Title
Polarons and Mobile Impurities Near a Quantum Phase Transition

Author
Shadkhoo, Shahriar

Publication Date
2015

Peer reviewed|Thesis/dissertation

UNIVERSITY OF CALIFORNIA

Los Angeles

Polarons and Mobile Impurities Near a Quantum Phase Transition

A dissertation submitted in partial satisfaction

of the requirements for the degree

Doctor of Philosophy in Physics

by

Shahriar Shadkhoo

2015

ABSTRACT OF THE DISSERTATION

Polarons and Mobile Impurities Near a Quantum Phase Transition

by

Shahriar Shadkhoo

Doctor of Philosophy in Physics

University of California, Los Angeles, 2015

Professor Robijn F. Bruinsma, Chair

This dissertation aims at improving the current understanding of the physics of mobile impurities in highly correlated liquid-like phases of matter. Impurity problems pose challenging and intricate questions in different realms of many-body physics. For instance, the problem of "solvation" of charged solutes in polar solvents, has been the subject of longstanding debates among chemical physicists. The significant role of quantum fluctuations of the solvent, as well as the break down of linear response theory, render the ordinary treatments intractable. Inspired by this complicated problem, we first attempt to understand the role of non-specific quantum fluctuations in the solvation process. To this end, we calculate the dynamic structure factor of a model polar liquid, using the classical Molecular Dynamics (MD) simulations. We verify the failure of linear response approximation in the vicinity of a hydrated electron, by comparing the outcomes of MD simulations with the predictions of linear response theory. This non-linear behavior is associated with the pronounced peaks of the structure factor, which reflect the strong fluctuations of the local modes. A cavity picture is constructed based on heuristic arguments, which suggests that the electron, along with the surrounding polarization cloud, behave like a frozen sphere, for which the linear response theory is broken inside and valid outside. The inverse radius of the spherical region serves as a

UV momentum cutoff for the linear response approximation to be applicable.

The problem of mobile impurities in polar liquids can be also addressed in the framework of the "polaron" problem. Polaron is a quasiparticle that typically acquires an extended state at weak couplings, and crossovers to a self-trapped state at strong couplings. Using the analytical fits to the numerically obtained charge-charge structure factor, a phenomenological approach is proposed within the Leggett's influence functional formalism, which derives the effective Euclidean action from the classical equation of motion. We calculate the effective mass of the polaron in the model polar liquid at zero and finite temperatures. The self-trapping transition of this polaron turns out to be discontinuous in certain regions of the phase diagram.

In order to systematically investigate the role of quantum fluctuations on the polaron properties, we adopt a quantum field theory which supports nearly-critical local modes: the quantum Landau-Brazovskii (QLB) model, which exhibits fluctuation-induced first order transition (weak crystallization). In the vicinity of the phase transition, the quantum fluctuations are strongly correlated; one can in principle tune the strength of these fluctuations, by adjusting the parameters close to or away from the transition point. Furthermore, sufficiently close to the transition, the theory accommodates "soliton" solutions, signaling the nonlinear response of the system. Therefore, the model seems to be a promising candidate for studying the effects of strong quantum fluctuations and also failure of linear response theory, in the polaron problem. We observe that at zero temperature, and away from the Brazovskii transition where the linear response approximation is valid, the localization transition of the polaron is discontinuous. Upon enhancing fluctuations—of either thermal or quantum nature—the gap of the effective mass closes at distinct second-order critical points. Sufficiently close to the Brazovskii transition where the nonlinear contributions of the field are significantly large, a new state appears in addition to extended and self-trapped polarons: an impurity-induced soliton. We interpret this as the break-down of linear response, reminiscent of what we observe in a polar liquid. Quantum LB model has been proposed to be realizable

in ultracold Bose gases in cavities. We thus discuss the experimental feasibility, and propose a setup which is believed to exhibit the aforementioned polaronic and solitonic states.

We eventually generalize the polaron formalism to the case of impurities that couple quadratically to a nearly-critical field; hence called the "quadratic polaron". The Hertz-Millis field theory and its generalization to the case of magnetic transition in helimagnets, is taken as a toy model. The phase diagram of the bare model contains both second-order and fluctuation-induced first-order quantum phase transitions. We propose a semi-classical scenario in which the impurity and the field couple quadratically. The polaron properties in the vicinity of these transitions are calculated in different dimensions. We observe that the quadratic coupling in three dimensions, even in the absence of the critical modes with finite wavelength, leads to a jump-like localization of the polaron. In lower dimensions, the transition behavior remains qualitatively similar to those in the case of linear coupling, namely the critical modes must have a finite wavelength to localize the particle.

The dissertation of Shahriar Shadkhoo is approved.

Alexander J. Levine

Michael Gutperle

Benjamin J. Schwartz

Robijn F. Bruinsma, Committee Chair

University of California, Los Angeles

2015

Dedicated to my parents

&

my one and only sister

TABLE OF CONTENTS

LIST OF FIGURES

LIST OF TABLES

ACKNOWLEDGMENTS

I would like to first express my deepest appreciation to my family, for their unconditional and everlasting support. I feel indebted to my parents, for first instilling in me a thirst for learning, and then teaching me how to strive for what I want; and to my sister for being "the" best friend, and always persuading and guiding me to achieve my goals.

I owe a debt of gratitude to my advisor, Professor Robijn Bruinsma, for generously supporting me in many respects, during the past four years. It has been a great honor to work under Robijn's supervision, who has greatly influenced my current knowledge and understanding of Physics. I am also very grateful to Professor Alexander Levine for always welcoming and helping me with questions I have come across. I feel very privileged to have had the opportunity to work with Robijn and Alex. From journal clubs and group meetings to short chats during the coffee or lunch break, I have been lucky to listen to their intuitions and viewpoints, and have gained deeper and deeper insight into Physics after each and every discussions.

This dissertation was primarily motivated by inspirational studies of Professor Benjamin Schwartz and Professor Gerard Wong, to whom I would like to give my sincerest thanks. Our further understanding of the problem would not have been possible without the theoretical and experimental studies of Ben and Gerard.

My first serious encounter with the subject of quantum field theory took place in two courses presented separately by Professor Michael Gutperle and Professor Eric D'hoker. I am very thankful to Michael and Eric for their unmatched lectures, which undoubtedly shaped my initial understanding of the topic.

VITA

2005 – 2009	B.S in Physics and Mechanical Engineering, Sharif University of Technology, Tehran, Tehran, Iran
2009 – 2010	M.S in Physics, Department of Physics and Astronomy, University of California, Los Angeles, California, USA
2010 – 2015	Graduate Research and Teaching Assistant, Department of Physics and Astronomy, University of California, Los Angeles, California, USA

PUBLICATIONS

Journal:

[1] S. Shadkhoo, R. Bruinsma, *Bose-Einstein Condensates: a model system for particle solvation?*, arXiv:1409.3329v1 (submitted, under revision at Phys. Rev. Lett.).

[2] F. Sedlmeier, S. Shadkhoo, R. Bruinsma, R.R. Netz, *Charge/mass dynamic structure factors of water and applications to dielectric friction and electroacoustic conversion*, The Journal of chemical physics, **140(5)**, 054512 (2014).

[3] S. Shadkhoo, G.R. Jafari, *Multifractal Detrended Cross-Correlation Analysis of Temporal and Spatial Seismic Data*, Eur. Phys. J. B, **72**, 679-683 (2009).

[4] S. Shadkhoo, F. Ghanbarnejad, G.R. Jafari, M.R. Rahimi Tabar, *Scaling behavior of earthquakes' inter-events time series*, Central European Journal of Physics, **7**, 620 (2009).

Conference:

[1] S. Shadkhoo, R. Bruinsma, *Impurity-doped Bose-Einstein Condensates in Multi-mode Cavities*, Bulletin of the American Physical Society, 2015 - APS.

[2] S. Shadkhoo, R. Bruinsma, *Wave-function Localization and Impurity-induced First Order Phase Transition in Correlated Liquids Near the Thermal Freezing Point*, Bulletin of the American Physical Society, 2014 - APS.

[3] S. Shadkhoo, R. Bruinsma, *Quantum Criticality of Charged Particles in Polar Liquids*, Bulletin of the American Physical Society, 2013 - APS.

[4] S. Shadkhoo, R. Bruinsma, *Small-to-Large Polaron Transition in Water*, Bulletin of the American Physical Society, 2012 - APS.

CHAPTER 1

Introduction

Scientific methods are strictly based upon "observations", which are performed by means of suitable apparatuses, and are intended to provide us with useful information about an unknown system. The basic idea is to treat any complex system as a black box; we learn about the system by sending signals and analyzing the outcome, *i.e.* the responses of the system to external perturbing stimuli. Depending on the properties of interest, we may apply various probes. As a general rule, signals with higher energies are required to probe the system at smaller scales of space and time.

The subject of condensed matter physics mainly concerns the collective behavior of many-body systems, and as a manifestation of the bulk behavior, studies different properties of the phases of matter and also the transitions between these phases. In particular, the theory of critical phenomena investigates the underlying mechanisms of phase transitions, which are accompanied by changes in the thermodynamic properties of the system. Interesting phenomena emerge as the energy scales of two competing contributions become comparable. Phase transitions take place as a consequence of the competition between different energetic and/or entropic contributions to the free energy of a system. Classical systems can undergo phase transitions which are driven entropically due to thermal fluctuations. The role of thermal fluctuations becomes less significant as the temperature falls below $k_B T \sim \hbar\omega$, where ω is the characteristic frequency scale of the low-lying excitations of the system. Quantum phase transitions—at absolute zero temperature—are thus driven by quantum fluctuations.

1.1 Impurities in Condensed Matter Systems

1.1.1 General Background

Impurities and defects are omnipresent in actual condensed matter systems. Defects come in various dimensions, from point-like (zero dimensional) to line dislocations and ruptures. They are mathematically represented by local potentials which depend on the nature of the defect. Point-like defects can be viewed as massive, immobile impurity particles in which the quantum zero-point motion is negligible. The renormalized coupling obtained upon integrating out the zero point motion, differs from the bare interaction.

In ultra-low temperature condensed matter systems, where the system is subject to strong quantum fluctuations, the problem of impurities becomes even more cumbersome. The role of interactions can be highly nontrivial, leading for example, to violations of Landau theory of Fermi liquids in some metallic systems near the magnetic phase transitions [1]. The Landau-Fermi-liquid theory is expected to be valid below a certain non-universal temperature T^*. The value of T^* depends on many parameters such as electron-phonon coupling strength. Non-Fermi-liquid (NFL) behavior, which is characterized by deviations from the Fermi-liquid scaling laws, appears above T^*. In order to observe NFL behavior down to zero temperature in the vicinity of a magnetic quantum phase transition, the mentioned energy scale T^* must disappear one way or the other. Immobile magnetic impurity (Kondo impurity) is a renowned example which amounts to the zero temperature residue of resistivity in metals [2], and also local NFL behavior [1]. The Kondo problem studies a magnetic impurity interacting with the itinerant electrons. Static nonmagnetic defects are also known to dominate the response of a system near a magnetic phase transition, which in certain cases results in the so-called Griffiths behavior [3]. The latter is another source of NFL, which is indeed caused by broadening the distribution of local T^* in the system, such that there remains no well-defined energy scale [1]. At zero temperature near a quantum phase transition, where

the imaginary-time enters as a new dimension, the role of the dynamics is very crucial in determining the dominating behaviors. In particular we note that at zero temperature, the static defects are perfectly correlated over this new dimension, and thus can have dramatic influence on the nature the phase transitions.

Light impurities, like single electrons, are subject to quantum zero-point fluctuations of the position-momentum conjugate pair. We refer to these impurities as mobile impurities. Mobile impurities behave quite differently when interacting with the surrounding medium. As a result of this interaction, the impurity can "polarize" the medium around itself; the induced polarization digs a potential well for the particle, and the particle tends to get localized. This iterative process goes on until the zero-point motion of the particle balances out the attractive self-trapping energy gain. The arising excitation is a quasiparticle consisting of the impurity and the induced polarization. Inspired by the original problem of electrons in polar crystals, this quasiparticle was coined "polaron" by Landau. The problem initially considered an excess electron interacting with longitudinal optical phonons of a crystal. However, the notion of polaron was later generalized to other structurally similar systems of impurities interacting with bosonic fields. Mobile impurities can be viewed as polarons, and when the effective mass of the impurity is sent to infinity, we essentially recover the physics of a static impurity (defect). Also the attractive nature of the polaron's self-interaction, which is counteracted by the zero-point pressure, eventually and at sufficiently strong couplings makes the particle self-trapped, a state which is characterized by a significantly large effective mass. As mentioned above, the strong coupling limit of the polaron problem can thus serve as a model for a static local defect with a renormalized coupling.

The problem of "polarons and mobile impurities near a quantum phase transition" was originally inspired by the interesting role of quantum fluctuations in the solvation process of a charged particle in polar liquids. Apart from the solvent-specific effects, the challenges that one deals with in the solvation problem are reminiscent of those in the polaron problem. The theoretical studies of impurities embedded in many-body

systems rely vastly on the linear response approximation. The impurity is considered as an external *weak* perturbation to the system, for which the leading order response is captured by the linear term. However, the strong quantum fluctuations in the solvation process or near a quantum phase transition, do not seem to be tractable via linear response formalism. In fact while the impact of a single impurity on the system is minuscule on average, and in the thermodynamic limit, this is not true in the vicinity of the impurity, and the linear response theory might become locally invalid.

Below we briefly mention a few conceptually important steps of derivation and also some of the consequences and corollaries of the linear response theory, such as Kubo formula and Fluctuation-dissipation theorem. Next, we discuss some of the difficulties that one faces in the study of solvation dynamics, and then introduce the formal notion of polaron.

1.1.2 Linear Response Theory

In the linear response formalism one first assumes that total Hamiltonian of the system is given by

$$\hat{\mathcal{H}}_{\mathrm{T}} = \hat{\mathcal{H}}_0 + \hat{\mathcal{H}}_{\mathrm{ext}}, \tag{1.1}$$

in which $\hat{\mathcal{H}}_0$ and $\hat{\mathcal{H}}_{\mathrm{ext}}$ represent the Hamiltonians of the isolated system and the external stimuli, respectively. The interaction picture of the above system can be constructed by splitting the dynamics of the system into that of the physical observables following $\hat{\mathcal{H}}_0$, and that of the states which is governed by $\hat{\mathcal{H}}_{\mathrm{ext}}$. Denoting the exact ground state of the system by $|G\rangle$, we calculate the expectation value of an observable $\hat{\mathcal{O}}(\mathbf{x}, t)$ under the influence of $\hat{\mathcal{H}}_{\mathrm{ext}}$:

$$\langle G|\hat{U}^{-1}(t)\hat{\mathcal{O}}(\mathbf{x}, t)\hat{U}(t)|G\rangle. \tag{1.2}$$

In the above expression $\hat{U}(t)$ is the evolution operator in the interaction picture, and is given by,

$$\hat{U}(t) = \mathtt{T}\ \exp\left(-\frac{i}{\hbar}\int_{-\infty}^{t} \mathrm{d}t'\, \hat{\mathcal{H}}_{\mathrm{ext}}(t')\right), \tag{1.3}$$

where T denotes the time ordering operator. Assumption of the weak perturbation allows us to expand the exponential in terms of external coupling. The change in the expectation value is given by

$$\delta\langle G|\hat{\mathcal{O}}(\mathbf{x},t)|G\rangle = \frac{i}{\hbar}\int_{-\infty}^{t} \mathrm{d}t'\,\langle G|[\hat{\mathcal{H}}_{\text{ext}}(t'),\hat{\mathcal{O}}(\mathbf{x},t)]|G\rangle, \tag{1.4}$$

in which it is implicitly assumed that $t > t'$, due to causality. For local observables like $\hat{\mathcal{O}}(\mathbf{x},t)$, there exists a conjugate external source $F(\mathbf{x},t)$ which couples linearly to the observable:

$$\hat{\mathcal{H}}_{\text{ext}}(t) = \int \mathrm{d}^d x\,\hat{\mathcal{O}}(\mathbf{x},t)F(\mathbf{x},t). \tag{1.5}$$

If the operators are normal ordered with respect to the vacuum, which implies that $\langle G|\hat{\mathcal{O}}(\mathbf{x},t)|G\rangle = 0$, we obtain for the *fluctuations* of the observable $\hat{\mathcal{O}}(\mathbf{x},t)$;

$$\langle G|\hat{\mathcal{O}}(\mathbf{x},t)|G\rangle = \int \mathrm{d}^d x' \int_{-\infty}^{t} \mathrm{d}t'\,\chi(\mathbf{x},t;\mathbf{x}',t')F(\mathbf{x}',t'), \tag{1.6}$$

where $\chi(\mathbf{x},t;\mathbf{x}',t')$ defines the generalized susceptibility or the correlation function of the observable $\hat{\mathcal{O}}(\mathbf{x},t)$. Alternatively, in the frequency domain we get

$$\langle G|\hat{\mathcal{O}}(\mathbf{x},\omega)|G\rangle = \frac{-i}{\hbar}\int \mathrm{d}^d x \int_{-\infty}^{0} \mathrm{d}t'\,\langle G|[\hat{\mathcal{O}}(\mathbf{x},t),\hat{\mathcal{O}}(\mathbf{x}',t+t')]|G\rangle F(\mathbf{x}',\omega). \tag{1.7}$$

The susceptibility is then obtained by:

$$\chi(\mathbf{x},\mathbf{x}';\omega) = \frac{-i}{\hbar}\int_{-\infty}^{0} \mathrm{d}\tau\, e^{i\omega\tau}\langle G|[\hat{\mathcal{O}}(\mathbf{x},0),\hat{\mathcal{O}}(\mathbf{x}',\tau)]|G\rangle. \tag{1.8}$$

This is called the *Kubo* formula [4, 5].

- **Fluctuation-Dissipation Theorem**

The response functions of a system can be calculated by using "fluctuation-dissipation theorem" which relates the non-equilibrium response function to the ensemble averages of equilibrium fluctuations, the structure factor. Structure factor is defined as an expectation value:

$$\Sigma(\mathbf{q},\omega) \equiv \int \mathrm{d}^d x \int \mathrm{d}t\, e^{i\omega t - i\mathbf{q}.\mathbf{x}}\langle\hat{\mathcal{O}}(0,0)\hat{\mathcal{O}}(\mathbf{x},t)\rangle. \tag{1.9}$$

Using the time ordering definition we find that $\Sigma(\mathbf{q}, -\omega) = e^{-\beta\hbar\omega}\Sigma(\mathbf{q}, \omega)$. According to fluctuation-dissipation theorem, the structure factor is related to the imaginary part of the susceptibility through

$$\mathrm{Im}\left\{\chi(\mathbf{q}, \omega)\right\} = \frac{\hbar}{2}\left(1 - e^{-\beta\hbar\omega}\right)\Sigma(\mathbf{q}, \omega). \tag{1.10}$$

This statement can be interpreted in terms of the intuitive argument, that the local observable is incapable of distinguishing the external perturbations from the inherent fluctuations, and hence responds similarly [4, 5].

1.1.3 Break down of Linear Response Theory in Solvation Problem

A challenging problem in chemical physics which has attracted so many physicists is the "solvation" (or *hydration*) of charged particles in polar solvents. The study of the solvation of particles in fluids is a fascinating area of chemical physics with an enormous literature [6, 7] that dates back to two centuries [8]. Solvated atoms and ions are surrounded by partially ordered shells of solvent molecules ("solvation shells"). On the other hand, solvent molecules surrounding solvated electrons appear to remain disordered [9]. Despite much recent progress, fundamental challenges remain, such as the breakdown of linear-response theory [10], solvent-specific effects that complicate continuum descriptions [11, 12] and the role of quantum fluctuations [13]. As an example, water—a very important solvent—is a highly correlated liquid characterized by complex, fluctuating patterns of hydrogen-bonding [14] which can be viewed as precursors of the freezing transition. The solvation of a particle in water depends on its compatibility with these fluctuations [15]. Path integral simulations of proton solvation in water indicate that the pattern of hydrogen bonding surrounding a solvated proton is subject to strong quantum fluctuations [16] while simulations of electrons in water [17] lead to wave-functions that are suggestive of Anderson localization [18]. In the remainder of this section, we elaborate on some of the mentioned issues.

In the process of solvation, the energy of the excited solute $\mathcal{E}^{\mathrm{exc}}$ decays to its ground

state $\mathcal{E}^{\text{gnd}}$, as a result of energy exchanging with the solvent. The solvation energy gap $\Delta\mathcal{E} = \mathcal{E}^{\text{exc}} - \mathcal{E}^{\text{gnd}}$ in the relaxation dynamics of the hydrated electron can be monitored through non-equilibrium solvent response function [19, 20]:

$$S(t) = \frac{\overline{\Delta\mathcal{E}}(t) - \overline{\Delta\mathcal{E}}(\infty)}{\overline{\Delta\mathcal{E}}(0) - \overline{\Delta\mathcal{E}}(\infty)}. \tag{1.11}$$

The overbar represents the non-equilibrium ensemble average under the initial condition that the electron is at the excited state at $t = 0$.

In the study of solvation dynamics, the applicability of linear response approximation is usually taken for granted. This is based on the Onsager regression hypothesis [21, 22], based on which the linear response of the system to an external perturbation is related to the equilibrium statistical fluctuations. The latter is characterized by:

$$C(t) = \frac{\langle \delta\Delta\mathcal{E}(0)\, \delta\Delta\mathcal{E}(t) \rangle}{\langle (\delta\Delta\mathcal{E})^2 \rangle}. \tag{1.12}$$

Here $\langle \bullet \rangle$ means equilibrium ensemble averaging, and $\delta\Delta\mathcal{E} = \Delta\mathcal{E} - \langle \Delta\mathcal{E} \rangle$ is the equilibrium fluctuations of the energy gap.

The validity of linear response theory in the process of solvation can be sometimes examined by comparing the non-equilibrium solvent response function $S(t)$, and the equilibrium solvation time correlation function $C(t)$. The two become identical when the linear response approximation is valid. The reverse statement, however, does not necessarily hold true; one cannot conclude the validity of linear response based on the similarity of the two functions [20]. In order to unravel the source of the failure of linear response one needs to be able to distinguish the effect of a *specific* type of molecular motions of the solvent (e.g. translational, vibrational, librational), on the solvation dynamics. A method was devised which employs the projection of the classical bath degrees of freedom onto the dynamics of *classical* solute [23]; this was hence utilized to explain the hidden break down of linear response for the problem of classical solvation [20]. Finally, the formalism was extended to the case of projection of classical molecular motions onto the solvation dynamics of a quantum solutes [19], and specifically the case of the photoexcited hydrated electron, e^-_{hyd}. Because of the similarities

between $S(t)$ and $C(t)$, it was believed for a long time, that the linear response theory holds for this system [24]. On the contrary, it was shown in the study of classical solvation, that linear response theory typically fails to capture the non-equilibrium solvation dynamics, when it involves size and/or shape changes of the solute particle [25]. Since the solvation of excited electron is accompanied by a shape change from s-like to p-like, the dynamics of non-equilibrium and equilibrium solvation processes are expected to exhibit different properties. This observation intrigued further investigations; mixed quantum-classical simulations (quantum solute in classical solvent) using the SPC-Flex model for water molecules which are interacting with an electron through a pseudopotential [26], and with a larger statistical sampling of the phase-space—than that used in [24]—reported the break down of linear response, and applied the projection method to investigate the sources of discrepancy between $S(t)$ and $C(t)$ [19]. It is noteworthy that in all the above studies, it was believed that the electron occupies a quasi-spherical region surrounded by the water molecules, the so-called cavity picture.

The commonly accepted cavity picture of the hydrated electron was challenged by a recent study which offered a different picture for the hydrated electron. According to this new picture which employed a rigorously derived pseudopotential that accounts for attractive oxygen and repulsive hydrogen features, the hydrated electron—in contrast to cavity picture—is spread over a region of size ~ 1 (nm), where the density of water is increased [17] (see Fig. (1.1)).

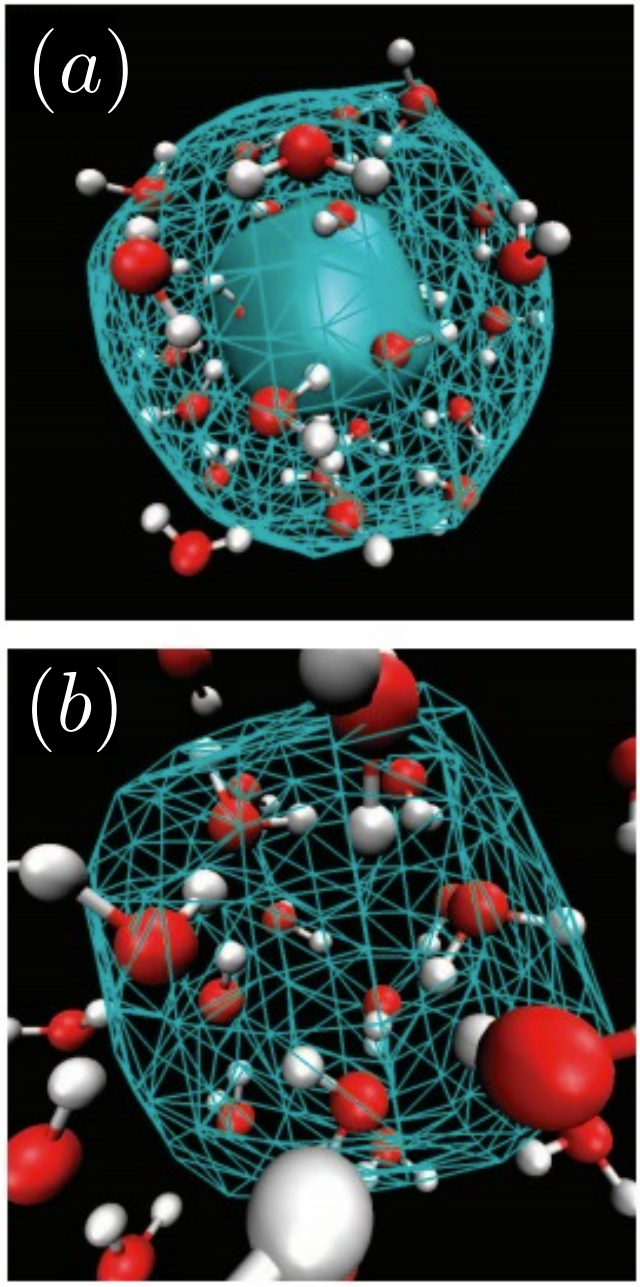

Figure 1.1: (From Ref. [17]) The top panel (a) shows the wave-function of the electron in liquid water. The outer meshed shell encloses $\%90$ of electrons distributions whereas the inner opaque shell encloses $\%50$ of that. The density of water is increased in these regions. (b) shows the zoomed-in inner shell.

1.1.4 Polaron Problem

According to the standard polaron problem, a quantum mechanical impurity (sometime interchangeably called "mobile impurity" in the literature and in context as well as throughout this dissertation), when interacting with longitudinal optical phonons, can acquire either extended or self-trapped polaronic states depending on the coupling constant. This is the standard Feynman's polaron which by means of an all-coupling variational approach, interpolates between the weak and strong coupling regimes, which were separately studied by Fröhlich, and, by Landau and Pekar.

The mode spectrum of the background medium, can drastically influence the polaron properties like effective mass and self energy. Parenthetically, we shall mention that these properties are commonly studied in (ultracold atomic) experiments through optical absorption and radio frequency (RF) spectroscopy. At finite temperatures where the quantum fluctuations of the field are largely suppressed, the particle is effectively interacting with a "frozen" field (or microscopically the constituents of the field). This mathematically corresponds to the so-called "Born-Oppenheimer" approximation. In this case if the background medium is in a disordered phase, as in the case of electrons in polar liquids, the impurity particle is effectively placed in a random potential. This problem, apart from the mathematical difficulties that may arise from, for instance, the complex mode spectrum, is conceptually easily approachable, and one might envision scenarios such as Anderson localization of waves in random potentials. However, for the regimes where the energy scale of the quantum fluctuations of the field become comparable to those of the thermal fluctuations and/or the zero point energy of the impurity, the interplay between different sources of fluctuations of the many-body as well as impurity degrees of freedom, makes the problem intractable at early stages.

In the next two sections, we introduce the general scenario of quantum phase transitions and eventually discuss the role of ultracold atomic physics and some approaches in studying mobile impurities in correlated systems.

1.2 Classical vs. Quantum Phase Transitions

Our formal understanding of the classical critical phenomena was initiated and developed based on the Landau-Ginzburg theory of symmetry-breaking. This phenomenological framework was later augmented by the idea of renormalization group, in part by Wilson. The theory of classical phase transitions is fairly well understood: phase transitions are classified based on the symmetries and the spatial dimensionality of the system. A key ingredient of Landau-Ginzburg-Wilson theory near a second order phase transition, is the notion of a long-wavelength macroscopic order parameter, which is zero in the symmetric phase and continuously takes on non-zero values below the critical point, *i.e.* in the symmetry-broken phase. The correlation length diverges upon approaching the critical point, and the scaling exponents are exclusive to universality classes. The statics and dynamics of the classical phase transitions are separable. The dynamics of the classical critical phenomena is usually defined according to the Halperin-Hohenberg classification [27].

In the simplest form of LGW theory (or ϕ^4-theory), the fluctuations occur around the wave-vector $q = 0$, which represents a single isolated point in momentum space. As mentioned, this gives rise to a second order (continuous) phase transition. The Gaussian fluctuations around the mean-field solution, modify the critical behavior in $2 \leq d \leq 4$. Hence $d_l = 2$ and $d_u = 4$ are called the lower and upper critical dimensions of the ϕ^4-theory, respectively. The lower critical dimension can be calculated according to the Mermin-Wagner theorem, which prohibits the spontaneous symmetry breaking in $d \leq 2$ for any positive temperature $T > 0$. In fact the effect of the strong fluctuations destroys the symmetry-breaking. The upper critical dimension is determined by using the Ginzburg criterion or renormalization group. This means that for $d < 4$, the critical behavior (e.g. exponents) of the theory is dominated by fluctuations; above $d > 4$, the scaling behavior can be predicted by mean-field theory.

In spite of a rather thorough understanding of the framework of classical critical

phenomena, quantum phase transitions pose significantly more difficult theoretical and experimental challenges. Apart from the nontrivial roles of entanglement and other properties which are absent in classical systems, statics and dynamics are no longer separable. In fact the equilibrium critical behavior of a system near a quantum phase transition is strongly influenced by its dynamics. This enters, for example, in the effective dimensionality of the system: near a quantum phase transition, correlation time, like the correlation length, diverges according to a power law. The scaling exponent is then related to the effective dimensions (see below).

1.2.1 Hertz-Millis Theory of Quantum Phase Transitions

A field theoretical approach to study quantum second-order phase transitions, was developed by Hertz and later modified by Millis [28, 29]. The theory resembles LGW theory, except dynamics is—near the quantum phase transition—essentially mixed with statics, unlike the classical cases where the statics and dynamics are uncorrelated and their fluctuations can be integrated out separately. Hertz-Millis formalism was intended to describe the itinerant-electron magnetization transitions (e.g. Stoner ferromagnetism). At zero temperature, $(k_B\beta)^{-1} \to 0$, the "imaginary-time" is an infinitely extended dimension; the effective dimensionality of the theory, D, is then increase by the dynamical exponent z (*i.e.* $D = d + z$), where z is obtained by the scaling relation between correlation time and length: $\xi_t \sim \xi^z$. At finite temperatures, the geometry of the domain of the order-parameter corresponds to a slab with a finite "length" $\beta\hbar$ in one dimension and infinitely long in other dimensions.

Depending on the type of dynamics, the dynamic exponent z can take different values. For example the in undamped dynamics case, where space and time enter on the same footing, we expect the dynamics to add "one" to the effective dimensions, hence $z = 1$. In overdamped, $z = 2$. In general $2/z$ turns out to be a measure of the importance of the quantum fluctuations to classical ones. The larger the z, the less important the quantum effects.

We now introduce a class of phase transitions which is not encapsulated in the traditional LGW theory.

1.2.2 Fluctuation-induced First Order Phase Transitions

Fluctuation induced first order phase transitions occur when the order parameter is coupled to a "gauge" field, whose fluctuations diverge at a *finite* wave-vector q_0. Examples include vector potential for superconductors or director field in smectic-A liquid crystals. As another example, in a ubiquitous class of phase transitions, the so-called crystallization, the order parameter seems to adopt a favored wave-vector of size $|\mathbf{q}| = q_0$. (Weak) crystallization is a transition between the disordered phase with continuous translational symmetry (liquid), and an ordered phase (crystal), modulated by one of the many degenerate modes with preferred wave-vector q_0. Therefore the divergent fluctuations occur—in spatial dimensions $d \geq 2$—around a hyper-sphere, forming a momentum shell in the momentum space.

The theory of weak crystallization was put forward by Brazovskii. In an attempt to describe the "crystallization" transition, and in accord with Landau's earlier trials, Brazovskii proposed a field theory. This field theory—if treated like a LGW theory, hence Landau-Brazovskii (LB) theory—results in a second order phase transition at mean-field level. However if the fluctuations are taken into account, the abundance of these critical modes keeps the renormalized distance from the transition positive (even below the mean-field critical point). Also, the quartic vertex becomes negative, but eventually a positive sixth-order term is generated in the RG procedure which stabilizes the free energy. Therefore the free energy density develops a nonzero minimum in addition to the zero Gaussian minimum. This implies that the order-parameter, at the transition where the minima are degenerate, jumps discontinuously from disordered zero to ordered nonzero value. We note that the consequence of adding the fluctuations is counterintuitive in the Brazovskii mechanism. The fluctuations are intuitively and generically expected to smear the singularity of the free energy, however in $d > 1$-

dimensional Brazovskii model, including the fluctuations results in a weakly first order phase transition, where the system avoids the critical point altogether, and prefers paying the latent heat energy in lieu of the fluctuations' entropic expense (which occur at wave-vector q_0). In superconductivity too, the fluctuating gauge field (vector potential), yields a similar effect. These phase transitions are commonly called the fluctuation-induced first order phase transitions.

In the vicinity of a first order transitions, the coexistence of the phases is permitted where the nucleated islands of the ordered phase are separated from the disordered bulk by a domain-wall with a thickness of the order of the correlation length, which is no longer divergent. Thus first order transitions are generically *not* described by a LGW-type continuum field theory. Nonetheless, in the case of *weakly* first order transitions, where the discontinuity of the order parameter is small, and where the correlation length, although finite, is very large, the coarse-graining and field theory formalism becomes valid again and the field theory description of the weak crystallization is legitimate. It is noteworthy that Landau-Brazovskii (LB) mechanism has been shown, in certain systems, to persist down to zero temperature making it a quantum phase transition (QLB).

1.2.3 Phase Transitions in Ultracold Quantum Gases

It was only recently around the turn of the twenty first century, that physicists succeeded in realizing quantum states of matter, and furthermore became capable of manipulating the systems and driving the transitions between different states. Ultracold atomic physics and cavity quantum electrodynamics have employed novel techniques such as laser cooling and/or evaporative cooling, to isolate the system from energy-exchanging environments and preserve the quantum characteristics of the system such as quantum coherence and entanglement, for time scales longer than those required in the experiment. Apart from the experimental interests, the fields provide ideal testbeds for theoretical models. Indeed designing the experiments for realizing *classical* model theories

through combinations of light-matter interactions of various sorts, is an active area of research. The engineering of quantum many-body cold atomic systems has been very successful as it usually provides us with a set of widely tunable knobs to explore the phase diagram of the system in hand. A commonly used technique, which allows us to explore the role of interactions (both strength and sign) in quantum gases, is Feshbach resonance. Through Feshbach resonance, one can tune the scattering length over a relatively large range, sometimes a few orders of magnitude. This can easily be applied to interactions between the same or different species of ingredients (atoms, molecules, etc.). Both pure and impure model systems have been employed to explore the role of quantum fluctuations and their interplay with inter- and intra-species interactions [30]. Furthermore, it is easily possible to change the dimensionality of the system in cold atomic experiments. Laser-pumping, for instance, can be used to confine the gas so tightly that the effective dimensionality of the system is reduced to lower than three.

Among the realizable phases, BECs are of special interest because of their long-range quantum coherence. Pure BECs are commonly described by the self-consistent nonlinear Gross-Pitaevski equation (GPE), and the fluctuations around the vacuum are approximated by the gapless Bogoliubov excitations. The self-interaction term in the GPE of an atomic condensate is represented by a local potential corresponding to the Lippmann-Schwinger s-wave scattering, in which the strength of the contact pseudopotential is proportional to the scattering length. The nonlinear nature of GPE, also supports non-dispersive solutions ("Solitons"), appearing concurrently in density and in the phase of the wave-function.

Optical lattices can be used to trap the bosonic atoms in a BEC, and they have been used to drive phase transitions. When the lattice depth is sufficiently large, the superfluid phase becomes unstable towards the Mott insulator phase. Here the explicit symmetry breaking determines the nodes into which the bosons get trapped. Cavities on the other hand, allow for a much richer and more complex collective behaviors through the photon-mediated interactions. These interactions in a single-mode cavity

result in the appearance of density modulation of a BEC which is trapped in a very wide parabolic well. Although the potential depth in the case of BEC in single mode cavity is emergent [31, 32, 33], the nodes are again determined by the cavity mode.

We eventually turn to the case of multimode cavities. The simplest example of a multimode cavity is a ring cavity with two counter-propagating waves. While the ordering transition can be observed in single-mode cavities, through an explicit symmetry-breaking, the multimode cavities allow for the "emergent" crystallinity. By emergent here we mean "*spontaneous*" symmetry-breaking. It has been proposed that spontaneous symmetry-breaking of translational symmetry in the form of crystallization transition can be observed in BECs in multimode cavities which are transversely pumped by a laser. The transverse laser provides a periodic potential (optical lattice) with parallel nodal and antinodal sheets. The atomic cloud is trapped in one of the antinodal sheets of the laser, and is also interacting with the cavity photons as well as the dissipative extracavity photons. The light-mediated interactions, softens the local modes of some finite wave-vector q_0. When the intensity of the transverse laser is tuned above a certain threshold, the transition takes place. This transition has been analytically shown to obey the Brazovskii mechanism of fluctuation-induced first order transition.

1.3 Outline

This dissertation is intended to be written in a self-contained manner and I try to provide the prerequisites of each topic, at the beginning of the corresponding chapter/section. In this section, we concisely illustrate the goals and results of each chapter.

Chapter 2: In order to study any impure system we first need to understand the background pure system. In our case of charged particles in polar liquids, the most relevant statistical quantity is the correlation function of the charge density fluctuations, *i.e.* the charge-charge structure factor. In the first part of this dissertation, we present and analyze the results of Molecular Dynamics (MD) simulations using the SPC/E

model of water. Furthermore, we calculate the dielectric drag force on a slowly moving charged particle, using a linear response theory. The discrepancy between the results obtained from the MD simulations, and those predicted by a linear-response Debye-like relaxation of the polarization field, signals the break-down of linear response. Next, by means of the Leggett's influence functional method, we propose an analytical model for calculating the effective mass and self-energy of the impurity. To this end, we use a model structure factor which is believed to capture the main features of a polar liquid. We observe, in certain circumstances, a first order transition in the effective mass of the impurity. When the system is viewed as a variant of polaron theory, the result can be contrasted against the Fröhlich polaron, in which the transition from the extended to the self-trapped state is smooth. We finally present the zero- and finite-temperature phase diagrams.

Chapter 3: In order to systematically study the role of quantum fluctuations of both the impurity and the medium, we adopt a model field theory, the so-called Landau-Brazovksii field theory. The model has been used extensively in its classical form to study the ordering transitions to lamellar phases of block-copolymers and liquid crystals. According to Brazovskii renormalization program, even though the model predicts a second-order phase transition in mean-field approximation, accounting for the fluctuations in spatial dimensions $d \geq 2$ renders the transition discontinuous. Brazovskii transition, is thus an example of the so-called fluctuation-induced first order phase transitions. A quantum generalization of the Landau-Brazovskii model (QLB) suggests that the first-order weak crystallization transition survives down to zero temperature, namely in the presence of the fully quantum mechanical fluctuations of the order-parameter (density field). It has been proposed that such emergent crystallization can be realized in ultracold Bose condensates, through light-mediated interactions, in transversely laser-pumped multimode cavities. When the laser intensity approaches a threshold, the resonant Bogoliubov excitations on top of the condensate vacuum, appear at finite wave-vectors which satisfy a condition that depends on the geometry of

the cavity.

The QLB theory and the proposed experiment seem to serve as promising candidates for examining the role of quantum fluctuations with finite wave-vectors on the polaron physics. Indeed, the laser intensity, an easily adjustable parameter in the experiment, is directly related to the distance from the Brazovskii transition; by tuning the laser intensity, one can tune the strength of fluctuations. Therefore, we adopt this model field theory to study the role of the *non-specific* quantum fluctuations of a solvent on the impurity and the phenomenon of solvation. We observe that far from the ordering transition, where the nonlinearities of the theory can be neglected, at zero effective temperature of the impurity particle, and also for frozen quantum fluctuations of the order-parameter (Born-Oppenheimer limit), the effective mass of the polaron undergoes a discontinuous transition (similar to the one from the phenomenological influence functional approach). At effective zero temperature, increasing the quantum fluctuations of the field gradually closes the jump of the effective mass at a second-order critical point. Alternatively, including the thermal fluctuations yields a qualitatively similar result. In the absence of the thermal and quantum fluctuations of the field, the "critical" coupling constant of the first-order transition of the effective mass, α_c, is calculated via a self-consistent approximation. This is shown to be proportional to the square root of the distance from the mean-field Brazovskii transition, which matches reasonably well with the numerical results. Therefore, away from the Brazovskii transition, the phase diagram consists of two branches of polaronic states corresponding to extended and self-trapped polarons, which are separated, in some regions of the phase diagram, by a line of first-order transition, which terminates at a critical point.

Chapter 4: This chapter begins with a quick overview of the soliton solutions the Gross-Pitaevskii equation. We discuss the density and phase solitons in atomic systems, and the role of interatomic interactions. Next, we turn to the case of impurity-induced solitons in BECs: close to the mean-field critical point of the QLB model, the effects of nonlinearities are no longer negligible, and indeed completely alter the

driving mechanism of the transition. We show, using the renormalized theory, that in addition to the aforementioned polaronic states, a new impurity-induced solitonic solution emerges, which correspond to the locally ordered structures of the symmetry-broken phase. The size of these solitons (also called "droplets") is of the order of the correlation length, which does not diverge at the first-order transition. We show that the soliton solutions are robust against Gaussian fluctuations, and also Derrick's instabilities. Gaussian fluctuations are shown to be irrelevant in spatial dimensions $d \geq 2$. Also according to Derrick's theorem, soliton solutions of scalar field theories are unstable against scaling transformations for $d \geq 2$. We show that a finite-size impurity is able to stabilize the solitons in any dimensions. Based on the currently accessible ranges of the intra- and inter-species interactions via Feshbach resonance, we estimate that many features of the theoretically explored phase diagram should be realizable in a atomic mixture, composed of a dilute impurity-gas of ^{6}Li atoms in a condensate of ^{23}Na atoms, and at temperatures of the order of nano-Kelvin.

Chapter 5: The analysis of mobile impurities near the quantum phase transitions is generalized in this chapter to the case of quadratic coupling of the impurity to the field. Inspired by the role of nonmagnetic impurities in itinerant-electron magnetic systems, a model system is proposed to produce this form of coupling: a magnetically polarizable mobile impurity interacting with the magnetization field of a system near a magnetic phase transition. The basic idea is that the induced magnetization of the impurity is proportional to the nearby magnetic field, which in turn is obtained by an integration over the contributions of the magnetization from all over the sample. In this chapter we focus mainly on the second-order transitions. The second-order quantum phase transition model is borrowed from Herz-Millis theory. Furthermore, we present the results for the case of fluctuation-induced first order transitions in magnetic systems. These transitions which follow the general scheme of Brazovskii transition, have been proposed to take place in paramagnon-magnetic roton phase transition, as well as paramagnet-helimagnet transition in itinerant magnets [34, 35].

We show in this chapter, that in three dimensions, the quadratic coupling induces a first order transition in the effective mass of the impurity, even in the absence of a preferred ordering wave-vector of the host system. We compare this result with those of the linear coupling formalism, where a minimum preferred wave-vector is required for discontinuous self-trapping of the particle to occur. In lower dimensions, a quadratic-type coupling alone cannot cause the first order transition of the effective mass, but like the case of linear coupling a finite q_0 is required for the localization to be discontinuous. We also present the results of some perturbative calculations, in small and large coupling limit.

Chapter 6: The appendix provides some supplementary materials as well as the theoretical backgrounds of different theories, which have been used throughout the previous chapters. These include (i) the details of MD simulations of chapter 2, (ii) an overview of the standard polaron notion and their properties, and (iii) a brief introduction to fluctuation-induced first order transition and Landau-Brazovskii theory of weak crystallization.

CHAPTER 2

Charged Particles in Polar Liquids

In this chapter, in line with our final goal of studying (quantum) impurities in polar liquids, we first aim at studying a ubiquitous and of course very important polar liquid, water. We determine time correlation functions and dynamic structure factors of the number and charge density of liquid water from molecular dynamics simulations. Using these correlation functions we consider dielectric friction and electro-acoustic coupling effects via linear response theory. From charge-charge correlations, the drag force on a moving point charge is derived and found to be maximal at a velocity of around 300 m/s. Strong deviations in the resulting friction coefficients from approximate theory employing a single Debye relaxation mode are found that are due to non-Debye-like resonances at high frequencies. From charge-mass cross-correlations the ultrasonic vibration potential is derived, which characterizes the conversion of acoustic waves into electric time-varying potentials. Along the dispersion relation for normal sound waves in water, the ultrasonic vibration potential is shown to strongly vary and to increase for larger wavelengths.

The last section of this chapter is devoted to a heuristic approach towards a path-integral formulation of the particle's degree of freedom. However the approach has some limitations which are discussed at the end of the section.

2.1 Classical Particles in a Classical Dielectric Medium

The dynamic structure factor $S(\vec{k},\omega)$ contains ample information on the structure and dynamics of condensed-matter systems. For water, where each molecule consists of one oxygen and two hydrogen atoms, various structure factors can be defined. The oxygen-oxygen structure factor S_{OO} is the dominant quantity for X-ray scattering experiments: Since X-rays interact predominantly with the electrons, the electron density is the relevant density related to the scattering cross section. In liquid water, due to the high electronegativity of the oxygen atom, the electron density is mainly centered around the oxygen atom and therefore one can determine the scattering cross section to a good approximation from the oxygen-oxygen structure factor using an isotropically averaged form factor [36, 37], which can be conveniently obtained from quantum chemistry calculations [38].

The recent usage of high intensity third generation synchrotron sources for inelastic X-ray scattering makes it possible to measure $S(\vec{k},\omega)$ for water over a wide range of wave vectors and frequencies [39] from which Greens functions and interfacial water dynamics have been reconstructed [40]. An interesting result of the inelastic scattering studies was that the excitation spectrum of water is richer than that of simple liquids, which is dominated by Rayleigh and Brillouin scattering. Water has two pronounced peaks in $S(\vec{k},\omega)$ with ω in the meV range and $|\vec{k}|$ in the inverse Angstrom range that are absent in simple liquids (see Fig. 2.1).

Neutrons on the other hand interact predominantly with the atomic nuclei, and have a high scattering cross section for hydrogen atoms. To model neutron scattering experiments one therefore has to take into account additionally the oxygen-hydrogen and hydrogen-hydrogen structure factors S_{OH} and S_{HH} [37].

For the case of acoustic perturbations, which are associated with mass displacements, the center of mass density structure factor $S_{\rho\rho}$ is relevant [41], while electrostatic fluctuations and correlations are embodied in the charge density structure factor

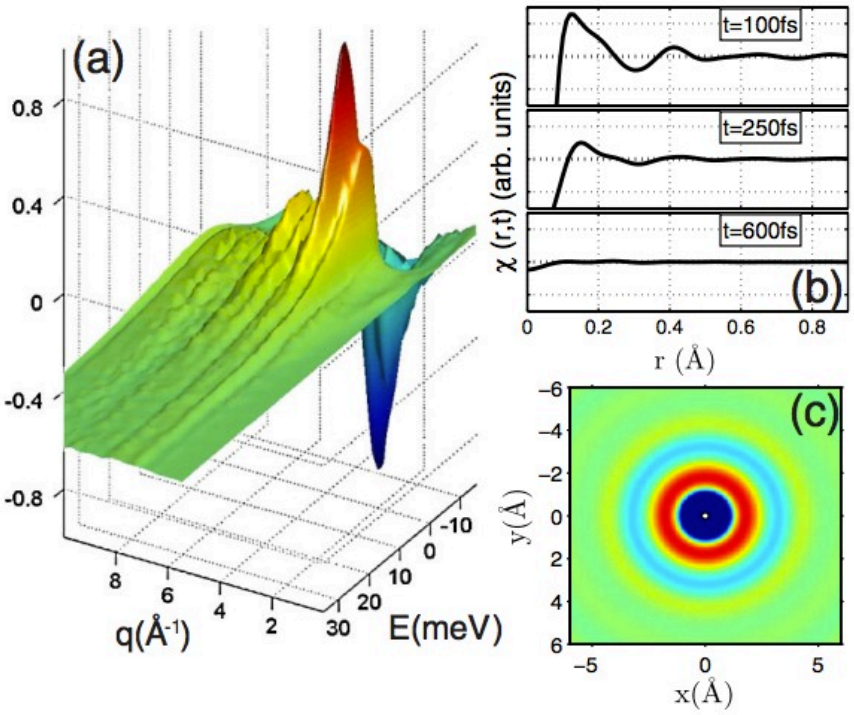

Figure 2.1: (From Ref. [39]) (a) shows the imaginary part of the response function Im$\chi(q,\omega)$ for water at ambient conditions. The double peaks occur at $q \simeq 3$ (Å^{-1}) and $\omega \simeq 1$ (meV) . (b) the response function $\chi(r,t)$ at times: 100 fs, 250 fs, and 600 fs. As observed from the bottom panel in (b), the hydration ripples are dissipated at $\gtrsim 600$ fs. A two-dimensional real-space representation of the hydration structure around a point negative charge. The red and blue rings correspond respectively to accumulation and depletion of oxygen density with respect to the background. The distance between the first and second hydration shells is $\simeq 2.6$ (Å).

S_{qq}, which determines also the solvation and dynamics of charged particles in water, like ions and electrons. In classical simulations, the structure factors $S_{\rho\rho}$ and S_{qq} can be constructed to a good approximation from the three site-site structure factors S_{OO}, S_{OH}, and S_{HH}, which therefore contain the complete structural and dynamical knowledge on the pair-correlation level. The importance of structure factors is due to a large extent to the fact that they are related to the linear response functions via the fluctuation dissipation theorem [42]. If, for example, one knows the charge density structure factor S_{qq} then one can directly obtain the imaginary part of the dielectric response function. This provides us with the polarization response of the medium to an external charge or potential distribution. To give an explicit application, the Bethe formula relates the stopping power of water for an electron to the dielectric response function of water [43].

In the following sections we determine the auto and cross-correlation functions and associated dynamic structure factors of the oxygen and hydrogen sites in liquid water over a wide range of wave vectors and frequencies. From those functions we derive diagonal and off-diagonal structure factors involving mass and charge densities. From the charge-charge dynamic structure factor we derive the dielectric friction force on a moving point charge via linear response theory. As a function of the point charge velocity, the drag force exhibits a pronounced maximum around a velocity of the order of $300\ m/s$. When compared with the standard theory for the friction of an electron in liquid water that employs a single Debye relaxation mode approximation, we find friction forces that are considerably larger. This deviation is due to non-Debye-like resonances at high frequencies in the simulated water susceptibility. The good agreement between single-Debye mode theory and experimental data for the electron mobility in water is nevertheless retained since the high-frequency domain is effectively preempted by a high-momentum cutoff that in a crude manner accounts for dielectric saturation effects. However, these non-Debye effects might be relevant for the kinetics and motion of partial molecular charges.

2.2 Dynamic Structure Factors

We define the auto- and cross correlation functions of the particle number and charge densities in reciprocal space as

$$F_{\alpha\beta}(\vec{k},t) = \frac{1}{N}\langle\alpha(\vec{k},t)\beta^*(\vec{k},0)\rangle, \tag{2.1}$$

where $\alpha,\beta = \mathrm{O},\mathrm{H},\rho,q$. For $\alpha = \mathrm{O},\mathrm{H},\rho$

$$\alpha(\vec{k},t) = \sum_{i=1}^{N} e^{-i\vec{k}\cdot\vec{r}_i^{\alpha}(t)}, \tag{2.2}$$

denotes the Fourier transform of the oxygen, hydrogen and molecule number density, while

$$q(\vec{k},t) = e\sum_{i=1}^{N}\sum_{\alpha=O,H,H} z_\alpha e^{-i\vec{k}\cdot\vec{r}_i^{\alpha}(t)}, \tag{2.3}$$

is the Fourier transform of the charge density. Here, z_α and $\vec{r}_i^{\alpha}(t)$ are the partial charge and the position of the atomic site $\alpha = \mathrm{O},\mathrm{H}$ while $\vec{r}_i^{\rho}(t)$ is the position of the center of mass of the i-th water molecule. The total number of water molecules is N, X^* denotes the complex conjugate of X and e is the elementary charge. The density-density autocorrelation function $F_{\rho\rho}(\vec{k},t)$ is also called the intermediate scattering function. The static structure factor is the $t \to 0$ limit of the correlation function, i. e., $S_{\alpha\beta}(\vec{k}) = F_{\alpha\beta}(\vec{k},0)$ for $\alpha,\beta = \mathrm{O},\mathrm{H},\rho,q$. The dynamic structure factor $S_{\alpha\beta}(\vec{k},\omega)$ is the Fourier transform of the correlation function,

$$S_{\alpha\beta}(\vec{k},\omega) = \frac{1}{2\pi}\int_{-\infty}^{\infty} F_{\alpha\beta}(\vec{k},t)e^{i\omega t}dt, \tag{2.4}$$

The structure factor $S_{\alpha\beta}(\vec{k},\omega)$ can be calculated from a simulation trajectory either by Eq. 2.4 or from the alternative expression,

$$S_{\alpha\beta}(\vec{k},\omega) = \frac{1}{2\pi}\langle\alpha_{\Delta t}(\vec{k},\omega)\beta^*_{\Delta t}(\vec{k},\omega)\rangle/(N\Delta t), \tag{2.5}$$

where the Fourier transform of the densities for the observation interval Δt is defined by

$$\alpha_{\Delta t}(\vec{k},\omega) = \int_0^{\Delta t}\alpha(\vec{k},t)e^{i\omega t}dt, \tag{2.6}$$

The charge density correlation functions can be expressed in terms of the site-site correlation functions as follows:

$$F_{qq} = e^2 z_{\mathrm{H}}^2 \left(4F_{\mathrm{OO}} - 4F_{\mathrm{OH}} + F_{\mathrm{HH}}\right), \tag{2.7}$$

$$F_{\mathrm{O}q} = e z_{\mathrm{H}} \left(-2F_{\mathrm{OO}} + F_{\mathrm{OH}}\right), \tag{2.8}$$

The static structure factors $S_{\rho\rho}(k)$, $S_{qq}(k)$, $S_{\mathrm{O}q}(k)$ and $S_{\rho q}(k)$ and the static site-site structure factors $S_{OO}(k)$, $S_{\mathrm{OH}}(k)$ and $S_{\mathrm{HH}}(k)$ are shown in Fig. 2.2a. It is seen that $S_{\rho\rho}(k)$ (filled circles) and $S_{OO}(k)$ (open circles) on the one hand and $S_{\rho q}$ (filled triangles) and $S_{\mathrm{O}q}(k)$ (open triangles) on the other hand almost perfectly overlap with each other. This reflects the fact that due to the small mass of H there is practically no difference between the oxygen and the center of mass positions in a water molecule. In the dynamic case there are differences as will be discussed below. The static site-site correlation functions $S_{OO}(k)$, $S_{\mathrm{OH}}(k)$ and $S_{\mathrm{HH}}(k)$ are shown in Fig. 2.2 b normalized by the site multiplicity. With this normalization they converge towards the same value in the long wavelength limit, since in this limit the small differences in the atomic positions are negligible with respect to the molecular position.

Figure 2.3 shows the autocorrelation functions $F_{\rho\rho}(k,t)$, $F_{\mathrm{OO}}(k,t)$ and $F_{qq}(k,t)$ and the corresponding dynamic structure factors $S_{\mathrm{OO}}(k,\omega)$, $S_{\rho\rho}(k,\omega)$ and $S_{qq}(k,\omega)$, while Fig. 2.4 shows the cross correlation functions $F_{\mathrm{O}q}(k,t)$ and $F_{\rho q}(k,t)$ and the corresponding dynamic structure factors $S_{\mathrm{O}q}(k,\omega)$ and $S_{\rho q}(k,\omega)$ for several values of $k = 3.5$, 10.5, 20.5, 28.5 and 36.5 nm^{-1}. Our results for the charge-charge correlation function compare well with the calculations of [44], who also used the SPC/E water model. Similar results for $F_{qq}(k,t)$ and $S_{qq}(k,\omega)$ have also been obtained for the TIP4P [45] and the BJH [46] water models.

If one compares $F_{\mathrm{O}q}(k,t)$ with $F_{\rho q}(k,t)$ for $k = 3.5$ nm^{-1}, it is evident that the high frequency oscillations present in $F_{\mathrm{O}q}(k,t)$ at short times $t < 0.3$ ps are absent in $F_{\rho q}(k,t)$. Correspondingly, the peaks in $S_{\mathrm{OO}}(k,\omega)$ and $S_{\mathrm{O}q}(k,\omega)$ around $\omega \approx 175$ ps^{-1} are absent for $S_{\rho\rho}(k,\omega)$ or much weaker for $S_{\rho q}(k,\omega)$. These differences can be ex-

plained by *librational modes* of the water molecules. These are small rotations around an axis through the center of mass of the molecules, which are manifest in the motion of the oxygen atom but not in the center of mass motion.

Site-site correlation functions $F_{\mathrm{OH}}(k,t)$ and $F_{\mathrm{HH}}(k,t)$ and the corresponding structure factors $S_{\mathrm{OH}}(k,\omega)$ and $S_{\mathrm{HH}}(k,\omega)$ are plotted in Fig. 2.5. Since $S_{\mathrm{OH}}(k,\omega)$ exhibits zero-crossings for several values of k we plot the absolute value.

Figures 2.6 - 2.9 show the logarithm of the dynamic structure factors $S_{\mathrm{OO}}(k,\omega)$, $S_{\rho\rho}(k,\omega)$, $S_{qq}(k,\omega)$, $|S_{\mathrm{O}q}(k,\omega)|$ and $|S_{\rho q}(k,\omega)|$ for the full k-ω-plane in 2D contour plots. An enlarged view of the low-k and ω region for $S_{\mathrm{OO}}(k,\omega)$, obtained from simulations of a system containing ≈ 33000 water molecules and a box size of $10 \times 10 \times 10$ nm^3, is shown in Fig. 2.7. Also included in Fig. 2.7 are the dispersion relations, $\omega(k) = c_{\mathrm{s}}k$, of propagating sound waves for hydrodynamic (dashed black line) and the hypothesized fast sound (dashed red line) modes [47]. The hydrodynamic (adiabatic) sound velocity is given by

$$c_{\mathrm{s}} = \sqrt{\frac{\gamma}{\kappa_T \rho_{\mathrm{m}}}}, \tag{2.9}$$

where $\gamma = c_{\mathrm{p}}/c_{\mathrm{v}}$ is the adiabatic index, κ_T is the isothermal compressibility, ρ_{m} is the mass density and c_{p} and c_{v} are the isobaric and isothermal heat capacities of water. For the SPC/E water model at $T = 300$ K we obtain $c_{\mathrm{p}} = 86.7$ J/(mol K) and $c_{\mathrm{v}} = 83.7$ J/(mol K) from linearly fitting the temperature dependence of the enthalpy and energy, respectively, yielding $\gamma = 1.037$. With $\kappa_T = 45.5 \cdot 10^{-11}$ Pa^{-1} and $\rho_{\mathrm{m}} = 0.999$ kg/l [48] we obtain $c_s = 1510$ m/s.

The literature discussion on the fast sound mode has a long and lively history: From the analysis of the dynamic structure factor $S_{\rho\rho}(k,\omega)$ obtained by MD simulations of the ST2 [49] water model [50] found two excitations, which they attributed to propagating modes with sound velocities of ≈ 1500 m/s and ≈ 3000 m/s. Many experimental [51, 52, 53, 54] and simulation [55, 56, 57] studies have been performed since and the current opinion is that rather than having two coexisting excitation modes, the ordinary sound branch with a sound velocity of $c_s \approx 1500$ m/s exhibits a gradual tran-

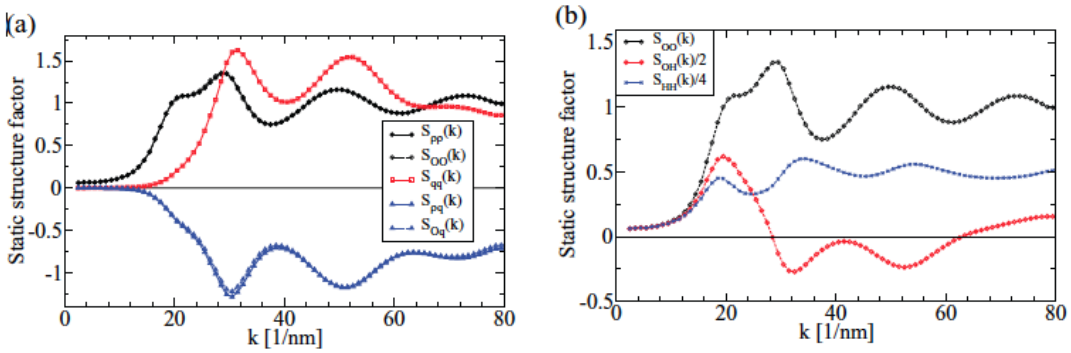

Figure 2.2: (a) Static structure factors $S_{\rho\rho}(k)$ (filled circles), $S_{\mathrm{OO}}(k)$ (open circles), $S_{qq}(k)$ (squares), $S_{\rho q}(k)$ (filled triangles) and $S_{\mathrm{O}q}(k)$ (open triangles). Note that $S_{\rho q}(k)$ and $S_{\mathrm{O}q}(k)$ are very similar, while $S_{\mathrm{OO}}(k)$ and $S_{\rho\rho}(k)$ are virtually indistinguishable. (b) Static site-site structure factors $S_{\mathrm{OO}}(k)$ (open circles), $S_{\mathrm{OH}}(k)$ (diamonds) and $S_{\mathrm{HH}}(k)$ (crosses). All data are obtained by MD simulations of SPC/E water at $T = 300$ K and $p = 1$ bar.

sition to the fast sound dispersion with a sound velocity of $c_{\mathrm{s}}' \approx 3500$ m/s [47] at higher wave vectors. In the k-range studied in this work, the Brillouin peak corresponding to the propagating sound wave is quite broad and overlaps with the central Rayleigh peak, which is due to diffusion of the water molecules. Consequently, it is only discernable as a slight shoulder and not as a pronounced maximum in Figure 2.3. The Rayleigh peak is reflected in Fig. 2.7 a by the slight bulge in the contour lines in between the two dashed lines. As indicated in Fig. 2.7 b, with increasing wave vector k the position of the shoulder moves from the position predicted by the dispersion relation of the normal sound c_s (filled spheres) towards the prediction of the dispersion relation for the fast sound c_s' (open spheres).

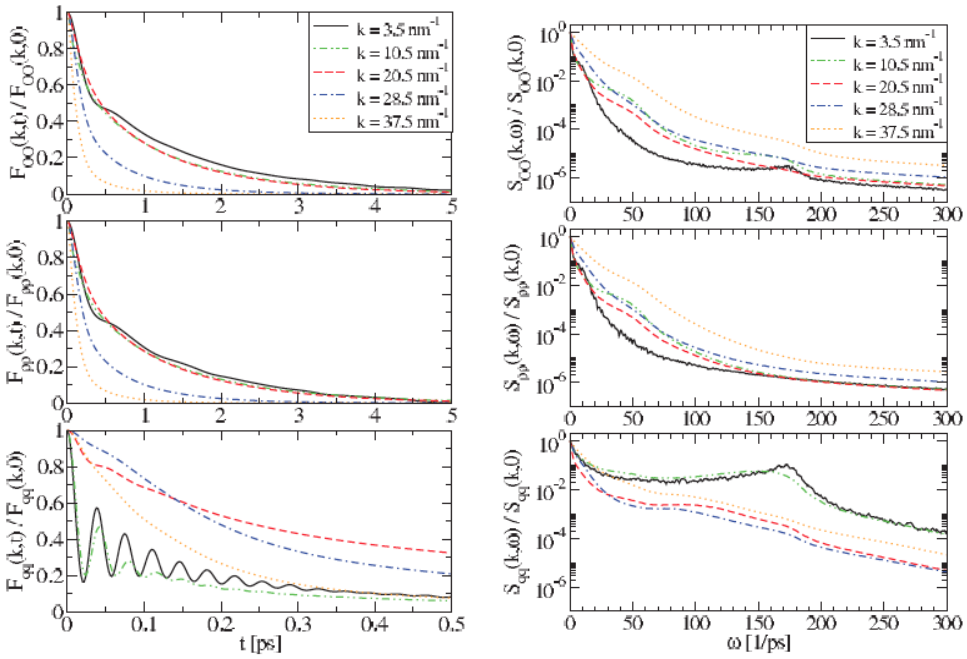

Figure 2.3: *Left panels*: Normalized autocorrelation functions $F_{\rho\rho}(k,t)$, $F_{\mathrm{OO}}(k,t)$ and $F_{qq}(k,t)$ for several values of the wave vector k. *Right panels*: Dynamic structure factors $S_{\mathrm{OO}}(k,\omega)$, $S_{\rho\rho}(k,\omega)$ and $S_{qq}(k,\omega)$ normalized by the $\omega = 0$ value for several different wave vectors k. All data are obtained by MD simulations of SPC/E water at $T = 300$ K and $p = 1$ bar.

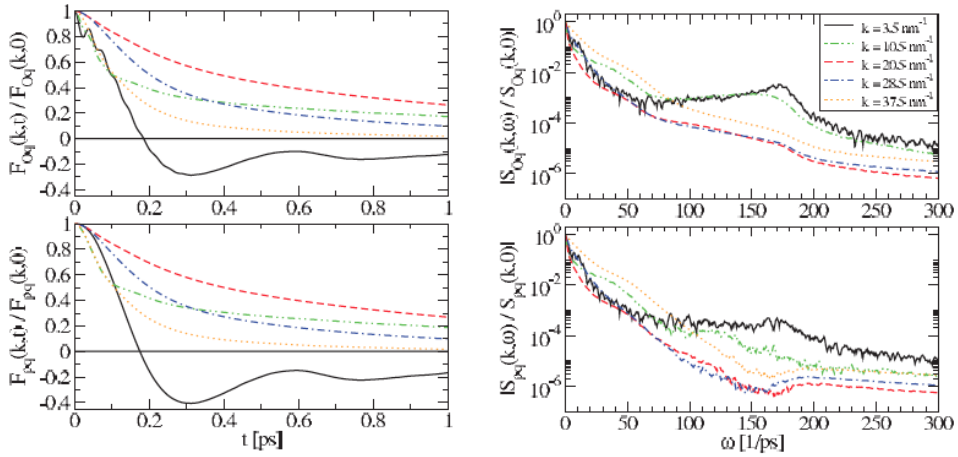

Figure 2.4: *Left panels*: Normalized cross correlation functions $F_{\mathrm{O}q}(k,t)$ and $F_{\rho q}(k,t)$ for several values of the wave vector k. *Right panels*: Dynamic structure factors $S_{\mathrm{O}q}(k,\omega)$ and $S_{\rho q}(k,\omega)$ normalized by the $\omega = 0$ value for several different wave vectors k. All data are obtained by MD simulations of SPC/E water at $T = 300$ K and $p = 1$ bar.

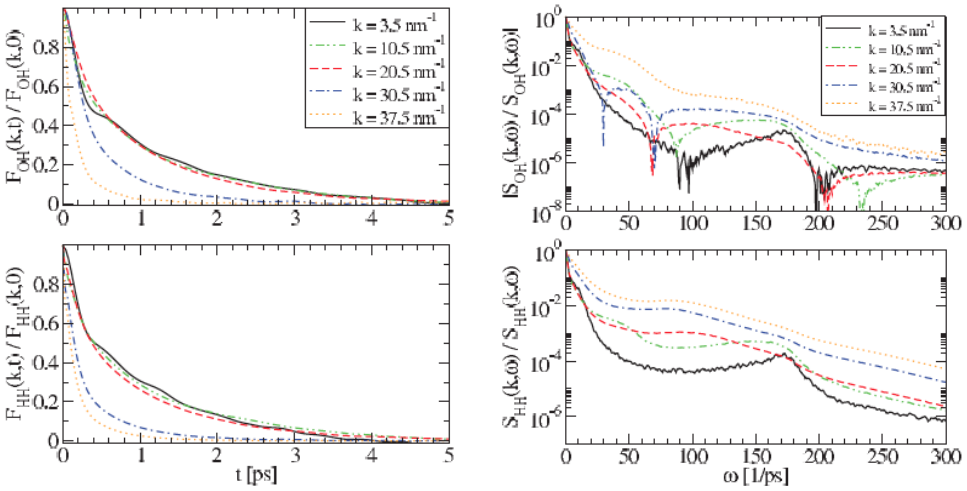

Figure 2.5: *Left panels*: Normalized site-site time correlation functions for several values of the wave vector k. *Right panels*: Corresponding dynamic structure factors normalized by the $\omega = 0$ value for several values of the wave vector k. All data are obtained by MD simulations of SPC/E water at $T = 300$ K and $p = 1$ bar.

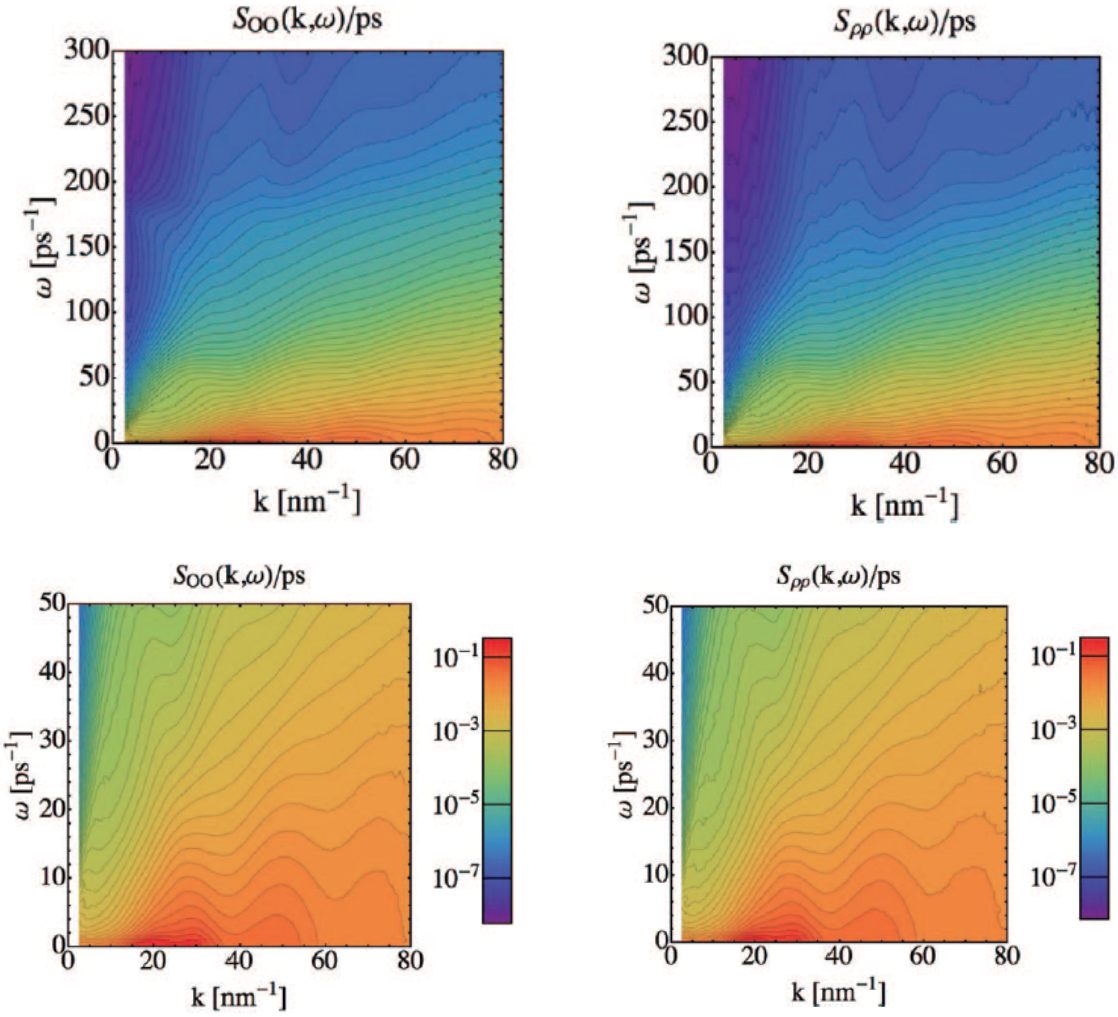

Figure 2.6: *Left panels*: Dynamic structure factors $S_{\mathrm{OO}}(k,\omega)$ (top row) and $S_{\rho\rho}(k,\omega)$ (bottom row) of SPC/E water at $T = 300$ K and $p = 1$ bar. *Right panels*: Close-up view of the low ω region.

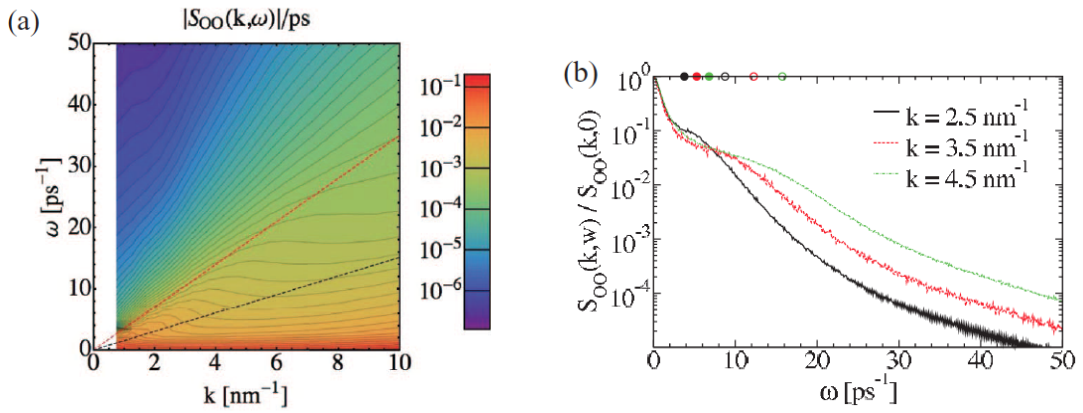

Figure 2.7: (a) Low k and ω region of the dynamic structure factors $S_{\mathrm{OO}}(k,\omega)$ of SPC/E water at $T = 300$ K and $p = 1$ bar, obtained from simulations of a system containing $\approx$ 33000 water molecules with a box size of $\approx 10 \times 10 \times 10$ nm^3. The black and red dashed lines show the dispersion relations of hydrodynamic and the hypothesized fast sound modes with sound velocities of $c_{\mathrm{s}} = 1510$ m/s and $c_{\mathrm{s}} = 3500$ m/s. (b) Normalized slices at fixed $k = 2.5$, 3.5 and 4.5 nm^{-1}. Filled and open circles show the positions of the expected Brillouin peaks for the normal and fast sound velocities.

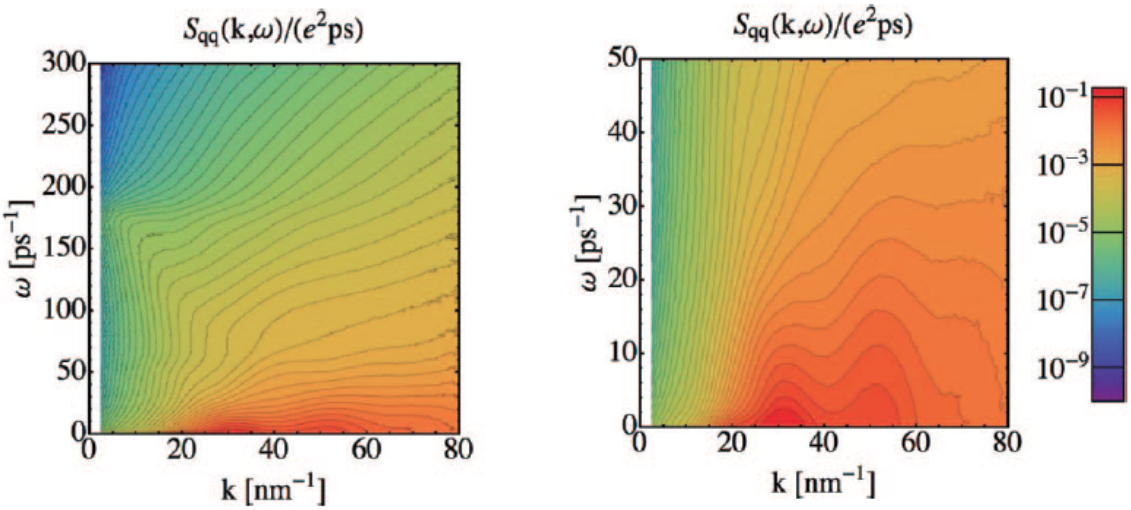

Figure 2.8: *Left panel*: Dynamic charge charge structure factor $S_{qq}(k,\omega)$ of SPC/E water at $T = 300$ K and $p = 1$ bar. *Right panel*: Close-up view of the low ω region.

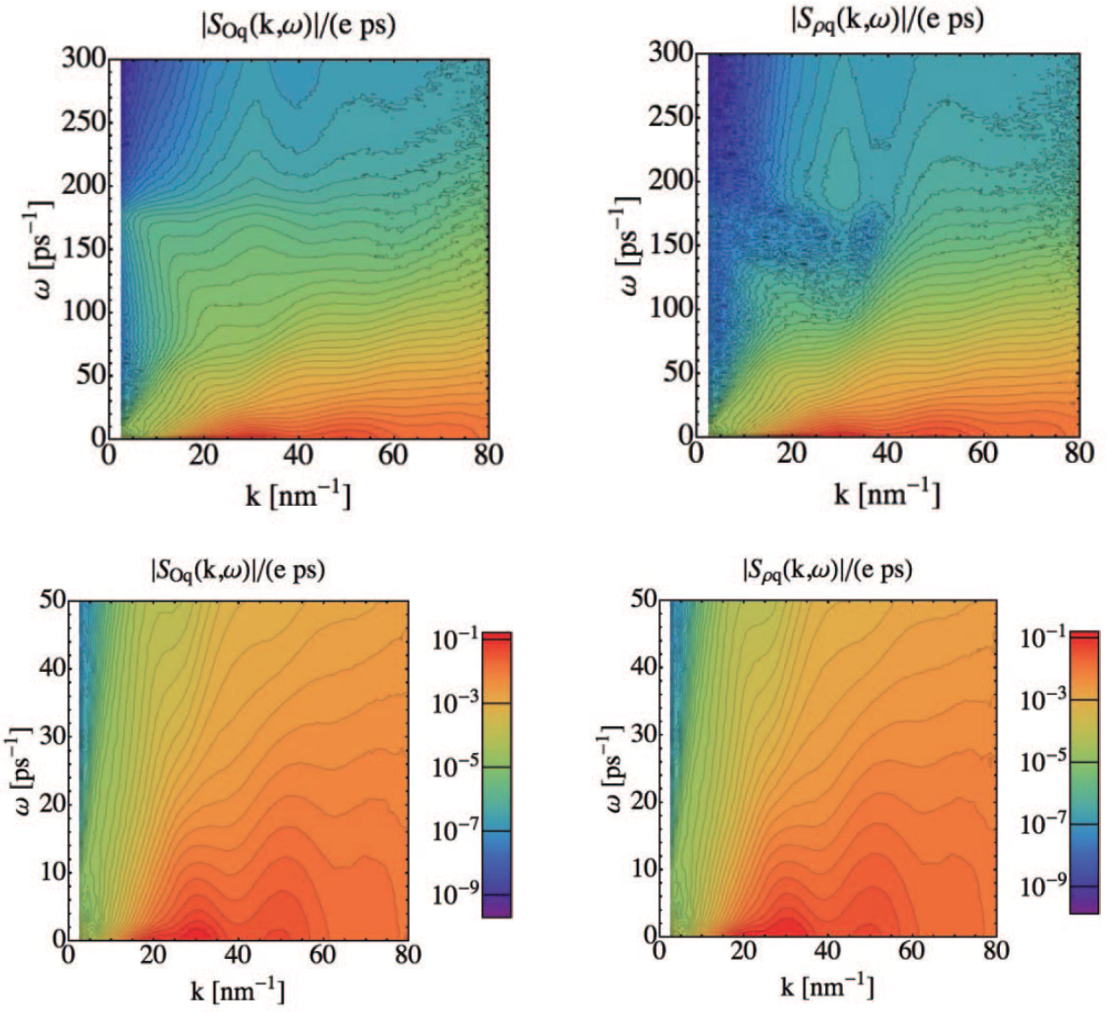

Figure 2.9: *Left panels*: Dynamic structure factors $S_{\mathrm{Oq}}(k,\omega)$ (top row) and $S_{\rho q}(k,\omega)$ (bottom row) of SPC/E water at $T = 300$ K and $p = 1$ bar. *Right panels*: Close-up view of the low ω region.

2.3 Electrostatic Effects

2.3.1 Linear Response Formalism

We briefly review here the basic definitions of electrostatic linear response theory which we will need in the following (see e.g. [46]). The dielectric response tensor $\chi_{\alpha\beta}$ is defined by the relation between the polarization density $\vec{P}$ and the dielectric displacement $\vec{D}$,

$$P_\alpha(\vec{r},t) = \int_V d^3r' \int_{-\infty}^{t} dt' \chi_{\alpha\beta}(\vec{r}-\vec{r}',t-t') D_\beta(\vec{r}',t'), \tag{2.10}$$

For a homogeneous medium the corresponding expression in Fourier space is

$$P_\alpha(\vec{k},\omega) = \chi_{\alpha\beta}(\vec{k},\omega) D_\beta(\vec{k},\omega), \tag{2.11}$$

In an isotropic medium the response tensor can be decomposed into longitudinal and transversal parts,

$$\chi_{\alpha\beta}(\vec{k},\omega) = \frac{k_\alpha k_\beta}{k^2}\chi_{||}(k,\omega) + \left(\delta_{\alpha\beta} - \frac{k_\alpha k_\beta}{k^2}\right)\chi_\perp(k,\omega), \tag{2.12}$$

with

$$\chi_{||}(k,\omega) = \frac{k_\alpha k_\beta}{k^2}\chi_{\alpha\beta}(\vec{k},\omega), \tag{2.13}$$

$$\chi_\perp(k,\omega) = \left(\delta_{\alpha\beta} - \frac{k_\alpha k_\beta}{k^2}\right)\chi_{\alpha\beta}(\vec{k},\omega), \tag{2.14}$$

The longitudinal response function is related to the charge density structure factor by the fluctuation dissipation theorem [42],

$$\mathrm{Im}\left[\chi_{||}(k,\omega)\right] = \frac{\pi}{k^2}\frac{\rho}{\varepsilon_0 k_\mathrm{B} T}\omega S_{qq}(k,\omega), \tag{2.15}$$

We further have

$$q_\mathrm{ind}(\vec{k},\omega) = -\chi_{||}(k,\omega) q_\mathrm{ext}(\vec{k},\omega), \tag{2.16}$$

where $q_\mathrm{ext}(\vec{k},\omega)$ and $q_\mathrm{ind}(\vec{k},\omega)$ are the Fourier transforms of an external and the induced charge density. In non-magnetic media and at low frequencies (quasistatic approximation), the transverse response function $\chi_\perp(k,\omega)$, does not enter the equations for the electrostatic potential, and will not be studied further in this work. It can be obtained directly from the polarization density correlation function [46].

2.3.2 Dielectric Friction and Drag Force on a Point Charge

Next, we derive an expression for the drag force on a charged point particle moving through a medium with velocity $\vec{v}$, using the linear response formalism. The external charge density arising from the moving charge then is $q_{\rm ext}(\vec{r},t) = q_0\delta(\vec{r}-\vec{v}t)$, where q_0 is the charge of the particle and $\delta(\vec{r})$ the Dirac delta function. Accordingly, the external charge density in Fourier space is

$$q_{\rm ext}(\vec{k},\omega) = 2\pi q_0\delta(\vec{k}\cdot\vec{v}-\omega). \tag{2.17}$$

The induced charge density follows from Eq. 2.16 as

$$q_{\rm ind}(\vec{k},\omega) = -2\pi q_0\chi_{||}(k,\omega)\delta(\vec{k}\cdot\vec{v}-\omega), \tag{2.18}$$

In the quasi-static approximation, the electric potential produced by the induced charge density is given by

$$\begin{aligned}\phi_{\rm ind}(\vec{k},\omega) &= \frac{1}{k^2}\frac{q_{\rm ind}(\vec{k},\omega)}{\varepsilon_0} &(2.19)\\ &= -\frac{1}{k^2}\frac{2\pi q_0}{\varepsilon_0}\chi_{||}(k,\omega)\delta(\vec{k}\cdot\vec{v}-\omega), &(2.20)\end{aligned}$$

Applying the inverse Fourier transform, we obtain

$$\begin{aligned}\phi_{\rm ind}(\vec{r},t) &= -\int\frac{d\omega}{2\pi}\int\frac{d^3k}{(2\pi)^3}\phi_{\rm ind}(\vec{k},\omega)e^{i(\vec{k}\cdot\vec{r}-\omega t)} &(2.21)\\ &= -\int\frac{d^3k}{(2\pi)^3}\frac{q_0}{\varepsilon_0 k^2}\chi_{||}(k,\vec{k}\cdot\vec{v})e^{i(\vec{k}\cdot\vec{r}-\vec{k}\cdot\vec{v}t)}, &(2.22)\end{aligned}$$

The force on the moving particle due to the induced charge density then is $\vec{F} = -q_0\nabla\phi_{\rm ind}(\vec{r},t)|_{\vec{r}=\vec{v}t}$, which yields

$$\vec{F} = i\frac{q_0^2}{(2\pi)^3\varepsilon_0}\int d^3k\frac{\vec{k}}{k^2}\chi_{||}(k,\vec{k}\cdot\vec{v}), \tag{2.23}$$

Without loss of generality we can assume $\vec{v} = v\vec{e}_z$ and write the integral in spherical coordinates,

$$\vec{F} = i\frac{q_0^2}{(2\pi)^3\varepsilon_0}\int_0^{2\pi}d\varphi\int_{-1}^{1}ds\int_0^{k_{\rm max}}dk\vec{k}\chi_{||}(k,kvs), \tag{2.24}$$

where $s = \cos(\theta)$ and we have introduced an upper wave vector cutoff $k_{\max}$.

It is easily seen, that the x and y components of $\vec{F}$ vanish and with $\vec{F} = F\vec{e}_z$ we obtain

$$F = i\frac{q_0^2}{(2\pi)^2\varepsilon_0}\int_{-1}^{1} ds \int_0^{k_{\max}} dkks\chi_{||}(k, kvs), \tag{2.25}$$

Writing the response function as $\chi = \chi' + i\chi''$, we have

$$\chi'(k,\omega) = \chi'(k,-\omega), \tag{2.26}$$

$$\chi''(k,\omega) = -\chi''(k,-\omega), \tag{2.27}$$

and therefore we obtain

$$F = -\frac{q_0^2}{(2\pi)^2\varepsilon_0}\int_{-1}^{1} ds \int_0^{k_{\max}} dkks\chi''(k, kvs), \tag{2.28}$$

The minus sign indicates here that F is a friction force in the direction opposite to that of the velocity. As expected, only the imaginary part of the susceptibility contributes to the rate of energy dissipation. Using Eq. 2.15 we can express the friction force in terms of the charge density structure factor as

$$F = -\frac{q_0^2\rho v}{4\pi\varepsilon_0^2 k_{\mathrm{B}}T}\int_{-1}^{1} ds \int_0^{k_{\max}} dks^2 S_{qq}(k, kvs), \tag{2.29}$$

The same result appears as an intermediate step in the derivation of the Bethe stopping power [58]. Figure 2.10 a shows the drag force F obtained using Eq. 2.29 and the dynamic structure factor of SPC/E water at $T = 300$ K and $p = 1$ bar as shown in Fig. 2.8. We find a pronounced dependence on the upper wave vector cutoff $k_{\max}$; the friction force increases with increasing cutoff. The highest cutoff we consider is $k_{\max} = 70\mathrm{nm}^{-1}$ since for higher wave vectors we expect the point-charge model employed in our classical MD simulations to become inaccurate. The friction force is shown to exhibit a maximal value at a velocity around $v = 300$m/s and to slowly decay for larger velocities, in stark contrast to Stokes friction. The concept of dielectric friction has a long history [59, 60], but note that previous simulation estimates for the friction of a moving charge in water used approximate theories and therefore could not

resolve the velocity dependence of the friction force in full detail [61]. Although it is clear that the dielectric friction and non-electrostatic friction are of course intimately coupled and difficult to disentangle [62], the decrease of friction with increasing velocity is certainly noteworthy and points to collective effects. For electrons in water, we expect non-electrostatic friction effects to be rather small and therefore the effect predicted in Fig. 2.10 a might be directly observable. In situations where the dielectric adsorption spectrum has features at lower frequencies than in bulk water, such as in water-filled protein cavities or close to membrane-water interfaces, we expect the velocity of maximal friction to be shifted to lower values. In Fig. 2.10 b we plot the friction coefficient $\gamma = F/v$ as a function of the velocity, which monotonically decays; here the crossover seen in the friction force is not directly seen. We note that in the limit of $\vec{v} \to 0$ Eq. (28) simplifies and the friction coefficient is given by

$$\gamma(v=0) = -\frac{2}{3}\frac{e^2\rho}{4\pi\varepsilon^2 k_B T}\int_0^{k_{\max}} \mathrm{d}k S_{qq}(k,0) \tag{2.30}$$

and takes on a finite value, as seen in Fig. 2.10(c).

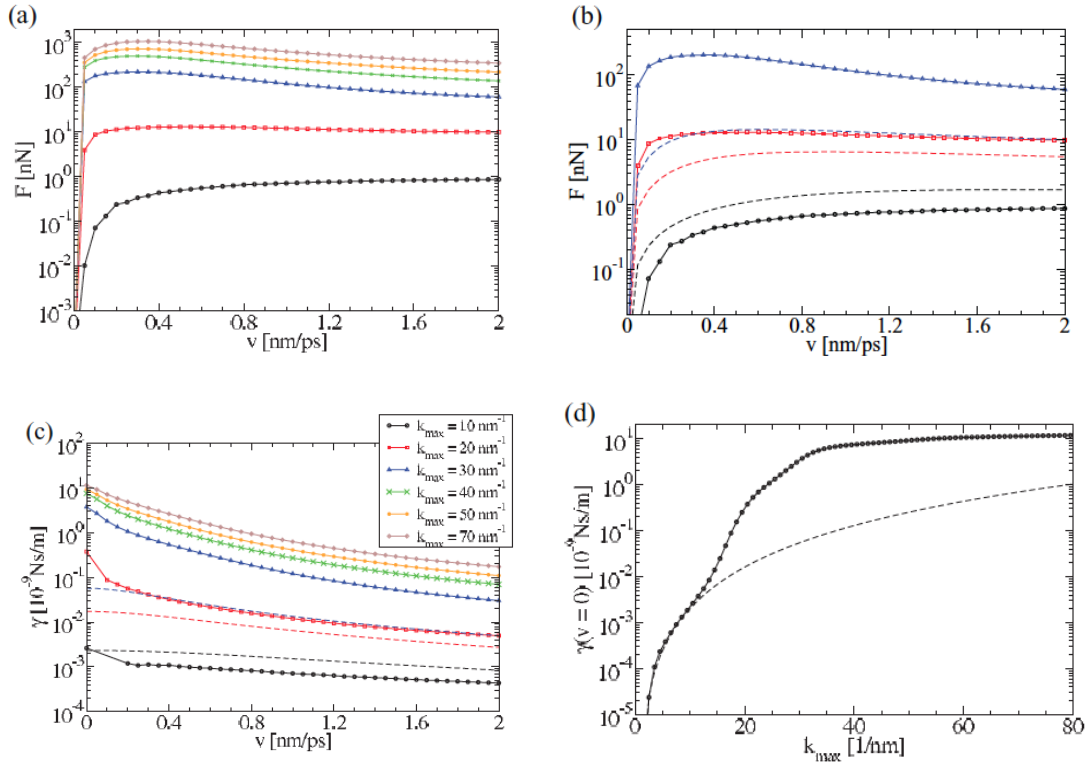

Figure 2.10: (a) and (b) Drag force F and (c) friction coefficient $\gamma = F/v$ of a charged particle with charge $q_0 = e^-$ as a function of the particle velocity v as obtained by Eq. (28) (open symbols and solid lines). Different symbol shapes and line colors denote results for different values of the upper wave vector cutoff $k_{\max}$. In (b) and (c) in addition results obtained using the single Debye peak approximation, Eq. (33), with $\varepsilon(0) = 80$, $\varepsilon(\infty) = 1$, and $\tau = 10$ (ps) are shown (dashed lines). (d) Comparison of the friction coefficient in the limit $v \to 0$ as a function of the wave vector cutoff $k_{\max}$ in Eq. (29) using the full susceptibility from the MD simulations (open symbols and solid lines) with the single Debye peak approximation, Eq. (35) (dashed line). The dynamic charge-charge structure factor used in the calculation is taken from SPC/E water at $T = 300$ K and $p = 1$ bar.

2.4 Break-down of Linear Response Theory; Limitations of the Single Debye-peak Approximation

To understand the strong cutoff dependence of the calculated friction forces and friction coefficients in Figs. 9(a) and 9(c) it is useful to compare our results to the limiting case of a single Debye relaxation mode, in which limit the calculation can be done exactly. First we note that the standard electrodynamic relations between the polarization density P, the displacement field D, and the electric field E, namely,

$$D = P + \varepsilon_0 E, \tag{2.31}$$

and $D = \varepsilon_0 \varepsilon E$, yield in comparison with our definition for the susceptibility in Eq. (10) the relation

$$\chi(k,\omega) = 1 - \varepsilon^{-1}(k,\omega) \tag{2.32}$$

The imaginary part of the susceptibility then equals:

$$\chi''(k,\omega) = \frac{\varepsilon''(k,\omega)}{|\varepsilon(k,\omega)|^2} \tag{2.33}$$

The original Debye model for the dielectric response (polarization decay), ignores the k-dependence:

$$\varepsilon(\omega) = \frac{\varepsilon(0) - \varepsilon(\infty)}{1 - i\omega\tau} + \varepsilon(\infty), \tag{2.34}$$

which describes a single relaxation mode with characteristic time τ. Then the imaginary part of the susceptibility for Debye model reads:

$$\chi''(\omega) = \frac{\omega\tau(\varepsilon(0) - \varepsilon(\infty))}{\varepsilon^2(0) + \varepsilon^2(\infty)(\omega\tau)^2}. \tag{2.35}$$

We note that while $\varepsilon''(\omega)$ has a maximum at $\omega = \tau^{-1}$, the maximum of $\chi''(\omega)$ is shifted to higher frequencies and occurs at $\omega = (\varepsilon(0)/\varepsilon(\infty))\tau^{-1}$. Inserting the single-Debye approximation Eq. (33) into the expression Eq. (27) we obtain an approximation for the friction force F. Choosing $\varepsilon(0) = 80$ as appropriate for the static dielectric constant of SPC/E water, choosing the dielectric constant in the optical to equal the

vacuum value $\varepsilon(\infty) = 1$, which reflects the absence of high-frequency polarization effects in the MD simulations, and a relaxation time of $\tau = 10$ (ps), which again is close to the actual relaxation time in SPC/E water, we obtain via numerical integration of Eq. (27) the broken lines in Fig. 9(b) which correspond to three different values of the upper momentum cutoff k_{max}. It is seen that for the smallest value $k_{\text{max}} = 10$ nm^{-1} denoted by a black broken line, the deviation from the result using the full susceptibility from the MD simulations (black circles and black solid line) is quite modest, but grows significantly for $k_{\text{max}} = 20$ nm^{-1} (red broken line and red data points) and for $k_{\text{max}} = 30$ nm^{-1} (blue broken line and blue data points). In Fig. 9(c) we show the single-Debye peak approximation for the friction coefficient $\gamma = F/v$ as a function of the velocity for the three smallest values of the upper wave vector cutoff k_{max} (broken lines). We again observe that for the smallest value $k_{\text{max}} = 10$ nm^{-1} (black broken line), the agreement with the result using the full susceptibility from the MD simulations (black circles and black solid line) is quite good, but significant deviations are seen for $k_{\text{max}} = 20$ nm^{-1} (red broken line and red data points) and for $k_{\text{max}} = 30$ nm^{-1} (blue broken line and blue data points).

In the limit of vanishing velocity of the point charge, $v \to 0$, the expression for the friction coefficient using the single-Debye peak approximation can be calculated in closed form and reads

$$\gamma(v=0) = -\frac{1}{18\pi^2}\frac{q_0^2(\varepsilon(0)-\varepsilon(\infty))\tau k_{\text{max}}^3}{\varepsilon_0\varepsilon^2(0)}. \tag{2.36}$$

Approximating $\varepsilon(0)-\varepsilon(\infty) \approx \varepsilon(0)$, defining the Bjerrum length as $\ell_B = \frac{q_0^2}{4\pi\varepsilon_0\varepsilon(0)k_BT}$ which for a unit charge $q_0 = e^-$ has a value of roughly $\ell_B \approx 1$ (nm), and relating the upper cutoff to an effective radius R as $k_{\text{max}} = \pi/R$, we obtain the simple expression

$$\gamma(v=0) = -\frac{2}{9\pi}\ell_B k_B T \tau k_{\text{max}}^3 = -\frac{2\pi^2}{9}\frac{\ell_B k_B T \tau}{R^3} \tag{2.37}$$

which has the same scaling and a very similar numerical prefactor as previously derived expressions. The cubic dependence of the friction coefficient on the upper wave

vector cutoff $k_{\max}$ explains why the data in Fig. 9 depend so sensitively on $k_{\max}$. Putting in numbers which presumably are appropriate for electrons in water, i.e., $\ell_B = 1$ (nm), $\tau = 10$ (ps), $k_BT = 4 \times 10^{-21}$ (J), $k_{\max} = \pi/R = 10^{10}$ m^{-1}, we obtain the value $\gamma(v = 0) \approx 2 \times 10^{-12}$ (Ns/m). Through Einsteins relation $D = k_BT/\gamma$ we obtain a diffusion constant of $D \approx 2 \times 10^{-9}$ m^2/s $= 2 \times 10^{-5}$ cm^2/s, which agrees well with experimental results for the electron diffusivity and previous theoretical estimates. Incidentally, an estimate of the hydrodynamic friction for a particle with a radius $R = 0.1$ (nm) gives, using Stokes law with a water viscosity of $\eta = 10^{-3}$ kg/(ms), a friction coefficient of $\gamma_{\rm hyd} = 6\pi\eta R = 2 \times 10^{-12}$ Ns/m which is identical to the dielectric friction estimate. This reflects that dielectric and hydrodynamic friction effects have very similar magnitudes for liquid water if the characteristic radii are chosen similarly and of the order of $R = 0.1$ nm. The static friction coefficient $\gamma(v = 0)$ according to Eq. (35) is shown in Fig. 9(d) as a function of $k_{\max}$ by a broken line and compared to the result using the full susceptibility in Eq. (29) (solid line and symbols). It is seen that for $k_{\max} < 10$ nm^{-1} the two calculations agree while for larger values of $k_{\max}$ the single Debye peak approximation underestimates $\gamma(v = 0)$ by roughly an order of magnitude. To understand the cause of this deviation in more detail, we show in Figs. 10(a) and 10(b) the susceptibility $\chi''_{\|}(k, \omega)$ for different fixed values of k as a function of ω. It is seen that for small values of k at $\omega \approx 175$ ps^{-1} a sharp peak is present, which by comparison with the results for S_{qq} in Fig. 2 is traced back to the fast librational motion of the hydrogen atoms. Figure 10(c) compares $\chi''_{\|}(k, \omega)$ in the small ω-region with the Debye form, Eq. (33), for a few different values of $\varepsilon(\infty)$. The overall agreement is not impressive, but the comparison shows that the small hump in $\chi''_{\|}(k, \omega)$ around $\omega \approx 10$ ps^{-1} is related to the dielectric Debye relaxation which only becomes accurate in the limit $k \to 0$.We conclude that the strong deviations in $\chi''_{\|}(k, \omega)$ at finite values of k from the simple Debye form lead to the pronounced deviations between the results based on the numerical integration over the full $\chi''_{\|}(k, \omega)$ and the single-Debye peak approximation in Fig. 9.

We finally want to explain how the upper wave vector cutoff $k_{\max}$ can be derived for a toy model of a charge distribution with a finite radius R. Considering a moving external charge that is distributed over a spherical shell with a radius R,

$$q_{\text{ext}}(\vec{r},t) = \frac{q_0}{4\pi R^2}\delta(|\vec{r}-\vec{v}t| - R), \tag{2.38}$$

the analogous calculation leading to the friction force, Eq. (28), gives for the present case of a charged spherical shell the friction force

$$F = -\frac{q_0^2\rho v}{4\pi\varepsilon_0^2 k_{\text{B}}T}\int_{-1}^{1}\mathrm{d}s\int_0^{k_{\max}}\mathrm{d}k s^2 S_{qq}(k,kvs)\times J_0^2(kR)\,, \tag{2.39}$$

where $J_0(x) = \sin x/x$ is the first spherical Bessel function. For vanishing sphere radius $R \to 0$ we recover the previous result from Eq. (28), but for finite R the squared Bessel function in the integral leads to fast convergence of the momentum integration, so that the upper integration boundary can be set to infinity. In an approximate way, the Bessel function can be thought of as imposing a smooth upper momentum cutoff at a value of roughly $k_{\max} \approx \pi/R$, so that the two expressions, Eqs. (28) and (37), are in fact equivalent.

It remains to be discussed why we need to impose a rather small upper cutoff $k_{\max} = \pi/R = 10^{10}$ m^{-1} in order to obtain a value for the friction coefficient that roughly matches the experimental one for an electron. In fact, the need to impose a cutoff $k_{\max}$ comes mainly from a breakdown of the assumption of linear response theory (in addition, the susceptibility obtained with the point charge SPC/E water model is also inaccurate at high momentum, but this effect is of secondary importance). As is easy to see, the electric charge of an electron is too large for linear response to hold and as a result of the strong polarization of the hydration water, a dielectrically saturated shell forms around the point charge with a radius of a few water molecules. Outside this radius linear response theory applies. A simple approximate remedy to this issue is to use a heuristic cutoff, leading to Eq. (28), or to consider the friction force on a charged shell with a radius R corresponding roughly to the dielectrically saturated

region, leading to Eq. (37).

In the remainder of this chapter, we introduce a prescription for quantizing the particle's degree of freedom, then we apply the method to our problem. We finally discuss the limitations of this approach.

2.5 Path Integral Quantization of the Particle's Degree of Freedom

Although one can treat heavy impurities (such as heavy ionic solutes) classically, lighter particles like electrons suffer from stronger quantum fluctuations, and one needs to quantize the corresponding degree of freedom. Caldeira and Leggett, in a seminal work [63, 64], and in an attempt to study the macroscopic quantum phenomena, proposed a prescription for calculating the tunneling rate of a quantum degree of freedom in a double-well potential, subject to an Ohmic dissipative force. Suppose that the classical equation of motion of the degree of freedom $q(t)$, is given by

$$M\ddot{q}(t) + \eta\dot{q}(t) + \frac{\partial V[q(t)]}{\partial q} = F_{\text{ext}}(t), \tag{2.40}$$

where M the inertia associated with $q(t)$, and η is the "Ohmic" dissipation coefficient, which results in the rate of dissipation $\eta\dot{q}^2$, and is independent of frequency, etc. Finally $V[q(t)]$, is a conservative potential associated with q. They proved that the tunneling rate can be calculated using

$$P_{\text{tunn}} = A\exp(-B/\hbar). \tag{2.41}$$

Here A is expressible in terms of the fluctuations around the saddle-point "bounce" trajectories between the wells of the potential and is therefore a function of the parameters in Eq. 2.40. Next, B is the effective WKB exponent for the saddle-point path. They further showed that in the presence of dissipation, the tunneling rate is *always* suppressed compared to the dissipationless case. This also implies the loss of quantum coherence of the coordinate, as a result of interaction with an energy-exchanging reservoir (environment). Noting that "measurement" (or perturbing with classical probes) results in

the collapse of wave-function in Copenhagen interpretation of quantum mechanics, this theoretical model, based on a minimal set of ingredients, can serve as the explanation of this collapse.

This formalism was later extended by Leggett to the cases where the coordinate q is acted upon by a rather general (frequency dependent) integro-differential operator, provided a number of commonly satisfied conditions hold. Let us assume that the classical equation of the motion is described by:

$$\hat{K}\, q(t) = -\frac{\partial V[q(t)]}{\partial q}, \tag{2.42}$$

in which $\hat{K}$ is a linear integro-differential operator, which obeys causality. In the case of Eq. 2.40, $\hat{K}$ reduces to: $\hat{K} = M\mathrm{d}^2/\mathrm{d}t^2 + \eta\,\mathrm{d}/\mathrm{d}t$. By means of the Fourier transform

$$f(\omega) = \int_{-\infty}^{+\infty} \hat{f}(t) e^{-i\omega t} \mathrm{d}t, \tag{2.43}$$

we write the above equation as:

$$K(\omega)\, q(\omega) = -\left(\frac{\partial V(q)}{\partial q}\right)(\omega), \tag{2.44}$$

where $K(\omega)$ is now a complex function, and is generally related to an impedance-like function. In the following subsection we briefly review the derivation of the Euclidean action from the classical equation of motion, via Leggett's prescription.

2.5.1 Leggett's Quantization Prescription

According to Caldeira-Leggett model, the environment which is in general an energy-exchanging heat reservoir, can be modeled by a bath of harmonic oscillators. The spectrum of such bath (usually denoted by $J(\omega)$) determines the induced dynamics, as a result of the particle-environment interaction. In the specific case of Ohmic damping, where the dissipative force is proportional to the conjugate velocity $\dot{q}$, we have: $J(\omega) =$

$\eta\,\omega$. The appropriate hamiltonian for such a coupled system is written as:

$$H(q,p;\{x_j,p_j\}) = \frac{p^2}{2M} + V_0(q) + \sum_j \left[\frac{p_j^2}{2m_j} + \frac{1}{2}m_j\omega_j x_j^2\right] - \sum_j [F_j(q,p)x_j + G_j(q,p)p_j] + \Phi(q,p). \tag{2.45}$$

In the above equation (2.45), (q,p) and $\{(x_j,p_j)\}$ are the (coordinate, conjugate momentum) pairs of the particle and harmonic oscillators of the environment, respectively. Also M, $\{m_j\}$ and $\{\omega_j\}$, represent the bare mass of the particle, masses of the environmental harmonic oscillators, and the frequencies of the harmonic oscillators, respectively. On the right hand side, the first line is the sum of the hamiltonians of the decoupled particle and bath system. The first term in the second line is the coupling between the particle and bath, which must be *linear* in the bath coordinates. Note that although F_j and G_j are labeled by the oscillators' indices, they are independent of the dynamical variables $\{(x_j,p_j)\}$. Finally $\Phi(q,p)$ is a real function which might in turn depend on the parameters m_j,ω_j,F_j,G_j but not on dynamical variables.

For the Leggett's prescription to be valid, there are constraints to be imposed on the Hamiltonian:

(**I**) The assumption of "weak" perturbation due to environment. This allows us to neglect the nonlinear effects of the bath, effectively keeping only the linear terms in bath degrees of freedom.

(**II**) The condition of "strict linearity". This means that the microscopic interaction Hamiltonian of the particle and environment, can only contain the terms either (a) linear in particle variables (q,p) when coupled to environment, or (b) quadratic in particle variables when the environment variables are absent.

(**III**) Time-reversal symmetry. This is not an essential assumption but simplifies the derivation.

Occurrence of the terms which include higher order terms than linear, in environmental degrees of freedom implies that the assumption of "weak" perturbation due to

environment is no longer valid and one needs to resort to other techniques such as adiabatic approximation. In order for the second condition to hold, we note that F_j, G_j must be linear in (q, p), whereas $\Phi(q, p)$ can be bilinear. This allows us to write down the interaction term in the following form:

$$H_{\text{int}} = -\frac{p}{M}\sum_j F_j x_j - q\sum_j \frac{1}{m_j} G_j p_j + \frac{1}{2}ap^2 + \frac{1}{2}bq^2, \tag{2.46}$$

where a, b are constants. The last two terms can be absorbed in the Hamiltonian of the bare particle, resulting in renormalization of the mass, and a shift in potential $V_0(q)$,

$$\widetilde{M}^{-1} = M^{-1} + a \tag{2.47a}$$

$$\widetilde{V}(q) = V_0(q) + \frac{1}{2}bq^2. \tag{2.47b}$$

After a set of canonical of the coordinates and Legendre transformations, we obtain the total Lagrangian of the system:

$$\begin{aligned}\mathcal{L}(q, \dot{q}; \{\tilde{x}_j, \dot{\tilde{x}}_j\}) =& \frac{1}{2}\widetilde{M}\dot{q}^2 - \widetilde{V}(q) + \frac{1}{2}\sum_j \widetilde{m}_j(\dot{\tilde{x}}^2 - \widetilde{\omega}_j^2\tilde{x}_j^2) \\ & - q\sum_j C_j\tilde{x}_j - q^2\sum_j \frac{C_j^2}{2\widetilde{m}_j\widetilde{\omega}_j^2}.\end{aligned} \tag{2.48}$$

It is now convenient to introduce the spectral density of the environment as:

$$J(\omega) \equiv \frac{\pi}{2}\sum_j \frac{C_j^2}{\widetilde{m}_j\widetilde{\omega}_j}\delta(\omega - \widetilde{\omega}_j), \tag{2.49}$$

and also a complex function of ω in the lower half of the complex plane:

$$\bar{K}(\omega) \equiv -\omega^2\left[\frac{2}{\pi}\int_0^\infty \mathrm{d}\omega' \frac{J(\omega')}{\omega'(\omega'^2 - \omega^2)} + \widetilde{M}\right], \tag{2.50}$$

such that $\mathrm{Im}\bar{K}(\omega) = J(\omega)$ for $|\mathrm{Im}\omega| \to 0$. Now if we calculate the equation of motion from Eq. 2.48, and eliminate the environmental degrees of freedom, we get for $q(\omega)$, the real-time Fourier transform of $q(t)$:

$$\bar{K}(\omega)q(\omega) = -\left(\frac{\partial\widetilde{V}(q)}{\partial q}\right)(\omega) \tag{2.51}$$

where $\omega = \mathrm{Re}\omega + i\epsilon$ and $\epsilon \to 0^+$. Therefore $\bar{K}(\omega)$ is identical to $K(\omega)$ for $|\mathrm{Im}\omega| \to 0$. Now following the Caldeira-Leggett prescription, we get for the effective Euclidean action in "imaginary-time":

$$\mathcal{S}_{\text{eff}}[q(\tau)] = \int_{-\infty}^{+\infty} \left[\frac{1}{2}\widetilde{M}\dot{q}^2 + \widetilde{V}(q)\right] \mathrm{d}\tau + \frac{1}{2}\iint_{-\infty}^{+\infty} \mathrm{d}\tau\mathrm{d}\tau'\alpha(\tau-\tau')[q(\tau)-q(\tau')]^2. \tag{2.52}$$

We call the last term $\Delta\mathcal{S}_{\text{eff}}$. In the above equation we $\alpha(\tau-\tau')$ is given by:

$$\alpha(\tau-\tau') \equiv \frac{1}{2\pi}\int_0^{\infty} J(\omega)e^{-\omega|\tau-\tau'|}\mathrm{d}\omega. \tag{2.53}$$

Now by defining the Fourier transform in the imaginary-time domain for the coordinate q,

$$\tilde{q}(\omega) \equiv \int_{-\infty}^{+\infty} q(\tau)e^{-i\omega\tau}\mathrm{d}\tau, \tag{2.54}$$

we get for $\Delta\mathcal{S}_{\text{eff}}$:

$$\Delta\mathcal{S}_{\text{eff}} = -\frac{1}{2\pi}\int_{-\infty}^{+\infty}[\alpha(\omega)-\alpha(0)]|\tilde{q}(\omega)|^2\mathrm{d}\omega, \tag{2.55}$$

where we have

$$\begin{aligned}\alpha(\omega) &= \frac{1}{(2\pi)^2}\int_{-\infty}^{+\infty}\mathrm{d}\tau\int_0^{\infty}\mathrm{d}\omega' e^{-\omega'|\tau|}e^{-i\omega\tau}J(\omega') \\ &= \frac{1}{2\pi^2}\int_0^{\infty}\frac{\omega' J(\omega')}{\omega'^2+\omega^2}\mathrm{d}\omega'\end{aligned} \tag{2.56}$$

From Eq. 2.55, we get:

$$\mathcal{S}_{\text{eff}} = \frac{1}{2\pi}\int_{-\infty}^{+\infty}\mathrm{d}\omega\left[\frac{1}{2}\widetilde{M}\omega^2 + \pi^{-1}\omega^2\int_0^{\infty}\mathrm{d}\omega'\frac{J(\omega')}{\omega'(\omega'^2+\omega^2)}\right]|\tilde{q}(\omega)|^2 + \mathcal{S}_V, \tag{2.57}$$

where,

$$\mathcal{S}_V \equiv \int_{-\infty}^{+\infty}\mathrm{d}\tau V[q(\tau)], \tag{2.58}$$

is the action of the potential $V[q(\tau)]$. From comparing Eq. 5.33, it is concluded that if the classical equation of motion governing $q(\omega)$ is,

$$K(\omega)q(\omega) = -\left(\frac{\partial V(q)}{\partial q}\right)(\omega), \tag{2.59}$$

then the effective action is given by the following expression:

$$\mathcal{S}_{\text{eff}}[\tilde{q}(\omega)] = \frac{1}{2\pi}\int_{-\infty}^{+\infty}\frac{1}{2}K(-i|\omega|)|\tilde{q}(\omega)|^2\mathrm{d}\omega + \mathcal{S}_V[\tilde{q}(\omega)]. \tag{2.60}$$

The prefactor of $\tilde{q}(\omega)$, for the simple Ohmic dissipation case, reduces to $\frac{1}{4\pi}(M\omega^2 + \eta|\omega|)$.

The Leggett's prescription facilitates the derivation of effective Euclidean action for a coordinate (corresponding to a single impurity in our problem), from the classical equation of motion, which in turn is expressible in terms of the *influence functional* $K(\omega)$ which is induced by the bath. In other words, by integrating out the harmonic degrees of freedom of the bath, we obtain the reduced density matrix of the particle, in terms of the influence functional. This implies that given a (phenomenological) influence functional which is—as mentioned above—related to an impedance-like quantity of the bath, we can construct the effective action for the particle. However we note that in order for the prescription to be strictly valid, the aforementioned three conditions must be satisfied. We will see below that the second criterion runs into difficulties in our system and some approximations are required in order to be able to utilize Leggett's formalism.

2.6 Influence Functional and Effective Action of a Charged Particle in a Dielectric Medium

In this section, we essentially follow the same lines as the beginning of this chapter, namely we find the dielectric drag force acting on a slowly moving particle. Inspired by the Leggett's formalism sketched above, we would like to find the influence function of the environment, from which the effective Euclidean action is straightforwardly concluded. So we begin with deriving the classical equation of motion of a particle in a dielectric medium. We wish to write it in the following form:

$$\mathcal{K}(\omega)\, R(\omega) = F(\omega). \tag{2.61}$$

Here R denotes the coordinate of the particle and plays the role of q in the original formalism. We note that the above formula is valid for a one dimensional system. A more general form reads:

$$\overleftrightarrow{\mathcal{K}}(\omega).\mathbf{R}(\omega) = \mathbf{F}(\omega). \tag{2.62}$$

where $\overleftrightarrow{\mathcal{K}}(\omega)$ is now the influence functional tensor, $\mathbf{R}$ the position vector of the particle and $\mathbf{F}$, the dielectric force which is naturally expected to be in opposite direction as $\dot{\mathbf{R}}(t)$.

We now start with a single classical charged particle which is moving very slowly at velocity $\vec{v}$ in a certain direction. As a result of the electrostatic interaction between the particle and surrounding medium, the medium gets polarized, as a consequence of the opposite displacements of positive and negative partial charges of the constituents of the medium. Thus as the particle moves through the medium, it has to drag the cloud of polarization. This clearly amounts to the increase of the inertia or effective mass of the particle. One can think of this problem (at this level) as the classical version of the polaron problem. Now Leggett's prescription is essentially designed to transform this classical problem to its quantum mechanical counterpart. Therefore one might hope that by deriving the influence function and then performing the consequent quantization, one would find the effective action of a polaron. However the strict linearity condition on the coordinate of the particle, inhibits us from making further mathematical progress, as this coordinate appears not quadratically but in fact as $\exp(i\mathbf{q}.\mathbf{R}(t))$, where q is the wavevector. We, however, note that starting off directly with quantum mechanical hamiltonian does not resolve this issue. In fact a similar mathematical difficulty arises in the polaron problem.

Now using the expression obtained for the dielectric force on the particle we get:

$$\mathbf{F}(t) = -i \int \mathrm{d}^3q \int \mathrm{d}\omega \Bigg[\frac{e^2\mathbf{q}}{2\pi^2 q^2} (\epsilon^{-1}(\mathbf{q},\omega) - 1) \times \int \frac{\mathrm{d}t'}{2\pi} \exp[i\mathbf{q}.(\mathbf{R}(t) - \mathbf{R}(t')) - i\omega(t-t')] \Bigg]. \tag{2.63}$$

where e is the charge of the particle and where $\epsilon(\mathbf{q},\omega)$ is the dielectric function of the medium. Now the classical equation of motion for the particle reads,

$$M\ddot{\mathbf{R}} = \mathbf{F}[\{\mathbf{R}(t)\}] \tag{2.64}$$

If the force $\mathbf{F}[\{\mathbf{R}(t)\}]$, after Fourier transform to frequency domain, could be written in the form $\overleftrightarrow{\mathcal{K}}(\omega).\mathbf{R}(\omega)$, we could deduce the influence function. It is not hard to see that such a simplification can be achieved by approximating the exponential $\exp[i\mathbf{q}.(\mathbf{R}(t)-\mathbf{R}(t'))]$ by $1-i\mathbf{q}.(\mathbf{R}(t)-\mathbf{R}(t'))$. This approximation is only valid for slowly moving particles where $\mathbf{q}.\mathbf{R}(\omega) \ll 1$. Therefore we can rewrite the force as:

$$\mathbf{F}(t) = -i\int \mathrm{d}^3q \int \mathrm{d}\omega \exp(-i\omega t)\left[\frac{e^2\mathbf{q}}{2\pi^2q^2}(\epsilon^{-1}(\mathbf{q},\omega)-1)\right](-i\mathbf{q}.(\mathbf{R}(\omega)-\delta(\omega)\mathbf{R}(t))). \tag{2.65}$$

Neglecting the zero frequency part, we arrive at:

$$\mathbf{F}(\omega) = -\frac{e^2}{2\pi}\int \mathrm{d}^3q \left[\frac{\mathbf{q}}{(2\pi^2)q^2}(\epsilon^{-1}(\mathbf{q},\omega)-1)\right](\mathbf{q}.\mathbf{R}(\omega)). \tag{2.66}$$

We note that this force is proportional to $-e^2$, hence negative and insensitive to the sign of the charge. From this we find the relation for influence function in terms of the dielectric function of the medium:

$$\overleftrightarrow{\mathcal{K}}(\omega) = -\frac{e^2}{2\pi}\int \mathrm{d}^3q \left[\frac{\mathbf{qq}}{2\pi^2q^2}(\epsilon^{-1}(\mathbf{q},\omega)-1)\right] \tag{2.67}$$

Now using Leggett's formalism, we can derive the effective Euclidean action of the particle. Further by means of the fluctuation-dissipation theorem, we can recast the above equation (expressed in terms of dielectric function) in terms of the charge-charge structure factor of the medium $S(\mathbf{q},\omega) = \langle|\rho(\mathbf{q},\omega)|^2\rangle$, which is the ensemble average of the charge density fluctuations $\rho(\mathbf{q},\omega)$.

$$\begin{aligned}\mathcal{S}_{\text{eff}} = -\int_0^{\beta\hbar}\frac{1}{2}M|\dot{\mathbf{R}}|^2 + \alpha\beta^{-1}\sum_{\omega_n}\int\frac{\mathrm{d}^3q}{(2\pi)^3}\frac{1}{q^4}S(\mathbf{q},\omega_n) \\ \times\iint_0^{\beta\hbar}\mathrm{d}t\mathrm{d}s\exp[-i\mathbf{q}.(\mathbf{R}(t)-\mathbf{R}(s))+i\omega_n|t-s|].\end{aligned} \tag{2.68}$$

Here α is the self-interaction coupling constant which depends on the charge of the particle and other characteristic constants of the system. Next, $\beta = 1/k_B T$ is the inverse temperature and $\omega_n = 2\pi n/\beta$ is the bosonic Matsubara frequency. We note that this action is derived for the Coulomb potential $V_{\mathbf{q}} = 1/q^2$. Note that in order to retain the original form of $\mathbf{R}$-dependence we have here (and after deriving the influence function), re-exponentiated the coordinate. With the above definition of the effective action, the equilibrium partition function of the particle can be written the following functional integral as: $\mathcal{Z} = \int \mathcal{D}[\mathbf{R}(t)] \exp(\mathcal{S}_{\text{eff}}[\mathbf{R}(t)]/\hbar)$, where $\mathcal{D}[\mathbf{R}(t)]$, denotes the path-integration measure.

Equation 2.68 suggests that *one approximate* strategy to study the quantum particles in dielectric media, could be to derive the structure factor and substitute that in Eq. 2.68. We shall mention here that the approximation of the quadratic dependence on $\mathbf{R}$, becomes more and more accurate as the mass of the impurity is increased. The heavier the impurity, the less significant the zero point motion of the particle and the more localized the wave-function, hence the more valid the Taylor expansion. In the language of polaron problem, this corresponds to large self-interaction, which causes the self-trapping localization. We also note that from the results of the MD simulations, we only can extract the classical $S(\mathbf{q}, \omega)$ at room temperature. Hence the quantum fluctuations of the environment are absent. The full quantum mechanical fluctuation-dissipation theorem between the response function and structure factor reads:

$$\text{Im}\{\chi(\mathbf{q}, \omega)\} = \frac{2\pi}{\hbar}(1 - e^{-\beta\hbar\omega}) S(\mathbf{q}, \omega). \tag{2.69}$$

This implies that the structure factor is not an even function in the full quantum mechanical form and is in fact obtained by a detailed-balance equation:

$$S(\mathbf{q}, -\omega) = e^{-\beta\hbar\omega} S(\mathbf{q}, \omega), \tag{2.70}$$

which in the classical limit $\beta\hbar\omega \to 0$, reduces to the classical form.

The dynamic structure factor of polar liquids, as numerically calculated for the case of water, reveals pronounced peaks in $(\mathbf{q}, \omega)$-plane, in the range of small frequencies.

One can fit the numerical results using a combination of simpler solvable models, e.g. Debye-like dynamics. For the imaginary part of the dielectric response function $\chi(\mathbf{q},\omega)$ is in general related to the structure factor via fluctuation-dissipation theorem. In the classical limit the relation takes the form: $\mathrm{Im}\{\chi(\mathbf{q},\omega)\} = 2\pi\beta\omega S(\mathbf{q},\omega)$. Fitting the response function $\chi(\mathbf{q},\omega)$ to the actual numerical data, suggests the following general form [46]:

$$\mathrm{Im}\{\chi(\mathbf{q},\omega)\} = 4\pi\beta S(q)\Bigg[\frac{A_1\tau_1}{1+\omega^2\tau_1^2} + \frac{A_2\tau_2}{1+\omega^2\tau_2^2} + \frac{A_3}{2}\left(\frac{\gamma}{(\omega_0+\omega)^2+\gamma^2} + \frac{\gamma}{(\omega_0-\omega)^2+\gamma^2}\right)\Bigg], \quad (2.71)$$

in which $A_1, A_2, \tau_1, \tau_2, \gamma$, are free parameters which are obtained by fitting. Based on this analytical model, obtained from the numerical analyses, we calculate the polaron properties in a model polar liquid.

For simplicity, we focus on the major component of the dynamics corresponding to the dissipative mode, namely the first term in the brackets in Eq. (2.71). The static structure factor $S(q)$, also has a peak at $q = q_0$. The peaks in the structure factors can be well modeled by Lorentzians. Following this common approach we propose the general form,

$$S(q) \sim \frac{1}{(q-q_0)^2 + (\Delta q)^2}. \quad (2.72)$$

In the above equation, Δq determines the width of the peak of the structure factor. We note that the sum-rule requires that the static structure factor satisfies

$$S(q) = \int_{-\infty}^{+\infty} \mathrm{d}\omega S(q,\omega), \quad (2.73)$$

which is the equal-time correlation of the fluctuations (a snapshot of the system). We now insert this phenomenological model in the effective action of the particle. The goal is to find the self-energy and the effective mass of this particle as a result of interaction with this dissipative local modes.

2.6.1 Zero Temperature Limit

From previous sections effective Euclidean action according to Leggett's formulation,

$$S_{\text{eff}}^{E}\big[\mathbf{R}(t)\big] = -\frac{m}{2}\int_{-\infty}^{\infty} \mathrm{d}t\, |\dot{\mathbf{R}}|^2 - \iint_{0}^{\infty} \mathrm{d}t\mathrm{d}s \int_{0}^{\infty} \frac{d\omega}{2\pi} \overleftrightarrow{\mathcal{K}}(\omega) e^{i\omega|t-s|}\, |\mathbf{R}(t) - \mathbf{R}(s)|^2\,, \tag{2.74}$$

where,

$$\overleftrightarrow{\mathcal{K}}(\omega) = -\frac{e^2}{\varepsilon_0}\int \frac{\mathrm{d}^3 q}{(2\pi)^3}\, \frac{\mathbf{qq}}{q^2}\, \mathrm{Im}\left\{\frac{1}{\varepsilon(\mathbf{q},\omega)}\right\}, \tag{2.75}$$

In the original Leggett's formalism, the coupling between the particle and medium is linear. It is not the case in our problem; the force is *n*ot linear in particle's degree of freedom. In order to match it with the Leggett's method, we expanded the exponential interaction to the linear order in terms of the generalized coordinates. The justification for such a generalization is the following. In the case of Feynman theory, where the electron interacts with a single dispersionless mode, the formulation matches with that of Leggett's where the linear coupling is a basic assumption, if we expand the force to the linear order. In our case, the electron is coupled to a distribution of modes which does not make any fundamental difference with Feynman's problem. Thus the natural and reasonable way to generalize the Leggett's theorem to find the effective action in our case seems to be the same. Therefore we re-exponentiate the linear term to the original form of the force. Eventually the effective Euclidean action takes the following form.

$$\begin{aligned} S_{\text{eff}} = -\frac{m}{2}\int_{0}^{\infty} \mathrm{d}t\, |\dot{\mathbf{R}}|^2 + \frac{e^2}{\varepsilon_0}\iint_{0}^{\infty} \mathrm{d}t\mathrm{d}s \int \frac{\mathrm{d}^3 q}{(2\pi)^3} \int \frac{\mathrm{d}\omega}{2\pi} \\ \times\ \frac{1}{q^2} e^{i\omega|t-s|} e^{i\mathbf{q}.(\mathbf{R}(t)-\mathbf{R}(s))} \mathrm{Im}\left\{\frac{1}{\varepsilon(\mathbf{q},\omega)}\right\}, \end{aligned} \tag{2.76}$$

We drop the superscript "E" denoting the Euclidean action hereafter. Note that a minus sign is already included in the effective action such that, $e^{-\beta F} = \int e^{S}\, \mathcal{D}[\mathbf{R}]$.

- **Variational Method**

Since the path integrals with the above actions are not analytically solvable, we introduce the following trial action with two free parameters to be fixed. The trial action is of the following form,

$$S_1 = -\frac{m}{2}\int_0^\beta |\dot{\mathbf{R}}|^2 \mathrm{d}t - \frac{C}{2}\iint_0^\beta |\mathbf{R}(t)-\mathbf{R}(s)|^2 e^{-D|t-s|}\mathrm{d}t\mathrm{d}s, \tag{2.77}$$

The free parameters are intuitively chosen in a way to determine two physically separate characteristics of the interaction. C is the strength of the interaction, while D shows how fast the distortions are mediated through the medium i.e. the temporal Kernel of interaction. This form of trial action reflecting pure dissipation is in consistence with the physical intuition of the polar liquids as mentioned before. The Debye-like decay is the most important contribution of the modes in polar liquids, approved by numerical methods. Exponent D, represents this time constant.

In the path integral representation of the free energy, the following relation exists between F, F_1, S and S_1, denoting the free energy of the original system, free energy of trial action, original Euclidean effective action and trial Euclidean effective action, respectively,

$$F \leq F_1 + \frac{1}{\beta}\langle S - S_1\rangle, \tag{2.78}$$

At the zero temperature limit the dominant term in the free energy is the ground state, such that we can replace the effective energy of both the original and the trial actions by the ground state energies which are denoted by E and E_1 respectively.

$$\frac{1}{\beta}\langle S - S_1\rangle = A + B, \tag{2.79}$$

where,

$$\begin{aligned} A =& \frac{1}{\beta}\frac{e^2}{\varepsilon_0}\iint_0^\infty \mathrm{d}t\mathrm{d}s \int \frac{\mathrm{d}^3 q}{(2\pi)^3}\int \frac{\mathrm{d}\omega}{2\pi} \\ & \times \frac{1}{q^2} e^{i\omega|t-s|}\left\langle e^{i\mathbf{q}.(\mathbf{R}(t)-\mathbf{R}(s))}\right\rangle \mathrm{Im}\left\{\frac{1}{\varepsilon(\mathbf{q},\omega)}\right\}, \end{aligned} \tag{2.80a}$$

$$B = \frac{1}{\beta}\frac{C}{2}\iint_0^\beta \langle|\mathbf{R}(t)-\mathbf{R}(s)|^2\rangle e^{-D|t-s|}\mathrm{d}t\mathrm{d}s, \tag{2.80b}$$

Note that all the averages are defined with respect to the weights, e^{S_1}. For later convenience we define a new parameter in terms of the primary variational parameters, $v^2 = D^2 + 4C/Dm$.

For brevity we call the last term in the integrand of Eq. (2.80a) , $\langle\exp\rangle^{(0)}$ hereafter (the superscript (0), becomes clear in the next section). This term is calculated by Feynman for the above-mentioned weights [65, 66, 67, 68],

$$\begin{aligned}\langle\exp\rangle^{(0)} =& \frac{\int \exp\left[i\mathbf{q}.(\mathbf{R}(t)-\mathbf{R}(s))\right]e^{S_1}\mathcal{D}[\mathbf{R}]}{\int e^{S_1}\mathcal{D}[\mathbf{R}]}\\ =& \exp\left[-\frac{2\hbar C q^2}{mv^3 D}\left(1-e^{-v|t-s|}\right)-\frac{\hbar D^2 q^2}{2mv^2}|t-s|\right]\\ =& \exp\left[-\frac{\hbar q^2}{2mv^2}\mathcal{G}(|t-s|)\right],\end{aligned} \tag{2.81}$$

where,

$$\mathcal{G}(u) = D^2 u + \frac{v^2-D^2}{v}\left(1-e^{-vu}\right), \tag{2.82}$$

Now we may calculate B,

$$\begin{aligned}B =& \frac{1}{\beta}\frac{C}{2}\iint_0^\beta \langle|\mathbf{R}(t)-\mathbf{R}(s)|^2\rangle e^{-D|t-s|}dtds\\ =& \frac{3C}{vD},\end{aligned} \tag{2.83}$$

which can be readily approved by taking the second derivative of $\langle\exp\rangle^{(0)}$ with respect to q.

$$E_1 = \frac{3}{2}(v-D), \tag{2.84}$$

Using Eqs.[2.78,2.79], we obtain the upper bound for the original ground state energy,

$$E = \frac{3}{4}\frac{(v-D)^2}{v} - A, \tag{2.85}$$

At this step we have to minimize Eq.[2.85] with respect to variational parameters D, v. These parameters are going to be used in the effective mass calculation later in this

paper. The minimizing set of variational parameters, we call (D^*, v^*) gives us an upper bound of the ground state energy. But let us first work out the integral in Eq. (2.80a).

$$\begin{aligned} A =& \frac{1}{\beta}\frac{e^2}{\varepsilon_0}\iint_0^\infty \mathrm{d}t\mathrm{d}s \int \frac{\mathrm{d}^3q}{(2\pi)^3}\int\frac{\mathrm{d}\omega}{2\pi} \\ & \times \frac{1}{q^2}e^{i\omega|t-s|}\langle e^{i\mathbf{q}.(\mathbf{R}(t)-\mathbf{R}(s))}\rangle \mathrm{Im}\left\{\frac{1}{\varepsilon(\mathbf{q},\omega)}\right\} \\ =& \frac{e^2}{\varepsilon_0}\iint_0^\infty \mathrm{d}t\mathrm{d}s \int \frac{\mathrm{d}^3q}{(2\pi)^3}\int\frac{\mathrm{d}\omega}{2\pi} \\ & \times \frac{1}{q^2}e^{i\omega|t-s|}\exp\left[-\frac{\hbar q^2}{2mv^2}\mathcal{G}(|t-s|)\right]\mathrm{Im}\left\{\frac{1}{\varepsilon(\mathbf{q},\omega)}\right\}, \end{aligned} \tag{2.86}$$

The integration over imaginary times t and s, needs to be discussed here. The upper limit of the integrals in the path-integral representation of the free energy is the inverse temperature which goes to infinity at zero temperature limit.

$$\begin{aligned} \lim_{\beta\to\infty}\iint_0^\beta \mathrm{d}t\mathrm{d}s\, f(|t-s|) &= \lim_{\beta\to\infty}\int_0^\beta 2(\beta-u)f(u)du \\ &= 2\beta\int_0^\infty f(u)du, \end{aligned} \tag{2.87}$$

for fast enough decaying function $f(u)$, and $u = |t-s|$. Equation (2.76) can be slightly simplified,

$$\begin{aligned} A =& \frac{4e^2}{\varepsilon_0}\int_0^\infty \mathrm{d}u \int \frac{\mathrm{d}^3q}{(2\pi)^3}\int\frac{\mathrm{d}\omega}{2\pi} \\ & \times \frac{1}{q^2}e^{-i\omega u}\exp\left[-\frac{\hbar q^2}{2mv^2}\mathcal{G}(u)\right]\mathrm{Im}\left\{\frac{1}{\varepsilon(\mathbf{q},\omega)}\right\}, \end{aligned} \tag{2.88}$$

Therefore, Eq. (2.85) reduces to the following,

$$\begin{aligned} E =& \frac{3}{4}\frac{(v-D)^2}{v} - \frac{4e^2}{\varepsilon_0}\int_0^\infty \mathrm{d}u \int \frac{\mathrm{d}^3q}{(2\pi)^3}\int\frac{\mathrm{d}\omega}{2\pi} \\ & \times \frac{1}{q^2}e^{-\omega u}\exp\left[-\frac{\hbar q^2}{2mv^2}\mathcal{G}(u)\right]\mathrm{Im}\left\{\frac{1}{\varepsilon(\mathbf{q},\omega)}\right\}, \end{aligned} \tag{2.89}$$

$$\tag{2.90}$$

In Fig. (2.11), we see the energy landscape as a function of the variational parameters (D, v), for three different α's, and for specific $\Delta q, \tau^{-1}$. Two minima coexist for intermediate coupling constants which defines the coexistence region, while one of them fades away beyond that.

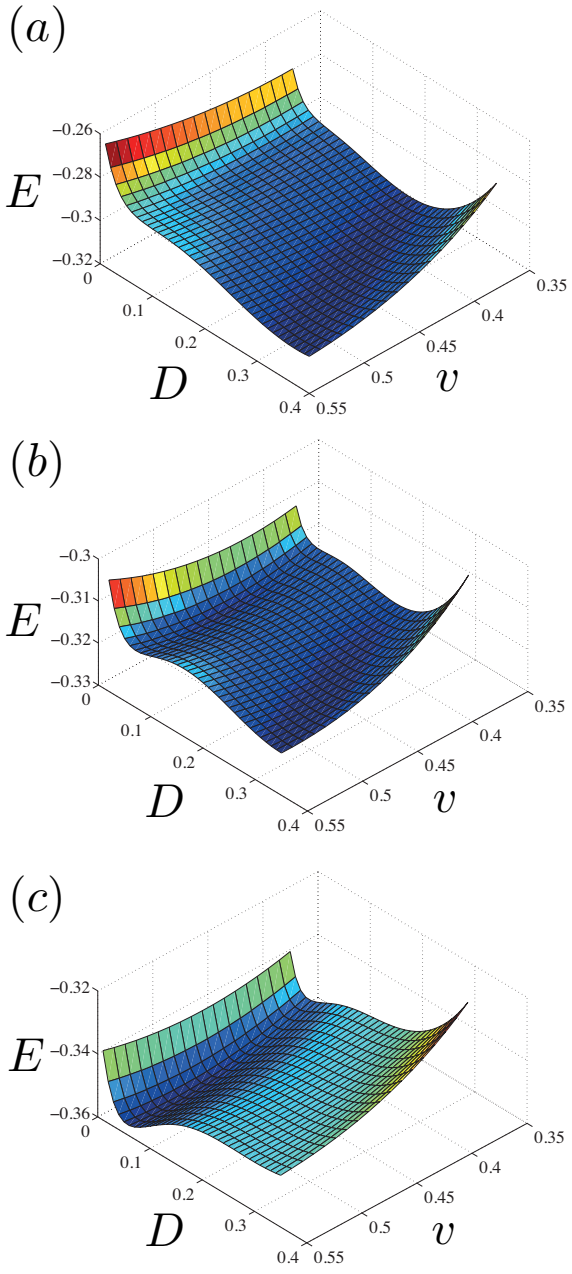

Figure 2.11: The energy-landscape for (a) below the transition, (b) the coexistence region, and (c) above the transition. In the landscapes of (a) and (c) there exists only one minimum, whereas in the coexistence range (b), the two minima coexist. This is a signature of the first order transition.

- **Effective Mass**

In order to calculate the effective mass, we use a mathematical trick, which was used by Feynman. We add a term, $\mathbf{U}(t-s)$ to $(\mathbf{R}(t)-\mathbf{R}(s))$ in the exponential, assuming that particle in moving with a constant "velocity" $\mathbf{U}$, in the imaginary time domain. Then we expand the exponential to the second order in $\mathbf{U}$. We eventually come up with a modified $\langle\exp\rangle$, defined in the previous section,

$$\begin{aligned}\langle\exp\rangle =& \exp\left[-\frac{\hbar q^2}{2mv^2}\mathcal{G}(|t-s|)\right] \\ & \times (1+i\mathbf{q}.U|t-s|-\frac{1}{2}q^2U^2|t-s|^2\cos^2\theta+\mathcal{O}(U^3)) \\ =&\langle\exp\rangle^{(0)}[1+i\mathbf{q}.U|t-s|-\frac{1}{2}q^2U^2|t-s|^2\cos^2\theta \\ & +\mathcal{O}(U^3)] \\ =&\langle\exp\rangle^{(0)}+\langle\exp\rangle^{(1)}+\langle\exp\rangle^{(2)}+\ldots\,, \end{aligned} \tag{2.91}$$

where θ is the angle between $\mathbf{U}$ and $\mathbf{k}$. The linear term vanishes after the integration because of isotropicity. We are now left with a $\mathbf{U}$-independent term and a quadratic term in $\mathbf{U}$, whose coefficient along with the kinetic term's coefficient gives us the effective mass.

The effective action turns out to be of the following form,

$$\langle S^E_{\text{eff}}\rangle = \left\langle -\frac{m}{2}\int|\dot{\mathbf{R}}|^2\,dt\right\rangle + A + A_2(\mathbf{U}), \tag{2.92}$$

where A, is the interaction part in the $U=0$ case, discussed in the previous section and $A_2(\mathbf{U})$, is the "velocity"-dependent term and takes the form,

$$\begin{aligned}A_2(\mathbf{U}) =& -\frac{1}{2}U^2\frac{4\beta e^2}{\varepsilon_0}\int_0^\infty \mathrm{d}u\int\frac{\mathrm{d}^3q}{(2\pi)^3}\int\frac{\mathrm{d}\omega}{2\pi} \\ & \times u^2\,\cos^2\theta\,e^{-\omega u}\exp\left[-\frac{\hbar q^2}{2mv^2}\mathcal{G}(u)\right]\mathrm{Im}\left\{\frac{1}{\varepsilon(\mathbf{q},\omega)}\right\}, \end{aligned} \tag{2.93}$$

The second equality results from zero temperature approximation discussed above and also integration over θ. The coefficient of U^2 in the energy is equal to $\frac{m^*}{2}$. Therefore

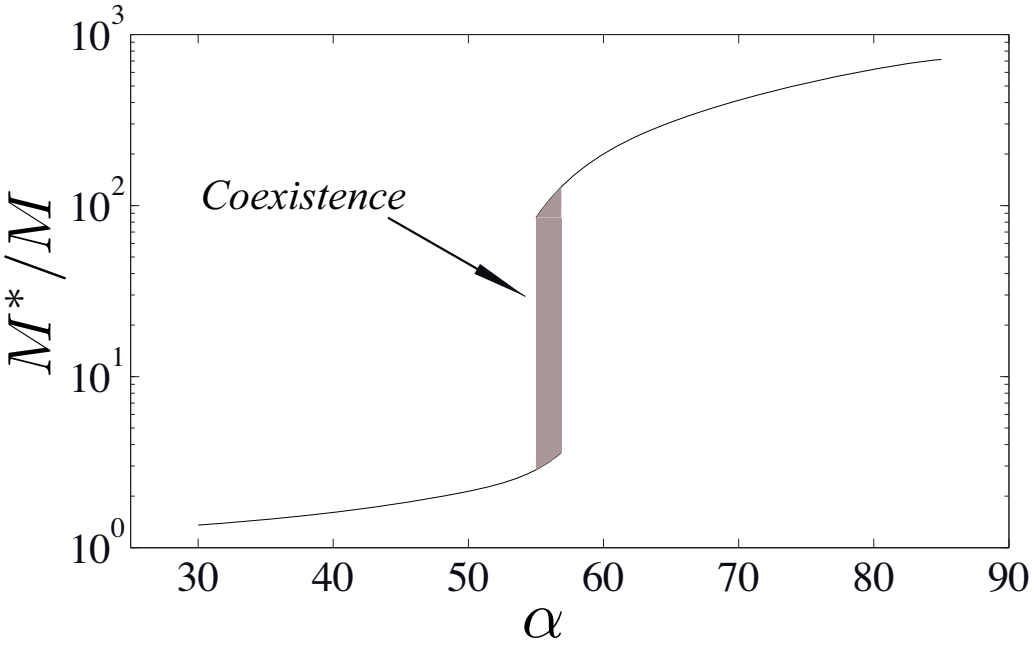

Figure 2.12: Effective mass against coupling constant. Other parameters are set at $\Delta q = 0.3\, q_0$ and $\tau = 10$. As shown in the picture, the polaron mass remains around the bare mass for coupling constants $\alpha \lesssim 55$. This corresponds to panel (a) of Fig. (2.11). As the coupling in enhanced, the effective mass undergoes a discontinuous jump by two orders of magnitude. This corresponds to the self-trapped polaron, panel (c). In between there exists a narrow range of the coupling constant, where the energy landscape develops two coexisting minima; see panel (c).

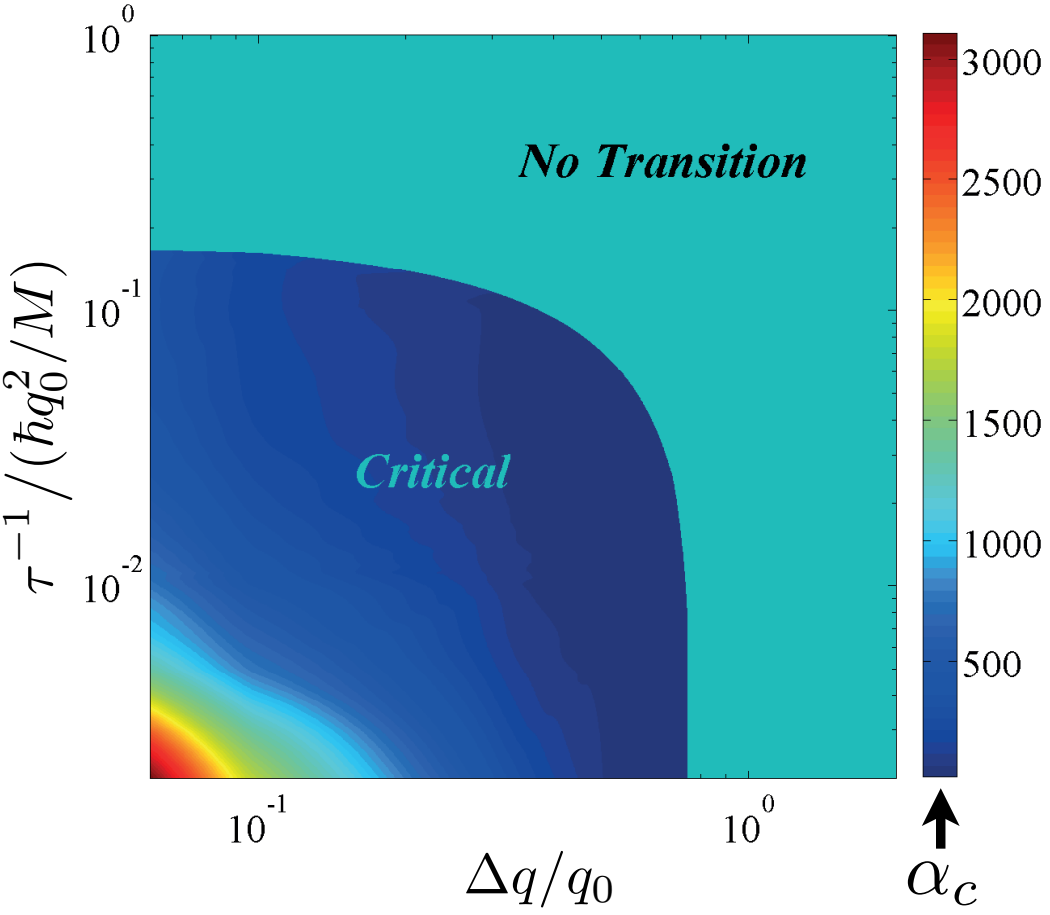

Figure 2.13: Zero-temperature phase diagram. The heat map of the critical coupling constant, as a function of the width of the static structure factor in q and that of the dynamic part τ^{-1}. The "critical" region, indicates the region where the first order transition exists. Therefore the effective mass is becomes discontinuous at the "critical" coupling constant. The value of this critical coupling can be read off the color code sidebar. The "No Transition" region is connected to the critical one by a line of second order transition, where the gap of the effective mass closes. We note that some values of the critical coupling, obtained from this model, might be unrealistic in actual systems.

the effective mass turns out to be,

$$\frac{m^*}{m} = 1 - \frac{2}{\beta}\frac{A_2(\mathbf{U})}{U^2}\bigg|_{(D^*,v^*)}, \tag{2.94}$$

where (D^*, v^*), are the values of the variational parameters minimizing the free energy. The result of the effective mass calculation is shown in Fig. (2.12). There coexistence region is specified in the figure. This type of behavior is observed for a so-called "Critical" area marked in Fig.[2.13], where Δq and τ, lie in a specific range. Therefore the border of this critical area defines a second order transition line which separates it from no transition part.

2.6.2 Finite Temperature

We derived the effective action in the case of zero temperature limit using the Leggett's influence functional theorem in Eq.[2.76], where the only allowed process is dissipating energy from the particle to the environment through the term $e^{-\omega|t-s|}$. However in the presence of thermal fluctuations, absorption processes play role as well as emission. Mathematically these processes are reflected in a more general form: $\{N+1\}e^{-\omega|t-s|} + \{N\}e^{\omega|t-s|}$, which is the result of integration over a bath of harmonic oscillators at finite temperature. Here $N = [\exp(\beta\hbar\omega) - 1]^{-1}$, is the Planck distribution function.
We now use the theory of a polaron at finite temperature [69], where we introduce a general form of the trial action,

$$S_1 = -\frac{m}{2}\int_0^\beta |\dot{\mathbf{R}}|^2 \mathrm{d}t - \frac{1}{2}\int_0^\beta\int_0^\beta \mathcal{K}(|t-s|)|\mathbf{R}(t) - \mathbf{R}(s)|^2 \mathrm{d}t\mathrm{d}s, \tag{2.95}$$

the kernel of the trial action, $\mathcal{K}(|t-s|) \equiv \mathcal{K}(u)$, reduces to $Ce^{-D|t-s|} = Ce^{-Du}$, in our case, allowing both negative and positive values of minimizing D, for emission and absorption of the excitations of medium respectively. Defining the Fourier components of the kernel in terms of Matsubara frequencies $\nu = \frac{2\pi n}{\beta}$, we have,

$$\mathcal{K}(u) = \frac{1}{\beta}\sum_\nu \tilde{\mathcal{K}}_n\, e^{i\nu u}, \tag{2.96}$$

where $\nu = 2\pi n/\beta$, and for the aforementioned form of trial action, we have,

$$\tilde{\mathcal{K}}_\nu = \frac{2CD}{\nu^2 + D^2}, \tag{2.97}$$

Similar to the vase of zero temperature, we would need to calculate the average of the actions for which we need,

$$\langle \exp \rangle^{(0)} = \exp\left[-\frac{\hbar q^2}{2m}\Lambda(|t-s|)\right], \tag{2.98}$$

where,

$$\Lambda(|t-s|) = \Lambda(u) = \frac{4}{\beta}\sum_{\nu>0} g_\nu(1-\cos\nu u), \tag{2.99a}$$

and,

$$\begin{aligned} g_\nu &= [\nu^2 + 2(\tilde{\mathcal{K}}_0 - \tilde{\mathcal{K}}_\nu)]^{-1} \\ &= \frac{1}{\nu^2 + \frac{4}{D}\frac{\nu^2}{D^2+\nu^2}}, \end{aligned} \tag{2.99b}$$

We can still use the first equality of Eq.[2.87], provided that the $\langle \exp \rangle^{(0)}$, is a function of $|t-s|$. Following the general formalism of variational method, discussed in previous sections,

$$F = F_1 - (A + B), \tag{2.100}$$

for which we need to calculate F_1, the free energy associated with the trial action, and eventually minimizing F with respect to variational parameters. According to [69], B can be easily calculated having the trial action in hand,

$$\begin{aligned} B =& \frac{3}{\beta}\sum_{\nu>0}\left(1-\nu^2 g_\nu\right) \\ =& \frac{3}{\beta}\sum_{\nu>0}\frac{\frac{4C}{D}\frac{\nu^2}{D^2+\nu^2}}{1+\frac{4C}{D}\frac{\nu^2}{D^2+\nu^2}}, \end{aligned} \tag{2.101}$$

The last equality could be easily verified in a few lines of simple algebra. The free energy of trial action F_1, also satisfies the following differential equation,

$$\begin{aligned} \frac{\mathrm{d}F_1}{\mathrm{d}C} =& \frac{B}{C} \\ =& \frac{3}{\beta}\sum_{\nu>0}\frac{\frac{4}{D}\frac{\nu^2}{D^2+\nu^2}}{1+\frac{4C}{D}\frac{\nu^2}{D^2+\nu^2}}, \end{aligned} \tag{2.102a}$$

with the boundary condition,

$$F_1(C=0)=0, \tag{2.102b}$$

which can be easily solved,

$$F_1=\frac{3}{\beta}\sum_{\nu}\ln\left(1+\frac{4}{D}\frac{\nu^2}{D^2+\nu^2}\right), \tag{2.103}$$

- **Effective Mass**

Using the method of Feynman we calculate the effective mass at finite temperature. This results in the following expression:

$$\frac{m^*}{m}=\frac{\beta^2}{24}\left[\sum_{\nu>0}g_\nu\right]^{-1}, \tag{2.104}$$

The effective mass experiences a first order transition at zero temperature as well as finite temperatures up to a certain point depending on the phase-space parameters $(\Delta q,\tau^{-1})$. Figure (2.14) shows α_c, as a function of Δq and temperature, at fixed τ^{-1}. As we see in figure (2.14), the transition happens at finite temperature as well, up to a certain temperature which depends on Δq and τ. According to the above figure, in the presence of thermal fluctuations, the first order transition of effective mass takes places at weaker couplings and goes away beyond a specific temperature.

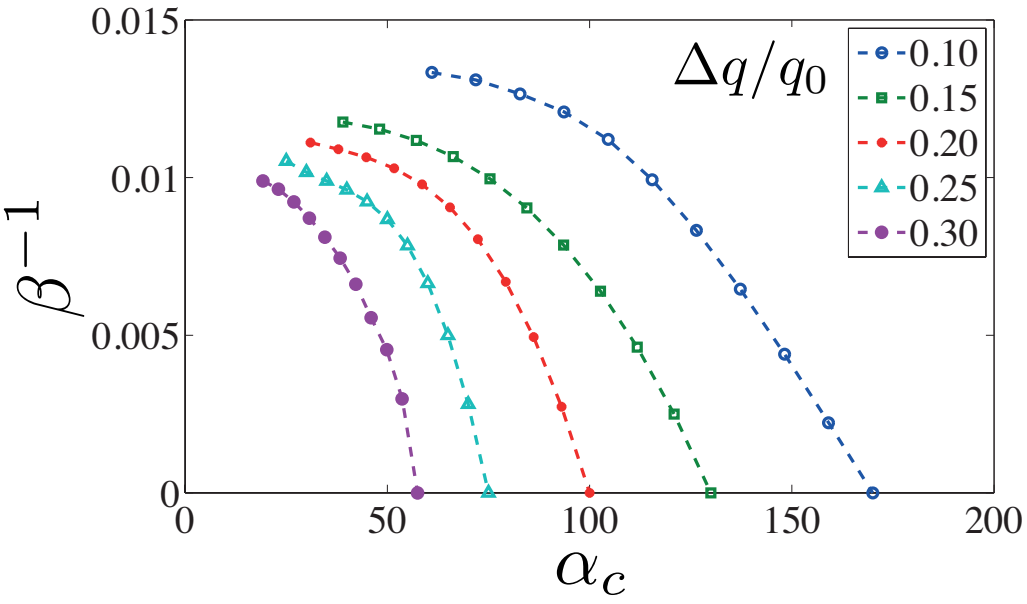

Figure 2.14: Finite temperature phase diagram at $\tau = 10$. At each $\Delta q/q_0$, *i.e.* width of the peak, the critical coupling constant α_c is reduced upon increasing the temperature β^{-1}. The discontinuity in the effective mass closes at a finite temperature.

2.7 Conclusions

Using classical MD simulations of the SPC/E water model at ambient pressure and room temperature, we determine the auto- and cross-correlation functions and associated dynamic structure factors of the oxygen and hydrogen sites in liquid water over a wide range of wave vectors and frequencies. Based on the diagonal and off-diagonal structure factors involving mass and charge densities we consider dielectric friction and electro-acoustic coupling effects in liquid water.

On the linear-response level, the friction force on a moving point charge is maximal at a velocity around $v = 300$ (m/s) and decays for larger velocities. This quasi-resonant friction feature is reminiscent of frequency-dependent Stokes friction, which also shows deviations from a linear velocity dependence. Although our calculation is strictly valid only on the linear-response level and thus neglects the nonlinear effects the presence of a point charge has on the water surrounding, this finding is interesting and points to complex dynamic phenomena for moving charges in liquid water. This might be even biologically relevant for electron and proton charge-transfer processes in proteins. In situations where the dielectric adsorption spectrum has features at lower frequencies than in bulk water, such as in water-filled protein cavities or close to membrane-water interfaces, we expect the velocity of maximal friction to be shifted to lower values. The friction forces we calculate are for elevated momentum cutoff values considerably larger than predicted by the single Debye relaxation mode approximation, which is due to non-Debye-like resonances related to librations at high frequencies in the simulated water susceptibility. For an electron a sufficiently low momentum cutoff basically eliminates the high-frequency domain, which can be thought of as to account for dielectric saturation effects in a heuristic manner. However, non-Debye effects can be relevant for the kinetics and motion of partial molecular charges which do not lead to dielectric saturation at small length scales (i.e., high momenta). We note that in the high-wave vector/high frequency regime classical MD simulations become unreliable

as polarization and quantum effects start to be important, therefore in this regime our results should be merely viewed as indicative.

Furthermore, in the last part of the chapter we proposed a heuristic and phenomenological approach, where a few approximations are needed, which in turn limit the applicability of our results. We used the Leggett's influence functional method to derive the effective Euclidean action of the particle as a result of the interaction with a presumably bath of harmonic oscillators. The formalism is based on linear-response theory. Whether this is a good approximation or not, thus depends on the validity of linear-response theory, and hence the strength of interaction. In the actual system of an excess electron in water, we observed from calculating the dielectric friction, that the linear response breaks down. This was justified using the discrepancy between the predictions of the linear-response relaxation of the polarization field (Debye-relaxation), and that of the molecular dynamics simulation data. However, this toy model gives us some clues about the effects of local modes on the properties of polarons. We observed that local modes are capable of localizing the polaron, at sufficiently large couplings. The transition is jump-like; the jump closes if the width of the peak of the structure factor or the characteristic frequency of damping are increase beyond a region shown in Fig. (2.13).

From chapter 3 on, we switch to a rather systematic approach: a model field theory which is also realizable in cold atomic experiments is proposed to be a good candidate for capturing some physical aspects of the phenomenon of solvation.

Inspired by the above discussion, we shall seek models involving nonlinear effects, which invalidate the perturbative expansion in coupling constant, and therefore linear response theory breaks down. In the case of an electron in water, we heuristically and phenomenologically interpreted the formation of hydration shell as a manifestation of the break-down of linear response theory. Hydration shell, in our phenomenology, can be thought of as a "frozen", dense layer of solvent molecules. This local structure corresponds to an ordered state, not achievable by expanding the free energy around

the liquid phase minimum.

The model we adopt in the next chapter describes a quantum field in the vicinity of a mean-field second order quantum phase transitions. We know, from the theory of critical phenomena, that near a critical point the fluctuation occur at all length scales, and consequently, the static structure factor $S_q \propto \langle|\rho_q|^2\rangle$ diverges. Here ρ_q is the Fourier mode of the density fluctuations. Therefore by moving close to or away from a critical point, one can tune the strength of the fluctuations. The model, near its transition, shows instabilities towards an ordered state with the characteristic length q_0^{-1}. This has dramatic consequences on both the nature of the transition in the bare system, and the polaron properties in the impurity problem. We investigate the role of quantum fluctuations of the medium on the solvation of the particle and the break-down of linear response theory which is characterized by the formation of solvation shell. We also address the experimental feasibility and discuss the possible realizations in an impurity-doped ultracold Bose gas.

CHAPTER 3

Ultracold Bose Gases and Mobile Impurities

Ultracold atomic quantum gases, specifically in the BEC state can be served as model systems for investigating the role of quantum fluctuations. Bose gases in shallow harmonic traps can simulate nearly ideal gases, when the interatomic scattering length $a_{\rm BB}$ is much smaller than the interatomic spacing, which is proportional to n^{-d}, where n is the density of the gas and d is the spatial dimensionality. For an ideal gas at temperature T, the mean momentum per particles is $p_T \sim \sqrt{M_{\rm B} k_B T}$, apart from a coefficient of order unity. Here M is the mass of the bosons and k_B is the Boltzmann's constant. From this, and the de Broglie's relation one can calculate the thermal wavelength $\lambda_T \sim h/p_T \sim h/\sqrt{M_{\rm B} k_B T}$, with h the Planck's constant. Therefore the short wavelength limit corresponds to, either $h \to 0$ or $T \to \infty$. This describes the classical limit with no quantum interference. When T is decrease below a critical temperature T_c, the thermal wavelength becomes of the order of n^{-d}. In this limit ($\lambda_T \gtrsim n^{-d}$), and also for lower temperatures, the quantum effects start playing significant roles.

Using Feshbach resonance techniques, one can change the scattering length, and thus the interaction strength, over a few orders of magnitude. For dilute alkali-metal atoms, the scattering length is of the order of a few nanometers. Feshbach resonance technique, allows us to remarkably increase this length, roughly by a factor of 10^3. When the interaction become important the ideal Bose gas theory fails and needs to be modified. Below, we discuss the famous Gross-Pitaevskii theory.

3.1 Nonlinear Gross-Pitaevskii Equation

The intraspecies interaction of a Bose gas is usually of the Lennard-Jones type. The low-energy s-wave scattering of the bosons is described by a short-range isotropic potential. For dilute enough gases, the potential can modeled by a local potential. In first quantized form, a bosonic gas, with inter-particle interaction $V_{\rm BB}(\mathbf{r}-\mathbf{r}') = g_{\rm BB}\delta(\mathbf{r}-\mathbf{r}')$, can be described the following Hamiltonian:

$$\hat{\mathcal{H}} = \sum_{i=1}^{N}\left(\frac{-\hbar^2}{2M_{\rm B}}\nabla_i^2 + V(\mathbf{r}_i)\right) + \sum_{i<j}\frac{4\pi\hbar^2 a_{\rm BB}}{M_{\rm B}}\delta(\mathbf{r}_i - \mathbf{r}_j), \tag{3.1}$$

where $M_{\rm B}$ is the mass of the boson, and where we used $g_{\rm BB} = 4\pi\hbar^2 a_{\rm BB}/M_{\rm B}$ for the contact pseudopotential. The many-body wave-function of the system in Hartree-Fock approximation, is a product state of the single particle states.

$$\Psi(\mathbf{r}_1, \mathbf{r}_2, ..., \mathbf{r}_N) = \psi(\mathbf{r}_1)\psi(\mathbf{r}_2)...\psi(\mathbf{r}_N). \tag{3.2}$$

The Gross-Pitaevskii equation is derived by applying the Hamiltonian to the many-body wave-function.

$$\mathscr{H} = \frac{\hbar^2}{2M_{\rm B}}|\nabla\Psi(\mathbf{r})|^2 + V(\mathbf{r})|\Psi(\mathbf{r})|^2 + \frac{g_{\rm BB}}{2}|\Psi(\mathbf{r})|^4. \tag{3.3}$$

Here $V(\mathbf{r})$ is an external potential, and $\nabla^2 \equiv \sum_i \nabla_i^2$ is the total laplacian operator. By minimizing the energy functional with respect to the many-body wave-function, for a conserved number of particles, we get the non-linear local Schrödinger equation.

$$\left(\frac{-\hbar^2}{2M_{\rm B}}\nabla^2 + V(\mathbf{r}) + g_{\rm BB}|\Psi(\mathbf{r})|^2\right)\Psi(\mathbf{r}) = \mu\Psi(\mathbf{r}). \tag{3.4}$$

The chemical potential μ is a Lagrange multiplier that can be found by applying the conservation of the particle number constraint:

$$N = \int \mathrm{d}^d r|\Psi(\mathbf{r})|^2. \tag{3.5}$$

In the Gross-Pitaevskii approach the many-body wave-function $\Psi(\mathbf{r})$ is reminiscent of the order parameter notion in the Landau-Ginzburg theory of second order phase transitions. The nonlinear Gross-Pitaevskii equation also allows for "*soliton*" solutions which will be discussed in some details in the following chapters.

3.2 Second Quantization Description and The Bogoliubov Theory

In the second quantized representation, and in the absence of the external potential, the Hamiltonian takes the form:

$$\hat{\mathcal{H}}_{\text{Boson}} = \sum_{\mathbf{q}} \frac{\hbar^2 q^2}{2M_{\text{B}}} a^{\dagger}_{\mathbf{q}} a_{\mathbf{q}} + g_{\text{BB}} \sum_{\mathbf{q},\mathbf{q}',\mathbf{k}} a^{\dagger}_{\mathbf{q}+\mathbf{k}} a^{\dagger}_{\mathbf{q}'-\mathbf{k}} a_{\mathbf{q}'} a_{\mathbf{q}}, \tag{3.6}$$

in which $(a_{\mathbf{q}}, a^{\dagger}_{\mathbf{q}})$ are the (annihilation,creation) operators of the bosons at momentum $\mathbf{q}$, and satisfy the canonical commutation relations:

$$[a_{\mathbf{q}}, a^{\dagger}_{\mathbf{q}'}] = \delta_{\mathbf{q},\mathbf{q}'}. \tag{3.7}$$

The ground-state of such a system forms a BEC. The fluctuations around the BEC state are commonly described by Bogoliubov approximation. The latter originates from the following: The vast majority of the bosons are assumed to form the BEC, and a small number of bosonic excitations are out of condensate. Mathematically, this is equivalent to say that the mode with $\mathbf{q} = 0$, is macroscopically occupied, and hence the BEC state $|\text{BEC}\rangle$, is insensitive to creation or annihilation of a single boson to the condensate: $a^{\dagger}_{\mathbf{q}=0}|\text{BEC}\rangle \approx a_{\mathbf{q}=0}|\text{BEC}\rangle \approx \sqrt{n_0}|\text{BEC}\rangle$. Here $n_0 = N_0/\Omega$ is the density of the condensate where N_0 is the number of bosons and Ω is the volume of the system. This means that we can replace the creation and annihilation operators of this mode by $\sqrt{n_0}$, where we have neglected 1 in comparison to $\sqrt{n_0}$.

Within the above approximation and using a canonical transformation from $(a_{\mathbf{q}}, a^{\dagger}_{\mathbf{q}})$ to a new set $(b_{\mathbf{q}}, b^{\dagger}_{\mathbf{q}})$ which are related to the former through:

$$b_{\mathbf{q}} = u_{\mathbf{q}} a^{\dagger}_{\mathbf{q}} + v_{\mathbf{q}} a_{\mathbf{q}}, \tag{3.8a}$$

$$b^{\dagger}_{\mathbf{q}} = u^{*}_{\mathbf{q}} a_{\mathbf{q}} + v^{*}_{\mathbf{q}} a^{\dagger}_{\mathbf{q}}, \tag{3.8b}$$

one can diagonalize the original Hamiltonian, such that:

$$\hat{\mathcal{H}} = \sum_{\mathbf{q}} \hbar\omega_{\mathbf{q}} b^{\dagger}_{\mathbf{q}} b_{\mathbf{q}}. \tag{3.9}$$

Here $\omega_{\mathbf{q}}$ is the dispersion of a Bogoliubov mode with wavevector $\mathbf{q}$ is equals:

$$\omega_{\mathbf{q}} = cq\sqrt{1 + (q\xi)^2/2}, \tag{3.10}$$

where $c = \sqrt{g_{\mathrm{BB}} n_0 / M_{\mathrm{B}}}$ is the speed of sound in the condensate, and $\xi = \sqrt{\frac{1}{2M_{\mathrm{B}} g_{\mathrm{BB}} n_0}}$ $= \frac{1}{\sqrt{2} M_{\mathrm{B}} c}$ is the healing length of the condensate.

The "canonical" transformation preserves the commutation relations such that:

$$[b_{\mathbf{q}}, b^{\dagger}_{\mathbf{q}'}] = [a_{\mathbf{q}}, a^{\dagger}_{\mathbf{q}'}] = \delta_{\mathbf{q},\mathbf{q}'}. \tag{3.11}$$

This results in the following relation:

$$|v_{\mathbf{q}}|^2 - |u_{\mathbf{q}}|^2 = 1, \tag{3.12}$$

so we can write them as:

$$v = e^{i\theta_1} \cosh r \tag{3.13a}$$

$$u = e^{i\theta_2} \sinh r \tag{3.13b}$$

3.3 Mobile Impurities in Bose-Einstein Condensates

Atomic gas mixtures with large concentration imbalance are used to study the impurities in many-body systems. While heavy impurities can be thought of as static defects and treated classically, the finite-mass quantum impurities ("polarons") can acquire either extended or self-trapped states [70, 71]. The interaction of a quantum impurity with *dispersionless gapped* longitudinal optical phonons results in a smooth transition from extended (Fröhlich) to self-trapped (Landau-Pekar) polaron [67]. However, the interaction with *gapless* acoustic phonons, in the presence of the momentum cutoff (edge of the Brillouin zone), yields a smooth self-trapping transition up to a critical cutoff, beyond which the effective mass of the polaron experiences a jump as the coupling constant is enhanced [72]. A quantum impurity coupled to the gapless Bogoliubov excitations ("Bose polaron") can be described by a Fröhlich-like Hamiltonian. In atomic

mixtures such as impurity-doped BECs, a momentum cutoff should be introduced to the Bogoliubov excitations; turns out that although the results are almost independent of the cutoff for realistic choices of the order of inverse interatomic interaction range, they show a pronounced crossover at a critical coupling constant from quasifree to self-trapped state; very similar to acoustic polaron [73].

3.3.1 Bose-polaron and Mapping to Fröhlich Hamiltonian

Low energy s-wave scattering of the impurity-boson atoms is described by a contact pseudopotential of the form:

$$V_{\mathrm{IB}}(\mathbf{R}-\mathbf{r}) = g_{\mathrm{IB}}\delta(\mathbf{R}-\mathbf{r}), \tag{3.14}$$

where $\mathbf{R}$ and $\mathbf{r}$ denote the impurity and boson position vectors, respectively. The Hamiltonian of quantum (mobile) impurities immersed in atomic BEC's can be written in the second quantized form as,

$$\begin{aligned}\hat{\mathcal{H}} =& \sum_{\mathbf{q}} \frac{\hbar^2 q^2}{2M_I} c^\dagger_{\mathbf{q}} c_{\mathbf{q}} + \sum_{\mathbf{k}} \epsilon_{\mathbf{k}} a^\dagger_{\mathbf{k}} a_{\mathbf{k}} + \frac{1}{2}\sum_{\mathbf{k},\mathbf{k}',\mathbf{q}} V_{\mathrm{BB}}(\mathbf{q}) a^\dagger_{\mathbf{k}'-\mathbf{q}} a^\dagger_{\mathbf{k}+\mathbf{q}} a_{\mathbf{k}} a_{\mathbf{k}'} \\ &+ \sum_{\mathbf{k},\mathbf{k}',\mathbf{q}} V_{\mathrm{IB}}(\mathbf{q}) c^\dagger_{\mathbf{k}+\mathbf{q}} c_{\mathbf{k}} a^\dagger_{\mathbf{k}'-\mathbf{q}} a_{\mathbf{k}'}.\end{aligned} \tag{3.15}$$

In the above equation, M_{I} is the mass of the impurity, and $(c^\dagger_{\mathbf{q}}, c_{\mathbf{q}})$ the (creation, annihilation) operators of the impurity with dispersion $\epsilon_{\mathbf{k}} = \hbar^2 k^2/2M_{\mathrm{B}} - \mu$, in which μ is the chemical potential of the condensate. The first and second terms represent the kinetic contributions of the free impurity and the free Bose gas, respectively. However it is more convenient to convert the impurity's degree of freedom to first quantized form. Therefore the contribution of the impurity to the Hamiltonian reads:

$$\hat{\mathcal{H}}_{\text{impurity}} = \frac{\hat{P}^2}{2M_{\mathrm{I}}} + \sum_{\mathbf{q},\mathbf{k}} V_{\mathrm{IB}}(\mathbf{q}) \hat{\rho}_{\mathrm{I}}(\mathbf{q}) a^\dagger_{\mathbf{k}-\mathbf{q}} a_{\mathbf{k}}, \tag{3.16}$$

where $\hat{P}$ is the momentum operator of the impurity, and $\hat{\rho}_{\mathrm{I}}(\mathbf{q})$ is the impurity density operator.

The third term in Eq. 3.15 is the boson-boson interaction which is elaborated in the previous section. The last term which accounts for the impurity-boson interaction, is the part we desire to recast an rewrite in the Fröhlich form. This mapping is possible through the Bogoliubov shift. The resulting second quantized Hamiltonian in terms of the Bogoliubov excitations reads,

$$\begin{aligned}\hat{\mathcal{H}} =&\frac{\hat{P}^2}{2M_{\rm I}} + \sum_{\mathbf{k}\neq 0} E_{\mathbf{k}} b^\dagger_{\mathbf{k}} b_{\mathbf{k}} + E_{\rm GP} + N_0 V_{\rm IB}(0) \\ &+ \sum_{\mathbf{k}\neq 0} \sqrt{\frac{\xi_{\mathbf{k}} N_0}{E_{\mathbf{k}}}} V_{\rm IB}(\mathbf{k}) \hat{\rho}_{\rm I}(\mathbf{k}) [b^\dagger_{-\mathbf{k}} + b_{\mathbf{k}}]. \end{aligned} \tag{3.17}$$

Here

$$E_{\mathbf{k}} = \sqrt{\xi_{\mathbf{k}}(\xi_{\mathbf{k}} + 2N_0 V_{\rm BB}(\mathbf{k}))}, \tag{3.18}$$

is the dispersion of the Bogoliubov excitations, and $\xi_{\mathbf{k}} = \hbar^2 k^2 / 2M_{\rm B} = \epsilon_{\mathbf{k}} + \mu$. Next $E_{\rm GP}$ is the Gross-Pitaevskii energy of the condensate:

$$E_{\rm GP} = N_0 \epsilon_0 + \frac{N_0^2}{2} V_{\rm BB}(0) + \frac{1}{2} \sum_{\mathbf{k}\neq 0} N_0 V_{\rm BB}(\mathbf{k}). \tag{3.19}$$

The forth term in Eq. 3.17, $N_0 V_{\rm IB}(0)$ is the interaction of the impurity with the homogeneous condensate in the background with total number of bosons N_0. Therefore the resulting Hamiltonian of the impurity-Bogoliubov interaction in the Fröhlich form reads,

$$\hat{\mathcal{H}}_{\text{Fröhlich}} = \frac{\hat{P}^2}{2M_{\rm I}} + \sum_{\mathbf{k}\neq 0} E_{\mathbf{k}} b^\dagger_{\mathbf{k}} b_{\mathbf{k}} + \sum_{\mathbf{k}\neq 0} V_{\mathbf{k}} e^{i\mathbf{k}.\mathbf{r}} [b^\dagger_{-\mathbf{k}} + b_{\mathbf{k}}] \tag{3.20}$$

with

$$V_{\mathbf{k}} = \sqrt{n_0}\, g_{\rm IB} \left(\frac{(\xi k)^2}{(\xi k)^2 + 2} \right)^{1/4}. \tag{3.21}$$

Now upon integrating out the Bogoliubov excitations in favor of the particle's degree of freedom, one can calculate the effective Euclidean action for the "Bose-polaron":

$$\mathcal{S} = \int_0^{\beta\hbar} \frac{M_{\rm I}}{2} |\dot{\mathbf{R}}|^2 {\rm d}t - \sum_{\mathbf{k}\neq 0} \frac{|V_{\mathbf{k}}|^2}{2\hbar} \iint_0^{\beta\hbar} {\rm d}t{\rm d}s\, \mathcal{G}(\mathbf{k}, |t-s|) \exp[i\mathbf{k}.(\mathbf{R}(t) - \mathbf{R}(s))]. \tag{3.22}$$

The propagator of the self-interaction term equals:

$$\mathcal{G}(\mathbf{k}, |t-s|) = \frac{\cosh(\omega_{\mathbf{k}}(|t-s| - \hbar\beta/2))}{\sinh(\hbar\beta\omega_{\mathbf{k}}/2)}, \tag{3.23}$$

where $\omega_{\mathbf{k}}$ is introduced in Eq. 3.10. It is apparent from Eq. 3.22, that the path-integral over the particle's coordinate is not possible because of non-quadratic form of the action. It is noteworthy that usually in the large coupling limit, the particle acquires a self-trapped localized state, in which the quadratic approximation of the action in terms of $\mathbf{R}$ is plausible.

3.3.2 Feynman's Variational Method

In order to deal with the non-linearities in the problem, one can employ variational methods to gain some intuition. Variational ansätze are usually designed to match perfectly in certain exactly (or perturbatively) solvable limits. A few free parameters are included in each ansatz to play effectively the role of some combinations of actual parameters. In order to determine and fix the free parameters, we demand that the free energy must be minimized with respect to all the free parameters.

Feynman's variational method makes use of the convexity of an exponential function, namely $\exp(\mathcal{S}/\hbar)$. In this method one introduces a trial action $\mathcal{S}_0$, which is presumably path-integrable, hence Gaussian. Now using the following equation for partition function,

$$\mathcal{Z} = e^{-\beta\mathcal{F}} = \int \mathcal{D}[\mathbf{R}(t)] e^{\mathcal{S}[\mathbf{R}(t)]/\hbar}, \tag{3.24}$$

we get, after a few lines of algebra,

$$\mathcal{F} \leq \mathcal{F}_0 + \frac{1}{\hbar\beta}\langle \mathcal{S}_0 - \mathcal{S} \rangle_{\mathcal{S}_0}. \tag{3.25}$$

In the above equation $\mathcal{F}_0$ is the trial free energy associate with $\mathcal{S}_0$, which is obtained by using Eq. 3.24. Also $\langle \bullet \rangle_{\mathcal{S}_0}$ denotes averaging $\bullet$ with weights $\exp(\mathcal{S}_0/\hbar)$. The right hand side of the above inequality contains adjustable parameters to "best" replicate the original action. The "best" is achieved by minimizing the free energy with respect to

these parameters. In the case of Feynman polaron, a simple yet powerful trial action is of the harmonic form with a self-interaction propagator, which at zero temperature $\beta \to \infty$ dies off like $e^{-D|t-t'|}$ in "imaginary-time"; D is one of the variational parameters. A prefactor or coupling constant C is also included which mimics the polaron coupling constant. At finite temperature the action reads:

$$\begin{aligned}\mathcal{S}_0 =& -\int_0^{\hbar\beta} \frac{1}{2}\left(\frac{\mathrm{d}\mathbf{R}}{\mathrm{d}t}\right)^2 \mathrm{d}t - \mathbf{f}.\int_0^{\hbar\beta} \mathbf{R}(t)\mathrm{d}t \\ & -\frac{1}{2}\iint_0^{\hbar\beta} \mathcal{K}(|t-t'|)|\mathbf{R}(t)-\mathbf{R}(t')|^2 \mathrm{d}t\mathrm{d}t', \end{aligned} \tag{3.26}$$

where

$$\mathcal{K}(\tau) = \frac{1}{\hbar\beta}\sum_{n=-\infty}^{+\infty} \mathcal{K}_n e^{i\omega_n\tau} = \frac{C}{4D}\frac{\cosh(D(\tau-\hbar\beta/2))}{\sinh(\hbar\beta D/2)}. \tag{3.27}$$

We note that the wave-vector dependence of the kernel is completely ignored in the variational action. The second term in Eq. 3.26 represents a constant force on the particle. This term is included for later calculations of the effective mass.

After mapping, the Bose-polaron Hamiltonian is of the Fröhlich form, thus the same variational action can be written as,

$$\begin{aligned}\mathcal{S}_0 =& -\int_0^{\hbar\beta} \frac{1}{2}\left(\frac{\mathrm{d}\mathbf{R}}{\mathrm{d}t}\right)^2 \mathrm{d}t - \mathbf{f}.\int_0^{\hbar\beta} \mathbf{R}(t)\mathrm{d}t \\ & -\frac{MW^3}{8}\iint_0^{\hbar\beta} \frac{\cosh(W(|t-t'|-\hbar\beta/2))}{\sinh(\hbar\beta W/2)}\,|\mathbf{R}(t)-\mathbf{R}(t')|^2 \mathrm{d}t\mathrm{d}t', \end{aligned} \tag{3.28}$$

where $M \equiv C/D^2$ and $W \equiv D$ are the variational parameters.

Using the above variational ansatz, Tempere, *et.al,* calculated the self-energy and effective mass of the Bose-polaron. The results share common properties with those of acoustic polaron. Note that Bogoliubov excitations look like acoustic phonos at large wave-lengths. The polaron crossovers sharply from extended state at small couplings to localized state at large couplings. The quantitative results are clearly dependent on the momentum cutoff, like in the case of acoustic polaron (see Fig. (3.1)).

The problem of Bose-polaron has been a center of attraction to the condensed matter and ultracold atomic physicists. With the advent of experimental techniques, several

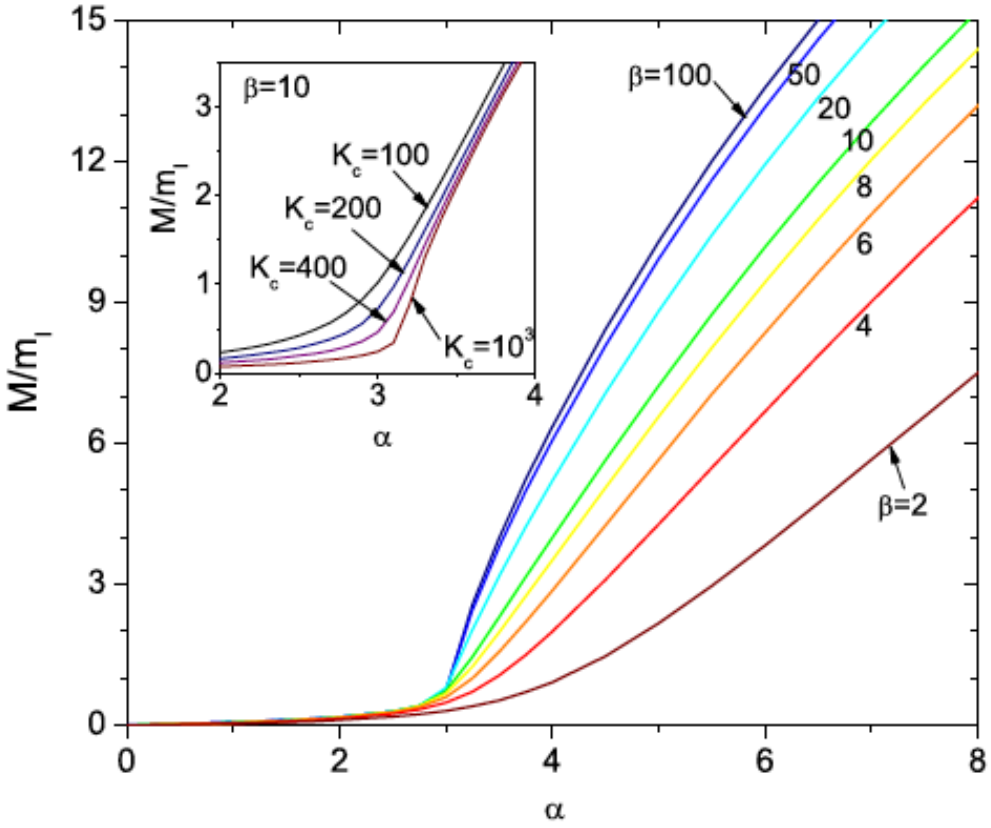

Figure 3.1: (From Ref. [71]) The effective mass of the Bose-polaron M/m_I, versus the dimensionless coupling constant α. Different curves correspond to different temperatures β^{-1}. The inset shows the dependence on the momentum cutoff at $\beta = 10$.

studies have considered various aspects of this problem. Besides the Feynman's variational method, other techniques such as second order perturbation theory, renormalization group, and Monte Carlo simulations have been applied to the problem. However the results seem to be considerably sensitive to the method for the intermediate coupling regime.

3.4 Bose-Einstein Condensates in Multimode Cavities

The first section of this chapter provides an overview of the calculations and results presented in Ref. [74]. First, consider a system of N bosonic atoms with the internal two-state structure. The atoms are both confined in an optical cavity and transversely pumped by a laser (along z direction). An interatomic interaction of the strength U is also included in the model. The geometry of the cavity is concentric, *i.e.* two spherical caps of mirrors with nearly coincident centers. Assuming that the level-spacing of the internal states of atoms is $\hbar\omega_a$, one can write down the Hamiltonian as:

$$\begin{aligned}\hat{\mathcal{H}} = &\sum_{i=1}^{N}\left[\frac{\hat{\mathbf{P}}_i^2}{2M_{\mathrm{B}}} + \hbar\omega_a\sigma_i^z\right] + U\sum_{1\le i<j\le N}\delta(\mathbf{x}_i-\mathbf{x}_j)\\ &+\sum_{\alpha}\hbar\omega_c a_\alpha^\dagger a_\alpha + i\hbar\sum_{i=1}^{N}\sum_{\alpha}[g_\alpha(\mathbf{x}_i)a_\alpha^\dagger\sigma_i^- - \text{H.c.}]\\ &+ i\hbar\Omega\sum_{i=1}^{N}\cos(k_L z_i)(\sigma_i^- - \sigma_i^+) + H_{\text{diss}}\ . \end{aligned} \tag{3.29}$$

In the above expression, $\mathbf{x}_i, \hat{\mathbf{P}}_i, \sigma_i$ are the position, momentum and Pauli matrices of atom i, respectively. The cavity-photon annihilation operators are represented by a_α. Also, $g_\alpha(\mathbf{x}) = g\,\Xi_\alpha(\mathbf{x})$, in which g is the atom-cavity coupling. For modes α the normalized mode functions are Ξ_α. This depends on the cavity geometry. In concentric cavity $\alpha = (l, m, n)$, where l is the number of nodes in the direction of the laser; m counts that in the angular direction and n in the radial direction. The Rabi frequency Ω is proportional to the laser intensity, with the wave-vector k_L. Finally the dissipation is included in H_{diss}, which includes terms the leaking of intracavity photons through cavity with rate κ. In a rotating-wave approximation for the laser frequency ω_L, red-detuned from the cavity mode. Both frequencies are in turn significantly red-detuned from the internal level-spacing: $\omega_L \gg \omega_a - \omega_L \gg \omega_c - \omega_L > 0$. We will use the following detuning frequencies in the next steps:

$$\Delta_a = \omega_a - \omega_c \simeq \omega_a - \omega_L, \tag{3.30a}$$

$$\Delta_c = \omega_c - \omega_L. \tag{3.30b}$$

First, the full action of the system can be written as:

$$\mathcal{S} = \mathcal{S}_{\text{atom}} + \mathcal{S}_{\text{photon}} + \mathcal{S}_{\text{int}} + \mathcal{S}_{\text{diss}} \tag{3.31}$$

where

$$\begin{aligned}\mathcal{S}_{\text{atom}} = \int \mathrm{d}^d x \mathrm{d}\tau \Bigg[& \psi_g^*(\mathbf{x},\tau)\left(\partial_\tau - \frac{\hbar\nabla^2}{2M_B} - \frac{\mu}{\hbar}\right)\psi_g(\mathbf{x},\tau) \\ & + \psi_e^*(\mathbf{x},\tau)\left(\partial_\tau - \frac{\hbar\nabla^2}{2M_B} + \omega_A - \frac{\mu}{\hbar}\right)\psi_e(\mathbf{x},\tau) \\ & + \frac{U}{2\pi\hbar}|\psi_g(\mathbf{x},\tau)|^2(|\psi_g(\mathbf{x},\tau)|^2 + |\psi_e(\mathbf{x},\tau)|^2)\Bigg],\end{aligned} \tag{3.32a}$$

where $\psi_{g,e}$ are the ground, excited coherent-states of the bosons, and μ is the chemical potential. Also τ is the imaginary time. Because of the large internal gap Δ_A of atoms, $|\psi_e|^2 \ll |\psi_g|^2$, hence the term $|\psi_e|^4$ is neglected. Next,

$$\mathcal{S}_{\text{photon}} = \int \mathrm{d}\tau \sum_\alpha a_\alpha^*(\tau)(\partial_\tau + \omega_c)a_\alpha(\tau), \tag{3.32b}$$

is the the action of the intra-cavity modes.

$$\begin{aligned}\mathcal{S}_{\text{int}} = \int \mathrm{d}\tau \mathrm{d}^d x \Bigg[& \sum_\alpha i g_\alpha(\mathbf{x})\psi_e^*(\mathbf{x},\tau)\psi_g(\mathbf{x},\tau)a_\alpha(\tau) + \text{H.c.} \\ & + i\Omega\psi_e^*(\mathbf{x},\tau)\psi_g(\mathbf{x},\tau) + \text{H.c.}\Bigg],\end{aligned} \tag{3.32c}$$

$$\mathcal{S}_{\text{diss}} = \int \mathrm{d}\tau \sum_\epsilon A_\epsilon^*(\partial_\tau + \omega_\epsilon)A_\epsilon + \sum_{\alpha,\epsilon} \kappa_{\alpha,\epsilon} a_\alpha^\dagger A_\epsilon + \text{H.c.}, \tag{3.32d}$$

Here A_ϵ represent the extracavity modes. In order to obtain an effective field theory for the condensate, one integrates out all the environmental degrees of freedom. The resultant action reads (see Ref. [74, 75]):

$$\begin{aligned}\mathcal{S}_{\text{eff}} = & \sum_n \int \mathrm{d}^d x\ \psi^*(\omega_\nu,\mathbf{x})\left[i\omega_\nu - \frac{\hbar\nabla^2}{2M_B} - \frac{\mu}{\hbar}\right]\psi(\omega_\nu,\mathbf{x}) \\ & - \zeta\sum_\alpha \int \mathrm{d}\tau \mathrm{d}^d x \mathrm{d}^d x' \Xi_\alpha(\mathbf{x})|\psi(\tau,\mathbf{x})|^2 \Xi_\alpha^*(\mathbf{x}')|\psi(\tau,\mathbf{x}')|^2 \\ & + \frac{U}{\hbar}\int \mathrm{d}\tau \mathrm{d}^d x |\psi(\tau,\mathbf{x})|^4 + \dots .\end{aligned} \tag{3.33}$$

Here we have used the following definitions: ω_n are the Matsubara frequencies, and the coupling constant

$$\zeta = \frac{g^2\Omega^2\Delta_c}{\Delta_a^2(\Delta_c^2+\kappa^2)}. \tag{3.34}$$

3.4.1 Order-parameter and Its Effective Action

One can define an order-parameter as the expectation value of the amplitude of the density modulation in mode α.

$$\langle\rho_\alpha\rangle = \int \mathrm{d}^d x \, \langle|\psi^*(\mathbf{x},\tau)|^2\rangle \, \Xi_\alpha(\mathbf{x}). \tag{3.35}$$

The relation expresses the expectation value of the amplitude of the density field with mode α, in terms the mode eigenfunctions Ξ_α. For example, in a concentric cavity with modes $\alpha = (l,m,n)$, the atoms would like to crystallize into modes which satisfy $l+m+n = q_0\mathcal{R}/2\pi$, where $\mathcal{R}$ is the radius of the cavity. In this case $l = 0$, that is the node at $z = 0$, contributes the most and has the largest amplitude. For the atomic clouds extended over many optical wavelengths, the orthonormal mode basis approximately satisfy,

$$\int \mathrm{d}^d x \Pi_i \Xi_{m_i,n_i}(\mathbf{x}) = \delta_{\sum_i m_i,0}\delta_{\sum_i n_i,0}, \tag{3.36}$$

analogous to the momentum conservation condition. Here Π_i denotes the product operation. After introducing some auxiliary fields and using identities, the effective action of the order parameter can be derived as presented in Ref. [74]:

$$\begin{aligned}\mathcal{S} = &\sum_\nu \sum_{m,n} \frac{1}{\zeta}\left[r' + \omega_\nu^2 + \chi(2\pi(m+n) - q_0\mathcal{R})^2\right]|\varrho_{\nu,m,n}|^2 \\ &+ \frac{U}{\hbar}\int \mathrm{d}\tau \mathrm{d}^d x |\varrho(\mathbf{x},\tau)|^4 + \dots .\end{aligned} \tag{3.37}$$

Here ϱ represents the Bogoliubov excitations in the condensate. Other parameters are given by:

$$r' = \left(\frac{\hbar q_0^2}{2M_\mathrm{B}}\right)^2 - \frac{\zeta N \hbar q_0^2}{2M_\mathrm{B}}, \tag{3.38}$$

and χ determines the width of the static structure factor of the model around q_0. The effective action obtained in Eq. (3.37) is reminiscent of the Brazovskii model for weak crystallization. The difference is in the mode basis into which the crystallization is favorable. The mean-field threshold of the laser field for the crystallization to happen is given by:

$$\Omega_{\rm MF}^2 = \frac{\hbar^2 q_0^2}{2M_{\rm B}} \frac{\Delta_a^2(\Delta_a^2+\kappa^2)}{N\hbar\Delta_c g^2}. \tag{3.39}$$

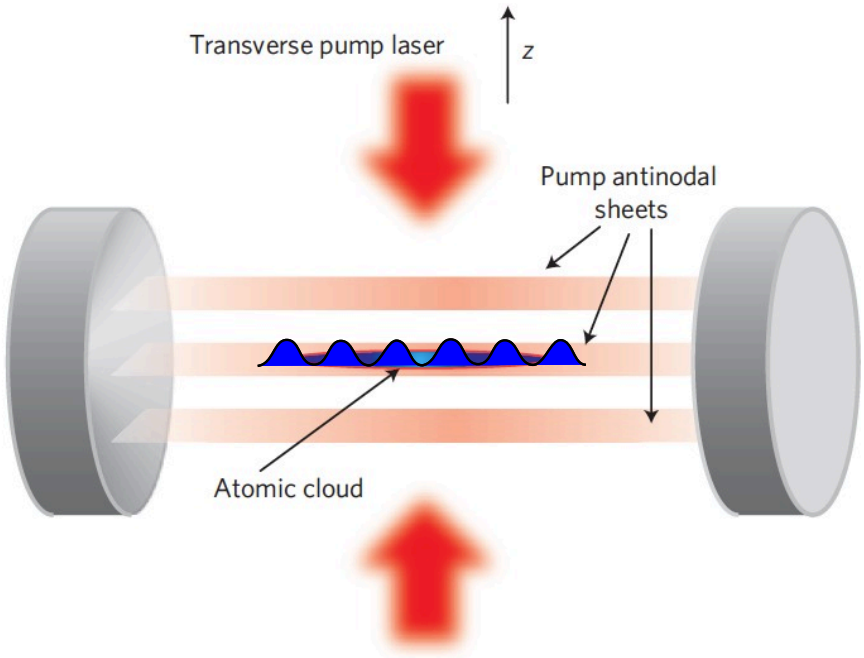

Figure 3.2: (From Ref. [74]) The picture is a schematic of a transversely pumped multimode concentric cavity. The atomic cloud is trapped in the center antinodal sheet with the least loss. The density field gets modulated when the laser reaches the Brazovskii threshold.

As Eq. (3.37) suggests, above the mean-field threshold $\Omega_{\rm MF}$, the density field undergoes a spontaneous symmetry-breaking transition which belongs to the Brazovskii class. Brazovksii renormalization calculation predicts that the transition point is shifted by [74, 75]:

$$\Omega_{\rm TH}^2 - \Omega_{\rm MF}^2 \simeq \left(\frac{g^2\Delta_c}{\Delta_a^2(\Delta_c^2+\kappa^2)} \frac{\Omega_{\rm TH}^8 M_{\rm B}\mathcal{R}^2}{\hbar N\chi}\right)^{1/3}. \tag{3.40}$$

It is clear as also mentioned in Ref. [74, 75], that the mode structure of the cavity is not a crucial component and the choice is only for simplicity of calculations. In the next section, we combine the Bose-polaron theory with the quantum Brazovskii field theory presented in this section, in order to study the effects of nearly critical fluctuations on the polaron physics. To this end, we ignore the specific mode basis of the concentric cavity geometry, and work in the plane-wave basis where

$$\Xi_\alpha(\mathbf{x}) = \exp(i\mathbf{q}.\mathbf{x}). \tag{3.41}$$

This choice is in particular convenient for the study of mobile impurities and polarons, and indeed generalizes the applicability of our treatment to actual crystallization in condensed matter systems. Therefore, we adopt a quantum Brazovskii model and include the interaction with the particle's degree of freedom which is also subject to quantum fluctuations.

3.5 Impurity-doped Bose-Einstein Condensates in Cavities

It is well known that ultracold atomic physics provides realizations of interesting quantum many-body systems [76, 77, 30]. In particular, and as discussed in the previous section, the emergence of spatial order and other forms of spontaneous symmetry breaking in quantum systems can be studied in BECs confined to transversely laser-pumped cavities [31, 32, 33, 74, 75]. We focus on the problem of an impurity in a correlated quantum liquid near a continuous (or weakly first-order) symmetry breaking transition. The role of quantum fluctuations on impurity solvation and transport in correlated liquids like water [9] is currently the subject of active debates in the physical chemistry literature. The failure of linear-response theory plays a central role in these debates [17].

As introduced in the previous sections, the physics of impurities in ultracold quantum gases [78, 79, 80] and in *uniform* BECs has already been well explored [81, 82, 83, 84, 85, 86]. The interaction between a (neutral) impurity and the Bogoliubov ex-

citations of the BEC maps onto the so-called Fröhlich Hamiltonian [70, 87, 88, 71], a linear-response theory that has been extensively applied to charged impurities in polarizable media (polarons). Such a "Bose-polaron" can undergo a transition from an extended state to a self-trapped—or Landau-Pekar (LP) [89, 90]—polaron as a function of the coupling constant [73].

In a transversely pumped, multi-mode cavity, a BEC undergoes a spontaneous phase transition from the uniform state to a state in which the the density of the condensate is periodically modulated, with density $\rho(\mathbf{r}) = \rho_0 e^{-i\mathbf{q}.\mathbf{r}} + \text{c.c.}$. This transition is described by a quantum version of the *Landau-Brazovskii* theory for fluctuation-driven first-order phase transitions (QLB)[74]. In this letter we will combine the Fröhlich Hamiltonian description for impurities and the QLB theory for symmetry breaking in BECs to investigate the fate of a BEC polaron near the onset of spontaneous positional ordering. The aim is to determine whether impurities in a BEC in a multi-mode laser-pumped cavity can serve as a model system for the study of the effects of quantum fluctuations on solvation and the breakdown of linear response theory without the molecular level complexities that hamper studies of impurities in correlated liquids like water.

- **Model**:

Our model is defined by a Lagrangian that is the sum of three terms, respectively referring to the impurity particle, the condensate, and the lossy cavity. The Lagrangian of an impurity particle in a BEC condensate is

$$L_{\rm I} = \frac{1}{2} M_{\rm I} |\dot{\mathbf{R}}|^2 - \int \mathrm{d}^3 r \, V(\mathbf{R}(t) - r) \rho(\mathbf{r}, t), \tag{3.42}$$

with $M_{\rm I}$ the impurity mass, $\mathbf{R}(t)$ the impurity location and $\rho(\mathbf{r})$ the deviation of the local density of the condensate from the mean density $n_0 = N_0/\Omega$ (N_0 and Ω are the number of bosons in the condensate and the volume of the system respectively). We note that $M_{\rm I}$ might be different from the bare mass of the impurity, and renormalized due to interaction with the laser and/or cavity modes. This is similar to the mass of the

Bloch electrons as a result of their interaction with a periodic potential. We only focus on the interaction with the BEC.

Next, $V(\mathbf{r})$ is the pseudopotential for the interaction of the impurity particle with the bosons. In the s-wave Fermi approximation,

$$V(\mathbf{R}-\mathbf{r}) = g_{\text{IB}}\delta^{(3)}(\mathbf{R}-\mathbf{r}) \tag{3.43a}$$

with

$$g_{\text{IB}} = 2\pi a_{\text{IB}}\hbar^2/M_{\text{r}} \tag{3.43b}$$

where a_{IB} is the impurity-boson s-wave scattering length and M_{r} the reduced mass of a impurity-boson binary system:

$$M_{\text{r}}^{-1} = M_{\text{I}}^{-1} + M_{\text{B}}^{-1}. \tag{3.44}$$

In order to adopt the Feynman's variational method, we first write down the classical Lagrangian of the field. The Lagrangian for the excitations of the BEC reads

$$L_{\text{B}} = \frac{1}{\Omega}\sum_{\mathbf{q}}\frac{\hbar}{\zeta_q}\left(|\dot{\rho}_{\mathbf{q}}|^2 - \omega(\mathbf{q})^2|\rho_{\mathbf{q}}|^2\right) + L_{\text{NL}}. \tag{3.45}$$

Here we used the Fourier transform definition,

$$\rho(\mathbf{r},t) = \Omega^{-1}\sum_{\mathbf{q}}\rho_{\mathbf{q}}(t)e^{i\mathbf{q}.\mathbf{r}} \tag{3.46}$$

and

$$\zeta_q = n_0\epsilon_0(q)/\hbar. \tag{3.47}$$

with

$$\epsilon_0(q) = \hbar^2q^2/2M_{\text{B}}, \tag{3.48}$$

the free boson dispersion relation. For a uniform BEC, the dispersion relation is given by the Bogoliubov spectrum

$$\hbar\omega_0(q) = \sqrt{\epsilon_0(q)(\epsilon_0(q)+2n_0g_{\text{BB}})}, \tag{3.49}$$

where

$$g_{\rm BB} = 4\pi a_{\rm BB}\hbar^2/M_{\rm B}, \tag{3.50}$$

is the pseudopotential for boson-boson scattering ($a_{\rm BB}$ is the boson-boson scattering length). Non-linear terms are represented by $L_{\rm NL}$. For BECs in an optical cavity, both the boson-boson and boson-impurity scattering length are experimentally adjustable parameters. The Fröhlich Hamiltonian of BEC polarons in uniform condensates is recovered upon canonical quantization of the linear and quadratic terms of equations (3.42) and (3.45).

The modes of a BEC inside a laser-pumped optical cavity, are mixed Bogoliubov excitations and electromagnetic modes [31, 32, 74, 75]. The mode frequencies are depressed and driven to zero around q_0, as the amplitude increases. Near the instability threshold, the spectrum can be approximated as [74, 75]:

$$\omega(\mathbf{q})^2 \simeq \Delta + \lambda\mathcal{R}^2(|\mathbf{q}| - q_0)^2, \tag{3.51}$$

where Δ is frequency squared of the lowest frequency mode, $\mathcal{R}$ the dimension of the cavity, and λ a phenomenological parameter determining the range of wave-vectors over which the depression takes place. It is itself determined by the width of the cavity resonance and other factors [74, 75]. In MF theory, this Lagrangian describes a continuous ordering transition at $\Delta = 0$ from a uniform phase to a density-modulated phase with modulation vector q_0 and modulation amplitude proportional to $|\Delta|^{1/2}$ [91, 92, 93].

In chapter 2, we introduced the Caldeira-Leggett formalism, where a classical degree of freedom can be quantized using path-integral formulation. The effective action of such a system is then obtained by the influence function of the bath. This formalism is in particular useful and can be conveniently incorporated in the field theory language. The modes of the BEC are also coupled to the electromagnetic modes outside the pumped cavity that act as a reservoir. These are included in the form of a distribution of harmonic oscillators coupled linearly to the BEC modes. Their Lagrangian

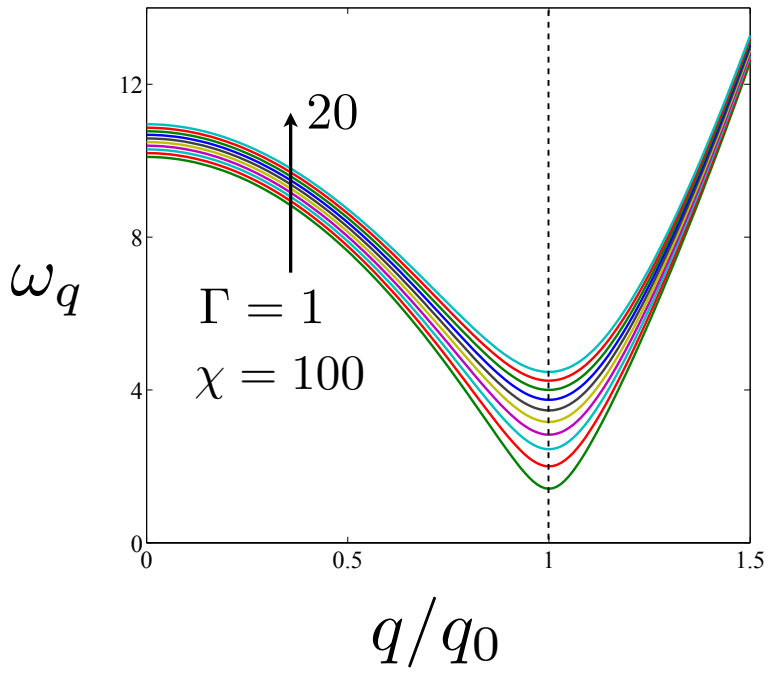

Figure 3.3: The dispersion of the Brazovskii modes $\omega_q^2 = \Gamma + \chi(q - q_0)^2$. Different colors correspond to different distances from the QLB mean-field transition from $\Gamma = 1$ to $\Gamma = 20$ at constant field rigidity, $\chi = 100$. The dimensionless parameters are introduced in the text (see below).

is

$$L_{\mathrm{E}} = \sum_j \frac{1}{2} m_j \{\dot{x_j}^2 - \omega_j^2 x_j^2\} - \sum_{j,\mathbf{q}} C_{j,q} \rho_{\mathbf{q}} x_j. \tag{3.52}$$

The nature of the dissipation is determined by the choice of the oscillator spectral density [63, 64].

$$J_q(\omega) = \frac{\pi}{2} \sum_j \left(\frac{{C_{j,q}}^2}{m_j \omega_j} \right) \delta(\omega - \omega_j) \tag{3.53}$$

We will restrict ourselves to the simplest case of "Ohmic" dissipation with $J_q(\omega) = \eta_q \, \omega$, for low frequencies where η_q is an effective friction coefficient. For higher frequencies, a UV cutoff should be introduced. The classical equation of motion for the

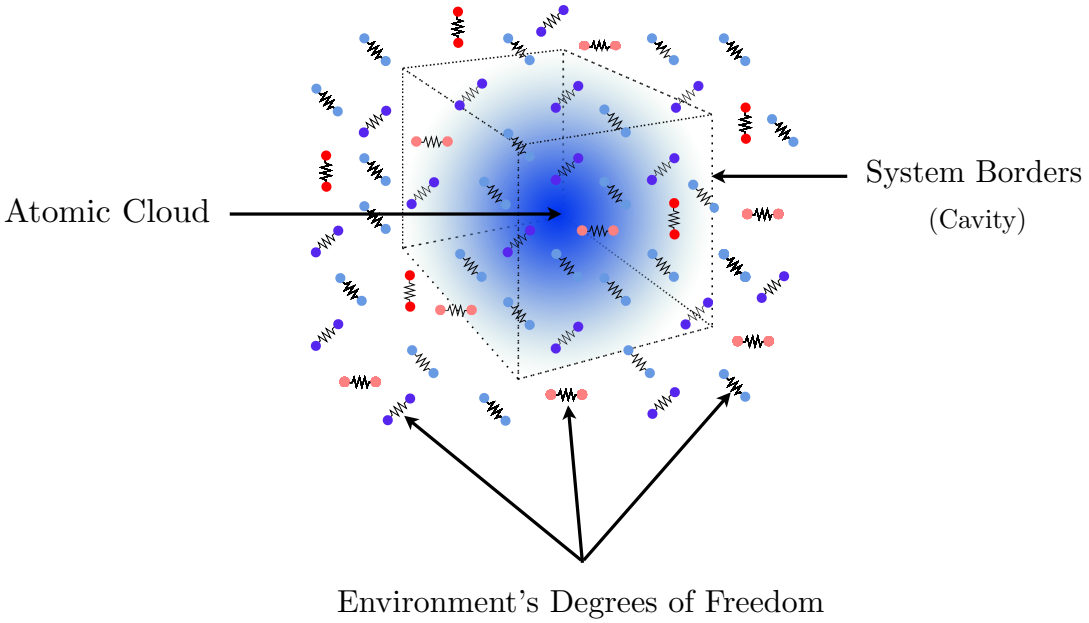

Figure 3.4: The dissipative environment, in general can be represented by a bath of harmonic oscillator whose displacement is linearly coupled to the system's degrees of freedom. The blue cloud indicates the atomic gas. The dotted edges are the imaginary boundaries of the system.

impurity, obtained by minimizing the total action, is of the Langevin form with a friction coefficient that diverges at the MF critical point as η_{q_0}/Δ^2.

The equilibrium partition function $\mathcal{Z}$ of the impurity is proportional to the functional integral

$$\int \exp(\mathcal{S}_{\rm T})\mathcal{D}\{\mathbf{R}(t)\}\mathcal{D}\{\rho_{\mathbf{q}}(t)\}\mathcal{D}\{x_j(t)\}, \tag{3.54}$$

over all degrees of freedom $\mathbf{R}(t), \rho_{\mathbf{q}}(t), x_j(t)$, which must obey periodic boundary conditions in "imaginary time" $0 \leq s \leq \beta$ ($\beta = 1/k_B T$). This condition is a consequence of tracing over bosonic degrees of freedom. We have,

$$\mathbf{R}(0) = \mathbf{R}(\beta), \quad \rho_{\mathbf{q}}(0) = \rho_{\mathbf{q}}(\beta), \quad x_{\{j\}}(0) = x_{\{j\}}(\beta). \tag{3.55}$$

Here, $\mathcal{S}_{\rm T}$ is the Euclidean action. The path integral over the environmental oscillators

can be carried out analytically because of their Gaussian form. This, in the case of Ohmic bath, adds a new overdamping term to the bare action of the density field of the form: $\gamma|\omega_n||\rho_{\mathbf{q},n}|^2$ (see below).

The remaining path integrals over condensate modes and particle trajectories will be discussed separately for positive and negative Δ.

3.6 Above the Mean-field Critical Point

For positive Δ, the non-linear terms ($L_{\rm NL}$) do not play a significant role. The density fluctuations can then be integrated out, leading to an effective action for the particle trajectories:

$$\begin{aligned}\mathcal{S} \simeq & -\int_0^{\tilde{\beta}} \frac{1}{2}\left(\frac{\mathrm{d}\tilde{\mathbf{R}}}{\mathrm{d}\tilde{s}}\right)^2 \mathrm{d}\tilde{s} - \tilde{\mathbf{f}}.\int_0^{\tilde{\beta}} \tilde{\mathbf{R}}(\tilde{s})\mathrm{d}\tilde{s} \\ & + \alpha \int \mathrm{d}^3\tilde{q} \iint_0^{\tilde{\beta}} \mathrm{d}\tilde{s}\mathrm{d}\tilde{s}' G^{(2)}_{\tilde{q}}(|\tilde{s}-\tilde{s}'|) e^{i\tilde{\mathbf{q}}.[\tilde{\mathbf{R}}(\tilde{s})-\tilde{\mathbf{R}}(\tilde{s}')]},\end{aligned} \tag{3.56}$$

where

$$\alpha = \frac{g_{\rm IB}^2 q_0^3 \zeta \hbar}{4(2\pi)^3}\left(\frac{M_{\rm I}}{\hbar^2 q_0^2}\right)^3, \tag{3.57}$$

plays the role of a dimensionless coupling constant. The kernel, for q around q_0, is given by

$$G^{(2)}_q(\tau) = \frac{1}{\beta}\sum_{n=-\infty}^{+\infty} \frac{e^{i\omega_n\tau}}{\chi(q-1)^2 + \Gamma + \gamma|\omega_n| + \omega_n^2}. \tag{3.58}$$

The summation is over dimensionless bosonic Matsubara frequencies

$$\omega_n = 2\pi n/\beta, \tag{3.59}$$

so the periodic boundary conditions in imaginary time are obeyed. The dimensionless distance to the MF critical point of the QLB is defined here as

$$\Gamma = \Delta(M_{\rm I}/\hbar q_0^2)^2, \tag{3.60a}$$

the dimensionless friction coefficient as

$$\gamma = \eta(M_{\rm I}/\hbar q_0^2) \tag{3.60b}$$

and the dimensionless field rigidity as

$$\chi = \lambda(M_{\rm I}/\hbar q_0^2)^2(\mathcal{R}q_0)^2. \tag{3.60c}$$

We shifted here to dimensionless quantities (indicated by tildes), by setting

$$M_{\rm I} = \hbar = q_0 = 1. \tag{3.61}$$

The energy is then measured in units of $\hbar^2 q_0^2/M_{\rm I}$; length is measured in units of q_0^{-1}, and time in units of $M_{\rm I}/(\hbar q_0^2)$. The dimensionless inverse temperature $\tilde{\beta} = (\hbar q_0)^2/M_{\rm I}k_BT$ is the ratio of the zero-point energy of the particle confined in a well with a dimension of order $1/q_0$ and the thermal energy. We drop the tildes for convenience hereafter, but will return to actual units when needed, to make the interpretations more straightforward. Also, in order to later compute the effective mass, an infinitesimal external force $\tilde{\mathbf{f}}$, is included in the action (see below).

- **Variational Action**:

As mentioned in the previous sections, the perturbation theory fails in the regime of most interesting cases of solid state. The coupling constant is usually of the order $\sim 1 - 10$. In ultracold quantum gas experiments, this coupling can be easily varied via Feshbach resonance. In order to cover the entire interesting possible values of coupling constant, a very successful method to adopt is the Feynman's variational method, specifically devised for the path-integral formulation. Therefore, the path integral over the particle trajectories is performed variationally [65, 66, 67, 68] by a defining suitable Gaussian trial action. For the present case we choose

$$\begin{aligned}\mathcal{S}_t = &-\int_0^\beta \frac{1}{2}\left(\frac{\mathrm{d}\mathbf{R}}{\mathrm{d}s}\right)^2 \mathrm{d}s - \mathbf{f}.\int_0^\beta \mathbf{R}(s)\mathrm{d}s \\ &-\frac{1}{2}\iint_0^\beta \mathcal{K}(|s-s'|)|\mathbf{R}(s)-\mathbf{R}(s')|^2 \mathrm{d}s\mathrm{d}s',\end{aligned} \tag{3.62}$$

where the kernel

$$\mathcal{K}(\tau) = \frac{1}{\beta} \sum_{n=-\infty}^{+\infty} \mathcal{K}_n e^{i\omega_n \tau}, \tag{3.63}$$

with

$$\mathcal{K}_n = C/(D + \gamma|\omega_n| + \omega_n^2), \tag{3.64}$$

is similar to the actual kernel. The constants C and D play the role of variational parameters.

- **Free Energy**:

The variational parameters C, D have to be adjusted to minimize the free energy. In particular, close enough to the phase transition, the integral is dominated by the q_0 mode. Therefore we expect the minimizing D to be of the same order as Γ. The free energy satisfies Feynman's inequality:

$$\mathcal{F} \leq \mathcal{F}_t + \beta^{-1} \langle \mathcal{S} - \mathcal{S}_t \rangle_t. \tag{3.65}$$

Here $\mathcal{F} = -k_B T \ln \mathcal{Z}$ is the free energy of the particle. Expectation values are computed using the Gaussian trial action. The right hand side of the inequality is a function of the variational parameters. By minimizing this expression with respect to C, D, we find an upper bound to the actual free energy.

- **Effective Mass**:

For a free particle with mass M^* subject to a force f, the second derivative of the free energy with respect to the applied force equals (in actual units).

$$\partial^2 \mathcal{F}/\partial f^2|_{f=0} = \hbar^2 \beta^2 / 12 M^*. \tag{3.66}$$

Using this as the definition of the effective mass [69] and applying the trial action gives (in dimensionless units):

$$M^* = \frac{\beta^2}{24} \left[\sum_{n>0} g_n \right]^{-1}, \tag{3.67}$$

where

$$g_n = \left[\omega_n^2 + \frac{2}{\beta}(\mathcal{K}_0 - \mathcal{K}_n)\right]^{-1}. \tag{3.68}$$

The minimizing C, D should be substituted in Eq. (3.68) to obtain g_n. This in turn is substituted in Eq. (3.67), to calculate the effective mass.

3.6.1 Zero Dissipation and Close to the Mean-field Critical Point

In the limit of $\gamma = 0$, and close to the mean-field critical point of the QLB transition, the effective action takes the following form:

$$\begin{aligned}\mathcal{S} \simeq & -\int_0^{\tilde{\beta}} \frac{1}{2}\left(\frac{\mathrm{d}\tilde{\mathbf{R}}}{\mathrm{d}\tilde{s}}\right)^2 \mathrm{d}\tilde{s} - \tilde{\mathbf{f}}.\int_0^{\tilde{\beta}} \tilde{\mathbf{R}}(\tilde{s})\mathrm{d}\tilde{s} \\ & + \alpha \int \mathrm{d}^3\tilde{q} \iint_0^{\tilde{\beta}} \mathrm{d}\tilde{s}\mathrm{d}\tilde{s}' \; \frac{1}{\omega_q}\frac{\cosh(\omega_q(|\tilde{s}-\tilde{s}'| - \beta/2))}{\sinh(\omega_q\beta/2)} \; e^{i\tilde{\mathbf{q}}.[\tilde{\mathbf{R}}(\tilde{s})-\tilde{\mathbf{R}}(\tilde{s}')]},\end{aligned} \tag{3.69}$$

where we have:

$$\omega_q = [\chi(q-1)^2 + \Gamma]^{1/2}. \tag{3.70}$$

Close enough to the QLB transition, the integral in momentum space is dominated by the shell $q = 1$. Therefore one can crudely assume that the kernel $G^{(2)}_{q=1}(\tau)$ decays as

$$G^{(2)}_{q=1}(\tau) \sim \exp(-\sqrt{\Gamma}\tau). \tag{3.71}$$

This looks like a Feynman polaron [65, 66, 67, 68] with the effective mass increasing smoothly as a function of α.

3.6.2 Large Dissipation Limit: Classical Field

When quantum fluctuations of the field are suppressed by taking the limit $\gamma \to \infty$, the only Matsubara frequency contributing to the summation in temporal kernel is the $n = 0$ term. We shall mention here that in our formulation, following the usual convention, we have absorbed $1/\zeta_{q_0} \equiv 1/\zeta$, the coefficient of ω_n^2 (let us call it the mode effective mass) in the definition of the coupling constant and set it equal to unity. Therefore we

need to take $\gamma \to \infty$ to reach the classical field limit. However, if we leave the effective mass of the mode as a free parameter, then $1/\zeta \to \infty$ limit, also serves as a classical field. From the experimental point of view, the latter is constrained by the zero-point motion of the Bose atoms, namely they should be of the same order of magnitude for the spatial order to emerge. On the other hand, a lossy environment could be more easily provided.

This limit corresponds to the Born-Oppenheimer approximation where a quantum particle interacts with a quasi-static configuration of the surrounding medium. In this limit, the kernel is independent of time and reduces to

$$G_q = [\beta(\chi(q-1)^2 + \Gamma)]^{-1}. \tag{3.72}$$

The effective action for the particle then reads:

$$\mathcal{S} = -\int_0^\beta \mathrm{d}s\, \frac{1}{2}\left|\frac{\mathrm{d}\mathbf{R}}{\mathrm{d}s}\right|^2 + \alpha \int \mathrm{d}^3q\, G_q \int_0^\beta \int_0^\beta \mathrm{d}s\mathrm{d}s' \exp[i\mathbf{q}.(\mathbf{R}(s) - \mathbf{R}(s'))]. \tag{3.73}$$

We need a criterion for the appearance of a self-trapped state. Assume that the trajectories $\mathbf{R}(s)$ that dominate the path integration in the partition function

$$\mathcal{Z} = \int \mathcal{D}[\mathbf{R}(s)] \exp(\mathcal{S}), \tag{3.74}$$

are confined isotropically in a spherical region around the origin and then, *a-posteriori*, verify the assumption. At low temperatures, the factor

$$f_q \equiv \beta^{-1} \int_0^\beta \mathrm{d}s' \exp[i\mathbf{q}.\mathbf{R}(s')], \tag{3.75}$$

samples a long trajectory and thus depend only on the magnitude q of the wavevector. The action can be written as:

$$\mathcal{S} = -\int_0^\beta \mathrm{d}s\, \frac{1}{2}\left|\frac{\mathrm{d}\mathbf{R}}{\mathrm{d}s}\right|^2 + \alpha\beta \int \mathrm{d}^3q\, G_q f_q \int_0^\beta \mathrm{d}s \exp[-i\mathbf{q}.\mathbf{R}(s)]. \tag{3.76}$$

A self-consistency condition for f_q is then

$$\frac{\mathrm{d}}{\mathrm{d}\alpha}F(\alpha) = -\beta \int \mathrm{d}^3q\, G_q |f_q|^2, \tag{3.77}$$

with $F = -1/\beta \ln \mathcal{Z}$. After integrating over the angular directions of the wavevector, the action reduces to

$$\mathcal{S} = -\int_0^\beta \mathrm{d}s\, \frac{1}{2}\left|\frac{\mathrm{d}\mathbf{R}}{\mathrm{d}s}\right|^2 - \int_0^\beta \mathrm{d}s\, U(R(s)). \tag{3.78}$$

where

$$U(R) = 4\pi\alpha\beta \int_0^\infty \mathrm{d}q\, q\, G_q f_q \frac{\sin(qR)}{R}. \tag{3.79}$$

This expression resembles the action of a particle in the radial potential $U(R)$. If this radial potential has one or more bound states, then the lowest bound state is isotropic and the path integral, indeed would be dominated at low temperatures by isotropic trajectories, as assumed. In order to determine whether there are bound states, we note that the integration over q is dominated (in dimensionless space) by $q = 1$ since G_q is peaked at $q = 1$ close to the transition. It follows that

$$U(R) \approx \frac{2\sqrt{2}\pi^2\alpha f_1}{\sqrt{\chi\Gamma}} \frac{\sin R}{R}. \tag{3.80}$$

For negative f_1 this represents a potential well near the origin (the case of interest), and for positive f_1 a repulsive potential. For small R, one can expand $U(R)$ to the second order in R, which leads for negative f_1 to a three dimensional harmonic oscillator potential:

$$U(R) \approx \frac{2\sqrt{2}\pi^2\alpha f_1}{\sqrt{\chi\Gamma}}(1 - R^2/3! + ...). \tag{3.81}$$

The ground-state energy level of the harmonic oscillator lies a distance $\Delta\epsilon = \frac{3}{2}\hbar\omega_0$ above $U(0)$, where $\omega_0 = \sqrt{\frac{4\pi\alpha|f_1|}{3\sqrt{\chi\Gamma}}}$. An approximate condition for the existence of at least one bound state is obtained by demanding that the lowest energy level $E(\alpha) = U(0) + \Delta\epsilon$ of the harmonic oscillator is negative. Here

$$E(\alpha) = -\frac{2\sqrt{2}\pi^2\alpha|f_1|}{\sqrt{\chi\Gamma}} + \frac{3}{2}\sqrt{\frac{2\sqrt{2}\pi^2\alpha|f_1|}{3\sqrt{\chi\Gamma}}}, \tag{3.82}$$

and consequently,

$$\alpha_c > \frac{3\sqrt{2}}{16\pi^2}\frac{\sqrt{\chi\Gamma}}{|f_1|}. \tag{3.83}$$

In the low temperature limit, with $F(\alpha) \simeq E(\alpha)$, the self-consistency condition for f_1 reduces to

$$-2\sqrt{2}\pi^2|f_1| + \frac{3}{4}\sqrt{\frac{2\sqrt{2}\pi^2\sqrt{\chi\Gamma}|f_1|}{3\alpha}} = -2\sqrt{2}\pi^2|f_1|^2. \tag{3.84}$$

Recalling that the minimum α value for a bound-state is $\alpha = \frac{3\sqrt{2}}{16\pi^2}\frac{\sqrt{\chi\Gamma}}{|f_1|}$ and inserting this into the self-consistency condition gives, $\sqrt{2}|f_1| = 2\sqrt{2}|f_1|^2$, with solutions $f_1 = 0$ and $f_1 = -1/2$. Taking the second solution to be the bound-state gives the final result

$$\alpha_c > \frac{3\sqrt{2}}{8\pi^2}\sqrt{\chi\Gamma}\,, \tag{3.85}$$

Therefore we see that, in the opposite limit of $\gamma \to \infty$, where the quantum fluctuations of the field are suppressed and only the $n = 0$ term remains (corresponding to MF classical static structure factor $\sim 1/[\chi(q-1)^2 + \Gamma]$, the model reduces to the Landau-Pekar theory of the small polaron. The effective mass indeed undergoes a discontinuous jump as a function of increasing coupling constant at a critical value $\alpha_c \sim \sqrt{\chi\Gamma}$. From Fig.3.6(a), as the damping coefficient is reduced, the effective mass discontinuity is reduced and goes to zero at a critical point.

According to Fig.3.5, the critical value of the critical coupling constant for the transition between the large and small polarons is strongly reduced as one approaches the ordering transition of the BEC. This is an important result: the transition from large to small polaron can be induced much easier in a BEC near the ordering transition.

3.6.3 Phase Diagrams

In this part, we calculate the effective mass and self-energy of the polaron in the general case of finite dissipation and temperature. The discontinuity of the effective mass occurs at a line of first order transitions which terminates as either the thermal fluctuations or the quantum fluctuations of the field is enhanced; see Figs. (3.6,3.7).

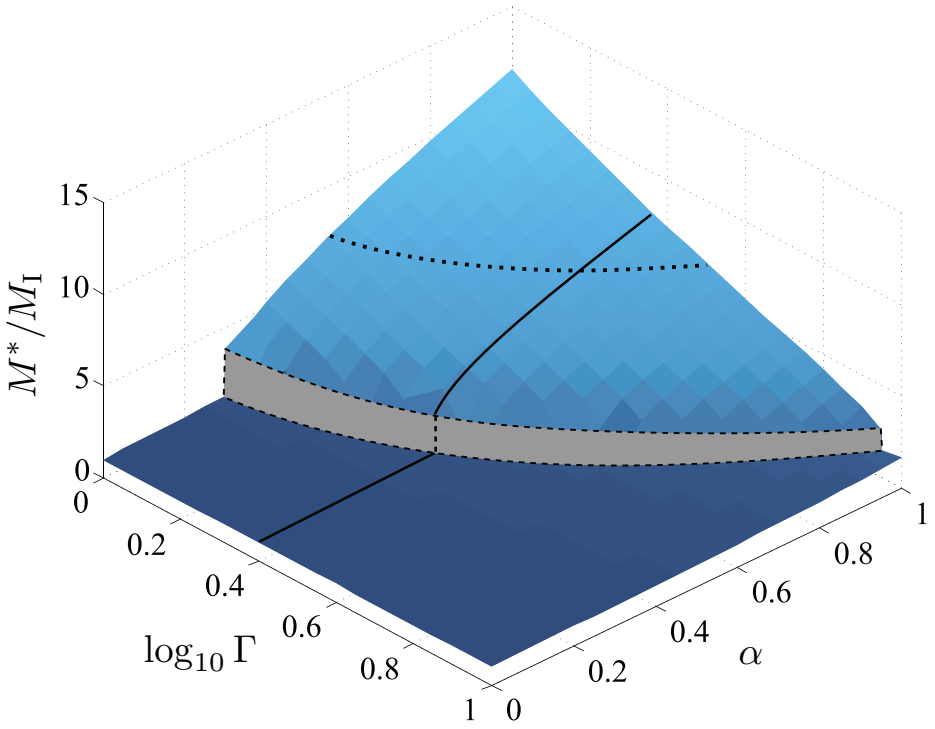

Figure 3.5: Effective mass versus dimensionless distance from the ordering transition Γ. Other parameters are set to: $\beta = \chi = \gamma = 100$.

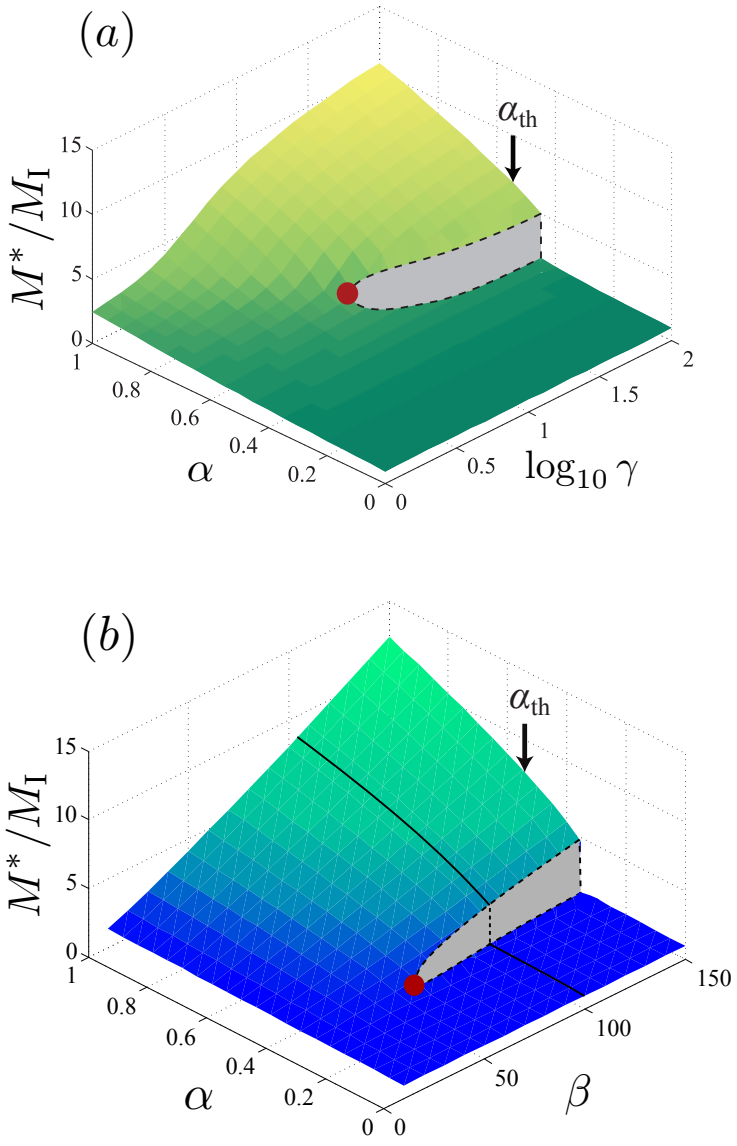

Figure 3.6: Effective mass versus dimensionless coupling constant and (a) dissipation, (b) temperature. Other parameters are set to: (a) $\beta = \chi = 100$ and $\Gamma = 1$, (b) $\gamma = \chi = 100$ and $\Gamma = 1$. In (a) and (b) the red dots indicate the critical points where the discontinuity of the effective mass closes. The dark arrows marked by $\alpha_{\rm th}$ corresponds to the value of the dotted line in Fig. 3.5, i.e. $\gamma, \beta \to \infty$, at $\Gamma = 1$.

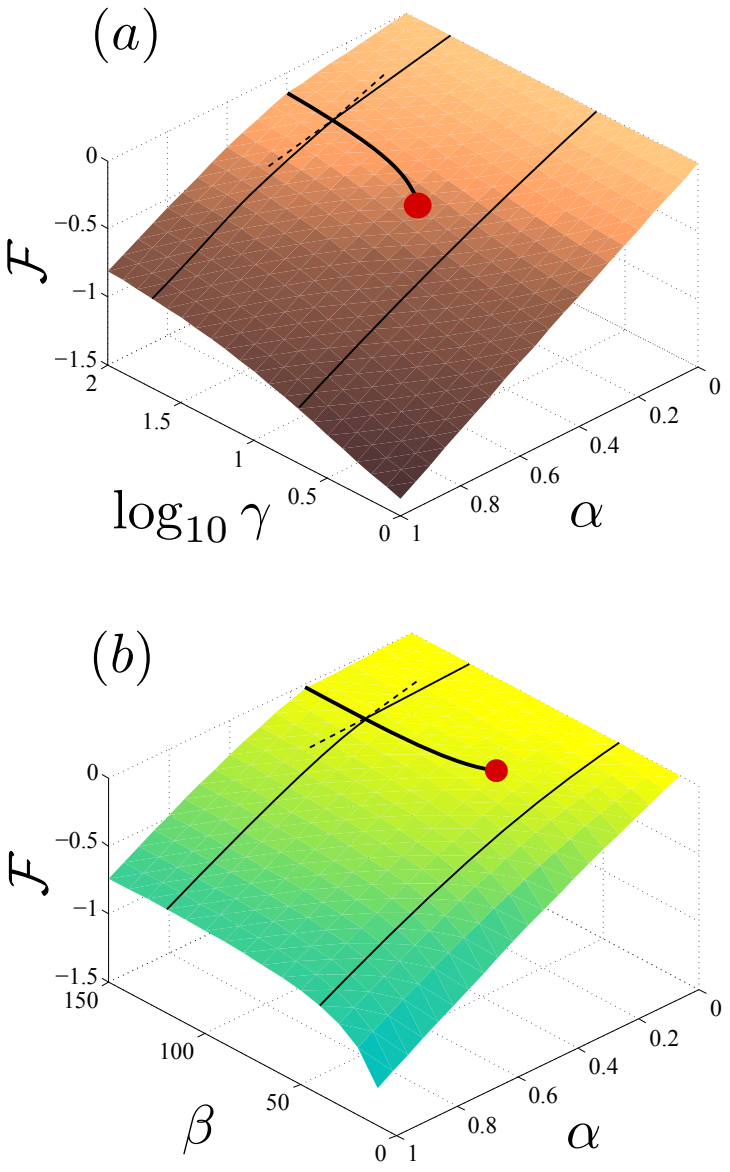

Figure 3.7: Free energy versus dimensionless coupling constant and (a) dissipation, (b) temperature. Other parameters are the same as those in Fig. 3.6. The red dots, again indicate the critical point, where the effective mass jump closes.

3.7 Conclusions

In this section, we first introduced the theory of trapped ultracold Bose gases and the effect of mobile impurities in them. We discussed how the Bogoliubov transformation can be applied to map the problem onto a Fröhlich Hamiltonian, the standard framework of the field-polaron model. Using this approach we presented the physics of Bose-polaron. As the Bogoliubov excitations look like acoustic phonons in the long wavelength limit, the behavior of the effective mass of the polaron, seems to be similar that of the acoustic polaron. The latter shows dramatic momentum cutoff dependence. As the cutoff is increased beyond certain values, the transition between extended (small coupling) to self-trapped (large coupling) shows a kink-like point, where the derivative of the effective mass becomes discontinuous.

Next, we introduced the theory of ultracold Bose gases in cavities, with a focus on multimode cavities. We discussed the main steps of the derivation of the effective action for the density field, and observed that the order parameter follows the scenario of a quantum Landau-Brazovskii first order transition. We then introduce a dilute impurity gas to the system. We studied the Bose-polaron physics away from the ordering transition, as a function of other parameters such as the dissipation of the order-parameter field and the effective temperature. We find that at zero temperature and infinite damping, (*i.e.* when quantum fluctuations of the bath are suppressed), the particle undergoes a first order transition. Adding either one of these sources of fluctuations, smears the jump in the effective mass. The gap finally closes at separate second-order critical point (similar to that of the liquid-gas transition). We note that although a similar behavior has been observed in acoustic polarons, in the latter the cause of jump-like self-trapping transition is the short wavelength fluctuations as the jump appears beyond a certain sharp cutoff, namely the edge of the Brillouin zone. In our model, the effective mass is insensitive to the cutoff and is instead dictated by a local mode q_0, which is not dependent on the microscopic details of the Bose gas. In fact as suggested q_0^{-1}, turns out to

be of the order of many interatomic distances. We also plot the phase diagram of effective mass versus coupling constant and the distance from the transition point. However we keep the distance large enough such that the nonlinear effects are not crucially important and can be neglected. We observe that as we move close to the transition, the transition to the self-trapped state is facilitated by the large fluctuations of the order parameter, and thus happens at a smaller coupling constant. We compared this with an analytical result obtained from self-consistent approximation at infinite damping and zero temperature.

In the next chapter, we devise a method for studying the impurities very close to the Brazovskii spatial ordering transitions, where the nonlinearities become important, so the perturbative solutions fail, and indeed a new type of interesting solutions appear: the solitons. We show how the new soliton state appears upon increasing the impurity-boson interactions; hence called the impurity-induced solitons.

CHAPTER 4

Solitons in Bose-Einstein Condensates

Bose-Einstein condensates are the matter analogues of light, where a condensate of photons give rise to coherent propagation of the electromagnetic waves. Bose-Einstein condensates are commonly described by the so-called nonlinear Gross-Pitaevski equation, which accounts for the self-interaction of the condensate. Gross-Pitaevskii equation is a mean-field model, very similar to the nonlinear Schrödinger equation. The latter is a key component in the field of nonlinear optics. Therefore BEC systems are promising candidates to be probed and gain insight into various systems from. The successful description of BECs by a mean-field model is due to the long-range (macroscopic) coherence of the wave-function. In the previous chapter, we studied the low-lying excitations in a condensate, by means of Bogoliubov transformation and approximation. Bogoliubov theory is a perturbation around the Gross-Pitaevskii equation which gives us the effective action of the fluctuations around the vacuum state. There are other types of solutions which are not predicted in this approach. These are the nonlinear solutions, e.g. solitons. Solitons in general refer to stable localized waves (envelopes) which propagate in a shape-preserved manner.

As mentioned above, a natural consequence of the nonlinear Gross-Pitaevski equation is the appearance of non-dispersive solutions, "solitons", which are stabilized agains dispersion, by a quartic nonlinear term. Indeed, the BEC solitons arise "spontaneously" as the system crosses the condensation transition, a second order symmetry breaking transition. If the interatomic interaction of the bosons is repulsive ($g_{\rm BB} > 0$ and thus $a_{\rm BB} > 0$), only dark solitons are allowed. In nonlinear optics the "dark" soli-

tons are the nonlinear solutions indicating the local "low-intensity" regions. The same term is thus being used for matter fields such the wave-function of a Bose-Einstein condensate. Alternatively, attractive interaction allows for "bright" solitons, where the amplitude of the soliton is above the homogeneous background density of the condensate. The solitonic solutions of nonlinear Gross-Pitaevskii occur concurrently in the amplitude and the phase of the Bose-Einstein condensate. The phase jump at the position of the density minimum, gives the dark solitons a topological nature (discussed below; also see Fig. (4.1)). One of the experimental methods for manipulating the wave-function is the quantum phase engineering. For instance, solitons in BECs can be generated by optical phase imprinting [94].

4.1 Solitonic Solutions of the Gross-Pitaevskii Equation

In this section we briefly overview the soliton solutions of the Gross-Pitaevskii equation. We start with the one-dimensional version of this equation in the absence of external potential of the trap.

$$\left(i\hbar\frac{\partial}{\partial t} + \frac{\hbar^2}{2M_{\rm B}}\frac{\partial^2}{\partial x^2} - g_{\rm BB}|\Psi(x,t)|^2 + \mu \right)\Psi(x,t) = 0. \tag{4.1}$$

where n_0 is the density of the condensate, $g_{\rm BB} = 4\pi\hbar^2 a_{\rm BB}/M_{\rm B}$ is the self-interaction of the BEC, and $\mu = g_{\rm BB}n_0$ is the chemical potential. The characteristic length scale dictated by the differential operator is $\ell_0 = \hbar/\sqrt{M_{\rm B}n_0 g}$. Therefore, Eq. (4.1) is a valid description of the macroscopic wave-function, as long as ℓ_0 is much larger than the mean inter-particle distances, *i.e.* $\ell_0 \gg 1/(n_0\sigma)$, where σ is the transverse cross section of the BEC.

4.1.1 Dark Solitons

Solitons can be considered as particle-like excitations. One can assign a degree of freedom, like a position and a conjugate velocity. For positive boson-boson scattering

length $a_{BB} > 0$, and thus $g > 0$, there exists a dark soliton solution with the $y-z$ nodal plane moving with velocity v in the x direction. This is expressed as:

$$\Psi(x,t) = \sqrt{n_0} e^{-i\mu t/\hbar} \left[\frac{iv}{c_S} + \sqrt{1 - v^2/c_S^2} \tanh\left(\sqrt{1 - v^2/c_S^2}\, (x - x_0)/\ell_0 \right) \right]. \quad (4.2)$$

in which x_0 is the location of the nodal plane on the x-axis (coordinate of the soliton as a particle), and c_S is the speed of sound:

$$c_S = \sqrt{\frac{g n_0}{M_{\rm B}}} \quad (4.3)$$

It is assumed that the velocity of the soliton v is smaller than the speed of sound: $v < c_S$. The energy of this state is:

$$\mathscr{H} = \frac{1}{3} \mathscr{M} c_S^2 \, (1 - v^2/c_S^2)^{3/2}, \quad (4.4)$$

where $\mathscr{M} = 4 n_0 \sigma \ell_0 M_B$, is the inertial coefficient of the soliton. If the velocity of the nodal plane is much smaller than the speed of sound: $v \ll c_S$, we get:

$$\mathscr{H} = \frac{1}{3} \mathscr{M} c_S^2 - \frac{1}{2} \mathscr{M} v^2. \quad (4.5)$$

4.1.2 Bright Solitons

For negative scattering length ($a_{BB} < 0$), corresponding to attractive interaction ($g < 0$), the soliton solutions is called a "bright" soliton. In principle, the attractive interaction allows for collapse of the wave-function. The Gross-Pitaevskii equation, or equivalently the nonlinear Schrödinger equation, admits singular or spreading solutions, in the presence of a focusing nonlinearity (*i.e.* negative scattering length). In two dimensions, collapse occurs when the total number of atoms exceeds a critical value. In three dimensions, however, the collapse may happen for any number of atoms. For a quasi-one-dimensional gas which is trapped in the radial direction with frequency ω_r, we define the radius of the trap

$$a_r = \sqrt{\frac{\hbar}{M_{\rm B} \omega_r}}. \quad (4.6)$$

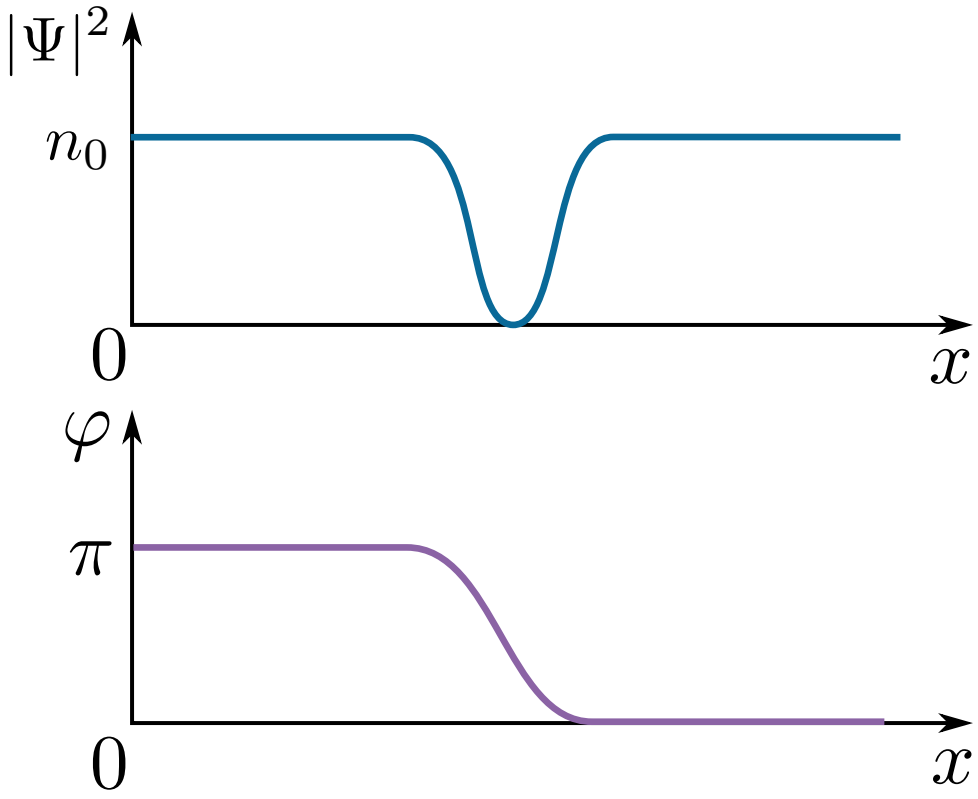

Figure 4.1: Top panel shows the density $|\psi(x)|^2$ of the BEC. The dip indicates the dark soliton. The bottom one depicts the phase of the wave-function $\varphi(x)$. The figure corresponds to the phase jump $\Delta\varphi = \pi$, where the density of the BEC locally reduces to zero, *i.e.* dark soliton.

The bright soliton is then expressed by the following expression:

$$\Psi(x,t) = \frac{a_r}{\sqrt{2|a_{\rm BB}|\kappa}}\,\mathrm{sech}\left(\frac{x-vt}{\kappa}\right)\exp\left[\frac{i}{\hbar}M_B v\,x - \frac{i}{\hbar}\left(\frac{M_{\rm B}v^2}{2} - \frac{\hbar^2\kappa^2}{2M_{\rm B}}\right)t\right]. \tag{4.7}$$

Here $\kappa = a_r^2/(|a_{\rm BB}|N)$ is the width of the soliton envelope.

4.2 Impurity-induced Solitons of BECs in Multimode Cavities

As discussed in the previous chapter, above the mean-field Brazovskii transition, in the large damping limit and/or at small temperatures, the impurity acquires either extended or self-trapped states for small and large couplings, respectively. We observed that adding the quantum fluctuations of the field, for example by decreasing the dissipation and allowing more Matsubara frequencies to contribute, finally closes the discontinuity of the effect mass at a critical point. On the other hand, increasing the thermal noise amounts qualitatively to the same effect, *i.e.* closes the jump of the effective mass at a distinct critical point.

We can get the system progressively closer to the mean-field transition point by cranking up the laser intensity closer to the mean-field threshold. For systems in spatial dimensions $D \geq 2$, the phase-space volume of the fluctuations corresponding to the modes around $q = q_0$, and consequently the entropic cost of these fluctuations, eventually become so large that the system avoids the second order critical point, and instead pays the latent heat expense, by jumping discontinuously to a non-zero minimum, which emerges during the renormalization procedure.

According to the renormalization flow of the parameters as a function of the dimensionless mean-field distance to the critical point Γ, the renormalized quartic coefficient $\bar{u}$ flips sign at around $\Gamma \simeq -3.5$. At this value of Γ, the renormalized distance to the critical point is $\bar{\Gamma} \simeq 1$. Therefore we see that for negative values of Γ, the nonlinear effects have to be taken into account. Practically this can be done by replacing the bare parameters with the renormalized ones, in the *full* bare action.

- **Below the Mean-field Critical Point of Quantum Brazovskii Model, $\boldsymbol{\Delta \lesssim 0}$:**

We start with the full Lagrangian again:

$$L_{\mathrm{B}} = \frac{1}{\Omega} \sum_{\mathbf{q}} \frac{\hbar}{\zeta_q} \left(|\dot{\rho}_{\mathbf{q}}|^2 - \omega(\mathbf{q})^2 |\rho_{\mathbf{q}}|^2 \right) + L_{\mathrm{NL}}. \tag{4.8}$$

For negative Δ, the non-linear terms of Eq. (4.8) must be taken into account. It can be shown that only even terms need to be included [74, 75]:

$$L_{\rm NL} = -u \int \mathrm{d}^3 r \, |\rho(\mathbf{r})|^4 - w \int \mathrm{d}^3 r \, |\rho(\mathbf{r})|^6 \, . \tag{4.9}$$

In order to perform the functional integrals for this non-linear case, first expand the free energy $F[\mathbf{R}(s)]$ in a Taylor expansion in powers of the impurity pseudopotential $g_{\rm IB}$. Then perform, term by term, the functional integrals using the non-linear action. The zero-order term in the expansion is the partition function of the condensate in the absence of the particle. The first order term is

$$F^{(2)}[\mathbf{R}(s)] = \frac{-g_{\rm IB}^2}{2!} \sum_{\mathbf{q},n} \mathcal{G}_q^{(2)}(\omega_n) \iint_0^\beta \mathrm{d}s \mathrm{d}s' e^{i\mathbf{q}\cdot[\mathbf{R}(s)-\mathbf{R}(s')]}. \tag{4.10}$$

Here, $\mathcal{G}_q^{(2)}(\omega_n)$ is the *full* two-point Green's function of the non-linear bare system. The second order term contains the full four-point vertex function of the pure system. These full correlation functions are obtained by a second expansion, now in powers of $L_{\rm NL}$. The non-linear terms can be included by the renormalization group method [74, 75]. To one-loop order, this leads to a renormalization of Δ to $\bar{\Delta}$ with

$$\bar{\Delta} \simeq \Delta + \mathcal{P} u \ln(\Delta_c/\bar{\Delta}), \tag{4.11}$$

where $\mathcal{P} \propto {q_0}^2$ and Δ_c a high-energy cutoff. The effective gap $\bar{\Delta}$ of the spectrum remains positive for negative values of Δ. The renormalized quartic coefficient $\bar{u}$ is given by

$$\bar{u} \simeq u \frac{1 - u\Pi}{1 + u\Pi}, \tag{4.12}$$

with $\Pi = \mathcal{P}/\bar{\Delta}$; so $\bar{u}$ becomes negative if the effective gap $\bar{\Delta}$ drops below $\mathcal{P}u$ (which happens for slightly negative Δ). The functional integral over the renormalized quadratic Lagrangian no longer suffers from strong fluctuations, even for negative $\bar{u}$. For negative $\bar{u}$ and decreasing Δ, a first-order phase transition takes place at

$$\bar{u}^2 = 4\hbar\bar{\Delta} w/\zeta. \tag{4.13}$$

At the transition, the modulation amplitude changes discontinuously from the symmetric phase $\rho = 0$ to the symmetry-broken phase at

$$\rho = \sqrt{2}(\hbar\bar{\Delta}/\zeta|\bar{u}|)^{1/2} \, . \tag{4.14}$$

Although the mean-field correlation length diverges at the second-order critical point, renormalization suggests that the correlation length remains finite at the first-order QLB transition. The correlation length at the ordering transition is

$$\xi = \mathcal{R}\sqrt{\lambda/\bar{\Delta}} \, . \tag{4.15}$$

This renormalized action $\mathcal{S}_{\mathrm{T}}^{\mathrm{R}}$ has the same form as the bare action $\mathcal{S}_{\mathrm{T}}$ but with u and Δ replaced by the renormalized ones: it can be analyzed by MF theory plus fluctuation corrections.

4.3 Static Impurities (Local Defects)

In this section we study the effect of the static impurities with a local potential, on a Brazovskii field, very close to its first order phase transition. In one dimension an exact solution is presented. In higher dimensions, in particular in three dimensions, we resort to a variational ansatz for the radial modulation profile of the field. The ansatz is of the form which can be obtained from linear-response theory.

4.3.1 Exact Solution in One Dimension

The mean-field Brazovskii free energy is minimized by a density modulation with the preferred wave-vector q_0:

$$\rho(x) = A \, \exp(iq_0 x) + \text{c.c.} \, . \tag{4.16}$$

By substituting the ansatz into the Brazovskii action, and keeping terms up to q^2, *i.e.* up to second order derivative ∇^2, we obtain an effective action for the modulation amplitude.

When the static impurity is added to the system, the modulation amplitude at the location of the impurity, serves as a free parameter which should determined by minimizing the total energy cost of the impurity interaction and that of the deformation of the field.

The energy cost of a soliton certainly depends on the value of the field at the boundaries. At the transition, the two vacua of the system corresponding to disordered and ordered phases are degenerate. Trivial homogenous solutions arise from the uniform boundary conditions, that is constant at the boundary (type I). The trivial solution is that the value of the order parameter remains constant across the system. Other types of boundary conditions can be imposed; for instance, in one dimension, one might demand that the boundary values are different at the two ends $x \to \pm\infty$ (type II). Then the saddle-point solution, namely the lowest energy field configuration is called a "kink". The kink solutions starts from the value at one end, remain mainly close to this value until a point far from the ends where the field amplitude is changed to the value at the other end. This decay occurs over the correlation length, which is finite at the first order transition, and small compared to the system size. It is worth mentioning that under the former boundary condition, and on top of the trivial uniform solution, there exist solutions consisting of even number of kinks. Configurations with odd number of kinks can be considered as excitations corresponding to the second type of boundary conditions.

We, in this section, are facing a new set of constraints: (i) the usual type I boundary conditions, plus (ii) a non-zero value at the origin, which should be found by minimizing the free energy. We name such soliton solutions, "droplets". A droplet is a local modulation of the ordered phase, embedded in the bulk disordered phase. At the transition and assuming that the field is cooled down from the high temperature phase, the nucleation of a droplet is in fact causes the coexistence of the phases which are separated apart by a domain-wall (kink) of the size of the correlation length.

$$\mathcal{F}[A(x)] = \int_{-\infty}^{+\infty} \mathrm{d}x \left\{ \lambda \mathcal{R}^2 \left(\frac{\mathrm{d}A(x)}{\mathrm{d}x} \right)^2 + \mathcal{V}(A(x)) \right\}. \tag{4.17}$$

According to our constraints, that is a non-zero value of A at the origin, we know that the everything is symmetric under parity transformation: $x \to -x$. We assume that the value of the field at the origin is some value A^*. Above the transition, any modulation on top the uniform field is costly. If the field is pinned at a non-zero value at the origin, it will have to fall down to the Gaussian minimum corresponding to the disordered phase. Right at the transition, the minima are degenerate. Upon imposing the aforementioned boundary conditions, the field is again forced to decay to zero (see Fig. (4.2)). We will calculate this deformation cost in the following. This situation is however costly, and its energy has to be provided in the actual system by the impurity potential. The value of the field at the origin is then determined by the counterbalancing forces which couple to the field.

In the above equation (4.17), the effective potential for the modulation amplitude is equal to:

$$\mathcal{V}(A(x)) = -V_0 \delta(x) A + \frac{\hbar \bar{\Delta}}{\zeta} A^2 + \bar{u} A^4 + w A^6. \tag{4.18}$$

We note that $\bar{u} < 0$. The Euler-Lagrange equation derived from minimizing the free energy in Eq. (4.17) reads:

$$\frac{\mathrm{d}^2 A(x)}{\mathrm{d}x^2} = \frac{1}{2\lambda \mathcal{R}^2} \frac{\mathrm{d}\mathcal{V}(A)}{\mathrm{d}A}. \tag{4.19}$$

For $x \neq 0$, the equation is that of the bare (*i.e.* without the impurity, but renormalized) field. We now need to calculate the total free energy of the system under the condition that the field is, after minimization, pinned at $A(x = 0) = A^*$, and decays to $A(x \to \infty) = 0$, following the Euler-Lagrange equation. The total free energy can be written in two terms:

$$\mathcal{F}(A^*) = -V_0 A^* + \mathcal{F}_{\text{drop}}(A^*) \, . \tag{4.20}$$

The two terms on the r.h.s arise respectively from the impurity and self-interaction of the field. As mentioned above, the system is invariant under parity. Therefore we know

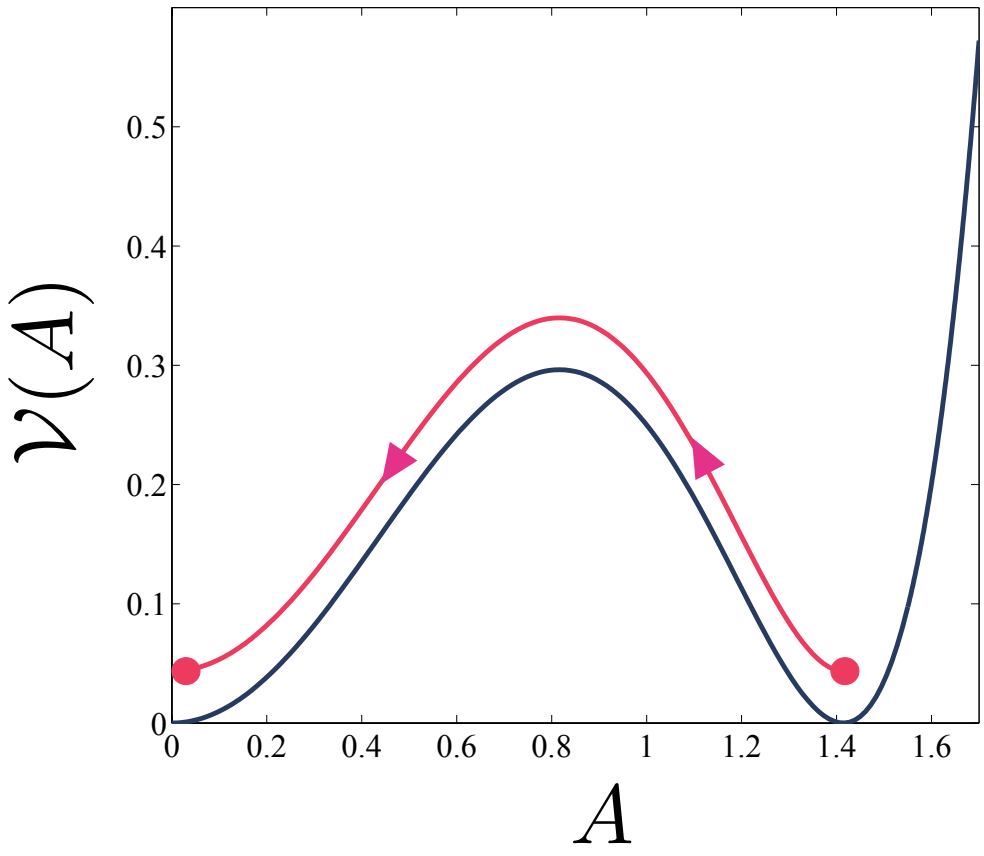

Figure 4.2: Dimensionless effective potential energy $\mathcal{V}(A)$, of the modulation coordinate A. At the transition, the potential clearly has a minimum at $A = \sqrt{2}$. The red curve with arrows, represents a saddle-point solution of the Euler-Lagrange equation, under the boundary condition that the field modulation at $x \to -\infty$ is pinned at $A = \sqrt{2}$, and goes to $A = 0$ at $x \to +\infty$.

that any such solution consists of two kink-like solutions, which are connected to one another at the origin. We call this a droplet. Thus,

$$\mathcal{F}_{\text{drop}} = 2\mathcal{F}_{\text{kink}}. \tag{4.21}$$

Consequently it suffices to calculate the kink energy as a function of its value at the origin. The kink energy is:

$$\mathcal{F}_{\text{kink}} = 2\lambda\mathcal{R}^2 \int_0^{+\infty} \mathrm{d}x \left\{ \frac{1}{2} \left(\frac{\mathrm{d}A}{\mathrm{d}x} \right)^2 + \overline{\mathcal{V}}(A) \right\}. \tag{4.22}$$

Here $\overline{\mathcal{V}}(A) = \mathcal{V}(A)/(2\lambda\mathcal{R}^2)$. Now using Euler-Lagrange equation we get:

$$\int_0^{+\infty} \mathrm{d}x \left\{ \frac{1}{2} \left(\frac{\mathrm{d}A}{\mathrm{d}x} \right)^2 + \overline{\mathcal{V}}(A) \right\} = \int_0^{A^*} \mathrm{d}A \sqrt{2\,\overline{\mathcal{V}}(A)}. \tag{4.23}$$

We note that we can exploit this relation *only* in one dimension. Therefore the total free energy of the system is:

$$\begin{aligned} \mathcal{F}(A^*) &= -V_0 A^* + 4\lambda\mathcal{R}^2 \int_0^{A^*} \mathrm{d}A \sqrt{2\,\overline{\mathcal{V}}(A)} \\ &= -V_0 A^* + 4\sqrt{\lambda\mathcal{R}^2} \int_0^{A^*} \mathrm{d}A \sqrt{(\hbar\bar{\Delta}/\zeta)A^2 + \bar{u}A^4 + wA^6}. \end{aligned} \tag{4.24}$$

At the transition there exist a relation between the coefficients: $\bar{u}^2 = 4w\hbar\bar{\Delta}_c/\zeta$, where $\bar{\Delta}_c$ is the value of the gap at the Brazovskii transition. By rescaling the field amplitude to, $\mathscr{A} = A\sqrt{\zeta\bar{u}/\hbar\bar{\Delta}_c}$, we can rewrite the free energy as:

$$\begin{aligned} \mathcal{F}(\mathscr{A}^*) &= -V_0 \sqrt{\hbar\bar{\Delta}_c/\zeta\bar{u}}\,\mathscr{A}^* \\ &\quad + 4\sqrt{\lambda\mathcal{R}^2} \left(\frac{\hbar\bar{\Delta}_c}{\zeta\bar{u}} \right)^{3/2} \int_0^{\mathscr{A}^*} \mathrm{d}\mathscr{A} \sqrt{\mathscr{A}^2 - \mathscr{A}^4 + \frac{1}{4}\mathscr{A}^6}. \end{aligned} \tag{4.25}$$

Note that the minimum of the new potential of the field $\mathscr{A}$ is at $\mathscr{A} = \sqrt{2}$. We define the dimensionless function $g(x)$, as follows

$$g(x) = \int_0^x dy \sqrt{y^2 - y^4 + \frac{1}{4}y^6}. \tag{4.26}$$

This is shown in figure (4.3).

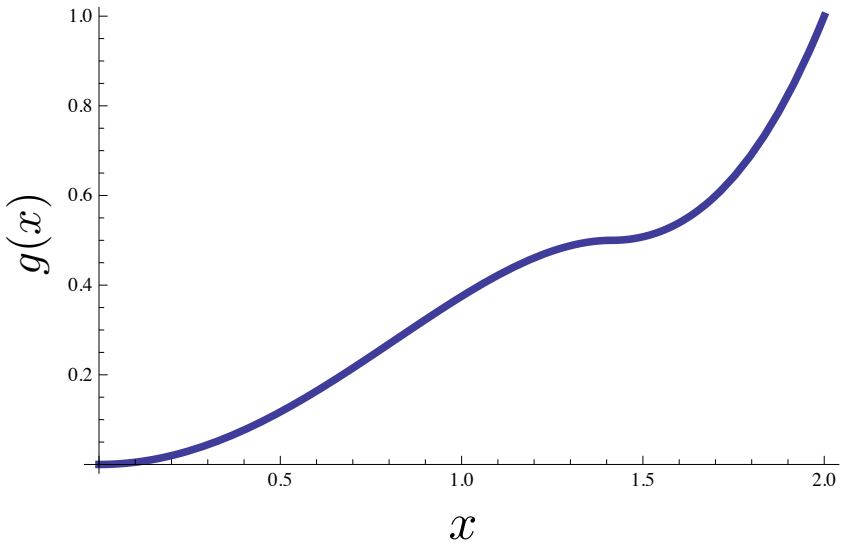

Figure 4.3: Dimensionless energy $g(x)$ of a radial modulation profile as a function of the displacement at the origin.

The plot of $g(x)$ shows that this function is monotonic in x. For small x, $g(x)$ is proportional to x^2. With increasing x, the second derivative of $g(x)$ becomes negative. The slope decreases to zero at $x = \sqrt{2}$ where $g(x)$ has a cusp singularity. For larger x, the slope starts to increase again and the second derivative is positive once again. The intermediate region where $g''(x)$ is negative is unstable. For dimensions above one, this expression is no longer the exact scale function but the qualitative features remain the same.

Using this definition we find:

$$\mathcal{F}(\mathscr{A}^*) \Big/ \sqrt{\hbar\bar{\Delta}_c/\zeta\bar{u}} = -V_0\,\mathscr{A}^* + 4\sqrt{\lambda\mathcal{R}^2}\left(\frac{\hbar\bar{\Delta}_c}{\zeta\bar{u}}\right)^2 g(\mathscr{A}^*). \tag{4.27}$$

The stable solution that minimize this free energy satisfies: $\delta\mathcal{F}/\delta\mathscr{A}^*|_{\mathscr{A}_s^*} = 0$ and $\delta^2\mathcal{F}/\delta\mathscr{A}^{*2}|_{\mathscr{A}_s^*} \geq 0$. When these conditions are applied, the minimizing $\mathscr{A}_s^*$ is obtained as plotted in Fig. (4.4) against the impurity potential.

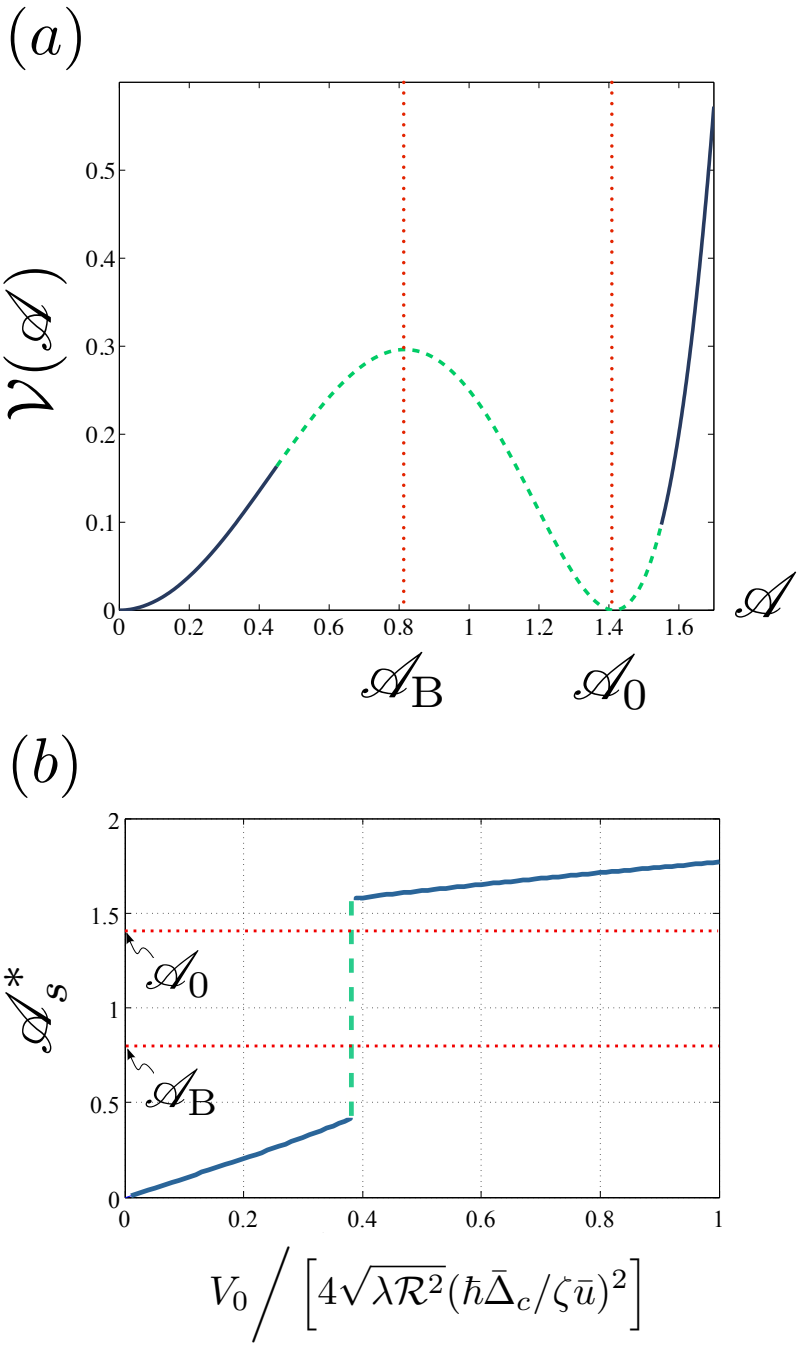

Figure 4.4: The amplitude of the modulation for the exact solution in one-dimension, against the impurity potential V_0.

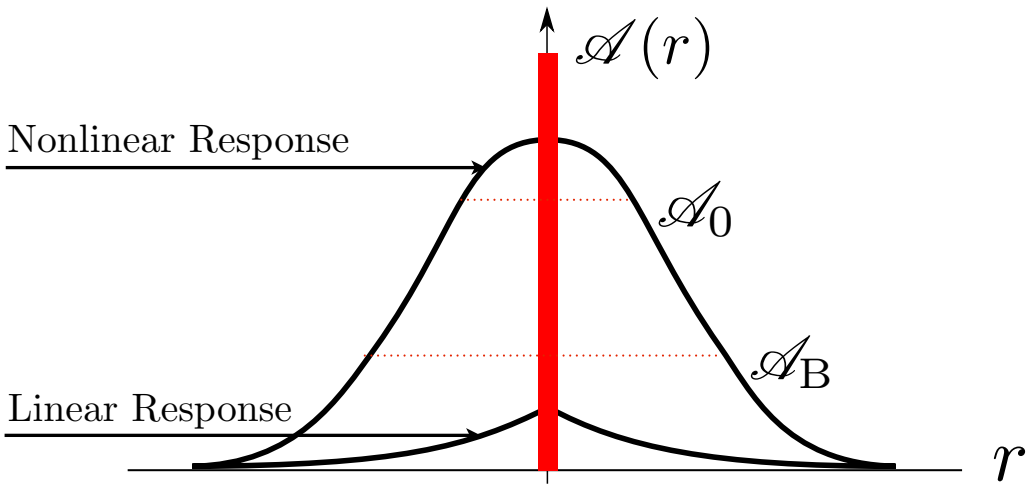

Figure 4.5: The figure shows a schematic of the modulation profile $\mathscr{A}(r)$. The red bar only indicates the location of static impurity and is of no other information. For small values of the external potential of the impurity, the minimizing profile of the field can be found within the linear response theory. As see in Fig. (4.4b), the value of the profile jumps discontinuously close to the other phase, invalidating the perturbative analysis. This is interpreted as nonlinear response regime.

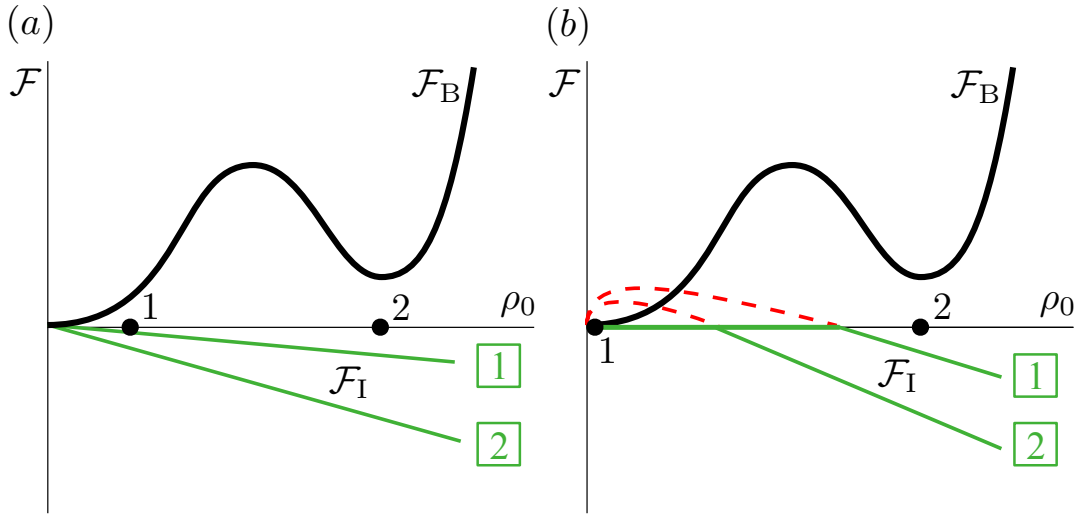

Figure 4.6: Variational free energies as a function of the modulation amplutude ρ_0. The black curves show the condensate energy $\mathcal{F}_{\rm I}(\rho_0)$. The dotted red and solid green curves show the free energy of the impurity for (1) smaller and (2) larger values of pseudopotential. (a) Massive impurities: the free energy of the impurity decreases linearly with ρ_0. The total free energy has minima indicated by 1 and 2. For increasing pseudopotential, the absolute minimum shifts from 1 to 2, corresponding to a transition from the small polaron to the soliton. (b) includes the zero point energy of a bound-state particle, which follows the green curves. The minimum at $\rho_0 = 0$ corresponds to the large polaron. For increasing pseudpotentials, there may be transitions from the large polaron to the small polaron and then to the soliton or a single transition directly from the large polaron to the soliton.

4.3.2 Variational Method in Three Dimensions

As mentioned above, the simplest case of the QLB model is the strong damping limit, when the condensate density modulation can be treated as quasi-static with respect to the dynamics of the impurity. We take $\gamma \to \infty$ to approach the classical field limit. The MF minimization of $\mathcal{S}_{\rm T}^{\rm R}$ leads to a radial density modulation around a static impurity at

the origin of the form

$$\rho(r) = \rho_0 \frac{\sin(q_0 r)}{q_0 r} \exp(-r/\xi). \tag{4.28}$$

Generally $\rho(r)$ retains this form if $q_0 r \gtrsim 1$. Using Eq. 4.28 as a trial function (with ρ_0 the free parameter), leads to non-linear MF free energy cost $\mathcal{F}_{\rm B}(\rho_0)$ for radial density modulations:

$$\mathcal{F}_{\rm B}(\rho_0) \simeq \frac{1}{\pi^2 q_0^3} \left(\frac{2\hbar\bar{\Delta}(q_0\xi)}{\pi\zeta} |\rho_0|^2 + \bar{u}|\rho_0|^4 + \frac{w}{2}|\rho_0|^6 \right) \tag{4.29}$$

where $\mathcal{F}_{\rm B}(\rho_0)$ has in general the form of a double-well potential with one minimum at $\rho_0 = 0$ and a second near the modulation amplitude $\rho^* = \sqrt{2|\bar{u}|/3w}$ of the ordered phase (see Fig.4.6). The second minimum represents the energy cost of a soliton-type spherically symmetric deformation of the condensate, the center of which has the structure of the ordered phase while far from the origin the condensate reduces to the uniform state. At the transition point, the energy cost of the soliton is $\mathcal{F}^* \simeq \frac{8\hbar}{\pi^3 q_0^3 \zeta}(\bar{\Delta}_c|\bar{u}|/w)(q_0\xi)$. If the mass of the impurity is so large ($M_{\rm I} \gg \hbar^2 q_0^2/\rho_0 g_{\rm IB}$) that quantum fluctuations of the impurity can be disregarded, the impurity free energy is $\mathcal{F}_{\rm I} \simeq -|g_{\rm IB}\rho_0|$ as shown in Fig.4.6(a):

For small $g_{\rm IB}$ the absolute minimum of $\mathcal{F}(\rho_0) = \mathcal{F}_{\rm B} + \mathcal{F}_{\rm I}$ as a function of ρ_0 is proportional to $g_{\rm IB}$ (marked "1" in Fig.4.6), which corresponds to the small polaron, while there is a metastable minimum near ρ^* that corresponds to the soliton (marked "2"). For larger values of $g_{\rm IB}$, the absolute minimum jumps near ρ^*. The soliton state has lower energy if

$$\frac{8\hbar}{\pi^3 q_0^3 \zeta}(\bar{\Delta}_c|\bar{u}|/w)(q_0\xi) \lesssim |g_{\rm IB}\rho^*| \, . \tag{4.30}$$

Since $\xi \propto \bar{\Delta}^{-1/2}$, the soliton state necessarily has a lower energy than the polaron state for sufficiently large correlation lengths and hence linear-response theory must break down for sufficiently large correlation lengths. When typical values for a pumped BEC condensate are inserted in this inequality, one finds that the polaron-soliton transition should be experimentally accessible.

4.4 Mobile Impurities: Including the Quantum Fluctuations

We studied the nonlinear saddle-point solutions of the Landau-Brazovskii model in the limit of large damping, where the dynamics of the field is quenched. We further showed that static impurities can locally stabilize the ordered phase, by lowering the free energy density of the field around itself. Therefore a "droplet" of the ordered phase can form (analogous to the "hydration" shell formation), when the impurity is so massive that can be considered static. Next, we include quantum fluctuations of the impurity particle. We intuitively expect this to be a destabilizing effect, which contributes a positive energy cost. This energy cost corresponds to the zero-point motion of the confined particle. However we will observe in this section that, the droplet survives against these quantum fluctuations, provided that certain conditions hold.

The effective Lagrangian is:

$$L_{\rm I} \simeq \frac{1}{2} M_{\rm I} |\dot{\mathbf{R}}|^2 + |g_{\rm IB}\rho_0| \frac{\sin(q_0 R)}{q_0 R} \exp(-R/\xi). \tag{4.31}$$

The impurity free energy $\mathcal{F}_{\rm I}$ is obtained from $L_{\rm I}$ by integrating over particle trajectories. This leads to

$$\mathcal{F}_{\rm I}(\rho_0) \simeq -|g_{\rm IB}\rho_0| + \frac{3}{2}\hbar\Omega(\rho_0) + \dots . \tag{4.32}$$

The first term is the earlier classical limit while the second term is the lowest-order correction due to quantum fluctuations. The natural frequency of the bound state impurity particle in the effective potential is:

$$\Omega(\rho_0) = \left(\frac{|g_{\rm IB}\rho_0| q_0^2}{3M_{\rm I}} \right)^{1/2} . \tag{4.33}$$

The bound state disappears if the right-hand side of Eq. (4.32) is positive, in which case $\mathcal{F}_{\rm I}$ should be set to zero (dotted red lines Fig.4.6(b)). The small polaron minimum is replaced by a minimum at $\rho_0 = 0$ that corresponds to the *large* polaron. The condition for the small polaron to survive in the presence of the zero-point fluctuations of the impurity is $g_{\rm IB} > g_{c1} = \sqrt{\frac{\hbar^3 \bar{\Delta}\xi}{M_{\rm I}\zeta}}$ or $\alpha_c \simeq \sqrt{\chi\bar{\Gamma}}$, which is just the earlier criterium for

Landau-Pekar self-trapping. The soliton state is significantly more stable against zero point fluctuations of the impurity than the small polaron state.

Quantum fluctuations of the condensate are included by treating $\rho_0(t)$ as a time-dependent coordinate with a kinetic energy $K = (2\pi\xi/q_0^2)\left(\mathrm{d}\rho_0(t)/\mathrm{d}t\right)^2$. In the double-well potential, the condensate coordinate now can tunnel between the two minima, allowing for a linear superposition of the small polaron and soliton states. As the strength of the quantum fluctuations of the condensate increases, the soliton state disappears, roughly when the zero point energy of the condensate coordinate exceeds the depth of the well. The transition between small polaron and soliton states can be viewed in terms of a variant of spin-boson model.

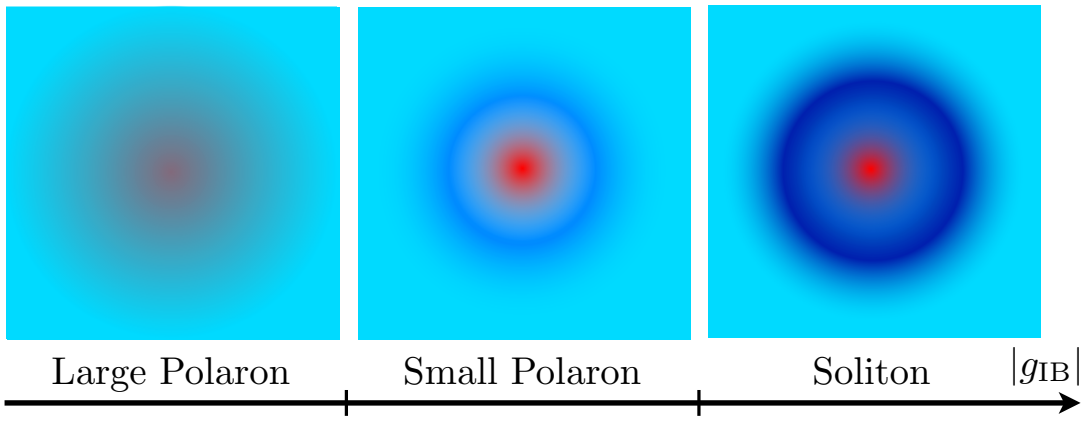

Figure 4.7: The different states of the BEC-impurity system. The blue color indicates the condensate modulation amplitude while the red cloud indicates the particle. From left to right, large polaron, small polaron, and the soliton.

An important concern regarding the soliton solutions is their instabilities in spatial dimensions $D > 1$, due to Derrick's theorem [95]. We show in the following that the coupling with the particle's degree of freedom stabilizes the soliton. Further, Gaussian fluctuations are shown to be irrelevant in $D \geq 2$.

In summary, the QLB theory predicts that impurity particles generate a variety of structures as the excitation spectrum is progressively depressed. Above the MF transi-

tion point, the impurity generates either a large or a small polaronic state, depending on the coupling and damping constant. Below the MF transition—but above the actual ordering transition—a new state appears: the soliton with a self-trapped impurity particle (see Fig.4.7).

4.5 Stability Analysis of Non-topological Solitons in Brazovskii Model

It is well known that any kind of stable solution must survive the fluctuations. The fluctuations can occur in different forms. A famous type of fluctuations is Gaussian fluctuations corresponding to the harmonic oscillations of the order parameter field around the saddle-point solutions. We first study the effect of these fluctuations, in the absence of the impurity. In other words, the stability conditions derived here are universal for the model theory.

Another relevant type of instabilities originate from stretching or compressing the solutions in space. Based on straightforward scaling arguments which utilize the fact that the free energy density of different terms scale differently under scaling the space coordinate, one can determine the stability conditions. This is called the Derrick's theorem, and can be viewed as a variant of the virial theorem.

4.5.1 Gaussian Fluctuations

In order to examine the stability of the soliton solution, we expand the action to quadratic order in fluctuations $\delta\tilde{A}$, so $\tilde{A} \rightarrow \tilde{A} + \delta\tilde{A}$. Here the tildes indicate the dimensionless quantities at the Brazovskii transition. For simplicity, we focus on the system right at the Brazovskii transition. It is clear that the generalization to slightly above the transition is straightforward by expanding the control parameter $\bar{\Delta}$ around its value at the transition. The free energy of the fluctuations reads:

$$\delta F = 2\beta \int \mathrm{d}^3\mathbf{r}\, \{\delta\tilde{A}(r)\hat{\mathcal{K}}\,\delta\tilde{A}(r)\}, \tag{4.34}$$

with

$$\hat{\mathcal{K}} = -\nabla^2 + U(r) \tag{4.35}$$

the operator of a Schrödringer equation with potential

$$U(r) = \frac{1}{2}\partial^2_{\tilde{A}}\tilde{\mathcal{V}}[\tilde{A}(r)]. \tag{4.36}$$

Stability requires all the eigenvalues of $\hat{\mathcal{K}}$ to be positive. When the field — at some distance from the origin — passes over the barrier of $\tilde{\mathcal{V}}(\tilde{A})$, the potential $U(r)$ becomes negative, because of the negative curvature of $\tilde{\mathcal{V}}(\tilde{A})$. The mean field solution is unstable if the ground state of the Schrödinger equation is a negative energy bound state of this potential well.

The ground state energy is greater than the minimum of $U(r)$ by

$$\Delta E = \frac{D}{2}\Omega, \tag{4.37}$$

where Ω is the frequency of small oscillations around the minimum of the potential $U(r_m)$, specifically, $\Omega = |\nabla^2 U|^{1/2}_{r=r_m}$, where r_m is the distance from the origin where U takes its minimum value. In terms of the amplitude $\tilde{A}$, the corresponding minimum is at $\tilde{A}_m = \sqrt{4/5}$ (see Fig. (4.8)). In order to have no bound states, we must demand $\frac{D}{2}\Omega$ to be larger than the barrier of $U(r)$. Also

$$U(r=0) = \frac{1}{2}\partial^2_{\tilde{A}}\tilde{\mathcal{V}}(\tilde{A}=\tilde{A}_0) = 4, \tag{4.38a}$$

and

$$U(r\to\infty) = \frac{1}{2}\partial^2_{\tilde{A}}\tilde{\mathcal{V}}(\tilde{A}=0) = 1. \tag{4.38b}$$

We have

$$\Omega = |\nabla^2 U|^{1/2}_{r=r_m} = \left[\frac{\partial^2 U}{\partial\tilde{A}^2}\left(\frac{\mathrm{d}\tilde{A}}{\mathrm{d}r}\right)^2\right]^{1/2} = \sqrt{24}\left|\frac{\mathrm{d}\tilde{A}}{\mathrm{d}r}\right|. \tag{4.39}$$

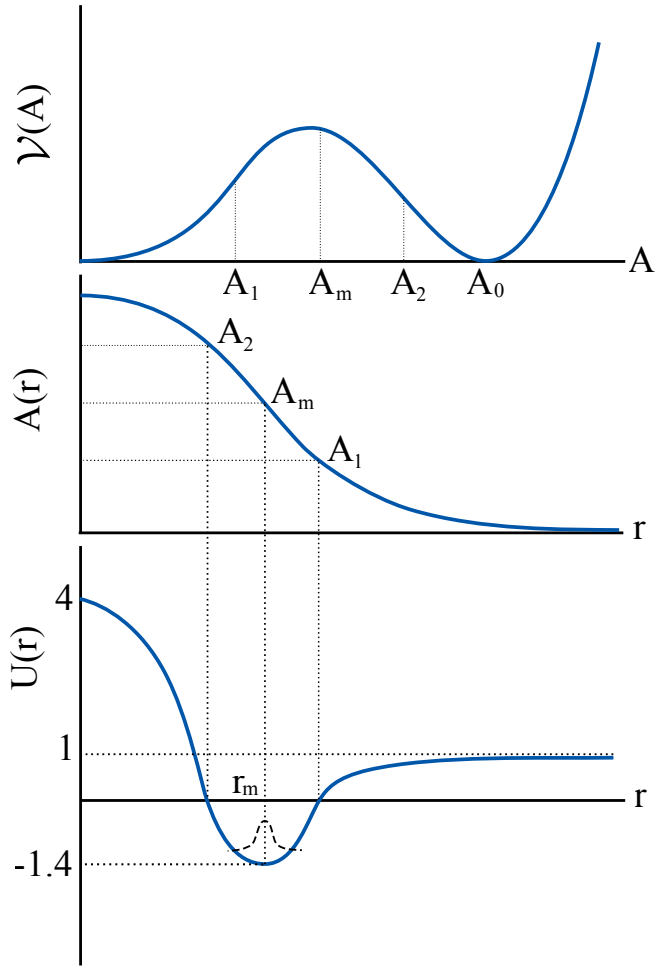

Figure 4.8: (Tildes dropped from the labels) The top panel shows $\mathcal{V}(A)$ at the transition. Points A_1 and A_2, indicate where the curvature flips sign, whereas A_m is where the curvature is minimum. The middle panel shows a schematic of the profile $A(r)$, taking all the values from A_0 down to 0. The bottom one plots the potential $U(r)$ for GFs. The dashed Gaussian wave-packet shows the ground state of the fluctuations around the minimum of $U(r)$.

We also know from Euler-Lagrange equation, that

$$\left[\frac{\mathrm{d}}{\mathrm{d}r}+\frac{2(D-1)}{r}\right]\left(\frac{\mathrm{d}\tilde{A}}{\mathrm{d}r}\right)^2=\frac{\mathrm{d}}{\mathrm{d}r}\tilde{\mathcal{V}}(\tilde{A}), \tag{4.40}$$

and hence,

$$\left|\frac{\mathrm{d}\tilde{A}}{\mathrm{d}r}\right|\leq|\tilde{\mathcal{V}}(\tilde{A})|^{1/2}=6\sqrt{5}/25, \tag{4.41}$$

and $\Omega\leq 2.74$. The equality is approached either for one dimension, or for large r_m in higher dimensions, where the effect of curvature is negligible. As shown in Fig. 4.8, the minimum of the potential is $U_m=-1.4$. If $U_m+\frac{D}{2}\Omega>1$, the bound state does not form. This is valid for $D\geq 2$ (for upper bound of Ω).

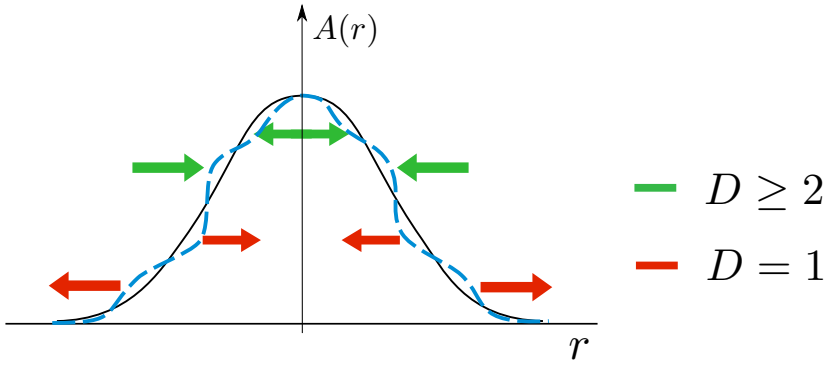

Figure 4.9: The figure shows a schematic of Gaussian fluctuations around the saddle–point solution, the soliton. The green arrows squeeze the fluctuations back towards the soliton, hence represent stability conditions. Red arrows, indicate the situation where the fluctuations destabilize the soliton.

4.5.2 Stability of Solitons in Scalar Field Theories: Derrick's Theorem

The soliton solutions of the scalar field theories are shown to be unstable in general, by Derrick's theorem. The idea is to consider the stretching-compressing transformations where the radial coordinate is scaled: $r\to\lambda r$. Following a few straightforward arguments on can see that in $D\geq 2$, the solitons are unstable. Suppose that the free energy

functional of the time-independent solution $\phi(r)$ can be written in the following form:

$$\mathcal{F} = \int \mathrm{d}^D r \left\{ (\nabla\phi(r))^2 + V[\phi(r)] \right\}. \tag{4.42}$$

The saddle-point solitonic solutions satisfy: $\delta\mathcal{F} = 0$, *i.e.* the first order variations of the free energy around the solutions vanish. We assume that a function $\varphi(r)$ satisfies this equation. The stability condition involves the second order variations: $\delta^2\mathcal{F} \geq 0$. We now perform the scaling $r \to \lambda r$, and denote the resultant free energies by $\mathcal{F}^{\lambda}_{1,2}$. Substituting this in the above equation gives:

$$\mathcal{F}_1 = \int \mathrm{d}^D r \ (\nabla\varphi(r))^2 \quad \Rightarrow \quad \mathcal{F}_1^{\lambda} = \lambda^{2-D}\mathcal{F}_1 \ , \tag{4.43a}$$

$$\mathcal{F}_2 = \int \mathrm{d}^D r \ V[\varphi(r)] \quad \Rightarrow \quad \mathcal{F}_2^{\lambda} = \lambda^{-D}\mathcal{F}_2 \ . \tag{4.43b}$$

Applying the first condition:

$$\left.\frac{\delta\mathcal{F}}{\delta\lambda}\right|_{\lambda=1} = 0, \tag{4.44}$$

we get:

$$(2-D)\mathcal{F}_1 - D\mathcal{F}_2 = 0. \tag{4.45}$$

So we have:

$$\mathcal{F}_2 = \frac{2-D}{D}\,\mathcal{F}_1. \tag{4.46}$$

Note that $\mathcal{F}_1 \geq 0$. So if we are expanding around the true vacuum for which $\mathcal{F}_2 \geq 0$, only $D = 1$ can satisfy the equation.

Now the stability condition requires that the energy cost of the second order variations about the solution be positive:

$$\left.\frac{\delta^2\mathcal{F}}{\delta\lambda^2}\right|_{\lambda=1} \geq 0. \tag{4.47}$$

Calculating the l.h.s gives:

$$(2-D)(1-D)\mathcal{F}_1 + D(D+1)\mathcal{F}_2 \geq 0. \tag{4.48}$$

Substituting Eq. (4.46), in the above equation also gives:

$$2(2-D)\mathcal{F}_1 \geq 0. \tag{4.49}$$

Again for $\mathcal{F}_1 \geq 0$, this suggests that the only acceptable answer is $D = 1$.

4.5.3 Derrick's Instabilities in the Presence of Impurity

Let $A(r)$ be a solution of the Euler-Lagrange equation (dropping tilde signs), including the impurity potential. The energy of a modulation pattern that is stretched in space by a scale factor λ, hence $A(\lambda r)$, is given by

$$\mathcal{U}(\lambda) = \lambda^{(2-D)}\mathcal{F}_1 + \lambda^{-D}\mathcal{F}_2 + \mathcal{F}_3 + \lambda^2\mathcal{F}_4 + ..., \tag{4.50}$$

where the coefficients

$$\mathcal{F}_1 = \int \mathrm{d}^D r \, \left(\frac{\mathrm{d}A(r)}{\mathrm{d}r}\right)^2, \qquad \mathcal{F}_2 = \int \mathrm{d}^D r \, \mathcal{V}[A(r)], \tag{4.51a}$$

$$\mathcal{F}_3 = -V_0 A(0), \qquad \mathcal{F}_4 = -\frac{1}{2}V_2 A''(0), \tag{4.51b}$$

are all positive. The dots stand for higher-order even powers of λ. We will drop these terms hereafter, in which case $\mathcal{U} \simeq \mathcal{F}_1 + \mathcal{F}_2 + \mathcal{F}_3 + \mathcal{F}_4$, is the energy of the original soliton. As a function of the scale factor, $\mathcal{U}(\lambda)$ has a single minimum that is stable. From the fact that $A(\lambda r)$ is a solution of the Euler-Lagrange equations for $\lambda = 1$, it follows that the minimum where $\mathrm{d}\mathcal{U}(\lambda)/\mathrm{d}\lambda = 0$ must be at $\lambda = 1$ so

$$(D-2)\mathcal{F}_1 + D\mathcal{F}_2 - 2\mathcal{F}_4 = 0\,, \tag{4.52}$$

which can be viewed as a virial theorem. Note that in the absence of the impurity potential, the soliton solution is unstable for $D > 1$, which is just Derrick's Theorem, but that the impurity potential suppresses the instability. Note also that the zeroth moment of the impurity potential does not enter in this expression, namely a localized static potential $V(r) = V_0\delta^{(D)}(r)$ does not suffice to stabilize the soliton in $D > 2$, simply because the contact interaction does not see the stretching and squeezing of the nearby field. Therefore we need to include higher moments of this potential. The odd moments vanish by analyticity and symmetry arguments. The first non-zero contribution comes from the first even moment, *i.e.* the second moment. It is worth mentioning that the broadening of the effective interaction range between the impurity and the field has in principle two origins. For static heavy impurities, the finite range can be assigned to the

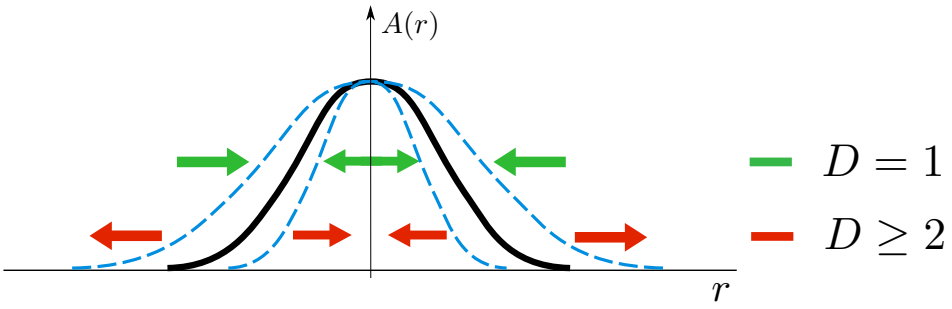

Figure 4.10: The figure shows a schematic of Derrick's instabilities around the saddle-point solution, in the absence of the impurity. Again, the green arrows squeeze the fluctuations back towards the saddle-point soliton, hence represent stable conditions. On the contrary, red arrows indicate the situation where the fluctuations destabilize the soliton.

size of the impurity. For lighter impurities, as we observed in the previous section, the particle gets trapped at a smaller coupling than the soliton formation. Thus the particle is confined within a cell of size q_0^{-1}. In this state, and to the first non-zero approximation, the wave-function of the particle (or equivalently the ensemble of the particle trajectories) is a Gaussian like with a finite width. Including the second moment of the potential also fixes the curvature of the modulation profile at the origin to be:

$$A''(0) = -\frac{(D-2)\mathcal{F}_1 + D\mathcal{F}_2}{V_2} < 0\,. \tag{4.53}$$

Since the zeroth moment of the impurity potential is of the order of one at the transition point between linear response and the soliton solution, and since $\mathcal{F}_{1,2}$ are positive numbers of the order of one, it follows that the curvature $|A''(0)| \sim (\xi/a)^2$ must be large.

4.6 Experimental Realization

For a uniform BEC condensate composed of ^{23}Na atoms with ^{6}Li impurities, the dimensionless coupling constant α can be tuned between $10^{-3} - 1$ through Feshbach resonance methods and the large to small polaron transition may or may not be accessible. However, by approaching the critical point, the critical value of α for the transition between large and small polarons can be decreased to about 0.3 (see Fig.3.6(c)) so the transition between the large and small polaron states now should be experimentally accessible. To estimate the onset of the soliton state, take $q_0 = 4(\mu m)^{-1}$, $\epsilon_0(q_0)/h = 2$ (kHz), a relative density modulation amplitude $(-\bar{u}/w)^{1/2}/n_0$ of the ordered phase of 0.1, a width δq of the depressed mode interval equal to $0.1q_0$—so $\lambda^{1/2} R\delta q = \epsilon_0(q_0)/h = 2$ (kHz)—then the condition reduces to the requirement that $a_{\rm IB}\xi q_0^2 \gtrsim 2.0$. For a scattering length $a_{\rm IB}$ enhanced by Feshbach resonance to 100 (nm), this requires that the correlation length ξ has only to exceed about ten times the repeat length ${q_0}^{-1}$ of the ordered phase.

For experimental realization, we choose the ^{23}Na condensate hosting a dilute ^{6}Li impurity gas with mass ratio $M_{\rm B}/M_{\rm I} = 3.8$ and hence $M_{\rm r} \simeq 0.8\, M_{\rm I}$. The Lippman-Schwinger scattering length of Li-Na two-body system is $a_{\rm IB} = 0.8$ nm. The coupling between the impurity particle and the Bogoliubov excitations has been proposed to be tunable via Feshbach resonance, over a few orders of magnitude, from $\alpha \sim 10^{-3}$ to $\alpha \sim 1$; hence bridging the small and large coupling regimes. To this end, we need to minimize the scattering length $a_{\rm BB}$ of sodium atoms, which is achieved at sodium Feshbach resonance near 907 G. The Li-Na scattering length—desired to be maximized—is tuned near the corresponding Feshbach resonance at 796 G or the predicted 1186 G resonance. The wavevector $q_0 \sim 10^{-3}$ nm$^{-1} = 1\ \mu$m^{-1}. Therefore the low temperature limit $\beta \sim 100$ is achieved at around $T \sim 1$ nK.

4.7 Conclusions

In this chapter we studied the problem of impurity-induced solitons in BECs near the Brazovskii transition. This new type of soliton should be discerned from the intrinsic soliton solutions of the GPE or equivalently those of the nonlinear Schödinger equation. Using the renormalized action, we showed that static impurities (local defects) are able to locally stabilize the ordered phase. We calculated, at the Brazovskii transition, the amplitude of the soliton at the location of the impurity. This can be calculated exactly in one-dimension, whereas we need to resort to a variational approach in general dimensions.

For the case of mobile impurities, we derived the conditions under which the zero-point fluctuations of the impurity do not destabilize the soliton. Furthermore, we addressed the Gaussian and Derrick's stability analysis, and observed that Gaussian fluctuations are irrelevant in $D \geq 2$, and Derrick's argument for instability of scalar field theories in $D \geq 2$ becomes invalid in the presences of the impurity.

Regarding the relevance to the phenomenology of solvation problem, in the introduction we posed the question whether impurities in a BEC can serve as a model system for the study of the role of quantum fluctuations and the breakdown of linear response theory in solvation theory. We have found that linear response theory breaks down when a pumped BEC system becomes increasingly correlated on approach of a spontaneous symmetry breaking transition, signaled by the formation of a soliton state. Does this agree, at least qualitatively, with solvation phenomena in conventional fluids? It is believed that the breakdown of linear response theory for small ions in water is related to the formation of partially ordered shells of water molecules ("solvation shells") around the ion [9]. Water is a highly correlated fluid and solvation shells indeed could be—crudely—viewed as local realizations of the low-temperature ordered phase (*i.e.* ice). On the other hand, the water molecules surrounding solvated electrons, with much stronger zero-point fluctuations, remain disordered. A recent mixed quantum-classical

simulation of electrons solvated in water have a wavefuntion that is relatively delocalized ("wet electron") [17]. According to the theory, a soliton state destroyed by the zero-point motion of the particle would have to be an extended polaron.

We also addressed the experimental feasibility of our model in a cold atomic experiment. Quantitative experimental studies of impurities in BECs in pumped optical cavities that would verify the association of the breakdown of linear response theory with solitons should, according to our estimates, be possible and would be of great value as a model system to study quantum effects on solvation in a system described by a general theory that does not require detailed assumptions about molecular interactions.

In the next chapter, we mainly follow the second aim of this dissertation: the physics of polarons in correlated disordered phases. We generalize our model to the case of a quadratic impurity-field interaction. The standard polaron problem, and in the previous chapters, the field appears linearly in the interaction term of the total action. Does the quadratic coupling influence the polaron properties qualitatively? How does the dimensionality affects the results? In chapter 6, we first introduce an actual model system in which the interaction is quadratic. Next, using the variational method as well as perturbation theory, answer the above questions.

CHAPTER 5

Polarons in the Vicinity of a Quantum Phase Transition

In order to understand the physics of impurities in critical systems, we first briefly review the most prominent theories of classical and quantum phase transitions. Second order phase transitions have been center of attraction since the early days of their observations. They exhibit macroscopic ordering transitions owing to the divergence of the correlation length ξ. This makes a continuum field theory, e.g. Landau-Ginzburg-Wilson (LGW), an appropriate approach to study these systems. There are numerous examples of systems with different symmetry-breaking scenarios between disordered and ordered phases, which fall into the general LGW scheme. The classical Ising model in $d \geq 2$, for instance, undergoes the ferromagnetic phase transition where the free energy continuously develops a non-zero minimum of the magnetization. The mean-field approach is known to be valid, *i.e.* the fluctuations do not modify the critical behavior, in spatial dimensions $d \geq d_u$, where d_u is the upper critical dimension of the theory ($d_u = 4$ for LGW). Also according to Mermin-Wagner theorem, at finite temperatures, the spontaneous continuous symmetry-breaking is not possible in $d \leq 2$. However in fundamentally discrete systems such as 2D Ising model, this does not hold true.

In the LGW and Hertz-Millis theories of the second-order transitions, the dispersion of the fluctuations is minimized at zero wave-vector $q = 0$. The crystallization-like transitions where the dispersion is minimized at q_0, are thus not captured by LGW-type theories. As we mentioned in the previous chapters, the theory of weak crystallization is well described by Brazovskii field theory. Apart from its traditional applications, in the recent years, more systems are found to obey the Brazovskii mechanism. One example

of artificial realization of such systems in ultracold quantum gases, was presented in the previous two chapters. In ultracold quantum gases, Bose-Einstein condensates are proposed to exhibit emergent crystallinity in transversely pumped multimode cavities, as a result of atom-light interaction [74, 75]. When the strength of the the transverse field reaches a threshold, the BEC self-organizes itself into a density modulation which breaks the continuous translational symmetry of the system. The emergent modes and their wavelengths depend on the geometry of the cavity and are larger than the inter-atomic distances of the BEC. This transition was shown to persist down to zero temperature, creating a quantum phase transition [74, 75]. In this variant of Brazovskii model, the effective action of the density field includes only even-powered terms, which results in transition to lamellar ordered phase. When including odd terms such as a cubic term, the ordered phase can exhibit three-dimensional unit cells e.g. tetrahedral structures [91, 92, 93].

Another example of the critical systems which fall into the fluctuation-induced Brazovskii first order transition class is the helimagnetic materials. Helimagnets possess partial order in the symmetry-breaking phase. The partial order is a result of two counteracting couplings, one favoring the ferromagnetic order on short length scales, competing with an antiferromagnetic term which favors staggered ordering on a larger length scale. This competition is characterized by a new length-scale, which turns out to be the pitch of the helix formed by the chiral order-parameter (discussed below). The microscopic origin of such partial ordering might come from the non-centrosymmetric structure of the unit cells of the lattice. The lack of inversion symmetry in these unit cell (most notably MnSi), allows the relativistic spin-orbit coupling interaction to play role, although the spin-orbit coupling is typically minuscule in solid state systems. If the spin-orbit coupling is absent, the partial order can still be imposed on the system using an external field (such as pressure) which utilizes the asymmetry of the underlying lattice.

A phenomenological approach to these systems was proposed by Dzyaloshinskii

and Moriya. They introduced a chiral interaction term to the action of the critical model. This chiral term is defined by a coupling $\mathfrak{D}$ which is commonly called the Dzyaloshinskii-Moriya (DM) interaction. The preferred wave-vector, or the inverse length-scale of the partial order is naturally dependent on DM interaction. In the absence of DM term, we retrieve the Hertz-Millis theory for the second order quantum phase transitions. For finite values of $\mathfrak{D}$, the antiferromagnetic order becomes important. The newly defined preferred wave-vector and the critical fluctuations of the corresponding modes, give rise to a fluctuation-induced first order transition similar to the Brazovskii scenario. In two dimensional thin films this results in the formation of Skyrmion lattices, which are promising candidates for topological magnetic data storage [96, 97, 98]. In order to perform any kind of computation, we need to understand the physics of bits or q-bits in the host system.

In this chapter we intend to study the physics of *mobile* nonmagnetic impurities (to be defined exactly below) near a magnetic quantum phase transition. Our goal and motivation are twofold. First, in line with the model used in the previous chapters (the Brazovskii model), we would like to explore other parts of the phase diagram (e.g. in terms of the preferred wave-vector), and bridge the gap between truly second order, and mean-field second-order transitions which turn first order upon including the finite wave-vector fluctuations. Second, this analysis complements the previously studied role of static defects near such phase transitions. We know that the attractive nature of the self-interaction (polaron self-energy), results in the localization of the particle at sufficiently large particle-field couplings. Whether or not this transition in a nearly critical environment is discontinuous or smooth is not trivial.

Nonmagnetic defects are usually assumed to couple quadratically to the magnetization field. The magnetic impurities with permanent magnetization (spin), couple linearly. However, magnetically polarizable impurities with zero permanent magnetic moment also couple quadratically to the magnetization field. This can be verified through a self-consistent condition: the potential energy of a magnetic dipole in an external field

is proportional to the dot product of the two vectors. But the induced magnetization of the impurity is itself proportional to the nearby magnetization. Therefore the coupling is quadratic in the external field and is in general nonlocal in both time and space. A simplifying model based on local interactions is presented in this chapter, using which we examine the physical properties of the mobile impurity. We will observe how the quadratic coupling changes the behavior of the polaron drastically in various respects.

In order to setup the basis of our model theory, we briefly introduce and discuss some features of the Hertz-Millis theory of quantum phase transitions. We first derive the Hertz-Millis effective action. Next, we introduce the chiral Dzyaloshinskii-Moriya interaction and present the consequences of this term. As expected, the treatment and the final result are very much similar to those of the original Brazovskii methodology for scalar field theories.

5.1 Hertz-Millis Theory of Quantum Phase Transitions

We start with a Hubbard Hamiltonian [28, 29]:

$$\mathcal{H}_{\text{Hubbard}} = -t \sum_{\langle i,j\rangle,\sigma} (c^{\dagger}_{i,\sigma} c_{j,\sigma} + c^{\dagger}_{j,\sigma} c_{i,\sigma}) + U \sum_{i=1}^{N} n_{i,\uparrow} n_{i,\downarrow}. \tag{5.1}$$

Here $c^{\dagger}_{i,\sigma}, c_{i,\sigma}$ are respectively the creation and annihilation operators of an electron at site i and with spin σ. The first term ($\mathcal{H}_0$) represents the non-interacting part which accounts for the hopping of electrons between neighboring sites denoted by $\langle i, j\rangle$ in the summation; the hopping coefficient is t. The second term is the on-site interactions of electrons with opposite spins (due to Pauli exclusion). The strength of the interaction is U. We now note that the interaction term ($\mathcal{H}'$) can be separated in terms of charge- and spin-density operators:

$$\mathcal{H}' = U \sum_{i=1}^{N} n_{i,\uparrow} n_{i,\downarrow} = \frac{U}{4} \sum_{i=1}^{N} (n_{i,\uparrow} + n_{i,\downarrow})^2 - \frac{U}{4} \sum_{i=1}^{N} (n_{i,\uparrow} - n_{i,\downarrow})^2. \tag{5.2}$$

In order to calculate the partition function: $\mathcal{Z} = \mathrm{Tr}\exp(-\beta\mathcal{H})$, we switch to interaction picture where we have:

$$e^{-\beta\mathcal{H}} = e^{-\beta\mathcal{H}_0}\, T\exp\left[-\int_0^{\beta\hbar} \mathrm{d}\tau \mathcal{H}'(\tau)\right], \tag{5.3}$$

where T is the time-ordering operator. We now use the Hubbard-Stratonovich transformation to obtain:

$$\begin{aligned}\mathcal{Z} = \mathrm{Tr}e^{-\beta\mathcal{H}} =& \mathcal{Z}_0 \int \mathcal{D}\Psi \exp\left(-\frac{1}{2}\int_0^{\beta\hbar} \mathrm{d}\tau \sum_i \Psi_i^2(\tau)\right) \\ &\times \left\langle \mathrm{Tr}\, T\exp\left(-\int_0^{\beta\hbar} \mathrm{d}\tau \sum_{i,\sigma} \sigma V_i(\tau) n_{i,\sigma}(\tau)\right)\right\rangle_0 .\end{aligned} \tag{5.4}$$

In the above relation $\mathcal{Z}_0$ is the partition function of the free system, and we have $V_i(\tau) = \sqrt{U/2}\Psi_i(\tau)$ is in fact the magnetic field at site i and imaginary time τ. Note that V accounts for spin fluctuations and we ignore the charge fluctuations as they are expected to be irrelevant. Now using the Green's function of the noninteracting system,

$$G^0_{i,j}(\tau,\tau') = \beta^{-1}\sum_{k,n} \frac{\exp[i\mathbf{k}.(\mathbf{R}_i - \mathbf{R}_j) - iE_n\tau]}{iE_n - \epsilon_k}, \tag{5.5}$$

we can simplify the partition function as:

$$\mathcal{Z} = \mathcal{Z}_0 \int \mathcal{D}\Psi\ \exp\left(-\frac{1}{2}\int_0^{\beta\hbar} \mathrm{d}\tau \sum_i \Psi_i^2(\tau) + \sum_\sigma \mathrm{Tr}\ln(1 - \sigma V G^0)\right). \tag{5.6}$$

Here V and G^0 are matrices. The elements of V are: $V_{i,j}(\tau,\tau') = V_i(\tau)\delta_{ij}\delta(\tau-\tau')$. The exponent in the above equation is then the free energy (or Euclidean action) associate with the order parameter $\mathcal{S}_{\text{Hertz}}$; we denote the free energy by $\mathcal{S}_{\text{Hertz}}[\Psi]$. Expanding the free energy in a power series in Ψ leads to the following general expression:

$$\begin{aligned}\mathcal{S}_{\text{Hertz}}[\Psi] =& \frac{1}{2}\sum_{\mathbf{q},\omega_n} v_2(\mathbf{q},\omega)|\Psi(\mathbf{q},\omega)|^2 + \frac{1}{4\beta N}\sum_{\mathbf{q}_i,\omega_i} v_4(\mathbf{q}_1\omega_1,\mathbf{q}_2\omega_2,\mathbf{q}_3\omega_3,\mathbf{q}_4\omega_4) \\ &\times \Psi(\mathbf{q}_1,\omega_1)\Psi(\mathbf{q}_2,\omega_2)\Psi(\mathbf{q}_3,\omega_3)\Psi(\mathbf{q}_4,\omega_4)\ \delta\left(\sum_{i=1}^4 \mathbf{q}_i\right)\delta\left(\sum_{i=1}^4 \omega_i\right) + \dots .\end{aligned} \tag{5.7}$$

Here v_2 and v_4 are the vertices. In certain cases the vertices can be calculated, and the full Euclidean action takes the form:

$$\mathcal{S}_{\text{Hertz}} = \frac{1}{\beta V}\sum_{\mathbf{q},\omega_n} \epsilon_0(\tau + \xi_0^2|\mathbf{q}|^2 + |\omega_n|/\gamma(q))\phi_{\mathbf{q},\omega_n}\phi_{-\mathbf{q},-\omega_n} + \mathcal{S}_4. \tag{5.8}$$

In the above relation ϵ_0 and ξ_0 are microscopic energy- and length-scales respectively. We note that the above calculation is carried out for a metallic system in which the particle-hole excitations cause the Landau damping, hence the dynamics of the order parameter is overdamped. In a more general form, the dynamic term is replaced by

$$\mathcal{S}_{\text{dyn}} = \frac{1}{2\beta V}\sum_{\mathbf{q},\omega_n}\left(\frac{1}{c_{\mathbf{q}}^2} + \frac{1}{\Gamma_{\mathbf{q}}|\omega_n|}\right)|\omega_n\phi(\mathbf{q},\omega_n)|^2. \tag{5.9}$$

We list four different systems and the corresponding dynamical coefficients, in table (5.1).

Class	$c_{\mathbf{q}}$	$\Gamma_{\mathbf{q}}$
Undamped Ising antiferromagnet	const.	$\to \infty$
Undamped Ising ferromagnet	$\sim 1/q$	const.
Metallic (overdamped) antiferromagnet	—	const.
Metallic Ising ferromagnet	—	$\sim q$

Table 5.1: The dynamical coefficients for different critical systems near the magnetic phase transition.

As mentioned in the introduction of this chapter, if we deal with systems with non-centrosymmetric structures (*i.e.* lacking the inversion symmetry), e.g. the unit cell of MnSi, the effect of spin-orbit coupling (SOC) term which also breaks the time-reversal symmetry becomes important. Such couplings collectively add a chiral term to the original Hertz-Millis action. This term is represented by a phenomenological coupling constant $\mathfrak{D}$, and is called the Dzyaloshinskii-Moriya (DM) interaction. The DM magnets (also called helimagnets) in three dimensions, exhibit a chiral phase below

the transition point. This is somewhat similar to the "Blue phase" of cholesteric liquid crystals. The static action of the bare field near the magnetization transition can be written as [34, 35]:

$$\mathcal{S}^{\text{stat}}_{\text{bare}} = \int_0^\beta \mathrm{d}t \int \mathrm{d}^d\mathbf{x} \left\{ \frac{\lambda}{2} \sum_i (\nabla \mathcal{M}_i)^2 + \mathfrak{D}\mathcal{M}.(\nabla \times \mathcal{M}) + \frac{\tau}{2}|\mathcal{M}|^2 + \frac{g}{4}|\mathcal{M}|^4 - \mathbf{H}.\mathcal{M} \right\}, \tag{5.10}$$

where $\mathcal{M}(\mathbf{r}, t)$ is the magnetization field ($\mathcal{M}$ and ϕ will be used interchangeably in the context), and where i lables $\{x_i\} = (x_1, ..., x_d)$; the d spatial coordinates. The second quadratic term is the Dzyaloshinskii-Moriya (DM) interaction due to lack of inversion symmetry and hence SOC. In spite of the relativistic nature of SOC, it can shown that this term (DM) dominates other contributions arising from anisotropies such as $\sum_i (\partial_i \mathcal{M}_i)^2$ and $\sum_i \mathcal{M}_i^4$ (see Ref. [34] and references therein). Next, τ measures the distance from the critical point of the mean-field model, and u measures the strength of forth order nonlinearities which is a positive constant to guarantee the stability. For convenience we choose the units in which $[\mathcal{M}(\mathbf{r}, t)]^2 = [\text{Length}]^{-d}$.

The dynamics of the order parameter is determined, for example, by coupling to the electron-hole excitations around the Fermi surface. Again in a general form the dynamic term is expressed as [34, 99]:

$$\mathcal{S}^{\text{dyn}}_{\text{bare}} = \frac{1}{\hbar\beta} \sum_{n=-\infty}^{+\infty} \frac{1}{\Gamma \epsilon_F} (\hbar|\omega_n|/\epsilon_F)^{2/z} |\mathcal{M}(\mathbf{r}, \omega_n)|^2, \tag{5.11}$$

where Γ^{-1} is the dimensionless dynamical coefficient. At finite temperature we introduce the Matsubara frequencies $\omega_n = 2\pi n/\beta\hbar$ as the Fourier conjugate of imaginary time.

5.1.1 Systems Without Inversion Symmetry: Helimagnets

Systems without inversion symmetry (chiral magnets), most notably MnSi, allow for SOC which collectively yields the DM interaction. In has been shown that such systems

exhibit a fluctuation-induced first order phase transition, which falls into a quantum version of the Brazovskii class of phase transitions, *i.e.* the kernel of the action takes the following form:

$$\chi_{\bar{q}}^{-1} = \theta + \mu(|\mathbf{q}| - Q)^2 + \Gamma^{-1}|\omega_n|^{2/z}, \tag{5.12}$$

where $Q = q_0\,\hbar/\sqrt{M\epsilon_F}$.

Here, we briefly review the MF analysis of a bare helimagnetic system [35]. At MF level, we use the following ansatz for the vectorial order parameter $\mathcal{M}$, to minimize the bare action. The ansatz contains terms which represent the para- and helimagnetic phases separately:

$$\mathcal{M} = \phi_0\hat{\phi}_0 + \psi_{\text{hel}}e^{i\mathbf{Q}.\mathbf{r}}\hat{e}^- + \psi^*_{\text{hel}}e^{-i\mathbf{Q}.\mathbf{r}}\hat{e}^+, \tag{5.13}$$

in which ϕ_0 and $\hat{\phi}_0$ are the paramagnetic background field and its direction and ψ_{hel} is the complex amplitude of the helical order with pitch vector $\mathbf{Q}$, a free parameter to be determined by minimizing the free energy, and finally $\hat{e}^{\pm} = (\hat{e}_1 \pm i\hat{e}_2)/\sqrt{2}$, such that $\hat{e}_1 \times \hat{e}_2 = \hat{\mathbf{Q}}$ and $\hat{\mathbf{Q}} = \mathbf{Q}/Q$. We assume that below the transition, there is an infinitesimal external magnetic field to single out a direction for the paramagnetic background of the ordered domains ($\hat{\phi}_0$) to be oriented along $\hat{\mathbf{H}}$, also parallel to the pitch vector $\hat{\mathbf{Q}}$. In general, even in the absence of external magnetic field, higher order contributions of SOC break the rotation symmetry by generating cubic anisotropies, e.g. $\langle 111\rangle$ is the preferred crystallographic direction in MnSi. For simplicity we neglect the cubic anisotropies and instead include a small external field.

Inserting the ansatz of Eq. (5.13) in the original static action, we get $\mathcal{S}^{\text{bare}}_{\text{stat}} = \beta L^d \mathfrak{f}_0$, where,

$$\begin{aligned}\mathfrak{f}_0 =& \frac{\theta}{2}\phi_0^2 + (\theta + \mu Q^2 - 2\mathscr{D}Q)|\psi_{\text{hel}}|^2 \\ &+ \frac{u}{4}(\phi_0^2 + 2|\psi_{\text{hel}}|^2)^2 - H\phi_0,\end{aligned} \tag{5.14}$$

is the free energy density which gives us the equation of state of the phase when minimized with respect to the fields and free parameters. In the above equation $\mathscr{D} =$

$\mathfrak{D}\,\hbar/\sqrt{M\epsilon_F^3}$, is the dimensionless DM coefficient, and $u = g\,(\sqrt{M\epsilon_F}/\hbar)^d/\epsilon_F$ is the dimensionless quartic coefficient. In the paramagnetic phase where $|\psi_{\text{hel}}| = 0$, the uniform magnetization ϕ_0 is parallel to the external field $\hat{\phi}_0 = \hat{\mathbf{H}}$ and satisfies the equation of state: $\theta\phi_0 + u\phi_0^3 = H$. The solutions of this equation in the limit $H \to 0$ are: zero for $\theta > 0$ and $\pm\sqrt{-\theta/u}$ for $\theta < 0$. Now minimizing with respect to the pitch vector $\mathbf{Q}$, we get: $Q = \mathscr{D}/\mu$. In the limit of zero external field, the minimized free energy density of the helimagnetic order parameter ψ_{hel} reads,

$$\mathfrak{f}_{\text{HM}} = \Delta|\psi_{\text{hel}}|^2 + u|\psi_{\text{hel}}|^4 \tag{5.15}$$

where $\Delta = \theta - \mu\,Q^2$ is the gap of the chiral mode, which is the paramagnetic gap shifted by the deformation cost of the mode Q. For $\Delta > 0$ the DM interaction is not large enough to overcome the paramagnetic gap θ and $|\psi_{\text{hel}}|$. When increasing the chiral interaction, Δ becomes negative for $\mathscr{D}^2 \geq \theta\mu$, the helical order parameter favors a finite magnitude $|\psi_{\text{hel}}| = \sqrt{-\Delta/2u}$. Below we discuss the consequences of this non-zero ordering wavevector Q, on a mobile impurity.

In the previous chapters we studied the interplay of a quantum mechanical particle linearly coupled to the density of an ultracold BEC which is interacting with a transverse as well as the photons of a multimode cavity. As mentioned above, the system undergoes an emergent crystallinity above a threshold laser intensity, and is describe by the LB theory. In particular the role of the large quantum/thermal fluctuations of the BEC was investigated on the quantum mechanical features of the particle. It was shown that the particle, far from the transition and at zero temperature, experiences a discontinuous self-trapping transition, which is closed at a "critical" point, as the quantum fluctuations of the field are enhanced. Thermal fluctuations also close the discontinuity. Close to the LB transition a new class of non-linear solutions appear which cannot be obtained perturbatively. In that system, the local tendency of the field towards order around the particle yields the emergence of a "droplet" of the ordered phase. The boundary between the coexisting ordered and disordered phases, is of the order of the finite correlation length.

In this chapter we study a single mobile impurity coupled to a field near a second order or a weakly first order quantum phase transition. To this end, we (i) generalize the case of study of chapters 3 and 4 to quadratic particle-field coupling, in (ii) general spatial dimensions d and dynamic exponents $z = 1$, and finally (iii) vary the preferred wave-vector q_0 from zero (corresponding to Hertz-Millis theory) to finite values corresponding to LB-type transitions. In particular for this model system of itinerant-electron magnetism, we discuss and derive—based on heuristic arguments—that non-magnetic impurities couple quadratically to the magnetization field. The case of linear coupling is already solved for many of the above-mentioned cases. For example, the case of $q_0 = 0$, at the critical point is similar to "acoustic polaron", where the particle is interacting with Goldstone phonons. Away from the critical point, where the mode spectrum has a gap at $q = 0$, the theory resembles the "optical polaron". These cases are well studied in the literature of polaron problem. Therefore, in the case of linear coupling we calculate the polaron properties as a function of this gap, in general dimensions, and also at finite q_0. We finally compare the results of the quadratic and linear couplings and find significant differences between the two. In particular, we observe in three dimensions, to one loop order and also using Born-Oppenheimer approximation for the field (corresponding to the frozen field dynamics in the limit of large effective mass of the mode), the quadratic coupling makes the wave-function collapse. Furthermore we show this localization takes place at a finite coupling constant when the quantum fluctuations of the field are added.

Our approach to this problem is mainly based on the Feynman's variational method to calculate the self-energy and effective mass of the polaron. Throughout this chapter, we keep the magnetic transition as our model system, mainly for concrete interpretation of the parameters.

5.2 Model Field Theory

We start with the Hamiltonian of the Hubbard model interacting with a dilute electrically neutral bosonic impurity gas in their zero magnetization single particle states. The impurity gas is assumed to be of low enough concentration such that the atoms do not see each other and we neglect this term in our Hamiltonian.

We write the partition function in the imaginary-time path-integral representation:

$$\mathcal{Z} = \int \mathcal{D}[\phi(\mathbf{x},t)]\mathcal{D}[\mathbf{R}(t)]\exp(-\mathcal{S}[\phi(\mathbf{x},t);\mathbf{R}(t)]/\hbar). \tag{5.16}$$

The action $\mathcal{S}$ is the full action of the system plus impurity which consists of three terms: bare field, free particle, and their interaction (see below). The path-integration is over all the spatial and imaginary-temporal configurations of the field $\phi(\mathbf{x},t)$ and particle coordinate $\mathbf{R}(t)$, under the periodic boundary condition in imaginary time i.e. $\phi(\mathbf{x},0) = \phi(\mathbf{x},\beta\hbar)$ and $\mathbf{R}(0) = \mathbf{R}(\beta\hbar)$. We start with the action of the quantum field plus particle.

- **Bare Action**:

For notational convenience we rename the magnetization field $\phi(\mathbf{r},t) \equiv \mathcal{M}(\mathbf{r},t)$. The full bare action of the field equals:

$$\mathcal{S}_{\text{bare}} = \frac{1}{2}\int \frac{\mathrm{d}^{d+1}\bar{q}}{(2\pi)^{d+1}}\,\phi^*_{\bar{q}}\,\chi^{-1}_{\bar{q}}\,\phi_{\bar{q}} + \frac{g}{4}\int\prod_{i=1}^{4}\left(\frac{\mathrm{d}^{d+1}\bar{q}_i}{(2\pi)^{d+1}}\phi_{\bar{q}_i}\right)\delta^{(d+1)}\left(\sum_{i=1}^{4}\bar{q}_i\right), \tag{5.17}$$

where $\bar{q} = (\mathbf{q},\omega)$ denotes the momentum $(d+1)$-dimensional vector, and we use the definition

$$\int \mathrm{d}^{d+1}\bar{q}/(2\pi)^{d+1} \equiv (\beta\hbar L^d)^{-1}\sum_{\mathbf{q},\omega_n} \tag{5.18}$$

for a d-dimensional system with linear size L at temperature β^{-1}.

In the quadratic kernel

$$\chi^{-1}_{\bar{q}} = \tau + \lambda(|\mathbf{q}| - q_0)^2 + \Gamma^{-1}\epsilon_F\left(\hbar|\omega_n|/\epsilon_F\right)^{2/z}, \tag{5.19}$$

ϵ_F is the Fermi energy of the itinerant electrons, and τ the distance to the critical point. The preferred wave-vector is $q_0 = \mathfrak{D}/\lambda$. The field stiffness λ and the dynamic coefficient Γ^{-1} are positive constants. The exponent $2/z$ measures the quantum-to-classical field crossover for increasing z. The important cases of $z = 1, 2$ correspond to undamped and overdamped (Landau damping) dynamics, respectively.

5.3 Quadratic Polaron

We now introduce an impurity which couples quadratically to the system. In a semi-classical approximation for the magnetization of the impurity with large total angular momentum, we assume that the induced magnetization is proportional to the local magnetic field which is in turn, predominantly determined by the nearby magnetization field of the host system. Thus in a self-consistent approach, for the magnetic interaction energy we have:

$$U = -\mathbf{m}(t).\mathbf{B}(\mathbf{R}(t)), \tag{5.20a}$$

$$\mathbf{m}(t) = \int^t \mathrm{d}t'\, \varpi(t-t')\mathbf{B}(\mathbf{R}(t')). \tag{5.20b}$$

where $\varpi(t-t')$ is the temporal kernel of the polarizability of the impurity magnetic moment. We approximate this polarizability by $\varpi(t-t') = \varpi\delta(t-t')$. For the magnetic field at the position of the impurity we have:

$$\mathbf{B}(\mathbf{R}(t)) = \int \mathrm{d}^d r\, \mathcal{J}(|\mathbf{R}(t)-\mathbf{r}|)\mathcal{M}(\mathbf{r},t). \tag{5.21}$$

We first use $\mathcal{J}(r) = \mathcal{J}_0\delta^{(d)}(\mathbf{r})$, and get:

$$U = -\varpi\mathcal{J}_0^2|\mathcal{M}(\mathbf{R}(t))|^2. \tag{5.22}$$

The sign of the magnetic polarizability of the impurity determines the nature of its effective magnetic interaction with the magnetization of the medium; either ferromagnetic or antiferromagnetic. However as we shall see below, up to one-loop order approximation of the self-energy, this sign is unimportant. For a finite mass impurity, there exists

a kinetic term. Then the total action of the impurity reads:

$$\mathcal{S}_{\text{imp.}} = \int_0^{\beta\hbar} \mathrm{d}t \frac{M}{2}|\dot{\mathbf{R}}|^2 + \frac{1}{2}\int_0^{\beta\hbar} \mathrm{d}t \iint \mathrm{d}^d\mathbf{r}\mathrm{d}^d\mathbf{r}'\, \mathcal{J}(\mathbf{r}-\mathbf{R}(t))\mathcal{J}(\mathbf{r}'-\mathbf{R}(t))\phi(\mathbf{r},t)\phi(\mathbf{r}',t). \tag{5.23}$$

The second term can be cast in Fourier form,

$$\mathcal{S}^{\text{int.}}_{\text{imp.}} = \frac{\varpi}{2}\int_0^{\beta\hbar} \mathrm{d}t \iint \frac{\mathrm{d}^d q_1}{(2\pi)^d}\frac{\mathrm{d}^d q_2}{(2\pi)^d}\phi^*_{\mathbf{q}_1}(t)\phi_{\mathbf{q}_2}(t)\mathcal{J}^*_{\mathbf{q}_1}\mathcal{J}_{\mathbf{q}_2}e^{-i(\mathbf{q}_2-\mathbf{q}_1).\mathbf{R}(t)}. \tag{5.24}$$

As discussed above, we can choose a potential of the form $\mathcal{J}(|\mathbf{r}|) = \mathcal{J}_0\,\delta^{(d)}(\mathbf{r})$, where $\mathcal{J}_0 \equiv -\varpi\mathcal{J}_0^2$. We note that when $|\phi(\mathbf{r},t)|^2$ has dimensions of $[\text{Length}]^{-d}$, we have $[\mathcal{J}_0] = [\text{Energy}]\times[\text{Length}]^d$.

Although the above equation is local in time, it can represent the most general bilinear coupling of the particle to the field in space. Another possibility which can be viewed as a model for the coupling of non-magnetic impurities to a magnetization field is [100, 99]:

$$\mathcal{S}^{\text{int.}}_{\text{imp.}} = \frac{1}{2}\int_0^{\beta\hbar} \mathrm{d}t \int \mathrm{d}^d r V(\mathbf{r}-\mathbf{R}(t))|\phi(\mathbf{r},t)|^2, \tag{5.25}$$

in which case the vertex product $\mathcal{J}^*_{\mathbf{q}_1}\mathcal{J}_{\mathbf{q}_2}$ in Eq. (5.24) is replaced by $V_{\mathbf{q}_1-\mathbf{q}_2}$ (see below). It is clear that the models are equivalent for $\mathcal{J}(\mathbf{r}-\mathbf{r}') = \mathcal{J}_0\delta^{(d)}(\mathbf{r}-\mathbf{r}')$, such that

$$\mathcal{J}_0^2\delta^{(d)}(\mathbf{R}-\mathbf{r})\delta^{(d)}(\mathbf{R}-\mathbf{r}') \equiv V_0\delta^{(d)}(\mathbf{r}-\mathbf{r}'). \tag{5.26}$$

The action of the full system is the sum of the actions of the bare field and impurity, and their interaction. Using the latter form of coupling, we derive the full action:

$$\begin{aligned}\mathcal{S} = &\int_0^{\beta\hbar} \mathrm{d}t\ \frac{M}{2}|\dot{\mathbf{R}}|^2 + \frac{1}{2}\int \frac{\mathrm{d}^{d+1}\bar{q}}{(2\pi)^{d+1}}\ \chi_{\bar{q}}^{-1}|\phi_{\bar{q}}|^2 \\ &+ \frac{g}{4}\int \prod_{i=1}^{4}\left(\frac{\mathrm{d}^{d+1}\bar{q}_i}{(2\pi)^{d+1}}\phi_{\bar{q}_i}\right)\delta^{(d+1)}\left(\sum_{i=1}^{4}\bar{q}_i\right) \\ &+ \frac{1}{2}\iint \frac{\mathrm{d}^{d+1}\bar{q}_1}{(2\pi)^{d+1}}\frac{\mathrm{d}^{d+1}\bar{q}_2}{(2\pi)^{d+1}}\ \phi^*_{\bar{q}_1}\phi_{\bar{q}_2}\int_0^{\beta}\mathrm{d}t\ \mathcal{V}_{-\bar{k}}(t).\end{aligned} \tag{5.27}$$

The first three terms correspond to the free particle and bare action, respectively, while the last term represents their interaction. Defining $\bar{k} = \bar{q}_2 - \bar{q}_1$ the interaction potential

equals:

$$\mathcal{V}_{-\bar{k}}(t) = V_{\mathbf{q}_1-\mathbf{q}_2} \exp[i(\omega_2-\omega_1)t - i(\mathbf{q}_2-\mathbf{q}_1).\mathbf{R}(t)]. \tag{5.28}$$

Due to the quadratic nature of the coupling the field-impurity interaction induces coupling between the diagonalizing modes of the field. We note that, away from the critical point, although the coupling to the impurity is a perturbative effect to the field, it can be disturbing enough to the particle to localize it.

Like in the case of polaron problem, we are interested in calculating the effective action for the particle. To this end, we integrate out the field's degrees of freedom. We thus consider the quartic and impurity-field interactions as perturbations to the diagonal quadratic action of the field. Defining

$$\begin{aligned}\mathcal{A}[\phi,\mathbf{R}] =& \frac{1}{2}\iint \frac{\mathrm{d}^{d+1}\bar{q}_1}{(2\pi)^{d+1}}\frac{\mathrm{d}^{d+1}\bar{q}_2}{(2\pi)^{d+1}}\ \phi^*_{\bar{q}_1}\phi_{\bar{q}_2}\int_0^\beta \mathrm{d}t\ \mathcal{V}_{\bar{k}}(t) \\ &+ \frac{g}{4}\int\prod_{i=1}^{4}\left(\frac{\mathrm{d}^{d+1}\bar{q}_i}{(2\pi)^{d+1}}\phi_{\bar{q}_i}\right)\delta^{(d+1)}\left(\sum_{i=1}^{4}\bar{q}_i\right),\end{aligned} \tag{5.29}$$

we get,

$$\mathcal{S}_{\text{eff}}[\mathbf{R}(t)] = \mathcal{S}^0_{\text{imp.}} + \langle\mathcal{A}\rangle_{\text{G}} - \frac{1}{2!}[\langle\mathcal{A}^2\rangle_{\text{G}} - \langle\mathcal{A}\rangle^2_{\text{G}}] + \dots\,, \tag{5.30}$$

where $\mathcal{S}^0_{\text{imp.}}$ action of the free impurity and $\langle\bullet\rangle_{\text{G}}$ is the average of $\bullet$ with respect to the unperturbed diagonal Gaussian field action. It is easy to see that $\langle\mathcal{A}\rangle_{\text{G}}$ is independent of $\mathbf{R}$, hence irrelevant. The second cumulant includes four-, six- and eight-point correlation functions. The first non-zero contribution is:

$$\mathcal{S}^{(1)}_{\text{imp.}} = -\frac{1}{2}\iint \frac{\mathrm{d}^{d+1}\bar{q}_1}{(2\pi)^{d+1}}\frac{\mathrm{d}^{d+1}\bar{q}_2}{(2\pi)^{d+1}}\ \chi_{\bar{q}_1}\chi_{\bar{q}_2}|V_{-\mathbf{k}}|^2\iint_0^\beta \mathrm{d}t\mathrm{d}t' e^{i\Omega|t-t'|-i\mathbf{k}.(\mathbf{R}(t)-\mathbf{R}(t'))}, \tag{5.31}$$

in which $\Omega = \omega_2 - \omega_1$ and $\mathbf{k} = \mathbf{q}_2 - \mathbf{q}_1$. For $V(\mathbf{r}) = V_0\delta^{(d)}(\mathbf{r})$ (contact interaction) we have $|V_{\mathbf{k}}| = V_0$. We note again that the sign of the polarizability becomes irrelevant in this approximation, as V_0 appears quadratically in Eq. (5.31).

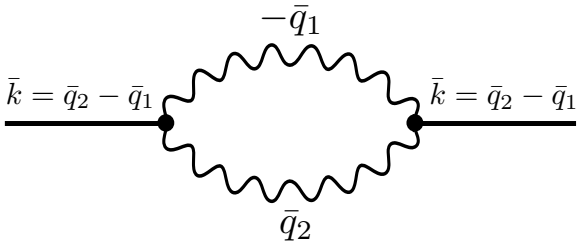

Figure 5.1: The Feynman diagram corresponding to equation (5.31) for quadratic polaron. Straight and wavy lines represent the particle and the field propagator, respectively. The incoming particle of momentum $\bar{k} \equiv (\mathbf{k}, \Omega)$, is scattered off the phonons with momenta $\bar{q}_1 \equiv (\mathbf{q}_1, \omega_1)$ and $\bar{q}_2 \equiv (\mathbf{q}_2, \omega_2)$. The space and time translation symmetry requires the conservation of momenta at each vertex, such that: $(\mathbf{k}, \Omega) = (\mathbf{q}_2 - \mathbf{q}_1, \omega_2 - \omega_1)$.

We now switch to dimensionless parameters by setting $\hbar = \epsilon_F = M = 1$. Thus length is measured in units of $\hbar/\sqrt{M\epsilon_F} = \lambda_F\sqrt{m_e/M}$, proportional to Fermi wavelength; m_e is the mass of electron. Time is measured in units of $\hbar/\epsilon_F$. Also $\beta \to \epsilon_F\beta$, $(\mathbf{q}, \omega) \to (\mathbf{q}\,\hbar/\sqrt{M\epsilon_F}, \omega\hbar/\epsilon_F)$. In these units we have:

$$\chi_{\bar{q}}^{-1} = \theta + \mu(|\mathbf{q}| - Q)^2 + \Gamma^{-1}|\omega_n|^{2/z}, \tag{5.32}$$

where $\theta = \tau/\epsilon_F$, $\mu = \lambda\, M/\hbar^2$, $Q = q_0\,\hbar/\sqrt{M\epsilon_F} = (\mathfrak{D}/\lambda)\,\hbar/\sqrt{M\epsilon_F}$ and thus χ_q^{-1}, are all dimensionless. So the effective action for the particle in dimensionless parameters reads:

$$\mathcal{S}_{\text{eff}}[\mathbf{R}(t)] = \frac{1}{2}\int_0^\beta \mathrm{d}t\, |\dot{\mathbf{R}}|^2 - \alpha \iint_0^\beta \mathrm{d}t\mathrm{d}t'\, |\tilde{\chi}(\Delta\mathbf{R}(t,t'); \Delta t)|^2, \tag{5.33}$$

where we introduced the shorthand notation $\Delta\mathbf{R}(t,t') \equiv \mathbf{R}(t) - \mathbf{R}(t')$ and $\Delta t = t - t'$ and $\tilde{\chi}(\mathbf{r}, t)$ is the inverse Fourier transform of $\chi_{\bar{q}}$. We introduced α, the dimensionless polaron coupling constant:

$$\alpha = \frac{1}{2}\left(\frac{V_0}{\epsilon_F}\right)^2 \left(\frac{M\epsilon_F}{\hbar^2}\right)^d. \tag{5.34}$$

We note that to first non-zero order in the coupling V_0, the effective action looks like that of the linear polaron, with the inverse correlation function squared.

For $z = 1$, time can be treated on the same footing as space. The correlation function decays in space and time over the correlation length (ξ) and correlation time ($1/\sqrt{\epsilon_F \Gamma \lambda}\ \xi$), respectively. In spatial dimensions d we get the following relations for the limiting cases (i) : $|\mathbf{r}|^2/\mu + \Gamma t^2 \ll \theta^{-1}$ and (ii) : $|\mathbf{r}|^2/\mu + \Gamma t^2 \gg \theta^{-1}$:

$$\tilde{\chi}_{z=1}(\mathbf{r},t) \simeq \begin{cases} \text{(i)}\ \frac{\mu^{-d/2}\Gamma^{1/2}}{(d-1)S_{d+1}}(|\mathbf{r}|^2/\mu + \Gamma t^2)^{-(d-1)/2}, \\ \text{(ii)}\ \frac{\mu^{-d/2}\Gamma^{1/2}\theta^{(d-2)/4}}{(d-1)S_{d+1}} \frac{\exp[-\sqrt{\theta(|\mathbf{r}|^2/\mu+\Gamma t^2)}]}{(|\mathbf{r}|^2/\mu+\Gamma t^2)^{d/4}}, \end{cases}$$

The above approximate expression is in general dimensions.

The general form of the action can be modified for gaining various insights. For instance, one can take the inverse Fourier transform to time domain, leaving the $\mathbf{q}$-dependence explicit:

$$\begin{aligned} \mathcal{S}^{(1)}_{\text{imp.}} = &- \frac{(\Gamma\epsilon_F)^2}{8} \iint_0^\beta \mathrm{d}t\mathrm{d}t' \iint \frac{\mathrm{d}^d q_1}{(2\pi)^d} \frac{\mathrm{d}^d q_2}{(2\pi)^d}\ |V_{-\mathbf{k}}|^2 \\ &\times \mathcal{G}(-\mathbf{q}_1, |t-t'|)\, \mathcal{G}(\mathbf{q}_2, |t-t'|) e^{-i\mathbf{k}.\Delta\mathbf{R}(t,t')} \end{aligned} \tag{5.35}$$

where the two-point correlation function is:

$$\mathcal{G}(\mathbf{q},u) = \frac{1}{\omega_{\mathbf{q}}} \frac{\cosh(\omega_{\mathbf{q}}(u-\beta/2))}{\sinh(\beta\omega_{\mathbf{q}}/2)}, \tag{5.36}$$

where $\omega^2_{\mathbf{q}} = \Gamma\epsilon_F(\tau + \lambda|\mathbf{q}|^2)$. The kernel reduces in the zero temperature limit ($\beta \to \infty$) to:

$$\mathcal{G}(\mathbf{q},u) = \frac{1}{\omega_{\mathbf{q}}} \exp[-\omega_{\mathbf{q}} u]. \tag{5.37}$$

This form is specifically useful for variational method.

- **Variational Method**

The path-integral over the degrees of freedom are most conveniently carried out using Feynman's variational approach. The effective mass and self-energy of the particle can be evaluated using this method. We introduce the trial action:

$$\mathcal{S}_t = \mathcal{S}^0_{\text{imp.}} + \frac{1}{2} \iint_0^\beta \mathrm{d}t\mathrm{d}t'\ \mathcal{K}(|t-t'|)|\Delta\mathbf{R}(t,t')|^2, \tag{5.38}$$

and use the Feynman's inequality $\mathcal{F} \leq \mathcal{F}_t + \frac{1}{\beta}\langle \mathcal{S}_{\text{eff}} - \mathcal{S}_t \rangle_t$, for the free energy of the impurity. The average is taken with respect to the Gaussian trial action. The trial kernel $\mathcal{K}(|t-t'|) = \beta^{-1}\sum_n \mathcal{K}_n e^{i\Omega_n|t-t'|}$, should be chosen to best mimic the actual kernel, yet contains free parameters to account for the difference in the form of $\mathbf{R}$-dependence, *i.e.* to minimize the free energy.

$$\mathcal{K}_n = \frac{\mathtt{C}}{\beta}\sum_m \left\{ \left[\mathtt{B} + \Gamma^{-1}|\omega_m|^{2/z}\right]\left[\mathtt{B} + \Gamma^{-1}|\omega_m + \Omega_n|^{2/z}\right] \right\}^{-1}, \tag{5.39}$$

or,

$$\begin{aligned}\mathcal{K}(u) &= \frac{\mathtt{C}}{\beta^2}\sum_{m,\ell}\left\{ \frac{e^{-i\omega_m u}}{\mathtt{B} + \Gamma^{-1}|\omega_m|^{2/z}} \frac{e^{+i\omega_\ell u}}{\mathtt{B} + \Gamma^{-1}|\omega_\ell|^{2/z}} \right\} \\ &= \mathtt{C}\,|\Phi_z(\mathtt{B}, \beta; u)|^2, \end{aligned} \tag{5.40}$$

with $\mathtt{C}$ and $\mathtt{B}$ the variational parameters playing the roles of coupling constant α and the distance to the critical point θ, respectively. Note that besides the fact that Γ is dimensionless, its presence is merely for later interpretational convenience. In general it can be absorbed in the definition of $\mathtt{C}, \mathtt{B}$. For $z = 1$, we have $\Phi_{z=1}(\mathtt{B}, \beta; u) \equiv \mathcal{G}(\mathbf{q} = 0, u)|_{\theta=\mathtt{B}}$.

With the trial kernel $\mathcal{K}_n$ we can calculate the upper bound of the free energy. After angular integration between the vectors $\mathbf{q}_1$ and $\mathbf{q}_2$ we get for the average of the interaction part of the original action:

$$\begin{aligned}\lim_{\beta\to\infty}\frac{\langle \mathcal{S}^{(1)}_{\text{imp.}}\rangle_t}{\beta\hbar} = \frac{-\alpha\Gamma^2 S_d^2}{(2\pi)^{2d}} \iint_0^\infty \mathrm{d}q_1 \mathrm{d}q_2 q_1^{d-2} q_2^{d-2} \int_0^{\beta\hbar} \mathrm{d}u\; \mathcal{G}^*(\mathbf{q}_1, u)\,\mathcal{G}(\mathbf{q}_2, u) \\ \times \frac{1}{\Lambda(u)}\left\{\exp[-|q_1 - q_2|^2\Lambda(u)] - \exp[-|q_1 + q_2|^2\Lambda(u)]\right\}, \end{aligned} \tag{5.41}$$

where $\Lambda(u)$ is given by:

$$\Lambda(u) = \frac{2}{\beta}\sum_{n>0} g_n[1 - \cos(\omega_n u)], \tag{5.42}$$

in which

$$g_n = \frac{1}{\omega_n^2 + 2(\mathcal{K}_0 - \mathcal{K}_n)}. \tag{5.43}$$

5.3.1 Quadratic Polaron Near a Classical Phase Transition

The limit of simultaneous classical order parameter and quantum impurity is achieved in the limit $\beta\,\epsilon_{\text{z.p}} \gg 1$ while $(\tau\Gamma)^{-1} \gg \beta^{2/z}$; altogether $\epsilon_{\text{z.p}}^{-1} \ll \beta \ll (\tau\Gamma)^{-z/2}$. In this regime the order parameter behaves classically and the phase transition is classical. However since the temperature is much smaller than the zero point motion of the particle, the latter ought to be treated quantum mechanically. In this limit, only the zero frequency terms of the order parameter correlation functions contribute to the action, and Eq. (5.31) reduces to:

$$\mathcal{S}^{(1)}_{\text{imp.}} = -\frac{\alpha}{2\beta^2}\iint \frac{\mathrm{d}^d q_1}{(2\pi)^d}\frac{\mathrm{d}^d q_2}{(2\pi)^d}\,\chi_{q_1}\chi_{q_2}|V_{-\mathbf{k}}|^2\iint_0^\beta \mathrm{d}t\mathrm{d}t' e^{-i\mathbf{k}.\Delta\mathbf{R}(t,t')}. \tag{5.44}$$

In three dimensions we get:

$$\begin{aligned}\mathcal{S}^{(1)}_{\text{imp.}} =& \frac{-\alpha}{2\beta^2\theta^2(2\pi)^4\xi^6}\iint_0^\beta \mathrm{d}t\mathrm{d}t'\,\frac{\exp(-2|\Delta\mathbf{R}(t,t')|/\xi)}{|\Delta\mathbf{R}(t,t')|^2/\xi^2}\\ =& \frac{-\alpha}{2\beta^2(2\pi)^4\mu^2}\iint_0^\beta \mathrm{d}t\mathrm{d}t'\,\frac{\exp(-2|\Delta\mathbf{R}(t,t')|/\xi)}{|\Delta\mathbf{R}(t,t')|^2},\end{aligned} \tag{5.45}$$

where $\chi_q \equiv \chi_{q,\omega=0} = (\theta + \mu q^2)^{-1}$. We note that this result is naturally independent of z. This corresponds to a single quantum mechanical particle in a time-independent potential. The ground-state energy of the particle is then achieved by the effective potential well, created by the field configuration. Far from the critical point, where $\lambda/\tau \ll m_e^2\epsilon_F/M\hbar^2 = \lambda_F^2 m_e/M$, the kernel is dominated by the exponential part with correlation length $\xi/2$.

This is equivalent to a nonlocal non-linear Schrödinger equation (NLSE) with a time-independent Hamiltonian. The potential is a two point function:

$$\hat{V}_{d=3}(\hat{\mathbf{x}},\hat{\mathbf{x}}') \propto \frac{\exp(-2|\hat{\mathbf{x}}-\hat{\mathbf{x}}'|/\xi)}{|\hat{\mathbf{x}}-\hat{\mathbf{x}}'|^2}. \tag{5.46}$$

The hat above the parameters indicates their operator nature. In the following, when they are projected onto x-space, we drop the hats. The time-independent Schrödinger equation is derived from the energy functional:

$$\left[\frac{-\hbar^2}{2M}\nabla^2 + \int \mathrm{d}^d x'|\psi(\mathbf{x}')|^2 V_d(|\mathbf{x}-\mathbf{x}'|)\right]\psi(\mathbf{x}) = E\psi(\mathbf{x}). \tag{5.47}$$

Such a problem has been shown to feature the "collapse" of the wave-function in $d \geq 2$, for singular potentials $V(\mathbf{x}, \mathbf{x}') \sim f(\mathbf{x} - \mathbf{x}')/|\mathbf{x} - \mathbf{x}'|^{\nu}$ with $\nu \geq 2$. The collapse is defined mathematically when the norm of the gradient of the wave-function diverges:

$$\textit{Collapse:} \qquad \left(\int \mathrm{d}^d x \, |\nabla \psi|^2 \right)^{1/2} \to \infty. \tag{5.48}$$

Therefore, it is clear that in the case of quadratic polaron, $d = 1, 2$ would not support the collapse. In $d = 3$, the potential has the required singularity to yield the collapse of wave-function. Note that this is the direct consequence of quadratic coupling. Linear-coupling in three dimensions, results in a potential decaying as $\sim 1/|\mathbf{x} - \mathbf{x}'|$ [101]. We will demonstrate in the following, that the localization (collapse) of the wave-function occurs at a finite coupling constant after adding the quantum fluctuations of the field.

5.3.2 Quadratic Polaron Near a Quantum Phase Transition

In the case of a quantum phase transition, dynamic terms of the field also contribute to the properties of the polaron. There are a few points that we need to mention here. The averages $\langle \mathcal{S}^{(1)}_{\text{imp.}} \rangle$ is convergent for linear coupling in all physical dimensions $d = 1, 2, 3$ and for the delta potential. In the case of quadratic coupling the integrals converge for $d = 1, 2$ and for delta potential but diverge for $d = 3$. This is the consequence of unphysical choice of the contact potential. The divergence originates from the equal-time ($u \to 0$) correlations. In order to regularize this, we introduce a soft cutoff of the form $\exp(-q^2/q_c^2)$, where q_c is the cutoff, and can be regarded as the range of the actual potential.

By introducing the cutoff we observe a similar behavior as in the acoustic polaron. The effective mass transforms smoothly from extended to localized for small cutoffs. For larger cutoffs, the transition becomes first order. The onset of this first order line signifies a critical point at around $q_c \simeq 20$. Below we present the results of effective mass of a quadratic polaron, at zero temperature and for $z = 1$:

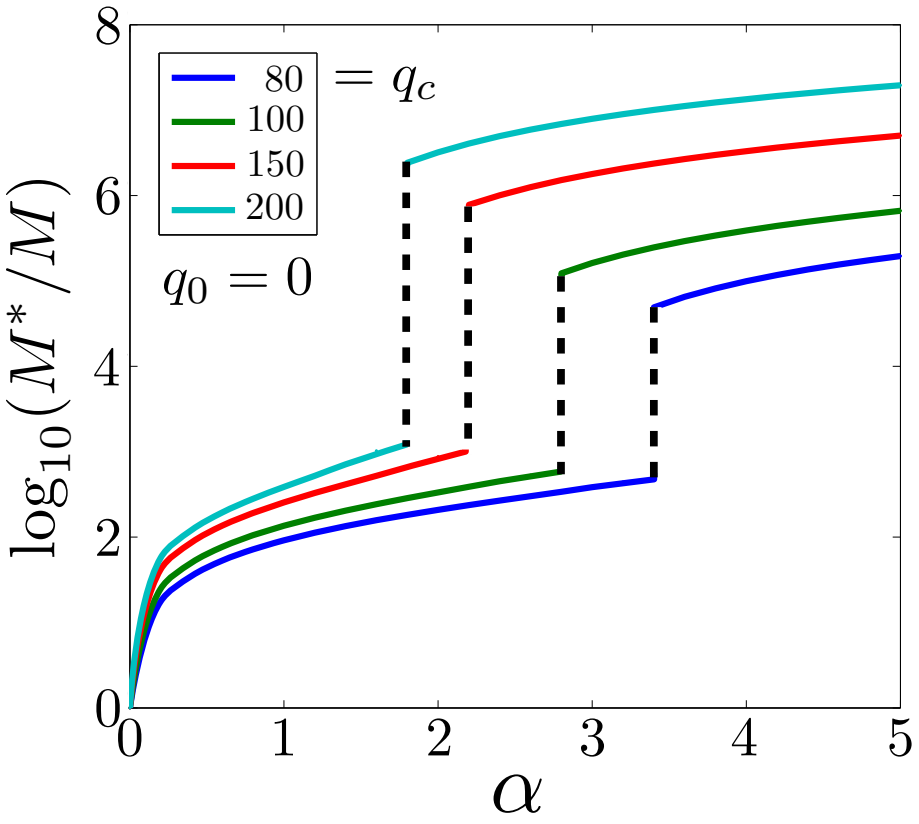

Figure 5.2: Effective mass of the quadratic polaron in $d = 3$ and for $q_0 = 0$. Different colors correspond to different cutoffs $q_c = 80, 100, 150, 200$, while other parameters are fixed at $\theta = \mu = 1$. As we see, in the case of quadratic coupling the effective mass exhibits a first-order localization, as opposed to the linear coupling in all dimensions (see for example Fig. 5.4), and also quadratic coupling in lower dimensions.

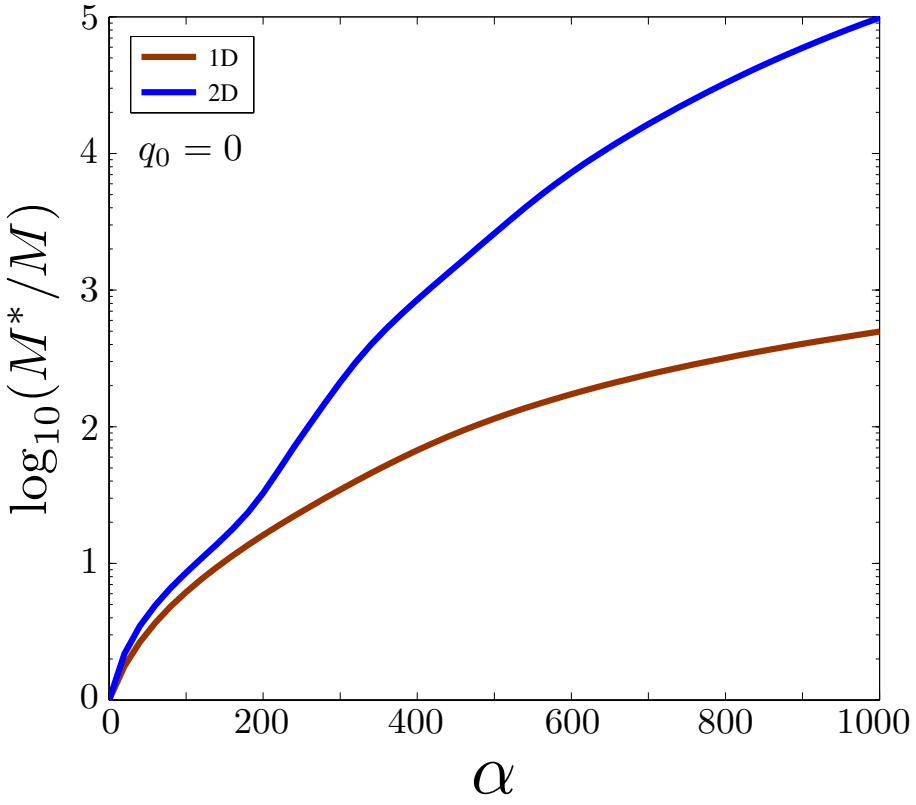

Figure 5.3: Effective mass of the quadratic polaron in $d = 1, 2$. The transition from extended to localized state is smooth for $q = 0$. In order to obtain a discontinuous transition, a minimum q_0 is required which increases for lower dimensions.

5.4 Linear Coupling and Comparison

Now, in order to compare our results, we study the case where an impurity is linearly coupled to a nearly critical field. We use the same parameters θ, μ, Γ, but we note that their physical interpretation might be different from the case studied in previous sections. The action of the impurity reads

$$\mathcal{S}^L_{\text{imp}} = \int_0^\beta \mathrm{d}t \, \left\{ \frac{M}{2} |\dot{\mathbf{R}}|^2 + \int \mathrm{d}^d\mathbf{r} \, V(\mathbf{r} - \mathbf{R}(t)) \phi(\mathbf{r}, t) \right\}. \tag{5.49}$$

Next, the action of the bare field is the same as in Eq. (5.17). Due to lack of the impurity-induced mode coupling, we can integrate out the field degrees of freedom exactly. This leads to the following effective action $\mathcal{S}_{\text{eff}}/\hbar$ for the impurity with a new dimensionless coupling constant for the linear coupling α_L.

$$\mathcal{S}^L_{\text{eff}} = \frac{1}{2} \int_0^\beta \mathrm{d}t |\dot{\mathbf{R}}|^2 - \alpha_L \iint_0^\beta \mathrm{d}t \mathrm{d}t' \int \frac{\mathrm{d}^{d+1}\bar{q}}{(2\pi)^{d+1}} \, \chi_{\bar{q}} \, e^{i\omega|t-t'| - i\mathbf{q}.\Delta\mathbf{R}(t,t')}, \tag{5.50}$$

where $\chi_{\bar{q}}$ is given by Eq. (5.32), and

$$\alpha_L = \frac{1}{4} \left(\frac{V_0}{\epsilon_F} \right)^2 \left(\frac{M\epsilon_F}{\hbar^2} \right)^{d/2}. \tag{5.51}$$

Note that the difference with the case of quadratic coupling is the power of the second factor on the r.h.s. For $\theta = 0$, the problem resembles a variant of acoustic polaron, whereas $\theta \neq 0$ corresponds to optical polaron, where the impurity interacts with a gapped optical phonon. An interesting question is the behavior of the effective mass as a function of gap. We will see below that this behavior is dependent on the dimensionality as well as the coupling constant.

The main features of linear coupling was captured in chapters 3 and 4. We here complement this analysis by extending the calculation to general dimensions and also their dependence on q_0.

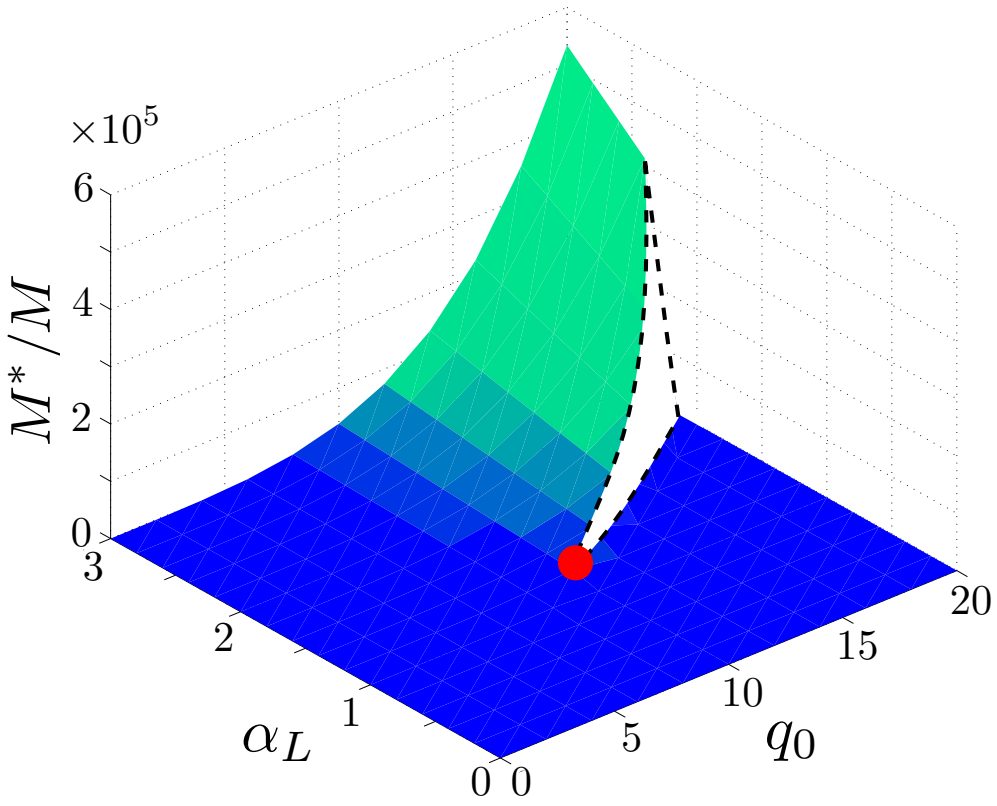

Figure 5.4: Effective mass as a function of the coupling constant and q_0 for $d = 3$. Here $\theta = \mu = 1$. As expected, a minimum q_0 is required for the first order transition in the case of linear coupling.

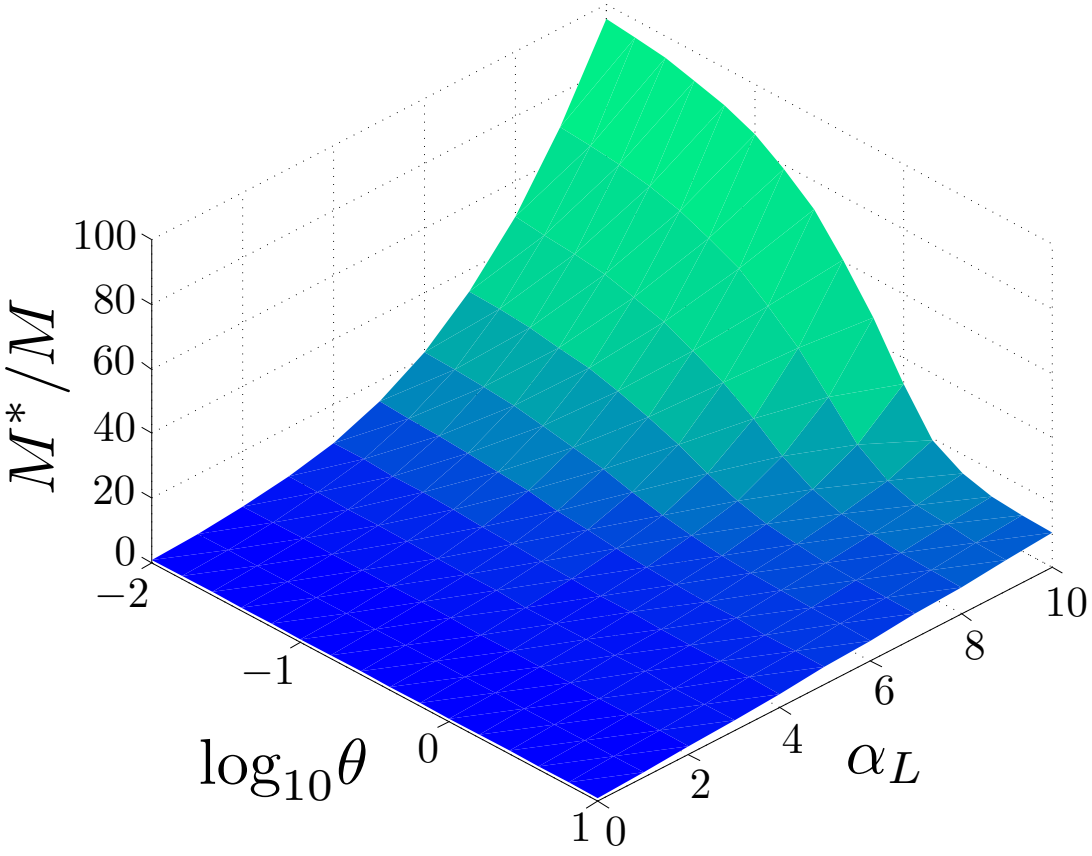

Figure 5.5: At $q_0 = 0$ and $\mu = 1$, the effective mass is plotted against α and $\log_{10}\theta$ is plotted for $d = 3$. For intermediate and large coupling constants, the effective mass decrease as we move away from critical point. This trend is not necessarily true for couplings $\alpha_L \lesssim 1$. The effective mass of the polaron develops a maximum at around $\theta \simeq 1$. Figures (5.6),(5.7) and (5.8), demonstrate this property for certain values of α_L, and compare the results with those of the one- and two-dimensional systems.

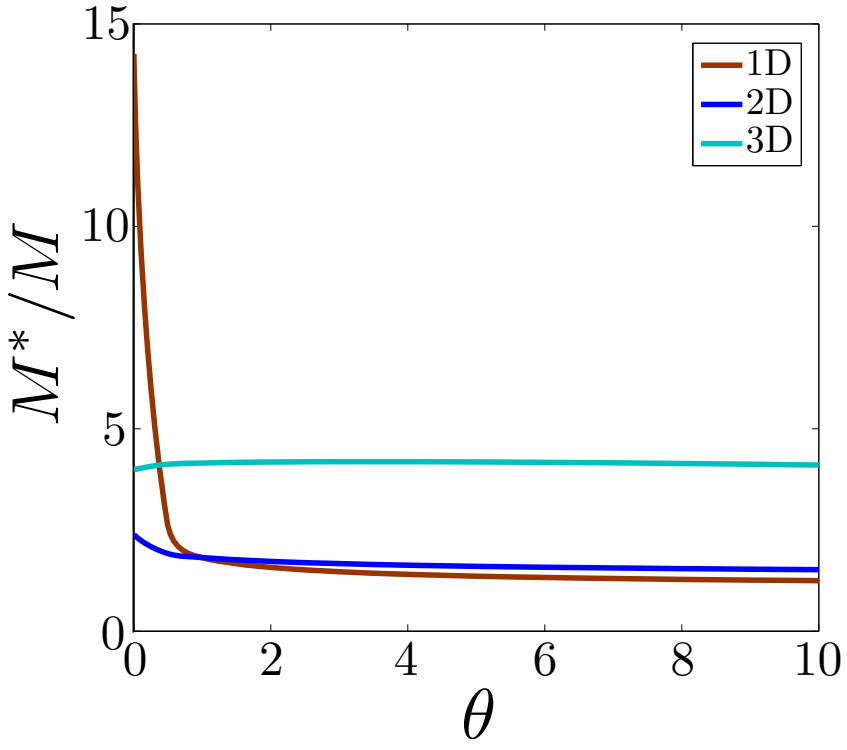

Figure 5.6: At $\alpha_L = 1$, $q_0 = 0$ and $\mu = 1$, the effective mass is plotted against θ for different dimensions. While for $d = 1, 2$ the effective mass decreases monotonically upon increasing θ, in $d = 3$, the effective mass shows a maximum.

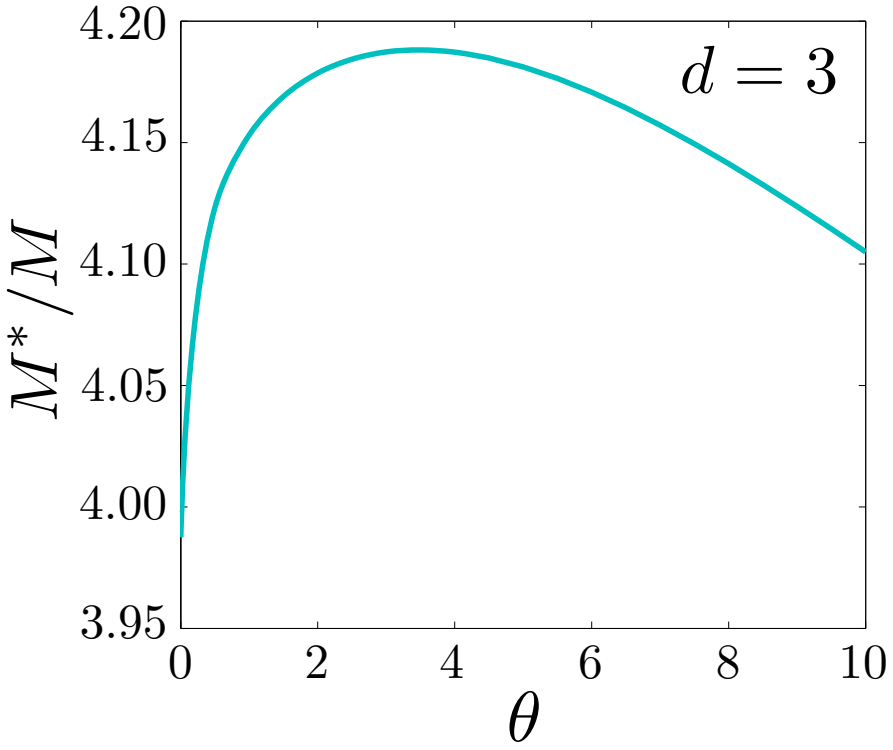

Figure 5.7: At $\alpha_L = 1$, $q_0 = 0$ and $\mu = 1$, the effective mass against θ is plotted for $d = 3$ (zoomed-in Fig. (5.6)).

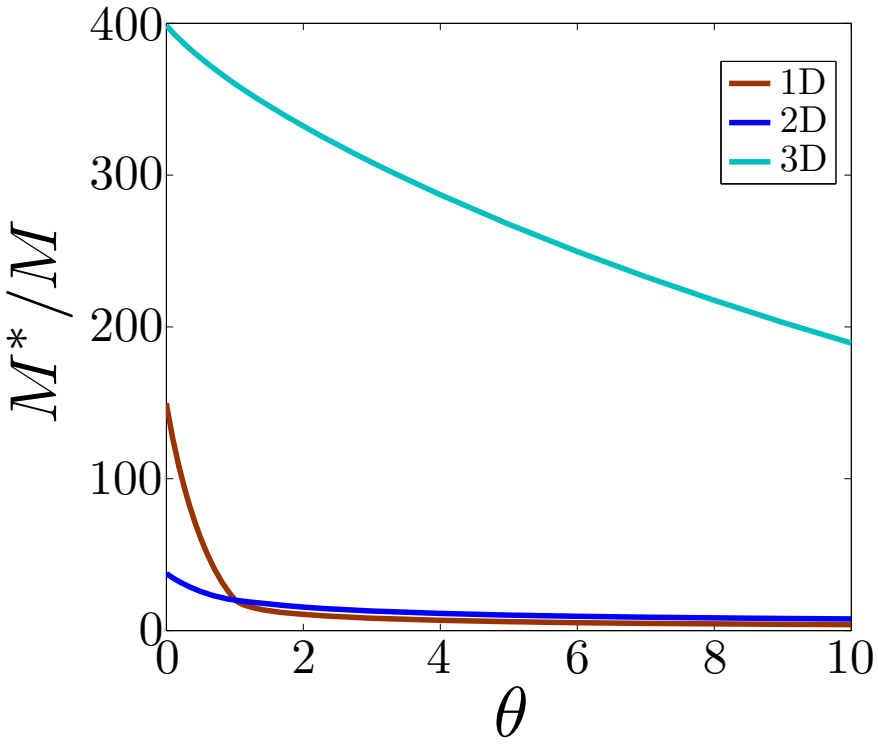

Figure 5.8: At $\alpha_L = 10$, $q_0 = 0$ and $\mu = 1$, the effective mass against θ is plotted for $d = 1, 2, 3$. In large enough couplings, the maximum of effective mass in $d = 3$ disappears.

5.5 Conclusions

In line with our second goal of understanding the role of quantum fluctuations on the polaron properties, we extended our model from the previous chapters, to the case of quadratic coupling. We proposed a model system which supports this coupling. We took the Hertz-Millis theory of second-order quantum phase transitions and its generalization to the case of helimagnets which requires an additive chiral term, the Dzyaloshinskii-Moriya interaction. This interaction induces a fluctuation-induced first order transition of the previously introduced Brazovskii form. Therefore the model seems to be a good candidate for studying the role of quadratic couplings within the same framework as in the previous chapters.

We observe that in three dimensions, the behavior of polaron is significantly altered by quadratic coupling. In the linear coupling case, a minimum preferred wave-vector q_0 of the field is required to localize the particle in all dimensions. However quadratic coupling in three dimensions was shown to cause the collapse of the wave-function in the classical field limit. After including the quantum fluctuations of the field, in three dimensions a divergence appears because of the nonphysical contact potential. We introduced a soft Gaussian cutoff to regularize this. For small cutoffs $q_c \lesssim 20$ the transition is smooth. Increasing the cutoff opens up a gap in the effective mass. This is very similar to the case of acoustic polaron. We note that the effective mass of the polaron increases very rapidly as a function of α, even before the discontinuity is approached. The numerical values are obtained for a specific set of parameters $\theta = \mu = 1$, and thus $\xi = 1$. For shorter correlation lengths, the transition takes place at smaller couplings. In $d = 1, 2$ the situation is qualitatively the same as the linear coupling. For $q_0 = 0$, the transition remains smooth, and a minimum q_0 is required to cause the first order transition. The minimum required value of q_0 is larger for lower dimensions (as expected), and is zero for $d = 3$.

Although the main features of the linear coupling case was addressed in chapters 3 and 4, we extended the phase diagram by varying q_0, so to compare the results with the quadratic case. At $q_0 = 0$, we also calculate at small $\alpha_L = 1$ and large couplings $\alpha_L = 10$, the effective mass as a function of distance from the critical point of the field. For $\alpha_L = 1$, the effective mass is monotonically decreasing for $d = 1, 2$ whereas it develops a maximum in $d = 3$ (see Figs. (5.6,5.7)). At larger couplings $\alpha_L \simeq 2$, the maximum of the 3D case disappears and becomes monotonically decreasing like 1D and 2D cases. It is noteworthy that the dimensionless coupling constants in both linear and quadratic cases, are themselves dependent on the dimensionality, and thus, have different expressions in terms of the actual parameters, for each dimension. In all the above calculations, we have absorbed this dependence in the definition of α.

CHAPTER 6

Appendix

In the appendix of this dissertation, we first present in section 6.1, the details of the molecular dynamics (MD) simulations performed to obtain the results of the classical charge particle in water. Next, in section 6.2, we review the traditional polaron problem and present their results based on perturbation theory and variational method. We finally introduce the formalism of the classical fluctuation-induced first order phase transitions in section 6.3, specifically the Brazovskii renormalization approach.

6.1 Molecular Dynamics Simulations

Molecular dynamics (MD) simulations are performed using the Gromacs simulation package. Throughout this study, the SPC/E water model is used, which consists of three point charges arranged in a fixed geometry with partial charges $z_{\mathrm{H}} = +0.4238$ on the hydrogen atoms and $z_{\mathrm{O}} = -0.8476$ on the oxygen atom. Dispersion interactions between the water molecules are modeled by a Lennard-Jones interaction centered on the oxygen atom.

We consider systems of two different sizes: The smaller system consists of 895 water molecules in a cubic box with periodic boundary conditions. At $T = 300\,\mathrm{K}$ this corresponds to a box size of roughly $3.0 \times 3.0 \times 3.0\ \mathrm{nm}^3$. We perform simulations at a temperature of $T = 300$ K and at a pressure of $p = 1\,\mathrm{bar}$. The system is equilibrated first in a NVT ensemble (constant particle number, volume and temperature) for $t = 50\,\mathrm{ps}$ and then in a NPT ensemble (constant particle number, pressure and tem-

perature) for $t = 10\,\mathrm{ns}$, in order to determine the box size corresponding to the pressure of $p = 1$ bar. The box size is then set to the average obtained in the NPT simulation and after an additional equilibration of $t = 50$ ps production runs are performed in the NVT ensemble for $t = 0.4\,\mathrm{ns}$. Configurations are saved with the full time resolution of $\delta t = 0.002$ ps. Additionally, longer simulations are run for $t = 2.0\,\mathrm{ns}$ and configurations are saved with a time resolution of $\delta t = 0.01$ ps. To determine the heat capacities at constant volume c_v and constant pressure c_p, additional simulations at temperatures of $T = 280$ and 320 K are performed in the NVT and NPT ensembles for $t = 10$ ns, respectively.

To reach lower wave vectors and to obtain a better resolution of the low-wave vector region of the dynamic structure factor, we also simulate a larger system containing ≈ 33000 water molecules, which corresponds to a box size of $10 \times 10 \times 10$ nm^3, in the NVT ensemble for $t = 2.0$ ns, where configurations are saved each $\delta t = 0.01$ ps, after equilibration in the NPT ensemble for $t = 2.0$ ns.

A Berendsen weak coupling thermostat and barostat with a relaxation time of $\tau = 1.0\,\mathrm{ps}$ is used for temperature and pressure control. All non bonded interactions are cut off at a radius of $r_\mathrm{c} = 0.9\,\mathrm{nm}$. Long-range electrostatic interactions are treated by the particle mesh Ewald method with tinfoil boundary conditions. For the Lennard-Jones interaction an analytic long-range correction is applied to energy and pressure. The bonds and angles in the water molecules are kept fixed using the analytic SETTLE algorithm, and a timestep of 2 fs is used for the integration of the equations of motion.

6.2 Polaron Theory

The notion of Polaron was first introduced by Landau. Searching for the possible sources of conductivity in ionic crystals, Landau and Pekar [102] considered the effects of fluctuations of the ion cores around their equilibrium position, *i.e.* phonons, on electrons. When the oscillations of ion cores are frozen, the electron is subject to a periodic potential with the periodicity of lattice constant. Such a problem is well understood; the electrons form the Bloch bands. Upon including the phonons, the Hamiltonian of this systems consists of three terms, corresponding to: (1) the kinetic energy of the electron, (2) the energy of the optical phonons, and (3) electron-phonon interaction. In the weak coupling regime, where the electron is extended over many lattice sites, the system is usually described by Fröhlich Hamiltonian:

$$\hat{H}_{\text{Fröh}} = \hat{H}_{\text{e}} + \hat{H}_{\text{ph}} + \hat{H}_{\text{e-ph}}. \tag{6.1}$$

where $\hat{H}_{\text{e}}$ and $\hat{H}_{\text{ph}}$ are the free electron and phonon Hamiltonians respectively, while the last term $\hat{H}_{\text{e-ph}}$ is their interaction. We introduce each term below.

$$\hat{H}_{\text{e}} = \sum_{\mathbf{q},n,s} \epsilon_{n,\mathbf{q},s} c^{\dagger}_{n,\mathbf{q},s} c_{n,\mathbf{q},s}, \tag{6.2a}$$

$$\hat{H}_{\text{ph}} = \sum_{\mathbf{k},\nu} \hbar\omega_{\mathbf{k},\nu} b^{\dagger}_{\mathbf{k},\nu} b_{\mathbf{k},\nu}, \tag{6.2b}$$

$$\hat{H}_{\text{e-ph}} = \sum_{\mathbf{q},\mathbf{k},n,n',s,\nu} \gamma_{n,n'}(\mathbf{q},\mathbf{k},\nu)\omega_{\mathbf{k},\nu} c^{\dagger}_{n',\mathbf{q},s} c_{n,\mathbf{q}-\mathbf{k},s} b_{\mathbf{k},\nu} + \text{H.c.} \tag{6.2c}$$

where $\epsilon_{n,\mathbf{q},s}$ is the eigen-energy of the free electron part in band n, momentum $\mathbf{q}$ and spin s. Similarly for the second contribution we have, $\hbar\omega_{\mathbf{k},\nu}$ is the energy of phonons with momentum $\mathbf{k}$ and band index ν. The last term is the electron-phonon interaction with vertex $\gamma_{n,n'}(\mathbf{q},\mathbf{k},\nu)$. This term accounts for electrons-phonon scattering. In the above we have used the shorthand notation: $\sum_{\mathbf{k}} \equiv \int \frac{\mathrm{d}^3 k}{(2\pi)^3}$.

Fröhlich Hamiltonian describes the polaron as an electron-field interaction. An electron-lattice model, in the limit of strong coupling where the electrons are localized is usually studied using the Holstein Hamiltonian,

$$\hat{H}_{\text{Hol}} = -t \sum_{\langle ij \rangle, s} (c^{\dagger}_{i,s} c_{j,s} + \text{H.c.}) + \hbar\omega_0 \sum_i b^{\dagger}_i b_i + g \sum_i n_i (b^{\dagger}_i + b_i). \tag{6.3}$$

Here i, j label the lattice sites, and $\langle ij \rangle$ means the summation over nearest neighbors. Therefore the first term accounts for hopping events between neighboring sites i, j. Also $(c^{\dagger}_i, c_i)$ and $(b^{\dagger}_i, b_i)$ denote the (creation,annihilation) operators of the electron and lattice ions respectively. Finally the last term represents with the local interaction of electron number $n_i = \sum_s c^{\dagger}_{i,s} c_{i,s}$, and the displacement of the ion cores.

6.2.1 Optical Polaron

Optical polaron forms as a result of the interaction of the electron with longitudinal optical phonon. The optical phonons have a relatively dispersionless spectrum where the frequency is—within the range of interest—independent of the wave-vector: $\omega_{\mathbf{k}} = \omega_{\text{opt}}$. The dispersion relations of the acoustic and optical phonons are shown in Fig. 6.1.

For simplicity, we can ignore and drop spin and band indices and assume the interaction of an electron with mass M, with a single optical mode. Setting $\hbar = \omega_{\text{opt}} = M_e = 1$, we get:

$$\hat{H} = \frac{\mathbf{P}^2}{2} + \sum_{\mathbf{k}} b^{\dagger}_{\mathbf{k}} b_{\mathbf{k}} + i(\sqrt{2}\alpha\pi)^{1/2} \sum_{\mathbf{k}} \frac{1}{|\mathbf{k}|} [b^{\dagger}_{\mathbf{k}} e^{-i\mathbf{k}.\mathbf{R}} - b_{\mathbf{k}} e^{+i\mathbf{k}.\mathbf{R}}]. \tag{6.4}$$

Here $(\mathbf{R}, \mathbf{P})$ are the canonical (position,momentum) coordinates of the electron. The components of these coordinates satisfy $[R_i, P_j] = i\hbar\delta_{i,j}$. Also α is the dimensionless electron-phonon coupling constant, given by:

$$\alpha = \frac{\text{e}^2}{2\hbar\omega_{\text{opt}}} \left(\frac{1}{\epsilon_\infty} - \frac{1}{\epsilon_0} \right) \left(\frac{2M\omega_{\text{opt}}}{\hbar} \right)^{1/2} \tag{6.5}$$

where e is the charge of the electron, and where ϵ_∞ and ϵ_0 are the high-frequency and static dielectric constants of the medium respectively.

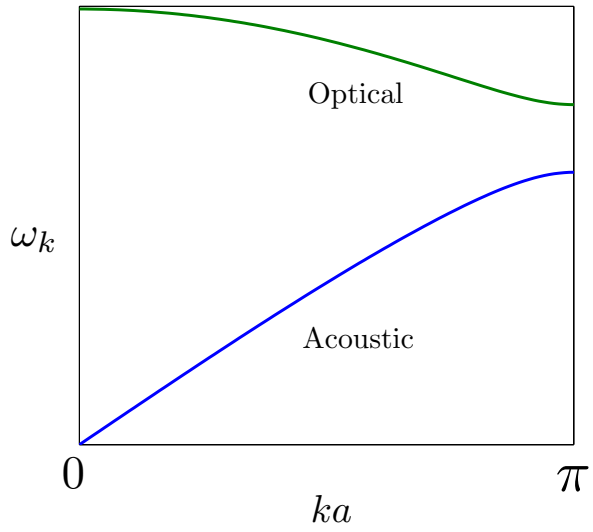

Figure 6.1: Dispersion relations of the acoustic and optical phonons. We note that optical branch is gapped whereas the acoustic branch is gapless at $k = 0$. In the general form, the gap at the Brillouin zone implies that there are more than one atoms per unit cell. For atoms with equal masses, the gap closes at the edge of the Brillouin zone $k = \pi/a$.

In the following we briefly review the results of second order perturbation theory, as well as variational method.

- **Second order perturbation theory:**

We consider the interaction term as a perturbation to the free terms. Therefore we would like to calculate the energy shift due to this interaction ΔE_0. We assume that the unperturbed Hamiltonian is diagonalized in the basis $|n\rangle$, which represent the simultaneous eigenstates of the particle and phonons. To second order perturbation we have:

$$\Delta E_0 = H^{00}_{\text{e-ph}} + \sum_n \frac{H^{0n}_{\text{e-ph}} H^{n0}_{\text{e-ph}}}{E^0_0 - E^0_n} + \dots , \tag{6.6}$$

where $H^{nm}_{\text{e-ph}} = \langle n|\hat{H}_{\text{e-ph}}|m\rangle$, and E^0_n is the n^{th} eigenvalue of the unperturbed Hamiltonian. We see from Eq. (6.4) that $\hat{H}_{\text{e-ph}}$ changes the number of phonons. Thus the first term in the above perturbative expansion vanishes. The second term is the first contribution, corresponding to an electron-phonon scattering. The initial and final states are, an electron with momentum $\mathbf{P}$ and with no phonons present, whereas the intermediate state corresponds to an electron with momentum $\mathbf{P}-\mathbf{k}$, and a phonon with momentum $\mathbf{k}$. We finally need to integrate over all possible $\mathbf{k}$'s. It turns out that the energy shift can be written in the following form:

$$\Delta E_0 = -4\sqrt{2}\pi\alpha \int \frac{\mathrm{d}^3k}{(2\pi)^3}\frac{1}{k^2(k^2-2\mathbf{P}.\mathbf{k}+2)} = -\alpha\,\frac{\sqrt{2}}{P}\sin^{-1}\frac{P}{\sqrt{2}}. \tag{6.7}$$

For the particle at rest, $P\to 0$, we get $\Delta E = -\alpha$. If we include higher orders of α, we get:

$$\Delta E = -\alpha + 0.0126\alpha^2. \tag{6.8}$$

If we instead expand the r.h.s of the last equality in Eq. (6.7) for small P, we get:

$$\Delta E = \frac{P^2}{2(1+\alpha/6)} - \alpha, \tag{6.9}$$

which suggests that the effective mass of the polaron can be obtained by:

$$M^*/M = 1+\alpha/6. \tag{6.10}$$

- **Variational method:**

Unlike the case of electron-photon interaction with coupling constant, $\alpha = \mathrm{e}^2/\hbar c = 1/137$, (with c the velocity of light), the coupling constant of electron-phonon interaction for typical polar crystals is of the order $\alpha\sim 3-6$. This implies that the perturbation theory fails very fast. In order to study the intermediate and large couplings, Feynman proposed an all-coupling variational approach based on path-integral formalism. This approach was introduced in treatment of the Bose-polaron problem where using the Bogoliubov shift, one can map the electron-atoms interaction to a Fröhlich type Hamiltonian. Here we present the results for the simplest case of an electron interacting with

longitudinal optical phonons, originally presented by Feynman. The advantage of this method (of course with the aid of computers) is its capability to bridge the small and large coupling regimes. The formulation starts with the definition of partition function:

$$\mathcal{Z} = e^{-\beta\mathcal{F}} = \text{Tr}[e^{-\beta H}] = \sum_i e^{-\beta E_i}. \tag{6.11}$$

The free energy $\mathcal{F}$ is dominated by the ground-state E_0 in the zero temperature limit $\beta \to \infty$. The trace in the above equation can be calculated using path-integral method;

$$\mathcal{Z} = \text{Tr}[e^{-\beta H}] = \int \mathcal{D}(\text{path}) e^{-S}. \tag{6.12}$$

In order to better make use of this representation it is convenient to transform the creation-annihilation operators of the phonon to their displacements and conjugate momenta, corresponding to the motion of crystal, namely:

$$q_{\mathbf{k}} = \frac{1}{\sqrt{2}}(b^\dagger_{\mathbf{k}} + b_{-\mathbf{k}}), \tag{6.13a}$$

$$p_{\mathbf{k}} = \frac{i}{\sqrt{2}}(b^\dagger_{-\mathbf{k}} - b_{\mathbf{k}}). \tag{6.13b}$$

If we use the present form of these coordinates, the electron-field interaction turns out to be $p_{\mathbf{k}}$-dependent, which is not suitable. By performing a canonical rotation in the $(q_{\mathbf{k}}, p_{\mathbf{k}})$ or in the $(b^\dagger_{\mathbf{k}}, b_{\mathbf{k}})$ spaces, we can resolve this issue. After these transformations we obtain the full Hamiltonian,

$$\hat{H} = \frac{\mathbf{P}^2}{2} + \sum_{\mathbf{k}} \frac{1}{2}\left(p^2_{\mathbf{k}} + q^2_{\mathbf{k}}\right) + \sqrt{2}(\sqrt{2}\pi\alpha)^{1/2} \sum_{\mathbf{k}} \frac{1}{|\mathbf{k}|} q_{\mathbf{k}} e^{i\mathbf{k}.\mathbf{R}}. \tag{6.14}$$

We can now interpret the shorthand measure $\mathcal{D}(\text{path})$:

$$\text{Tr}[e^{-\beta H}] = \int_{\substack{\mathbf{R}(0)=\mathbf{R}(\beta) \\ q_i(0)=q_i(\beta)}} e^{-S}\, \mathcal{D}[\mathbf{R}(u)]\mathcal{D}[q_2(u)]\mathcal{D}[q_1(u)]... \tag{6.15}$$

where the action is,

$$S = \int \mathrm{d}u \left\{ \frac{|\dot{\mathbf{R}}(u)|^2}{2} + \sum_{kk} \frac{1}{2}\left(\dot{q}^2_{\mathbf{k}}(u) + q^2_{\mathbf{k}}(u)\right) + \sqrt{2}(\sqrt{2}\pi\alpha)^{1/2} \sum_{\mathbf{k}} \frac{1}{|\mathbf{k}|} q_{\mathbf{k}}(u) e^{i\mathbf{k}.\mathbf{R}(u)} \right\}. \tag{6.16}$$

We note that the path-integral over the field degrees of freedom can be carried out due to its Gaussian form. We are then left with and effective Euclidean action for the particle:

$$S = \frac{1}{2}\int_0^\beta \mathrm{d}t\ |\dot{\mathbf{R}}|^2 - \sqrt{2}\pi\alpha \iint_0^\beta \mathrm{d}t\mathrm{d}s \int \frac{\mathrm{d}^3k}{(2\pi)^3}\frac{1}{k^2} e^{-|t-s|} e^{i\mathbf{k}.(\mathbf{R}(t)-\mathbf{R}(s))}. \tag{6.17}$$

As we see, the coordinate of the particle does not appear quadratically. Therefore the path-integral cannot be performed exactly. We now introduce a trial action, with a few adjustable parameters to minimize the free energy.

$$S_t = \frac{1}{2}\int_0^\beta \mathrm{d}t\ |\dot{\mathbf{R}}|^2 + \frac{C}{2}\iint_0^\beta \mathrm{d}t\mathrm{d}s\, e^{-W|t-s|}|\mathbf{R}(t)-\mathbf{R}(s)|^2 \tag{6.18}$$

where we assume the particle is interacting through a spring with constant $K = MW^2$ and a coupling constant $C = MW^3/4$.

The Feynman's variational inequality utilizes the convexity of the exponential function e^{-f} and, thus the inequality $\langle e^{-f}\rangle \geq e^{-\langle f\rangle}$. Using this inequality, an appropriate relation can be derived between the free energies of the original and trial actions, and their actions:

$$\mathcal{F} \leq \mathcal{F}_t + \frac{1}{\beta}\langle S - S_t\rangle_t. \tag{6.19}$$

The subscript t in $\langle\bullet\rangle_t$ means averaging using the weights e^{-S_t}, corresponding to the trial action. In the zero temperature limit, one can replace $\mathcal{F}$ and $\mathcal{F}_t$ by ground-state energies E and E_t, respectively. According to the above inequality, we need to calculate $\langle S\rangle_t$, *i.e.* the average of the original action with respect to trial action. We note that this can be done by calculating,

$$\langle e^{-i\mathbf{k}.(\mathbf{R}(t)-\mathbf{R}(s))}\rangle_t = \exp\left[-\frac{k^2}{2}\left\{\frac{W^2}{V^2}|t-s| + \frac{4C}{WV^3}[1-e^{-|t-s|V}]\right\}\right], \tag{6.20}$$

in which the dependent parameter V is defined by $V^2 \equiv W^2 + 4C/W$, for later convenience. We can also calculate E_0 and $\langle S_t\rangle_t$ immediately, using the fact that $E_t(C=0) = 0$. Consequently the Feynman's inequality reads:

$$E \leq \frac{3}{4V}(V-W)^2 - \frac{\alpha V}{\sqrt{\pi}}\int_0^\infty \mathrm{d}u\, e^{-u}\left[W^2u + \frac{V^2-W^2}{V}(1-e^{-uV})\right]^{-1/2}. \tag{6.21}$$

We now need to minimize the above action with respect to W, V. This can only be done analytically for the small and large α, separately.

Small coupling: For small α, we expect C to be very small, thus one can take $V = W(1 + \epsilon)$. Using this approximation we will obtain for the ground-state energy and the effective mass of the polaron,

$$E \leq -\alpha - 0.0123\alpha^2, \tag{6.22a}$$

$$M^*/M = 1 + \frac{\alpha}{6} + 0.025\alpha^2. \tag{6.22b}$$

We remember that from perturbation theory, the result is

$$E = -\alpha - 0.0126\alpha^2. \tag{6.23}$$

Large coupling: In the large coupling regime, we use another approximation: $V/W \gg 1$. This leads to the following relations:

$$E \leq -\alpha^2/2\pi - \frac{3}{2}(2\ln 2 + \gamma) - \frac{3}{4} + \mathcal{O}(1/\alpha^2), \tag{6.24a}$$

$$M^*/M = (2\alpha/3\pi)^4. \tag{6.24b}$$

In the first equation γ is the Euler-Mascheroni constant, $\gamma = 0.5772$.

The intermediate coupling regime can be explored using numerical methods. As a result of exact minimization with respect to W, V, we obtain the following result: Figure (6.2) shows that upon cranking up the coupling constant, the extended polaron with an effective mass of the order of the bare mass, is transformed *continuously* to a self-trapped polaron with large effective mass.

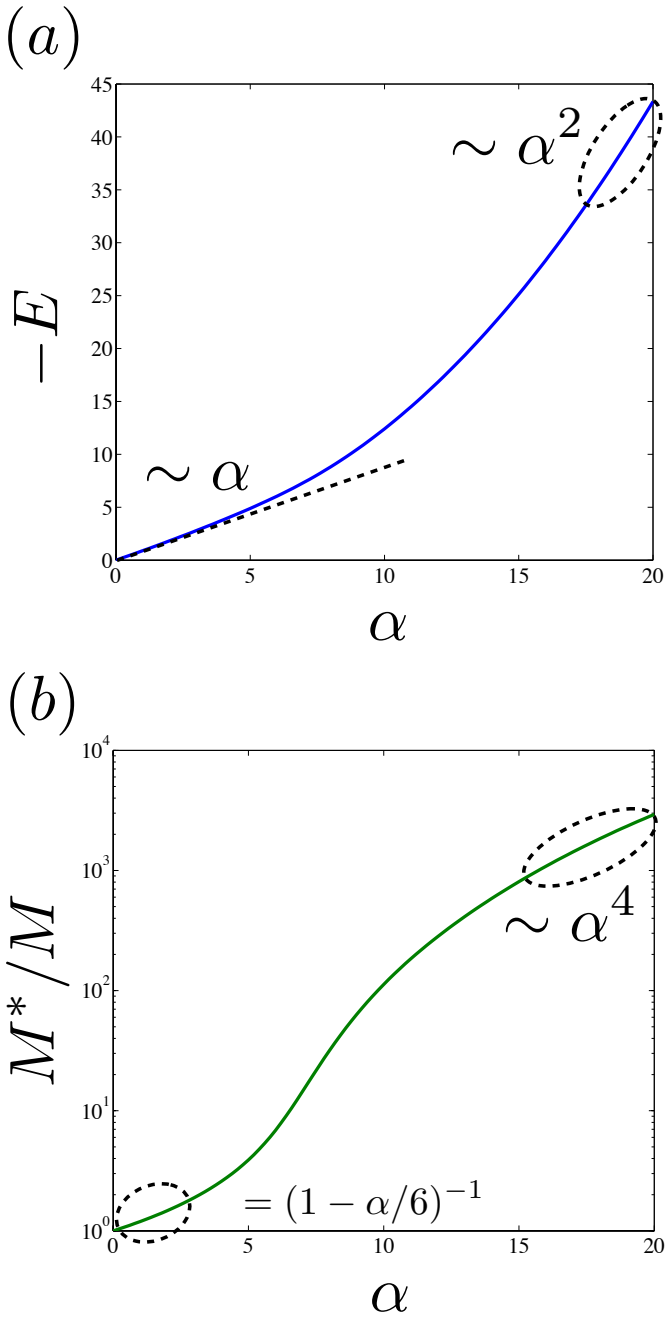

Figure 6.2: Top panel (a) shows the minimized ground-state energy as a function of the dimensionless coupling constant. (b) shows effective mass versus α. We note that the transition between the small and large coupling is smooth.

6.2.2 Acoustic Polaron

In addition to the optical phonons where the neighboring lattice sites oscillate out of phase, there exists another branch of phonons, the "acoustic" phonons. Acoustic phonons are gapless Goldstone modes, which arise as a result of continuous translational symmetry. For ionic mass m, and elastic constant of the interatomic potential K, we define $\omega = \sqrt{K/m}$, in terms of which the dispersion relation of the acoustic phonons reads (see Fig. 6.1):

$$\omega_k = 2\omega \left|\sin(ka/2)\right|, \tag{6.25}$$

where a is the lattice constant. In the $k \to 0$ limit, the dispersion becomes linear: $\lim_{k\to 0} \omega_k = \omega a|k|$.

Acoustic polaron is created when an impurity particle is added to a bath of acoustic phonons. We can follow the same lines as in the case of optical polaron. According to Peeters and Devreese [72], the final result of the effective mass and self-energy of acoustic polaron is dependent on the momentum cutoff. Beyond a certain large cutoff, the effective mass of the polaron indicates a discontinuity at a critical coupling constant of order $\alpha \sim 0.1$.

Figure (6.3) shows that for large enough momentum cutoffs k_0, upon cranking up the coupling constant, the extended polaron with an effective mass of the order of the bare mass, is transformed *discontinuously* to a self-trapped polaron with large effective mass. We note that this is similar to the behavior of Bose-polaron in harmonic traps. The similarity is mainly because the Bogoliubov excitations look like acoustic phonons in the small k regime.

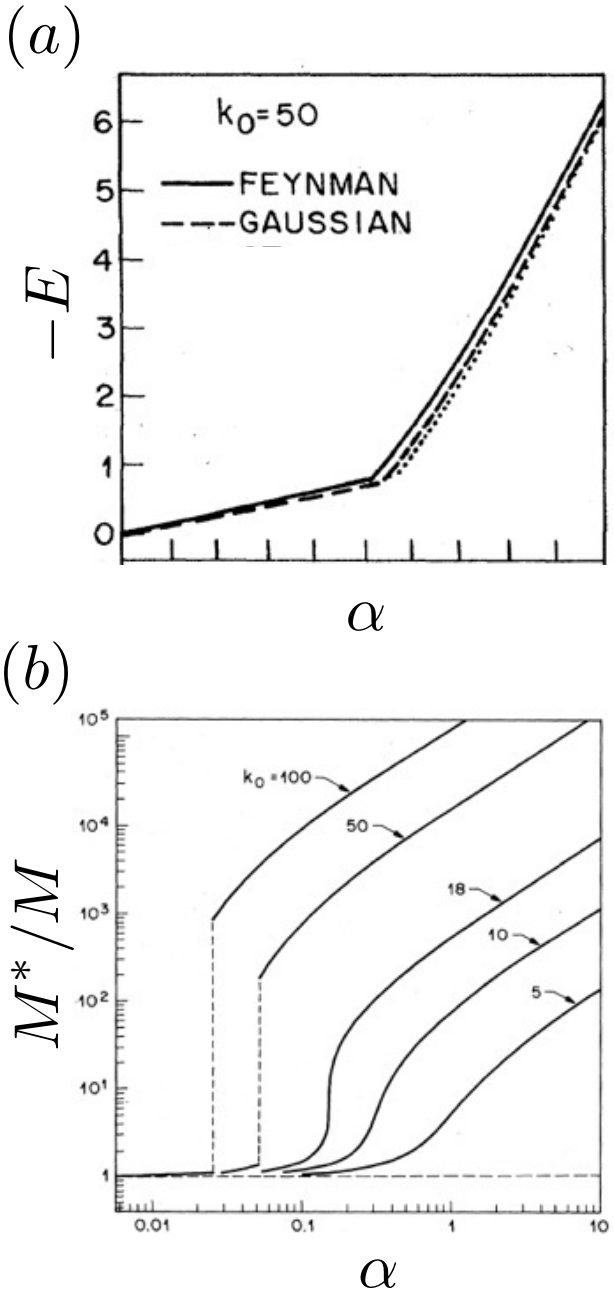

Figure 6.3: (From Ref. [72]) Top panel (a) shows the minimized ground-state energy as a function of the dimensionless coupling constant. (b) shows effective mass versus α. Beyond a certain cutoff k_0, the transition becomes discontinuous.

6.3 Fluctuation-induced First Order Phase Transitions

We repeatedly discussed the importance of the critical modes with finite wave-vector, and used in particular the consequences of the Brazovskii renormalization approach. We mentioned that in spatial dimensions $d \geq 2$, the fluctuations around the momentum shell with radius q_0, renders the second-order mean-field transition, a weakly first-order transition. This is also called the weak crystallization theory, as the first order jump remains small; hence a large correlation length. In fact the justification of a field theoretic (continuum) description of a first order transition lies in the weakness of transition. In this section we demonstrate the renormalization procedure of a class of the Brazovskii action.

6.3.1 Brazovskii Class of Phase Transitions

We start with the Euclidean action of the Brazovskii model, which can be written as a sum of a quadratic and a quartic terms; $\mathcal{S} = \mathcal{S}^{(2)} + \mathcal{S}^{(4)}$:

$$\mathcal{S} = \frac{1}{2!} \sum_{\mathbf{q},\nu} \phi^*_{\mathbf{q},\nu} \left(\omega_\nu^2 + \Delta + \lambda \mathcal{R}^2 (|\mathbf{q}| - q_0)^2 \right) \phi_{\mathbf{q},\nu} + \mathcal{S}^{(4)}. \tag{6.26}$$

The first term of the r.h.s corresponds to the quadratic part $\mathcal{S}^{(2)}$. The dynamics is assumed to be undamped. We note that $u > 0$ is required for stability. The second term, the quartic contribution, can be written in the Fourier form:

$$\mathcal{S}^{(4)} = \frac{U}{4!} \sum_{\{\mathbf{q}_i\},\{\nu_i\}} \phi_{\mathbf{q}_1,\nu_1} \phi_{\mathbf{q}_2,\nu_2} \phi_{\mathbf{q}_3,\nu_3} \phi_{\mathbf{q}_4,\nu_4} \delta^{(d)} \left(\sum_{i=1}^{4} \mathbf{q}_i \right) \delta \left(\sum_{i=1}^{4} \nu_i \right). \tag{6.27}$$

A class of static saddle-point solutions can be suggested as:

$$\phi(\mathbf{x}, \tau) = A \exp(i \mathbf{q}_0 . \mathbf{x}), \tag{6.28}$$

which correspond to modes (in all directions), with wave-vector $\mathbf{q} = \mathbf{q}_0$. The amplitude of this mode is denoted by A. The modes clearly are time-independent corresponding to $\omega_\nu = 0$, where the quantum fluctuations are quenched. The Euler-Lagrange equation

for A, determines the amplitude of the mode:

$$\frac{\delta \mathcal{S}}{\delta A} = \Delta A + u A^3 = 0. \tag{6.29}$$

For $\Delta > 0$, the acceptable solution is $A = 0$. The amplitude can be nonzero for $\Delta < 0$. In this case we get: $A = \sqrt{-\Delta/u}$.

This mean-field order-parameter is equivalent to the one used in the classical model where the frequency summation is dominated by $\omega_\nu = 0$ term. In the classical form the quadratic term reads:

$$\mathcal{S}^{(2)}/\hbar \equiv \beta \mathcal{F} = \frac{1}{2!} \sum_{\mathbf{q}} \phi^*_{\mathbf{q}} \left(\Delta + \lambda \mathcal{R}^2 (|\mathbf{q}| - q_0)^2 \right) \phi_{\mathbf{q}}. \tag{6.30}$$

In any case, when the action is treated like a Landau-Ginzburg model, *i.e.* assuming a large correlation length in the vicinity of the transition, such that the coarse-graining procedure is legitimate, the Brazovskii model, at the mean-field level, predicts a second order critical point at $\Delta = 0$. This is, however, not the correct fate of the story. In order to investigate the effects of fluctuation, one needs to design an appropriate renormalization analysis, where the high-energy modes around $q = q_0$ are integrated out step-by-step. Their effects are then included in the renormalized coefficients.

6.3.2 Renormalization Procedure

The renormalization procedure in classical systems can be carried out separately in space and time (if required). The statics and dynamics of classical systems are independent. At zero temperature, where the quantum effects are most significant, space and time are no longer independent. One needs to carefully integrate out the high-energy modes in momentum and frequency spaces *simultaneously*. In other words, in each step of this process, the momentum- and frequency-shells shrink together. The RG program presented in this section is based on the one presented in Ref. [75].

We first recast the action in a more convenient form for RG process:

$$\mathcal{S}^{(2)} = \frac{1}{2!}\int \mathrm{d}1\Delta(1,2)\phi(1)\phi(2)\delta(1+2), \tag{6.31a}$$

and,

$$\mathcal{S}^{(4)} = \frac{1}{4!}\int \mathrm{d}1\mathrm{d}2\mathrm{d}3\mathrm{d}4\, u(1,2,3,4)\phi(1)\phi(2)\phi(3)\phi(4)\,\delta(1+2+3+4). \tag{6.31b}$$

In the above notation, we have

$$\int \mathrm{d}1 \equiv \frac{1}{(2\pi)^d}\int \mathrm{d}\Omega_1 \int_{|q-q_0|<Q} q_0^{d-1}\mathrm{d}q_1 \int_{-\infty}^{+\infty}\mathrm{d}\omega_1, \tag{6.32}$$

where Ω is the solid angle, and Q is the renormalization group scale. We are now ready to perform the RG transformation, by first integrating out the modes in a momentum shell that satisfy: $Q/b \leq |q-q_0| \leq Q$, with $b = 1+\ell$, and $\ell \ll 1$, and second rescaling the length-scales which results in: $q \to bq$ and $\phi \to \phi/b$. Under these transformations the two-point vertex transforms to:

$$r(Q) \to r(Q/b) = b^2\left(\Delta(Q) + \mathcal{P}u_1(Q)\int_{Q/b}^{Q}\mathrm{d}q\,\frac{1}{\Delta(Q)+q^2}\right), \tag{6.33}$$

where $\mathcal{P} \propto q_0^2$ is called the self-energy coefficient. Using $b = 1+\ell$, we get:

$$\frac{\mathrm{d}r}{\mathrm{d}\ell} = 2\Delta(Q) + \frac{Q\mathcal{P}u_1(Q)}{[\Delta(Q)+Q^2]^{1/2}}. \tag{6.34}$$

We note that the four-point vertex now renormalizes in different manners, depending on how many of the fields (two or four) are identical. Hereon, u_1 refers to the one with two identical fields, whereas u_2 corresponds to the four identical fields part. For the two renormalized vertices (u_1, u_2) we get:

$$\frac{\mathrm{d}u_1}{\mathrm{d}\ell} = 2u_1 - \frac{\mathcal{P}u_1^2 Q}{\Delta(Q)+Q^2} + \frac{\mathcal{P}w_1 Q}{[\Delta(Q)+Q^2]^{1/2}}, \tag{6.35a}$$

$$\frac{\mathrm{d}u_2}{\mathrm{d}\ell} = 2u_2 - 2\frac{\mathcal{P}u_1^2 Q}{\Delta(Q)+Q^2} + \frac{\mathcal{P}w_2 Q}{[\Delta(Q)+Q^2]^{1/2}}. \tag{6.35b}$$

Here, w denotes the six-point vertex, which becomes essential as u might flip sign and is then insufficient for the stability of the free energy. For exactly the same reason as for u, the six-point vertex also renormalizes depending on whether two, four, or six fields

are identical. But in order to make the RG flow equations dimensionless, we first make the following change of cariables:

$$\mathcal{Q} = Q\, e^{-\ell}/\sqrt{\mathcal{P}U}, \tag{6.36a}$$

$$\bar{\Delta}(\mathcal{Q}) = \Delta(\ell)\, e^{-2\ell}/(\mathcal{P}U), \tag{6.36b}$$

$$\bar{u}_{\{i\}}(\mathcal{Q}) = u_{\{i\}}(\ell)\, e^{-2\ell}U, \tag{6.36c}$$

$$w_{\{i\}}(\mathcal{Q}) = w_{\{i\}}(\ell)\, e^{-2\ell}\mathcal{P}^2/U. \tag{6.36d}$$

In terms of the new RG scale parameter $\mathcal{Q}$ and others, we can write down the flow equations as follows:

$$\frac{\mathrm{d}\bar{\Delta}}{\mathrm{d}\mathcal{Q}} = -\frac{\bar{u}_1}{\left[\bar{\Delta}+\mathcal{Q}^2\right]^{1/2}}, \tag{6.37a}$$

$$\frac{\mathrm{d}\bar{u}_1}{\mathrm{d}\mathcal{Q}} = \frac{\bar{u}_1^2}{\bar{\Delta}+\mathcal{Q}^2} - \frac{w_1}{\left[\bar{\Delta}+\mathcal{Q}^2\right]^{1/2}}, \tag{6.37b}$$

$$\frac{\mathrm{d}\bar{u}_2}{\mathrm{d}\mathcal{Q}} = \frac{2\bar{u}_1^2}{\bar{\Delta}+\mathcal{Q}^2} - \frac{w_2}{\left[\bar{\Delta}+\mathcal{Q}^2\right]^{1/2}}, \tag{6.37c}$$

$$\frac{\mathrm{d}w_1}{\mathrm{d}\mathcal{Q}} = \frac{3\bar{u}_1 w_1}{\bar{\Delta}+\mathcal{Q}^2} - \frac{2\bar{u}_1^3}{\left[\bar{\Delta}+\mathcal{Q}^2\right]^{3/2}}, \tag{6.37d}$$

$$\frac{\mathrm{d}w_2}{\mathrm{d}\mathcal{Q}} = \frac{4\bar{u}_1 w_1 + \bar{u}_2 w_2}{\bar{\Delta}+\mathcal{Q}^2} - \frac{4\bar{u}_1^3}{\left[\bar{\Delta}+\mathcal{Q}^2\right]^{3/2}}, \tag{6.37e}$$

$$\frac{\mathrm{d}w_3}{\mathrm{d}\mathcal{Q}} = \frac{8\bar{u}_1 w_2}{\bar{\Delta}+\mathcal{Q}^2} - \frac{12\bar{u}_1^3}{\left[\bar{\Delta}+\mathcal{Q}^2\right]^{3/2}}. \tag{6.37f}$$

The numerical integration of the above equations results in the renormalized parameters, which are shown in Fig. (6.4).

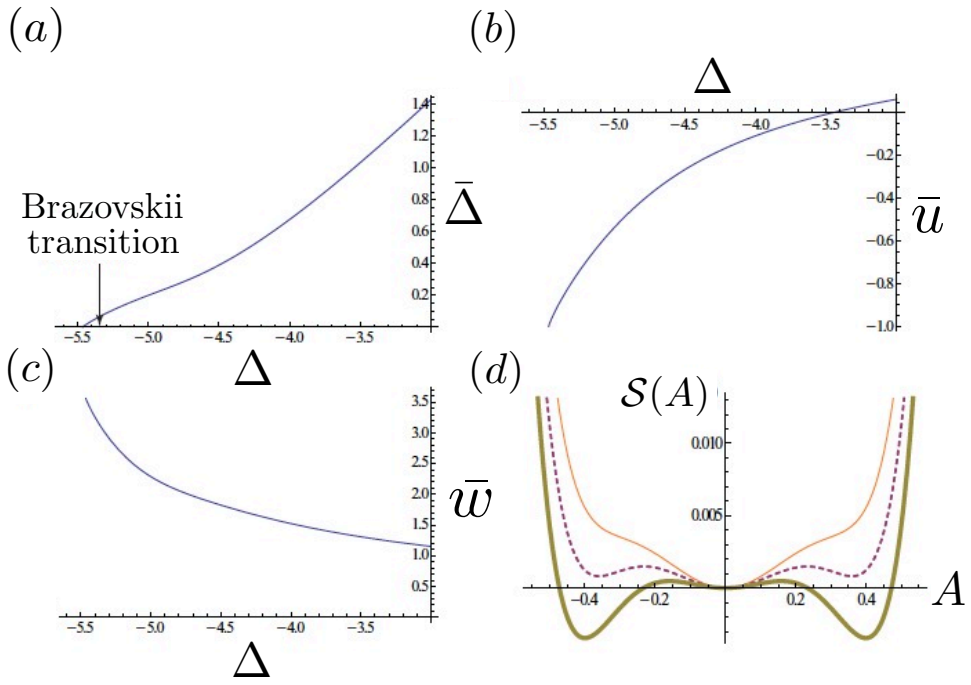

Figure 6.4: (From Ref. [75]) The renormalization group flows of different parameters in the quantum Brazovskii model. (a) shows how the renormalize gap $\bar{\Delta}$ decreases as the bare gap Δ is lowered below the mean-field transition value $\Delta = 0$. (b) shows the same diagram for renormalized quartic coefficient $\bar{u}$. As apparent from the figure, $\bar{u}$ flips sign around $\Delta \simeq -3.5$, where according to (a), $\bar{\Delta} \simeq 1$. When $\bar{u}$ becomes negative, the stabilization of the free energy is destroyed. However (c), demonstrates how during the renormalization process, a positive sixth-order nonlinearity with the coefficient w, emerges which is required for the stabilization. Finally (d) shows the resultant free energy (action), as a function of the order parameter, the amplitude of the mode q_0.

REFERENCES

[1] Hilbert von Löhneysen, Achim Rosch, Matthias Vojta, and Peter Wölfle. Fermi-liquid instabilities at magnetic quantum phase transitions. *Reviews of Modern Physics*, 79(3):1015, 2007.

[2] Jun Kondo. Resistance minimum in dilute magnetic alloys. *Progress of theoretical physics*, 32(1):37–49, 1964.

[3] Thomas Vojta. Quantum griffiths effects and smeared phase transitions in metals: Theory and experiment. *Journal of Low Temperature Physics*, 161(1-2):299–323, 2010.

[4] Ryogo Kubo. Statistical-mechanical theory of irreversible processes. i. general theory and simple applications to magnetic and conduction problems. *Journal of the Physical Society of Japan*, 12(6):570–586, 1957.

[5] Ryogo Kubo. The fluctuation-dissipation theorem. *Reports on progress in physics*, 29(1):255, 1966.

[6] JL Rivail, D Rinaldi, and J Leszczynski. Computational chemistry: Review of current trends. *World Scientific Publishing*, 1995.

[7] Y Marcus. Thermodynamic functions of transfer of single ions from water to nonaqueous and mixed solvents: Part 4-the selection of extra thermodynamic assumptions. *Pure and Applied Chemistry*, 58(12):1721–1736, 1986.

[8] CJT De Grotthuss. *Mémoire sur la décomposition de l'eau: et des corps qu'elle tient en dissolution à l'aide de l'électricité galvanique*. publisher not identified, 1805.

[9] E. J. Hart and M. Anbar. The hydrated electron. *Wiley*.

[10] Damian Aherne, Vu Tran, and Benjamin J Schwartz. Nonlinear, nonpolar solvation dynamics in water: The roles of electrostriction and solvent translation in the breakdown of linear response. *The Journal of Physical Chemistry B*, 104(22):5382–5394, 2000.

[11] B Abel, Ua Buck, AL Sobolewski, and W Domcke. On the nature and signatures of the solvated electron in water. *Physical Chemistry Chemical Physics*, 14(1):22–34, 2012.

[12] Christopher J Cramer and Donald G Truhlar. Implicit solvation models: equilibria, structure, spectra, and dynamics. *Chemical Reviews*, 99(8):2161–2200, 1999.

[13] Christopher J Cramer and Donald G Truhlar. Structure and reactivity in aqueous solution. 1994.

[14] JE Enderby, GW Neilson, and F Franks. Water: A comprehensive treatise. *by F. Franks, Plenum Press, New York*, 6:1, 1979.

[15] Ronald Wilfrid Gurney and Ronald W Gurney. Ionic processes in solution. 1953.

[16] Dominik Marx, Mark E Tuckerman, Juerg Hutter, and Michele Parrinello. The nature of the hydrated excess proton in water. *Nature*, 397(6720):601–604, 1999.

[17] Ross E Larsen, William J Glover, and Benjamin J Schwartz. Does the hydrated electron occupy a cavity? *Science*, 329(5987):65–69, 2010.

[18] Daniel Laria, David Wu, and David Chandler. Reference interaction site model polaron theory of the hydrated electron. *The Journal of chemical physics*, 95(6):4444–4453, 1991.

[19] Michael J Bedard-Hearn, Ross E Larsen, and Benjamin J Schwartz. Projections of quantum observables onto classical degrees of freedom in mixed quantum-classical simulations: Understanding linear response failure for the photoexcited hydrated electron. *Physical review letters*, 97(13):130403, 2006.

[20] Michael J Bedard-Hearn, Ross E Larsen, and Benjamin J Schwartz. Hidden breakdown of linear response: Projections of molecular motions in nonequilibrium simulations of solvation dynamics. *The Journal of Physical Chemistry A*, 107(24):4773–4777, 2003.

[21] Lars Onsager. Reciprocal relations in irreversible processes. i. *Physical Review*, 37(4):405, 1931.

[22] Lars Onsager. Reciprocal relations in irreversible processes. ii. *Physical Review*, 38(12):2265, 1931.

[23] Branka M Ladanyi and Mark Maroncelli. Mechanisms of solvation dynamics of polyatomic solutes in polar and nondipolar solvents: A simulation study. *Journal of Chemical Physics*, 109:3204–3221, 1998.

[24] Benjamin J Schwartz and Peter J Rossky. Aqueous solvation dynamics with a quantum mechanical solute: computer simulation studies of the photoexcited hydrated electron. *The Journal of chemical physics*, 101(8):6902–6916, 1994.

[25] Damian Aherne, Vu Tran, and Benjamin J Schwartz. Nonlinear, nonpolar solvation dynamics in water: The roles of electrostriction and solvent translation in the breakdown of linear response. *The Journal of Physical Chemistry B*, 104(22):5382–5394, 2000.

[26] Peter J Rossky and Jurgen Schnitker. The hydrated electron: Quantum simulation of structure, spectroscopy, and dynamics. *The Journal of Physical Chemistry*, 92(15):4277–4285, 1988.

[27] Pierre C Hohenberg and Bertrand I Halperin. Theory of dynamic critical phenomena. *Reviews of Modern Physics*, 49(3):435, 1977.

[28] JA Hertz. Quantum critical phenomena. *Phys. Rev. B*, 14:1165, 1976.

[29] AJ Millis. Effect of a nonzero temperature on quantum critical points in itinerant fermion systems. *Phys. Rev. B*, 48:7183, 1993.

[30] I. Bloch, J. Dalibard, and W. Zwerger. Many-body physics with ultracold gases. *Rev. Mod. Phys.*, 80:885, 2008.

[31] D. Nagy, J.K. Asboth, P. Domokos, and H. Ritsch. Self-organization of a laser-driven cold gas in a ring cavity. *Europhys. Lett.*, 74:254–260, 2006.

[32] D. Nagy, G Szirmai, and P. Domokos. Self-organization of a bose-einstein condensate in an optical cavity. *Eur. Phys. J. D*, 48:127–137, 2008.

[33] D. Nagy, G. Konya, G. Szirmai, and P. Domokos. Dicke-model phase transition in the quantum motion of a bose-einstein condensate in an optical cavity. *Phys. Rev. Lett.*, 104:130401, 2010.

[34] J Schmalian and M Turlakov. Quantum phase transitions of magnetic rotons. *Phys. Rev. Lett.*, 93:036405, 2004.

[35] Marc Janoschek, Markus Garst, Andreas Bauer, Pascal Krautscheid, Robert Georgii, Peter Boeni, and Christian Pfleiderer. Fluctuation-induced first-order phase transition in dzyaloshinskii-moriya helimagnets. *Physical Review B*, 87(13):134407, 2013.

[36] J. M. Sorenson, G. Hura, R. M. Glaeser, and T. Head-Gordon. What can x-ray scattering tell us about the radial distribution functions of water? *J. Chem. Phys.*, 113:9194–9161, 2000.

[37] T. Head-Gordon and G. Hura. Water structure from scattering experiments and simulation. *Chem. Rev.*, 102:2651–2669, 2002.

[38] J. Wang, T. N. Awadh, and V. H. Smith. Chemical binding and electron correlation effects in x-ray and high energy electron scattering. *J. Chem. Phys*, 101:4842–45, 1994.

[39] R. Coridan, N. Schmidt, G. Lai, R. Godawat, M. Krisch, S. Garde, P. Abbamonte, and G. Wong. Hydration dynamics at femtosecond time scales and angstrom length scales from inelastic x-ray scattering. *Phys. Rev. Lett.*, 103:237402, 2009.

[40] R. H. Coridan, N. W. Schmidt, G. H. Lai, P. Abbamonte, and G. C. L. Wong. Dynamics of confined water reconstructed from inelastic x-ray scattering measurements of bulk response functions. *Phys. Rev. E.*, 85:031501, 2012.

[41] J. P. Hansen and I. R. McDonald. Theory of simple liquids. *Math. Ann.*, 281:247–254, 2006.

[42] R. Kubo. Statistical-mechanical theory of irreversible processes. i. general theory and simple applications to magnetic and conduction problems. *J. Phys. Soc. Jpn.*, 12:570–586, 1957.

[43] H. Bethe. Zur theorie des durchgangs schneller korpuskularstrahlen durch materie. *Annalen der Physik*, 397:325–400, 1930.

[44] B. Ladanyi and B. Perng. Computer simulation of wavevector-dependent dielectric properties of polar and nondipolar liquids. *AIP Conf. Proc.*, 492:250, 1999.

[45] I. P. Omelyan. Longitudinal wavevector-and frequency-dependent dielectric constant of the tip4p water model. *Mol. Phys.*, 93:123, 1998.

[46] Philippe A. Bopp, Alexei A. Kornyshev, and Godehard Sutmann. Frequency and wave-vector dependent dielectric function of water: Collective modes and relaxation spectra. *J. Chem. Phys.*, 109:1939, 1998.

[47] G. Ruocco and F. Sette. The history of the "fast sound.

[48] Felix Sedlmeier, Dominik Horinek, and Roland R. Netz. Spatial correlations of density and structural fluctuations in liquid water: A comparative simulation study. *J. Am. Chem. Soc*, 133:1391, 2011.

[49] F. H. Stillinger and A. Rahman. Improved simulation of liquid water by molecular dynamics. *J. Chem. Phys.*, 60:1545, 1974.

[50] A. Rahman and F. H. Stillinger. Propagation of sound in water. a molecular-dynamics study. *Phys. Rev. A*, 10:368, 1974.

[51] J. Teixeira, M. Bellissent-Funel, S. Chen, and B. Dorner. Observation of new short-wavelength collective excitations in heavy water by coherent inelastic neutron scattering. *Phys. Rev. Lett.*, 54:2681, 1985.

[52] F. Sette, G. Ruocco, M. Krisch, U. Bergmann, C. Masciovecchio, V. Mazzacurati, G. Signorelli, and R. Verbeni. Collective dynamics in water by high energy resolution inelastic x-ray scattering. *Phys. Rev. Lett*, 75:850, 1995.

[53] F. Sette, G. Ruocco, M. Krisch, C. Masciovecchio, R. Verbeni, and U. Bergmann. Transition from normal to fast sound in liquid water. *Phys. Rev. Lett.*, 77:83, 1996.

[54] G. Ruocco, F. Sette, U. Bergmann, M. Krisch, C. Masciovecchlo, V. Mazzacurati, G. Signorelli, and R. Verbeni. Equivalence of the sound velocity in water and ice at mesoscopic wavelengths. *Nature*, 379:521, 1996.

[55] U. Balucani, G. Ruocco, A. Torcini, and R. Vallauri. Fast sound in liquid water. *Phys. Rev. E*, 47:1677, 1993.

[56] F. Sciortino and S. Sastry. Sound propagation in liquid water: The puzzle continues. *J. Chem. Phys.*, 100:3881, 1994.

[57] T. Komatsu, N. Yoshii, S. Miura, and S. Okazak. A large-scale molecular dynamics study of dynamic structure factor and dispersion relation of acoustic mode in liquid and supercritical water. *Fluid Phase Equilib.*, 226:345, 2004.

[58] L. D. Landau and E. M. Lifshitz. Electrodynamics of continuous media. *Pergamon Press, Oxford*, 2nd ed, 1984.

[59] R. Zwanzig. Dielectric friction on a moving ion. ii. revised theory. *J. Chem. Phys.*, 52:3625, 1970.

[60] J. Hubbard. Dielectric dispersion and dielectric friction in electrolyte solutions. ii. *J. Chem. Phys.*, 68:1649, 1978.

[61] M. Bruehl and J. T. Hynes. Dielectric friction and solvation dynamics: a molecular dynamics study. *J. Phys. Chem.*, 96:4068, 1992.

[62] P. Kumar and M. Maroncelli. The non-separability of dielectric and mechanical friction in molecular systems: A simulation study. *J. Chem. Phys.*, 112:5370, 2000.

[63] A. O. Caldeira and A. J. Leggett. Influence of dissipation on quantum tunneling in macroscopic systems. *Phys. Rev. Lett.*, 46:211, 1981.

[64] A. O. Caldeira and A. J. Leggett. Quantum tunneling in a dissipative system. *Annals of Physics*, 149.

[65] R. P. Feynman and A. R. Hibbs. *Statistical Mechanics, A Set of Lectures*. Addison-Wesley, 1972.

[66] R. P. Feynman and A. R. Hibbs. *Quantum Mechanics and Path Integrals*. McGrow-Hill and Company, 1965.

[67] R. P. Feynman. Slow electrons in a polar crystal. *Phys. Rev.*, 97:660–665, 1955.

[68] R. P. Feynman, RW Hellwarth, CK Iddings, and PM Platzman. Mobility of slow electrons in a polar crystal. *Phys. Rev.*, 97:660–665, 1955.

[69] M. Saitoh. Theory of a polaron at finite temperatures. *Journal of the Physical Society of Japan*, 49:878–885, 1980.

[70] D. K. K. Lee and J. M. F. Gunn. Polarons and bose decondensation: A self-trapping approach. *Phys. Rev. B*, 46:301, 1992.

[71] J. Tempere, W. Casteels, M. K. Oberthaler, S. Knoop, E. Timmermans, and J. T. Devreese. Feynman path-integral treatment of the bec-impurity polaron. *Phys. Rev. B*, 80:184504, 2009.

[72] FM Peeters and JT Devreese. On the existence of a phase transition for the froehlich polaron. *Physica Status Solidi (b)*, 112:219–229, 1982.

[73] J. Vlietinck, W. Casteels, K. van Houcke, J. Tempere, J. Rykebusch, and J. Devreese. Diagrammatic monte carlo study of the acoustic and the boseeinstein condensate polaron. *New J. Phys.*, 17:033023, 2015.

[74] S. Gopalakrishnan, B. L. Lev, and P. M Goldbart. Emergent crystallinity and frustration with boseeinstein condensates in multimode cavities. *Nat. Phys.*, 5:845, 2009.

[75] S. Gopalakrishnan, B. L. Lev, and P. M Goldbart. Atom-light crystallization of bose-einstein condensates in multimode cavities: Nonequilibrium classical and quantum phase transitions, emergent lattices, supersolidity, and frustration. *Phys. Rev. A*, 82:04362, 2010.

[76] D. Jaksch, C. Bruder, J. I. Cirac, C. W. Gardiner, and P. Zoller. Cold bosonic atoms in optical lattices. *Phys. Rev. Lett.*, 81:3108, 1998.

[77] M. Greiner, O. Mandel, T. Esslinger, T. W. Haensch, and I. Bloch. Quantum phase transition from a superfluid to a mott insulator in a gas of ultracold atoms. *Nature*, 415:39–44, 2002.

[78] Bryce Gadway, Daniel Pertot, Ren Reimann, and Dominik Schneble. Superfluidity of interacting bosonic mixtures in optical lattices. *Phys. Rev. Lett.*, 105:045303, 2010.

[79] N. Spethman, F. Kindermann, S. John, C. Weber, D. Meschede, and A. Widera. Dynamics of single neutral impurity atoms immersed in an ultracold gas. *Phys. Rev. Lett.*, 81:3108, 1998.

[80] T. Fukuhara, A. Kantian, M. Endres, M. Cheneau, P. Schauss, S. Hild, D. Bellem, U. Schollwoeck, T. Giamarchi, C. Gross, I. Bloch, and S. Kuhr. Quantum dynamics of a mobile spin impurity. *Nat. Phys.*, 9:235, 2013.

[81] Krzysztof Sacha and Eddy Timmermans. Self-localized impurities embedded in a one-dimensional bose-einstein condensate and their quantum fluctuations. *Phys. Rev. A*, 73:063604, 2006.

[82] M. Bruderer, A. Klein, S. R. Clark, and D. Jaksch. Polaron physics in optical lattices. *Phys. Rev. A*, 76:011605, 2007.

[83] D. H. Santamore and E. Timmermans. Multi-impurity polarons in a dilute bosee-instein condensate. *New J. Phys.*, 13:103029, 2011.

[84] A. A. Blinova, M. G. Boshier, and E. Timmermans. Two polaron flavors of the bose-einstein condensate impurity. *Phys. Rev. A*, 88:053610, 2013.

[85] Weiran Li and S. Das Sarma. Variational study of polarons in bose-einstein condensates. *Phys. Rev. A*, 90:013618, 2014.

[86] F. Grusdt, Y. E. Shchadilova, A. N. Rubtsov, and E. Demler. Renormalization group approach to the froehlich polaron model: application to impurity-bec problem. *arXiv:1410.2203v1*.

[87] F. M. Cucchietti and E. Timmermans. Strong-coupling polarons in dilute gas bose-einstein condensates. *Phys. Rev. Lett.*, 96:210401, 2006.

[88] W. Casteels, J. Tempere, and J. T. Devreese. Bipolarons and multipolarons consisting of impurity atoms in a bose-einstein condensate. *Phys. Rev. A*, 88:013613, 2013.

[89] L. D. Landau. Electron motion in crystal lattices. *Phys. Zeit. Sowjetunion*, 3:1933, 664.

[90] A M Stoneham, J Gavartin, A L Shluger, A V Kimmel, D Muoz Ramo, H M Rnnow, G Aeppli, and C Renner. Trapping, self-trapping and the polaron family. *J. Phys. Condens. Matter*, 19:255208, 2007.

[91] S.A. Brazovskii. Phase transition of an isotropic system to an inhomogeneous state. *Zh. Eksp. Teor. Fiz.*, 68, 1975.

[92] S.A. Brazovskii, I.E. Dzyaloshinskii, and A. R. Moratov. Theory of weak crystallization. *Zh. Eksp. Teor. Fiz.*, 93:1110–1124, 1987.

[93] E. I. Kats, V. V. Lebedev, and A. R. Muratov. Cold bosonic atoms in optical lattices. *Phys. Rep*, 288:91, 1993.

[94] J Denschlag, JE Simsarian, DL Feder, Charles W Clark, LA Collins, J Cubizolles, L Deng, EW Hagley, K Helmerson, WP Reinhardt, et al. Generating solitons by phase engineering of a bose-einstein condensate. *Science*, 287(5450):97–101, 2000.

[95] G.H. Derrick. Comments on nonlinear wave equations as models for elementary particles. *J. Math. Phys.*, 5:1252–1254, 1964.

[96] UK Rößler, AN Bogdanov, and C Pfleiderer. Spontaneous skyrmion ground states in magnetic metals. *Nature*, 442(7104):797–801, 2006.

[97] XZ Yu, Y Onose, N Kanazawa, JH Park, JH Han, Y Matsui, N Nagaosa, and Y Tokura. Real-space observation of a two-dimensional skyrmion crystal. *Nature*, 465(7300):901–904, 2010.

[98] XZ Yu, N Kanazawa, Y Onose, K Kimoto, WZ Zhang, S Ishiwata, Y Matsui, and Y Tokura. Near room-temperature formation of a skyrmion crystal in thin-films of the helimagnet fege. *Nature materials*, 10(2):106–109, 2011.

[99] AJ Millis, DK Morr, and J Schmalian. Quantum griffiths effects in metallic systems. *Physical Review B*, 66(17):174433, 2002.

[100] AJ Millis, DK Morr, and J Schmalian. Local defect in metallic quantum critical systems. *Phys. Rev. Lett*, 16:167202, 2001.

[101] F Maucher, S Skupin, and W Krolikowski. Collapse in the nonlocal nonlinear schroedinger equation. *Nonlinearity*, 24(7):1987, 2011.

[102] LD Landau and SI Pekar. Polaron effective mass. *Zh Eksp Teor Fiz*, 18(5):419, 1948.